SITE CHARACTERISATION FOR LNAPLs INVESTIGATION USING ELECTRICAL RESISTIVITY TOMOGRAPHY (ERT) SURVEY.

by

John Kalala Ngeleka

Thesis submitted in partial fulfillment of the requirements for the degree of

Master of Science

in the Faculty of Natural and Agriculture Sciences, at the Institute for Groundwater Studies, University of the Free State, Bloemfontein, South Africa

Supervisor: Dr. Danie Vermeulen

Co- Supervisor: Prof. Simon Lorentz

November 2009

Now unto him that is able to do exceeding abundantly above all that we ask or think, according to the power that worketh in us, unto him be glory in the church by Christ Jesus throughout all ages, world without end. Amen.

Ephesians 3:20-21

DECLARATION

I, John Kalala Ngeleka, declare that this dissertation hereby submitted by me for the Magister Scientiae degree in the Faculty of Natural and Agricultural Sciences, Department of Geohydrology at the University of the Free State is my own independent work and has not previously been submitted by me at another university/faculty. I furthermore cede copyright of the dissertation/thesis in favour of the University of the Free State. All sources cited are indicated in the References section.

…….. ……...

J.K. NGELEKA 25 November 2009

ACKNOWLEDGEMENTS

I would hereby like to express my sincere thanks to the people who have supported and encouraged me during the process of achieving my thesis:

- To my Supervisor, Dr. Danie Vermeulen, and my co-Supervisor Professor Simon Lorentz, thank you for your guidance, advice and support throughout the project.

- To all the lecturers at the Institute for Groundwater Studies, I gratefully express appreciation for sharing their knowledge and expertise.

- To Modrek Gomo, Kevin Vermaak, Dumi Gqiba, Michael Bester and many other colleagues and students at the Institute for Groundwater Studies, thank you for all your advice and the hours spent in research discussion.

- To my dear wife Garden Miandabu and my children Grace, David, Joyce and Jubilee, thank you for all your love and encouragement.

- Last, but not least, my Heavenly Father. Without Him at my side, I would not have been able to complete this thesis.

TABLE OF CONTENTS

LIST OF FIGURES

LIST OF TABLES

LIST OF ACRONYMS

ERT	Electrical Resistivity Tomography
LNAPLs	Light Non - Aqueous Phase Liquids
VOC	Volatile Organic Carbon
PID	Photo Ionic Detector
MNA	Monitored Natural Attenuation
TPH	Total Petroleum Hydrocarbon
BTEX	Benzene Toluene Ethylbenzene Xylene
MTBE	Methyl Tert–Butyl Ether
SP	Spontaneous Potential
EC	Electrical Conductivity
EM	Electromagnetic
IP	Induced Polarization
BEEH	School of Bioresources Engineering and Environment Hydrology

1. INTRODUCTION

South Africa is increasingly facing groundwater contamination due to Light Non-Aqueous Phase Liquids (LNAPLs) spills as a consequence of an increase in the demand for fuel in the automotive, agricultural and industrial sectors. Petro-chemical industries, service stations and petroleum depots form the main urban sources and potential sources of hydrocarbon contaminants.

The South African government, together with research institutions, has the task of proving for the appropriate protection of groundwater resources in order to secure the supply of water of acceptable quality. For this purpose, investigations have been initiated to understand the whole process of groundwater vulnerability to hydrocarbon pollution (Pretorius *et al.*, 2008).

The East London Joint Fuel Depot site has been selected to investigate the fate and transport of LNAPLs in groundwater. Site characterization has been initiated as the first step of the investigation to provide detailed information on the geological and hydrogeological conditions of the site. Such information is important as its lead to a better understanding of the position and flow of LNAPLs in the sub-surface and how the groundwater is affected.

In this investigation one of the geophysical methods, Electrical Resistivity Tomography (ERT) is tested to characterize the Joint Fuel Depot site geology units, aquifer setting and LNAPLs preferential flow pathways, as well as to establish its ability to identify LNAPLs contaminant plumes.

ERT is a 2-D electrical resistivity technique which uses an automatic multi-electrode instrument to inject a current into the ground through two electrodes and which measures the voltage drop at two other electrodes. The injection of a current and the measurement of voltage drop are sequentially repeated along a line of several electrodes to produce a 2-D distribution of resistivity of the subsurface. In order to use the ERT method effectively for a particular noisy site such as the Joint Fuel Depot site, the Wenner array has

been found more appropriate as it has the ability to discriminate noises and give better results.

1.1 Research Framework

The study on the fate and transport of LNAPLs pollutants in groundwater in South Africa has been initiated as part of a strategy to protect groundwater resources and to secure the supply of water of acceptable quality. This study was conducted in the Joint Fuel Depot in East London. From previous investigations on the site, leakage had been identified around the tanks and piping, with the potential of contaminating the groundwater, given that vertical fractures and bedding plane fractures in the Karoo aquifers are likely to facilitate the expansion of the LNAPLs plumes. In the context of the Karoo aquifers, the following approaches have been adopted and applied for LNAPL site characterization in East London:

- The use of geophysical methods to characterize the subsurface materials and to detect LNAPL product flow pathways and contaminants plumes, have been applied at this site. The geophysics has included Electrical Resistivity Tomography (ERT), Induced Polarization (IP) and Electromagnetic (EM) surveys.
- Both the core drilling and auger methods were used to collect soil samples at different depths on site, in order to characterize the overburdening and to identify hydrocarbon contaminants in this layer of the site.
- The drilling of new boreholes on site has made geological logs available that characterize the lithostratigraphy of the geological formations.

Geophysics results are finally interpreted in terms of the geological setting, the hydrogeological setting and the contaminant plume setting, by integrating them together with borehole logs and hydrocarbon test results. This integrated interpretation is used to conceptualise the geology and hydrogeology of the site.

1.2 Aims of Dissertation

In order to determine the pathways and extent of LNAPLs plumes in the subsurface, it is important to start the investigation by characterizing the geological and hydrogeological conditions of the site, as well as contamination status of the LNAPLs. Although there are several approaches to be considered for such an investigation, the main aim of this dissertation is to test the applicability of the Electrical Resistivity Tomography (ERT) method which will allow for the following:

- Characterization of the geological units of the site (distinguishing overburden and bedrocks) and geohydrological settings (localising water-bearing rocks).
- Localisation of weathered zones and fractured zones which are considered as groundwater and contaminant preferential flow paths.
- Identification of LNAPLs contaminant zones at a real field site.
- Defining a conceptual model of the study area.
- Discussing the applicability of ERT on LNAPLs site characterization.

1.3 Structure of this Dissertation

The Dissertation comprises ten chapters, and the various chapters are set-up as follows:

- Chapter One gives an introduction to the study, outlining the motivation for undertaking the study, as well as the aims and objectives of the study;
- Chapter Two is the Literature Review, which briefly describes the application of ERT in various case studies;
- Chapter Three describes the site location, as well as the general geology and hydrogeology of the study area;

- Chapter Four outlines, in steps, the approaches undertaken for site characterization using ERT;
- Chapter Five reviews the use of ERT described in the literature, the background on the Electrical Resistivity Methods for LNAPLs contaminated sites, data acquisition techniques on site and the interpretation process of the data collected;
- Chapter Six presents the results of field testing used to complement ERT, including soil analysis, groundwater analysis and geological logs;
- Chapter Seven presents a comparison of the field test results and the ERT results in an integrated data interpretation result;
- Chapter Eight describes an updated conceptual model;
- Chapter Nine discusses the applicability and limitation of the use of ERT methods for LNAPLs site characterization; and
- Chapter Ten draws conclusions on the characterisation for the study site and provides recommendations for future research on LNAPLs investigations using ERT.

2. LITERATURE REVIEW

Surface geophysical techniques such as gravity, magnetic, seismic and electrical methods are used to map, locate and characterize subsurface features by measuring physical, electrical and chemical properties at the surface. The increased interest in field investigation to study the fate and the transport of LNAPLs in the groundwater has lead to a need for an accurate characterization of the site's geology and hydrogeology.

The review of available literature has revealed that Electrical Resistivity Tomography (ERT) surveys have played a major role in such investigations for several years. ERT has been widely and successfully used for site characterization and for detecting hydrocarbon contaminant plume in groundwater. These literature studies contribute to establishing the applicability of ERT in the geological and hydrogeological characterization of a site and its ability to delineate LNAPLs plume in aquifers.

2.1 Movement of Light Non-Aqueous Phase Liquids in the Sub-surface

Light Non-Aqueous Phase Liquids (LNAPLs) are organic chemicals that, once in contact with either water or air, remain in a lighter-than-water, immiscible phase. When released into the subsurface, LNAPLs exist in four phases including a free phase, a residual phase, a volatile phase and a dissolved phase. The free phase is the mobile constituent, which under gravity is free to migrate downward to the water table, forming a contaminant plume on the surface of the water table. The free phase will then migrate generally in the direction of the groundwater gradient following groundwater preferential pathways, which are weathered zones and fractured zones. The residual phase is that portion left behind in the vadose zone after the migration of the free phase. A volatile phase takes place in the pore spaces around and above the residual and free phase, creating a vapour plume. The dissolved phase is a component of the LNAPLs that dissolve in the groundwater, the movement of

which will be controlled by conventional groundwater transport mechanisms (advection, dispersion and diffusion) (Refer to Figure 2.1).

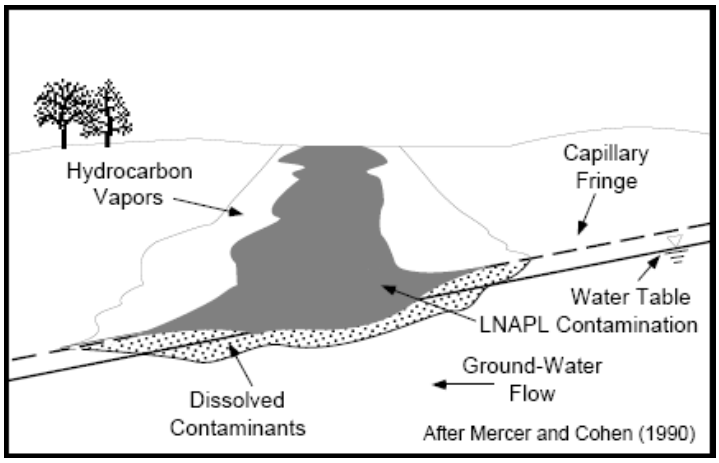

Figure 2.1 Simple model illustrating the release and migration of LNAPL in the vadose zone (after Newell *et al.*, 1995).

It has been noticed that Light Non-Aqueous Phase Liquids (LNAPLs) do not behave similarly in fractured rocks and in porous media. The groundwater surface fluctuation in the fractured rocks can greatly affect the entrapment and migration of LNAPLs (Hardisty *et al.,* 1998). The LNAPLs will follow the movement of the water table under the influence of gravity. The LNAPLs will then migrate suddenly through larger vertical fractures with high transmissivity and laterally through less steeply dipping fractures. Every time the groundwater surface rises up, the LNAPLs will find their way to new lateral fractures which allow their vertical migration.

2.2 Previous Works

In December 2005, SRK Consulting undertook an environmental contamination investigation after the seepage of the free phase product from the concrete was discovered on the boundary between the two facilities of the Joint Depot Facility (JDF). SRK Consulting then proposed to investigate the potential source of the contamination by digging holes in strategic positions with a hand auger on the facility, as well as along the boundary of the JDF. An

assessment on the contamination history and the way forward in detecting the suspected contamination plume at each of the sites, was conducted by SRK and Georem.

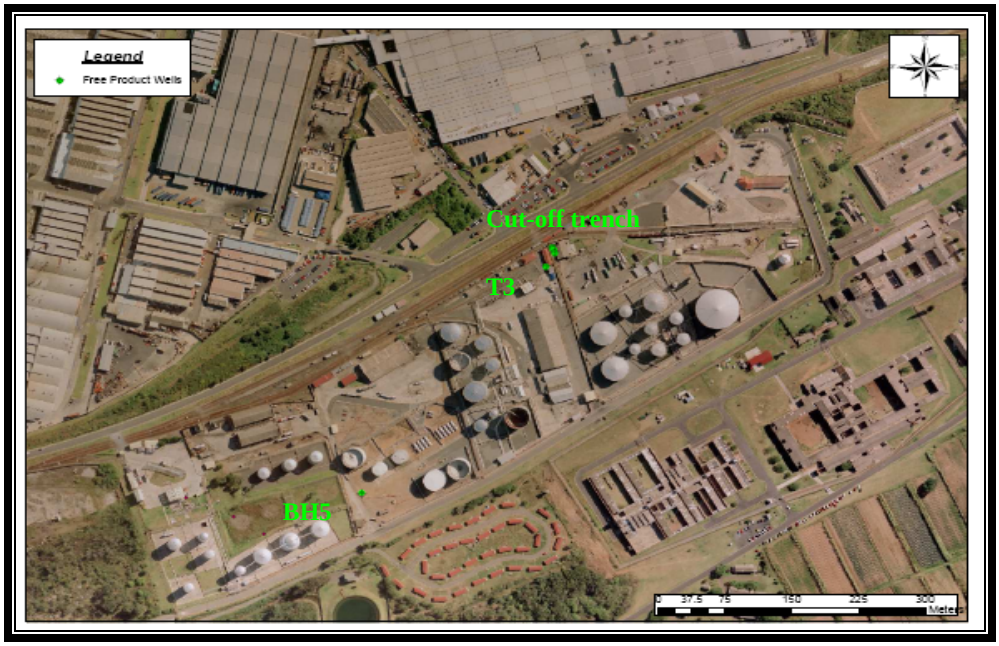

Figure 2.2 Locality of free product wells (Modified after Du Plooy, 2007).

- The borehole BH5, T3 and the cut-off trench were purged on a weekly basis and the product disposed of in supplied drums and separator pits; and
- Interface levels were measured and recorded and from the results a decrease in the free product thickness could be observed in all the wells where the free product was detected. This therefore suggests that the Pump and Treat method applied, achieved the required results i.e. the declining of the free product on the water.

SRK created a groundwater contour map for the joint fuel depot site based on information obtained from the National Ports Authority and water levels measured on site. The groundwater contour map was then used to determine the preferred groundwater flow directions. The general groundwater flow direction (excluding minor flow regimes) can be given as flowing in an east north-easterly direction.

The information obtained from this investigation (following on the desk study conducted) suggests that the product found at the lower site could have originated from the spill that occurred at the upper site during September 2005 (Du Plooy, 2006). Besides that, free product was already reported on the water in this borehole during 2003 and the borehole is located "up-gradient" from the tank where the product spill occurred.

The free product found in the wells was analysed for the degree of degradation. The product was compared with the peak retention times of commercial diesel and no variance of note could be found, thus suggesting that the free product discovered at the lower site originates from a recent spill/contamination event (Du Plooy, 2006).

2.3 Role of ERT in Geological and Hydrogeological Characterization

2.3.1 Resistivity for soil characterization

Electrical resistivity surveys have been applied to soil study for many decades. The electrical resistivity experience was found to be a proxy for the partial and temporal variability of many physical soil properties. A relationship has been established between the electrical resistivity and soil characteristics such as particle size distribution and mineralogy, arrangement of voids (porosity, pore size distribution, connectivity), degree of water saturation (water content), electrical resistivity of the fluid (solute concentration) and temperature.

It should be noticed that air is infinitively resistive, the resistivity of a water solution depends on the ionic concentration and the resistivity of solid grains is a function of the electrical charge density at the surface of the constituents.

The electrical resistivity of soils ranges from 1 Ωm for saline soil to several 10^5 Ωm for dry soil. Clay soil has a low electrical resistivity compared to coarse-texture soils because of the higher electrical charge density on clay particle surfaces.

Robain *et al.* (1996) established a relationship between the structure of soil materials and resistivity variations: the higher the porosity of soil materials the higher the resistivity values.

- **Resistivity related to nature and arrangement of solid constituents**

Archie's law allows for estimating the porosity of a saturated soil medium from its electrical property. For a saturated soil without clay the porosity can be estimated by the following equation:

$$F = \frac{\rho_a}{\rho_w} = a\phi^{-m} \qquad (1)$$

Where:

F = the formation factor

a = coefficient of saturation

ϕ = porosity

$_m$ = cementation factor

ρ_a = resistivity of the formation

ρ_w = resistivity of pore-water

Knowing the pore-water resistivity and the constants a and $_m$, the apparent porosity can be calculated from the resistivity value, assuming that the whole void space is filled only with water.

These porosities were subsequently used to estimate the hydraulic conductivity through the Kozeny-carman-Bear equation expressed as:

$$K = (\delta_w g / \mu)(d^2/180)\left[\phi^3/\left(1-\phi^2\right)\right] \qquad (2)$$

Where:

d = grain size

δ_w = fluid density (1000kg/m3)

μ = dynamic viscosity taken to be 0.0014kg/ms.

- **Resistivity related to water content.**

The electrical current in soil is based on ion displacement in pore water. The electrical current in soils is therefore a function of the water content in pores and the presence of dissolved salts. It has been established from laboratory experiments that electrical resistivity deceases when water content increases (McCarter, 1984; Michot *et al.*, 2000; Fukue *et al.*, 1999).

Archie (1942) has established that for coarse-grained soil, water saturation is a function of formation resistivity ρ and water resistivity ρ_w as indicated by the equation below:

$$S^n = \frac{F\rho_w}{\rho} \qquad (3)$$

Combining with equation (1) the following equation is obtained:

$$S^n = \frac{a\rho_w}{\phi^n \rho} \qquad (4)$$

Where:

S = the degree of saturation

$_n$ = parameter related to the degree of saturation

This relationship was successfully used for water content estimation in numerous studies (Binley *et al.*, 2002; Zhou *et al.*, 2001) and to determine

temporal variations in soil moisture profile using electrical resistivity data obtained at different times (Aaltonen, 2001; Michot *et al.*, 2003).
Goyal *et al.*, (1996) and Gupta and Hanks (1972) established an empirical linear relationship between resistivity and water content as follows:

$$\rho_{(z,t)} = a + b\theta_{(z,t)} \quad (5)$$

Where a and b are empirical constants characteristic of soil and water (porosity, temperature, salinity).

Rhoades *et al.* (1976b) proposed a new equation which takes into account the clay content in a solid matrix as follows:

$$\frac{1}{\rho} = \frac{1}{\rho_w}\left(a\theta^2 + b\theta\right) + \frac{1}{\rho_s} \quad (6)$$

Where ρ_w and ρ_s represent the pore-water resistivity and the solid matrix, respectively.

- **Resistivity related to pore fluid composition**

The estimation of the water content by resistivity measurements requires knowledge of the concentration of the dissolved ions (Samouelian *et al.*, 2005). Since salts have to be in an ionized form to conduct the current, the amount of water in the soil determines the available paths of conduction.
Shea and Lathin (1961) found a close linear relationship between electrical resistivity and salinity for a soil water content ranging from saturation to -3KPa water potential. The soil salinity should be measured at saturation, which is considered as the standardized condition.

Because of concentration and ionic composition variations in different areas of the soil, there will be a large range of possible electrical resistivities. From this principle, electrical resistivity surveys can successfully be used to delineate landfill structures (Bernston *et al.*, 1998) and to map salt water

intrusion into the coastal area (Nowroozi *et al.*, 1999; Acworth, 1999; Yaramanci, 2000).

- **Resistivity related to temperature**

The increase the soil temperature causes an increase in ion agitation and a decrease in fluid viscosity (Samouelian *et al.,* 2005). The electrical resistivity therefore decreases when the temperature increases. From this principle, comparisons of electrical resistivity data sets require the expression of electrical resistivity at a standardized temperature.

Campbell *et al.* (1948) demonstrated from a laboratory experience that conductivity increases by 2.02% per ºC between 15 ºC and 35 ºC. Therefore the correction to measure electrical conductivity is done using the following equation to express electrical conductivity at a standardized temperature:

$$\sigma_t = \sigma_{25°C}\left[1 + \alpha\left(T - 25°C\right)\right] \qquad (7)$$

Where:

σ_t = conductivity at the experiment temperature

$\sigma_{25°C}$ = conductivity at $25°C$

α = correction factor equal to 2.02%

Mostly temperature effect is not corrected for electrical resistivity measurements done every day at the same time over a short period, because the assumption is made that the temperature remains stable (Bottraud *et al.*, 1984b). But the correction of field electrical resistivity measurements for temperature effect is required at annual scale. It is therefore important to know the seasonal variation of the temperature and its impact on electrical resistivity measurements to avoid misinterpretation of filed data when comparing resistivity measurements obtained at the same place, but on different dates or seasons.

- Resistivity for clay characterization

Aritodemou and Thomas-Betts (2000) applied the ERT technique to characterize the landfill waste in terms of both resistivity and chargeability, to determine the base of the landfill and to identify clay layers which are considered as natural barriers to the downward movement of a contaminant plume.

From resistivity inversion results and fluid electrical conductivity measurements in the boreholes, aquifer properties such as porosity and hydraulic conductivity could be estimated. Both profiling and sounding surveys were used to collect data over a period of two years.

Six profiling survey lines were undertaken using Wenner and Dipole-Dipole arrays. Five lines were set up as closely as possible to monitor boreholes in the landfill area and one line was set up outside the landfill which was considered as a control line. Two sounding survey lines were carried out using the Schlumberger array in the centre of the landfill.

With resistivity and chargeability results, it was possible to distinguish the southern and northern sections of the landfill, as well as the saturated zone, which had received different types of waste. The ERT results were calibrated with geological logs in order to characterize lateral extent and the nature of different geological units. The chargeability results were able to reveal the position of clay aquitard at a 28m depth.

2.3.2 Resistivity for aquifer characterization

At Sawmills in Zimbabwe, Electrical Resistivity Tomography surveys were undertaken with the objective of finding suitable aquifers for water supplies in the city of Bulawayo (Dahlin, 2001). The geology of the study area consists mainly of a basaltic formation covering the upper Karoo sandstone, which was the target aquifer. Data was collected on an 800m long transect using Wenner and Schlumberger's arrays. The inversion results have provided true resistivity models which were correlated to different hydrogeological units. The fresh

basalt was related to the higher resistive middle layer, the weathered top part of the basalt is related to low resistivity zone as well as the upper Karoo sandstone underneath, which was the targeted aquifer.

2.3.3 Resistivity for a weathered zone characterization

Gioa *et al*. (2008) has proposed an effective approach to locate the boundary between the weathered and unweathered granite rocks on the hillside by integrating a conceptual weathering profile model and the results of ERT data inversion model. The mentioned approach included:

- The application of diverse field procedures, using more than one electrode array for resistivity data acquisition;
- A careful review of resistivity values of granite rocks form different sources;
- The inversion of ERT data using different algorithms and software considering the effect of topography; and
- Incorporation of the conceptual weathering model proposed by Ruxton and Berry (1957) in the interpretation of ERT results.

Investigation done by many scientists indicated that weathered granitic rock has a lower resistivity value then fresh granitic rock. The resistivity of weathered granite can be as low as 100 Ωm, while the resistivity of fresh granite can be as high a few thousands Ωm. The resistivity of granitic rocks, weathered and unweathered, depends on water content, water salinity and fractures.

2.3.4 Resistivity for a fractured zone characterization

Zhou *et al*. (2002) undertook an ERT survey to map enlarged fractures in Nashville, Tennessee. The geology of the study area consists of horizontal Ordovician Carters Limestone Formation. The Sting (Swift) system was used with Dipole-Dipole array to collect apparent resistivity data over a 305m

transect and RES2DINV (Loke and Barker 1995) was used for data inversion processes.

The result of this ERT investigation reveals the presence of two enlarged fractured zones at 280 feet and 220m on the profile (Refer to Figure 2.3) where low resistivity zones are found sandwiched vertically by the high-resistivity of the limestone around them.

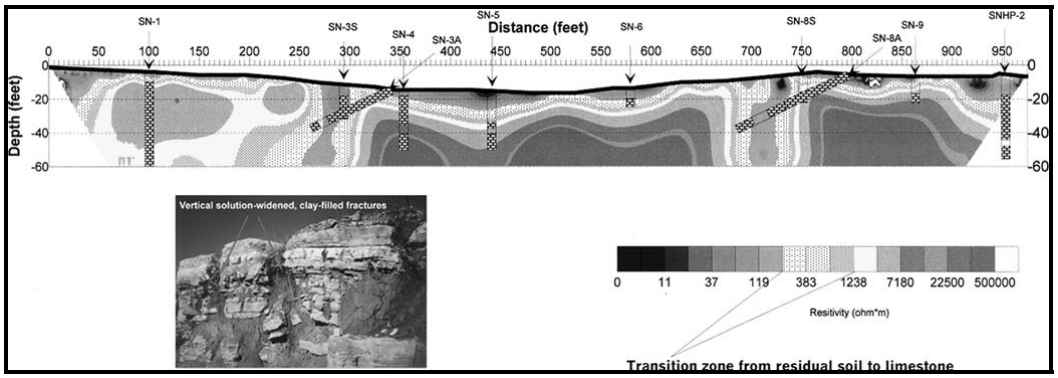

Figure 2.3 Comparison of geo-electrical profile using dipole–dipole array with geologic cross section using boring data (Zhou *et al.*, 2002).

The ERT findings were confirmed by geological logs from two directional boreholes (SN-3A and SN-8A) drilled across the location of the two interpreted fractured zones. It has been found that the boreholes logs and the resistivity model matched reasonable well (Zhou *et al.*, 2002).

2.3.5 Resistivity for site characterization

In general, Site Characterization starts with on-site observations which can provide an initial insight of the basic site geology and geomorphology. By inspecting road cuts, available open trenches or quarries one can depict geological features such as overburden, bedrock interfaces, fractures and weathered zones (Figure 4).

Figure 2.4 Road cut revealing geological features (Technos, 2004).

These on-site observations also aim to orientate the surface geophysical methods which will provide a wide special covering. Surface Electrical Resistivity methods have been successfully applied to detect and map fractures, cavities and other karsts features (Technos, 2004). Figure 2.5 is a result of the use of electrical resistivity methods to map variations in overburden thickness, top of rock, cavities, fracture zones and zones of highly weathered rock (Technos, 2004).

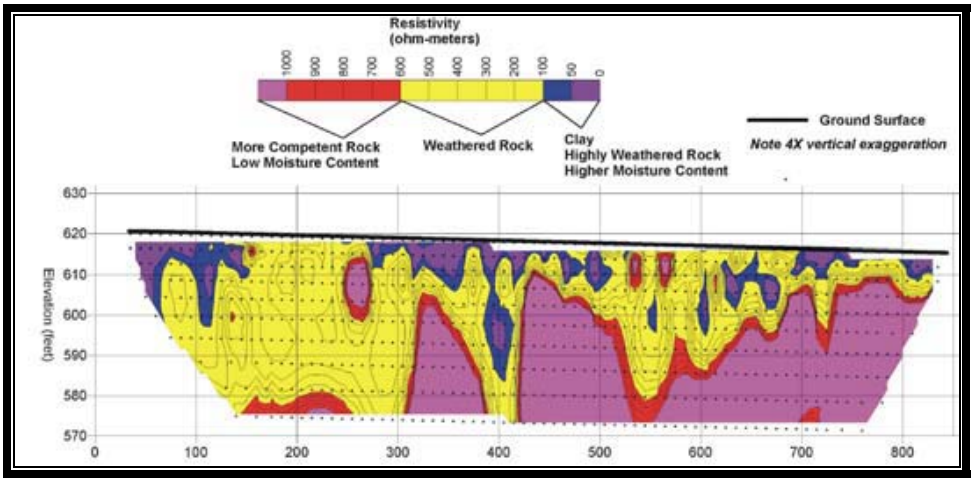

Figure 2.5 Resistivity Model showing highly weathered rock (Technos, 2004).

It has generally been concluded that a single method may not be able to provide all the site characterization needs. It may require other multiple observations and measurements using other geophysical techniques so that

multiple results may be compared each other for a higher level of confidence in geological and hydrogeological interpretations.

2.4 Role of ERT in Delineating LNAPLs Plumes in Groundwater

2.4.1 First case study

A laboratory pollution study was undertaken by Adepelumi *et al.* (2006) to simulate the field situation of a hydrocarbon spill environment. ERT was used to investigate its feasibility for detecting and monitoring LNAPLs (diesel in this case) spilled and/or leaked into clayey-sand aquifer.

- Model tank set-up

A model tank setup is referred to Figure 2.6. To simulate a moderately conductive clayey-sand medium, the tank was filled in a proportion of 3:1 with a mixture of sand and clay soil. This mixture was subsequently saturated with 20 litres of water before the injection of 10 litres of diesel through the four perforated PVC pipes BH1, BH2, BH3 and BH4. The PVC pipes with a 2 cm diameter were sealed at the bottom and inserted into the clayey-sand medium next to the ERT traverses. The resistivity of the diesel fuel used was measured prior to the experiment using an MC Conductivity meter. An approximate value of 25000 Ωm was determined. Two wooden boards (1.18m long) perforated every 1cm were placed on each traverse with 21 station positions to serve as electrode platforms during data acquisition. With an electrode spacing of 4cm, Dipole-Dipole array was used because of its ability to resolve vertical structures and an ABEM SAS 300C Terrameter was used for data acquisition.

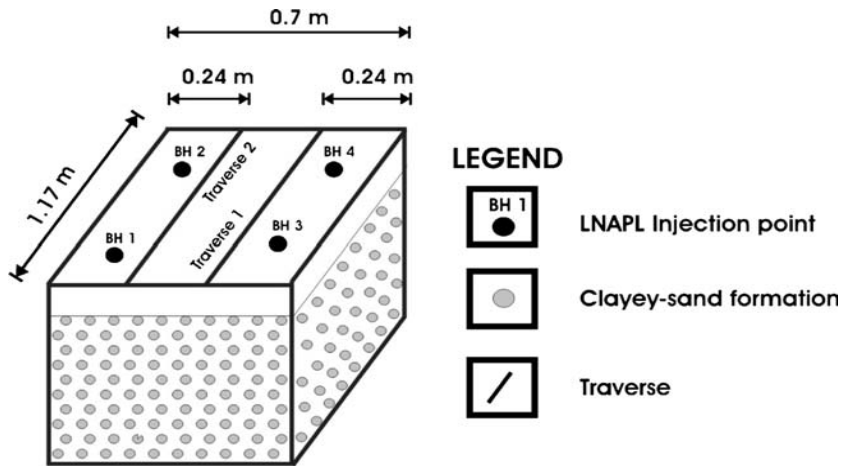

Figure 2.6 Model tank setup for ERT experiment.

- Data acquisition and inversion processes

The experiment was carried out in two main stages:

Pre-contamination: Before the injection of diesel into the medium, a 2-D resistivity measurement was performed on both two traverses to acquire the background resistivity of the clayey-sand medium.

Post-contamination: Ten minutes after the LNAPLs injection, a second 2-D resistivity measurement was run on both two traverses with the same electrode spacing of 4cm as for pre-injection. Other post-injection resistivity reading was taken at regular intervals of 190, 790, 1150 and 2050 minutes respectively on the two traverses. The 2-D resistivity inversion was performed using DIPRO software which employs the finite-element approach based on the smoothness-constraint least square optimization technique.

- Results and interpretation

Pre-contamination results: Two-dimensional resistivity structures recovered from inversion of the pre-injection resistivity data obtained on traverse TR1 and TR 2. The upper panel shows the acquired synthetic laboratory data, while the 2D model is shown in the lower panel. TR1's rms error 1.95% and TR2's rms error 1.71%.(refer to Figure 2.7).

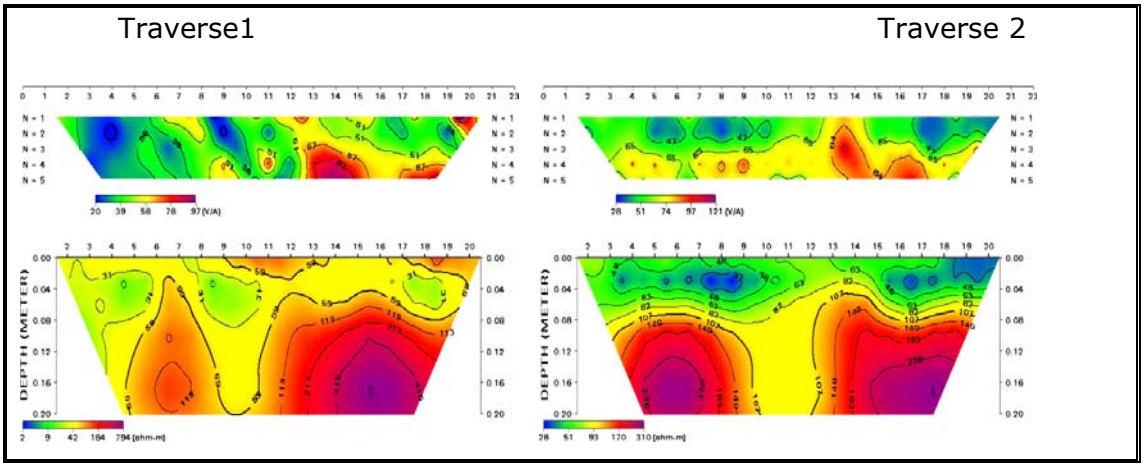

Figure 2.7 Pre-contamination results.

Pre-contamination interpretation:

- Upper part of the section (0 to 0.05m) is characterized by lower resistivity values ranging from 10 to 50 Ωm. This resistivity is interpreted as clayey-sand.
- The lower part of the section (0.05 to bottom) is characterized by high resistivity values compared to the upper part. This is interpreted as the presence of more resistive material (lower clay content) at depth.

These results indicate the heterogeneity of the clayey-sand medium.

Post-contamination results: Post-injection Time lapse 2D resistivity image beneath traverse TR 2. The upper and lower panels show the gathered laboratory data and the corresponding 2D resistivity model obtained through inversion. The rms errors of the 2D models range from 1.18% to 1.50%. (refer to Figure 2.8).

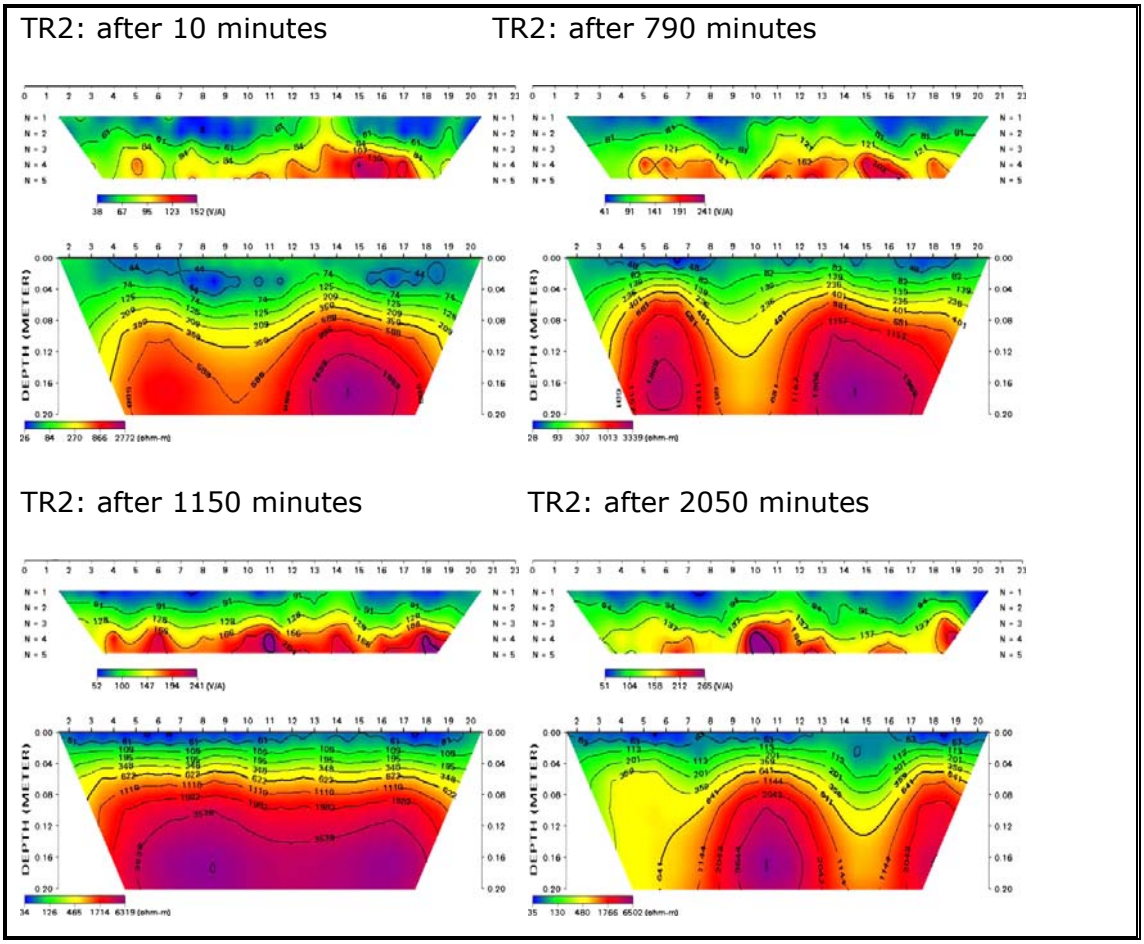

Figure 2.8 Post-contamination results.

Post-contamination interpretation:

- 10 minutes after the injection of LNAPLs, the inversed section is characterized by very high resistivity with values ranging between 900 and 2,700 Ωm beyond a 0.12m depth. These high values indicate that the LNAPLs have spread out laterally to this zone. It is thus inferred that the LNAPLs are moving toward areas of higher permeability (Adefelumi *et al.,* 2006).
- 790 minutes after injection, the LNAPLs form two discontinuous pools at the sides of the section. The resistivity values range from 900 to 2,500 Ωm on the left side and 600 to 3,000 Ωm on the right side.

- 1,150 minutes after injection, convincing evidence of the continuous spreading of LNAPLs plume has been obtained. The plume has migrated toward the center with an increase of resistivity values as high as 6,000 Ωm.
- 2,050 minutes after injection, the plume has finally formed a pool at the center of the section between station positions 8 and 14. The resistivity values of the plume had dropped to 4,000 Ωm.

- Conclusion

In this case study, the ERT has successfully characterized the movement of the LNAPLs in the unsaturated zone. The inverted resistivity data indicates very high resistivity values over the zone of LNAPLs plume, allowing the extent and migration pattern of the plume to be effectively mapped. It should also be noticed that as the plume residence time increases, the plume resistivity starts decreasing probably due to the draining of LNAPLs to a deeper level (Adepelumi *et al.*, 2006).

2.4.2 Second case study

A study of hydrocarbon-contaminated soil was undertaken by Hamzah (2009) using ERT surveys, together with Ground Penetrating Radar (GPR) and a Vertical Resistivity Probe (VRP). These geophysical surveys were successfully used to map geological structures and hydrocarbon plume in groundwater at Sungai Kandis. The study area was underlain by alluvial deposits consisting of 25 to 30 m of soft to firm silty clay with some intermediate sandy layers. A weathered zone covers a quartzite bedrock at 40m. The water table was located at 70 to 80 cm from the surface.

ERT measurements were made along 9 traverse lines using the ABEM Terrameter SAS 1000 instrument and the Schlumberger array. Data collected in the field was inverted using RES2DINV software (Loke and Baker, 1996). ERT results revealed an oil-contaminated layer with a higher resistivity value ranging form 60 to 200 Ωm sandwiched between the conductive top sand-silt

and the underlying conductive thick soft clay. This oil-contaminated layer shown in all inverse models of the 2-D electrical survey was confirmed by GPR and VRP results. The VRP results show apparent high resistivity values ranging from 200 to 10000 Ωm associated with an oil-contaminated layer (Hamzah *et al.,* 2009).

2.4.3 Third case study

Lago *et al.* (2008) demonstrated that the ERT survey and GPR survey could be effectively used to identify areas contaminated by a lubricant oil waste in the city of Ribeirao Preto, Brazil. The study site had been receiving waste generated by an oil company for 25 years. The lubricating oils consisted mainly of polycyclic aromatic hydrocarbon (PAHs) and inorganic additives. The waste was disposed of in four trenches with an approximate length of 41 to 49 m, a width of 24 to 36 m and a mean depth of 6 m, and no protection liners were used in the bottom and laterals of the disposal trenches (Lago *et al.,* 2008).

The area was located in a sedimentary basin made of two distinct geological units including a reddish sandstone layer baring groundwater called Guarani aquifer which is the main source of water supply of the city and dark grey basaltic dikes and sills. On top and between them are found residual sandy soil and clayey silts.

Using a Dipole-Dipole array, 2-D electrical resistivity surveys were undertaken across each disposal trench. RES2DINV program was used for smooth modelling and the inversed resistivity models interpreted below was obtained.

- Resistivity Section C3 across Trench 1 presents a contrast between the trench and the natural soil around it. The soil around it is more resistive (>800 Ωm) than the trench filled with residue (< 800 Ωm). The very low resistivity values (38 Ωm) below 12.7m is interpreted as an occurrence of contamination due to migration in the saturated zone of the waste trench materials (Refer Figure 2.9).

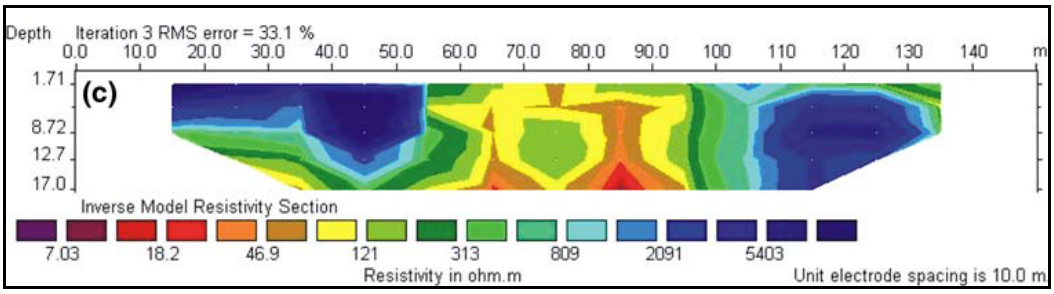

Figure 2.9 Resistivity section of the line C3 across trench 1.

- Besides the contrast shown between natural soil and trench materials, there is also a zone of lower resistivity (40 Ωm) at a depth of 14m inside the saturated zone. The zone also suggests the occurrence of contamination processes from the migration of waste materials inside the trench at a distance between 60 and 70 m (refer to Figure 2.10).

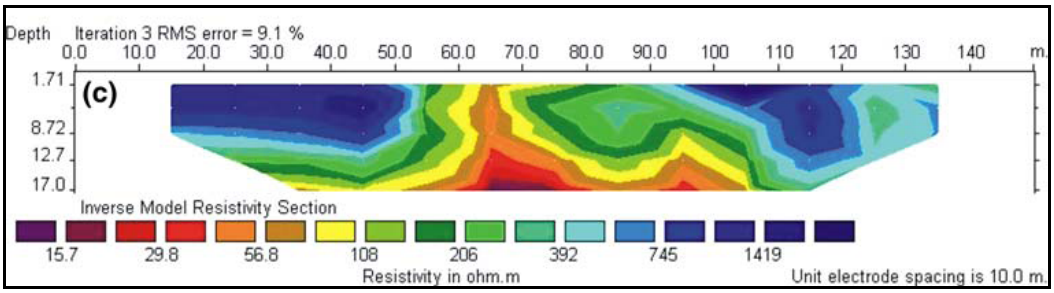

Figure 2.10 Resistivity section of the line C8 across trench 2.

- The line C14 across Trench 3 presents a zone of high resistivity (above 2,900 Ωm) between 65 and 85 m inside the trench filled by waste. This increase of resistivity compared to the above trenches is explained by the fact that this trench is chronologically more recent (Lago *et al.*, 2008). A conductive zone below the trench (resistivity < 100 Ωm) reveals the migration of contaminant downward to the bottom of the trench (refer to Figure 2.11).

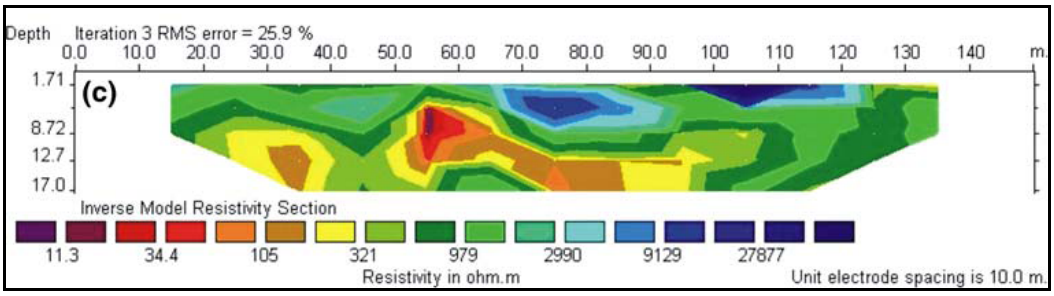

Figure 2.11 Resistivity section of the line 14 across trench 3.

- The line C17 across the trench presents a first layer of higher resistivity (>3,000 Ωm) between 75 and 110 m known as a trench filled by waste. The second layer of low resistivity (<185 Ωm) underneath is the result of the contaminant migration (refer to Figure 2.12).

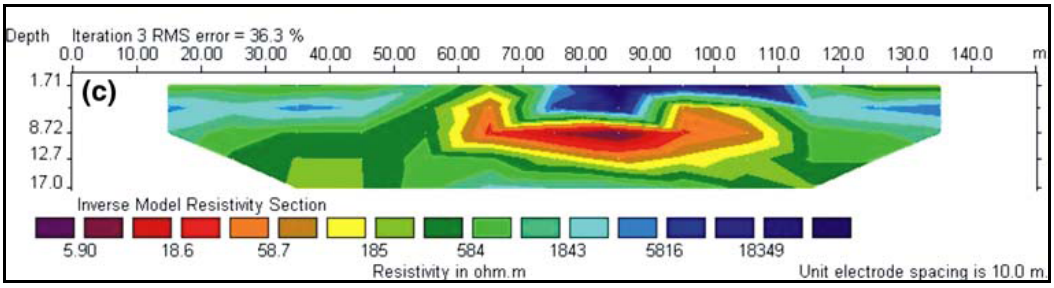

Figure 2.12 Resistivity section of the line 17 across trench 4.

In conclusion, the results of this study have indicated that electrical resistivity detected the presence of lubricant oil residues disposed of in the soil. Sauck (2000) shows that organic residues suffer greater bacteriological activity when the exposition time is increased, resulting in an enhancement of the electrical conductivity of the environment. This phenomenon is observed in the electrical resistivity of the trenches, where Trench 1 (the oldest) is less resistive in comparison with Trenches 2, 3 and 4 (which are younger and more resistive). The bacteriological activity is therefore the cause of lubricant oil degradation which reduces its resistivity values over time (Sauck, 2000).

2.4.4 Fourth case study

Godio and Naldi (2003) studied the effect of long-term diesel oil pollution due to leakage from buried tanks using the electrical resistivity tomography technique and established the applicability of this technique in delineating a hydrocarbon plume. From the results of both the electrical resistivity shown below (Figure 2.13) and the geochemical investigation, the authors suggested that the low resistivity zone, related to as the contaminant plume, is the result of a biodegradation due to organic activity. It was concluded that subsoil which has been saturated with diesel oil for a long period of more then 20 years, exhibits an increased conductivity.

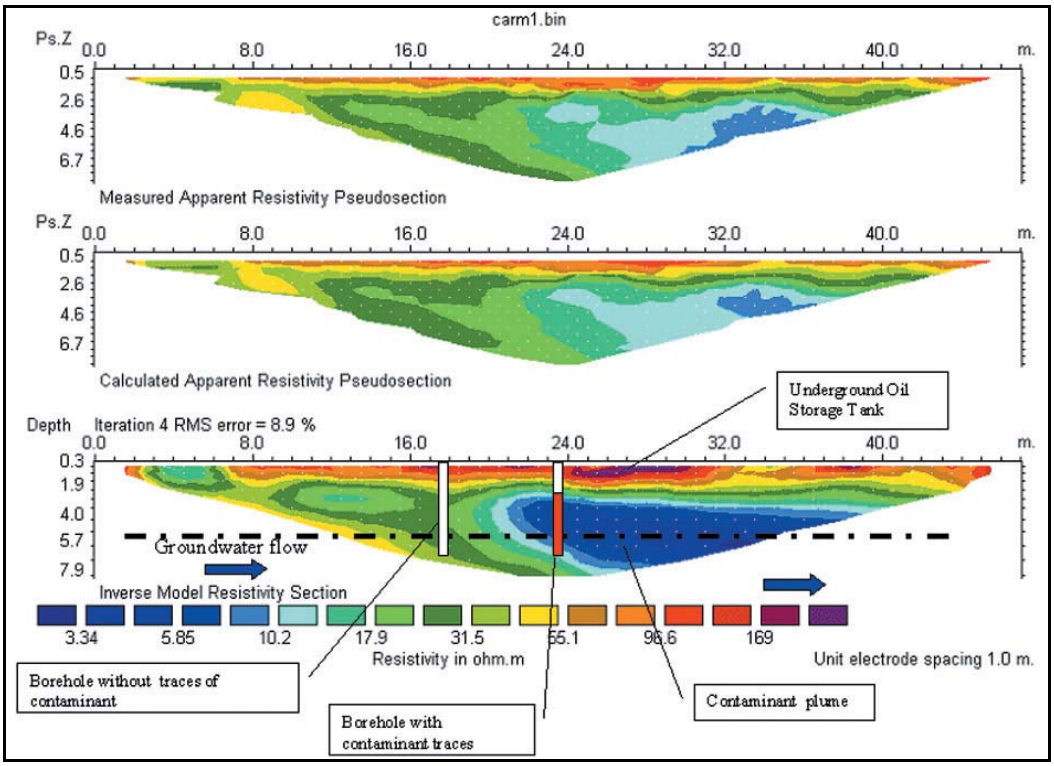

Figure 2.13 Electrical resistivity tomography result, showing positions of the boreholes (Godio *et al.,* 2003).

2.5 Summary of Literature Review

The literature review clearly summarized that the LNAPLs spill site's response to Electrical Resistivity is time- and space-dependant. The following processes are likely to be found on site when attempting to characterize the LNAPLs contaminate plume with the electrical resistivity survey:

- The presence of LNAPLs in the zone including the upper aquifer and lower vadose zone may initially be characterized by anomalously high resistivity (Sauck, 2000);

- Over time, biodegradation and chemical reaction are likely to occur, producing iron-rich leachates which cause a change to the response of the LNAPLs plume to a very conductive anomaly.

Study cases found in literature review demonstrate the ability of the ERT survey to depict changes in subsurface resistivity distribution due to the changes of soil water content, soil porosity, soil temperature and clay content.

The ERT survey has proved to be appropriate to locate aquifers position and extent as well as fractured and weathered zones. It is also possible with ERT survey to trace groundwater and LNAPLs movement in the subsurface.

3. SITE DESCRIPTION

3.1 Location and Topography

The Joint Fuel Depot facility is part of the industrial suburb of West Bank in East London, in the province of the Eastern Cape (refer to Figure 3.1). It is located between 27º 53´ 30.79" and 27º 53´ 59.66" longitudes East and between 33º 01´ 47.18" and 33º 02´ 07.31" latitudes South.

From the north-eastern to the south-western the site is occupied by four oil companies, one next to the other in the following order from the south west: BP/Shell, Engen, Chevron and Total. They are surrounded by the Department of Correctional Services facilities in the south and the industrial and residential areas in the north.

Each company has a number of tanks for the storage of petrol, diesel, paraffin, oil and fuel additives. Underground and surface piping is located between and surrounding the tanks. Next to the fuel storage facilities are loading zones, offices, warehouses and storerooms, mostly with concrete-paving around and between them. The site is thus inaccessible to heavy vehicles and the level of noise hampers conventional geophysical surveys on the site.

According to the 1:10 000 topographic map below (Figure 3.2) of the site and surroundings, the site is located at between approximately 60 and 40m above mean sea level (m.s.l). The regional topography of the area slopes to the north-east at a slope of approximately 2 per cent.

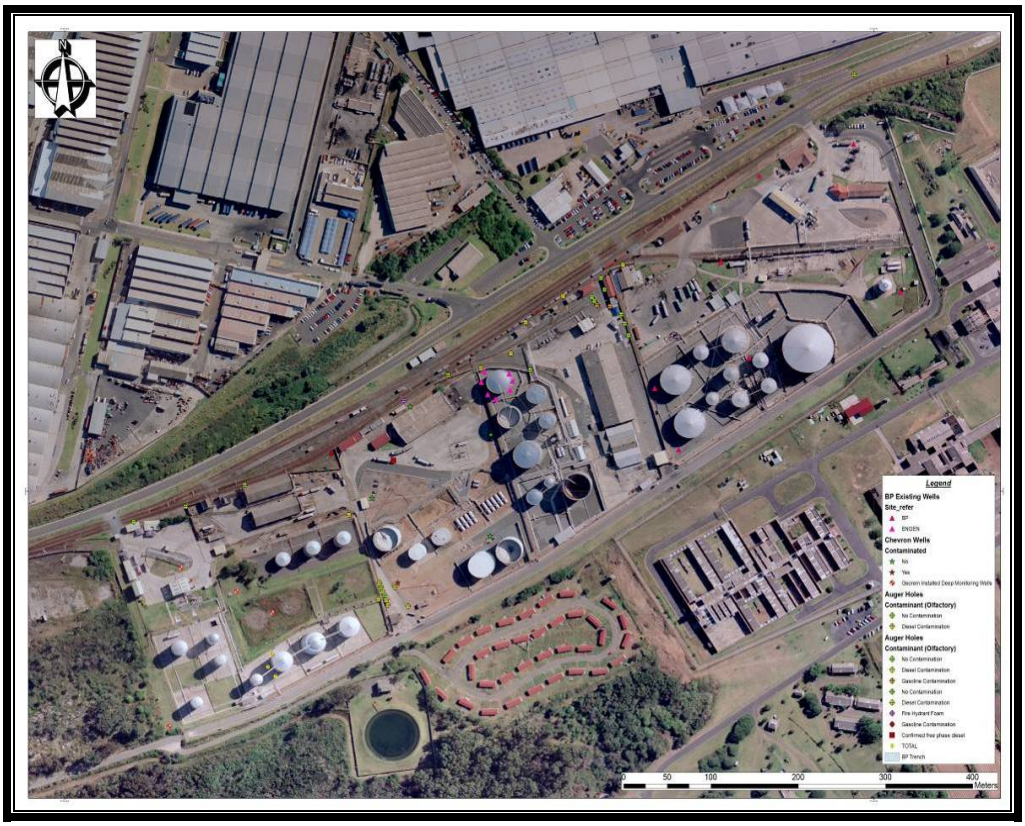

Figure 3.1 Location of the joint fuel depot site in East London (Source: SRK Consulting).

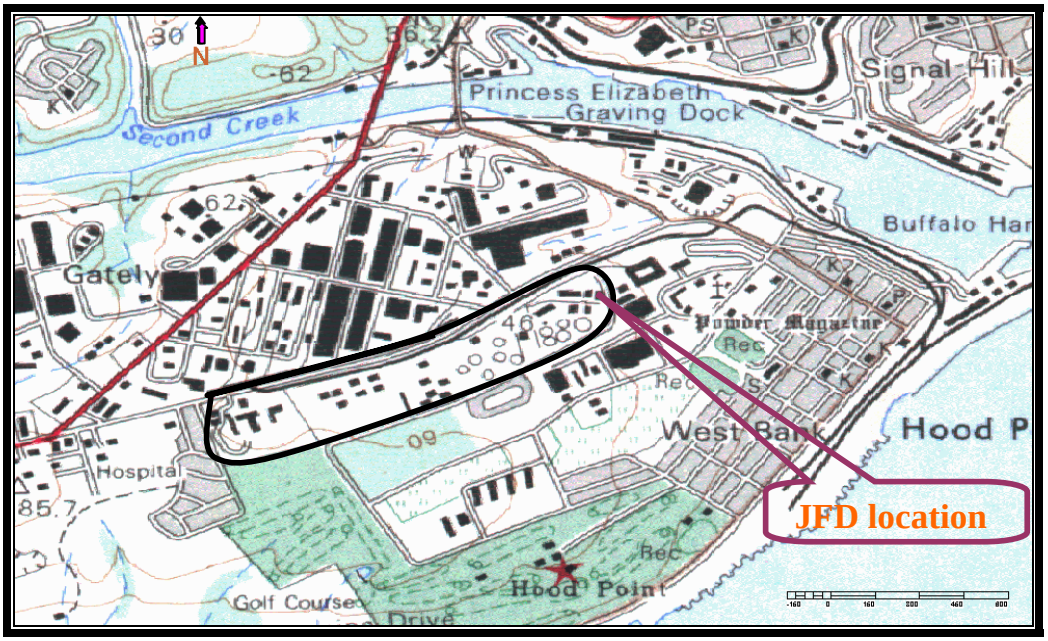

Figure 3.2 Topographic map of the site and surroundings (Source: BEEH).

3.2 Site Geology

The site is located on the geological unit of the late Permian Adelaide sub-group, which is the lower part of Beaufort group. The Beaufort group is lithographically divided into two major units including the Tarkastad sub-group on top and Adelaide beneath, which are part of the Karoo supergroup (Vegter, 2001). The south-eastern part of Adelaide which underlies the study area comprises mainly from the bottom to the top of Koonap, Middleton and Balfour Formations (Johnson *et al.,* 2006) (refer to Figures 3.3, 3.4 and 3.5).

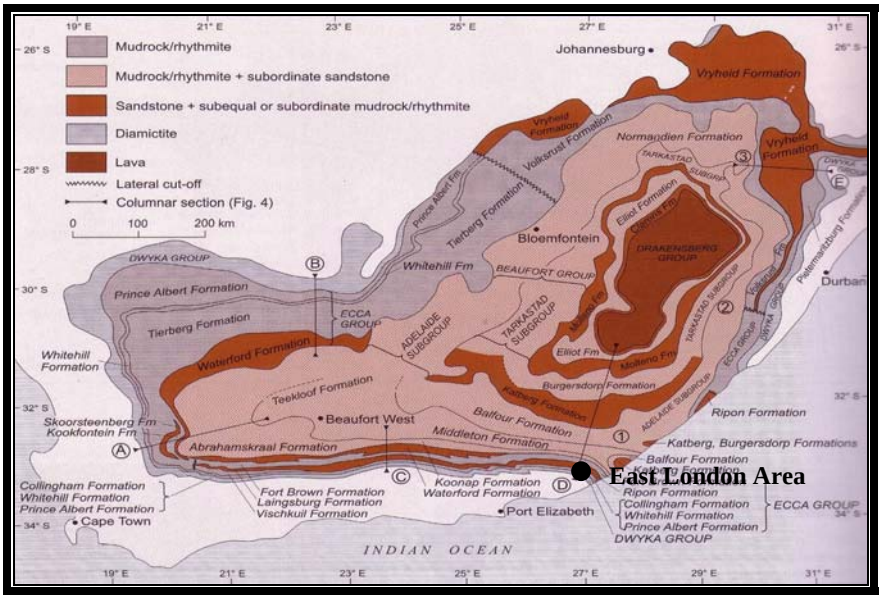

Figure 3.3 Aerial distribution of lithostratigraphic units in the Main Karoo Basin. (Modified after Johnson *et al.*, 2006).

Referring to the aerial distribution of lithographic units in the Main Karoo Basin in Figure 3.3, it was noticed that East London was geologically covered by the Balfour formation and the Middleton Formation. The bulk of the sediment that formed the sedimentary rocks of the Adelaide sub-group was derived from a source area situated to the south and south-east of the basin and deposited under fluvial conditions (Johnson *et al.,* 2006) (refer to Figure 3.4). The high mud/sand ratios and fine-grained character of the sandstones is the indication that the meandering rivers with the sandstone have formed as channel

deposits and that the mudstone represents overbank deposits (Johnson *et al.,* 2006).

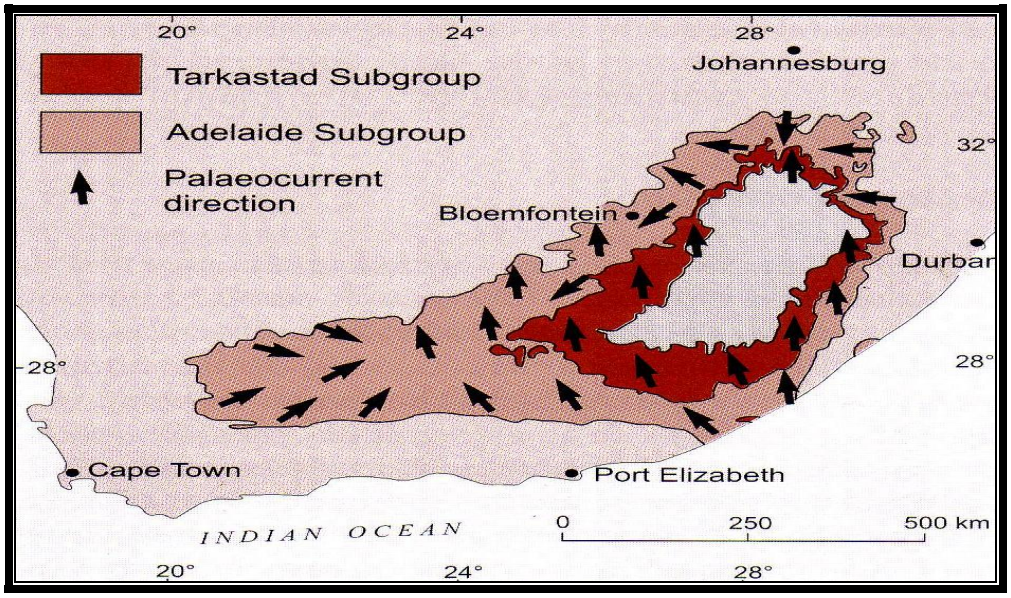

Figure 3.4 Palaeocurrent directions of Adelaide and Tarkastad Subgroup (after Johnson, 2006).

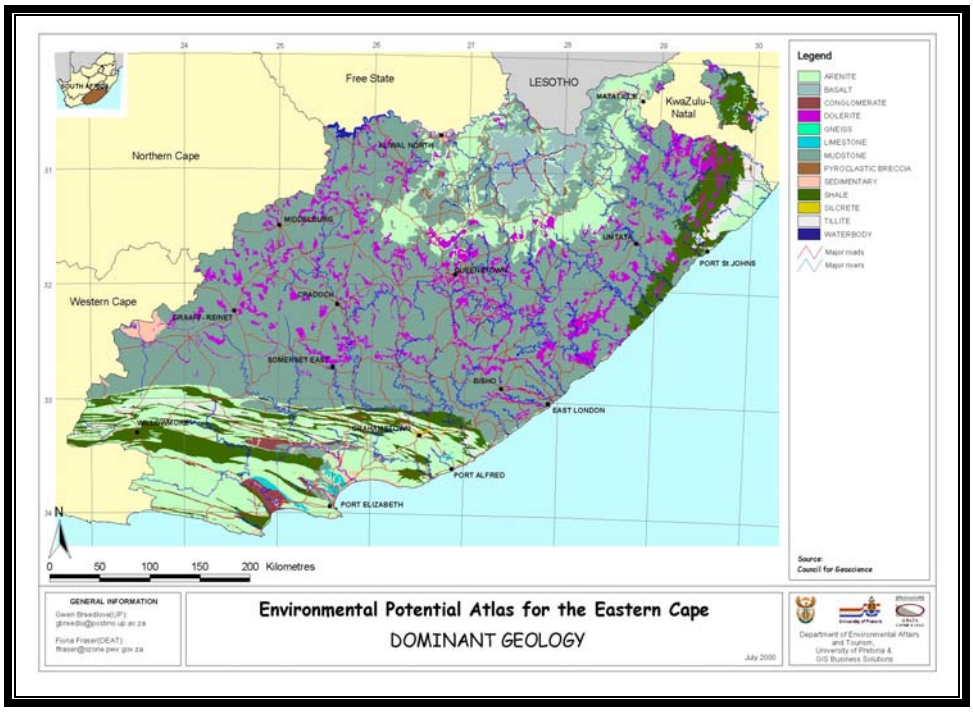

Figure 3.5 Dominant geology of the Eastern Cape (source: Council of Geoscience).

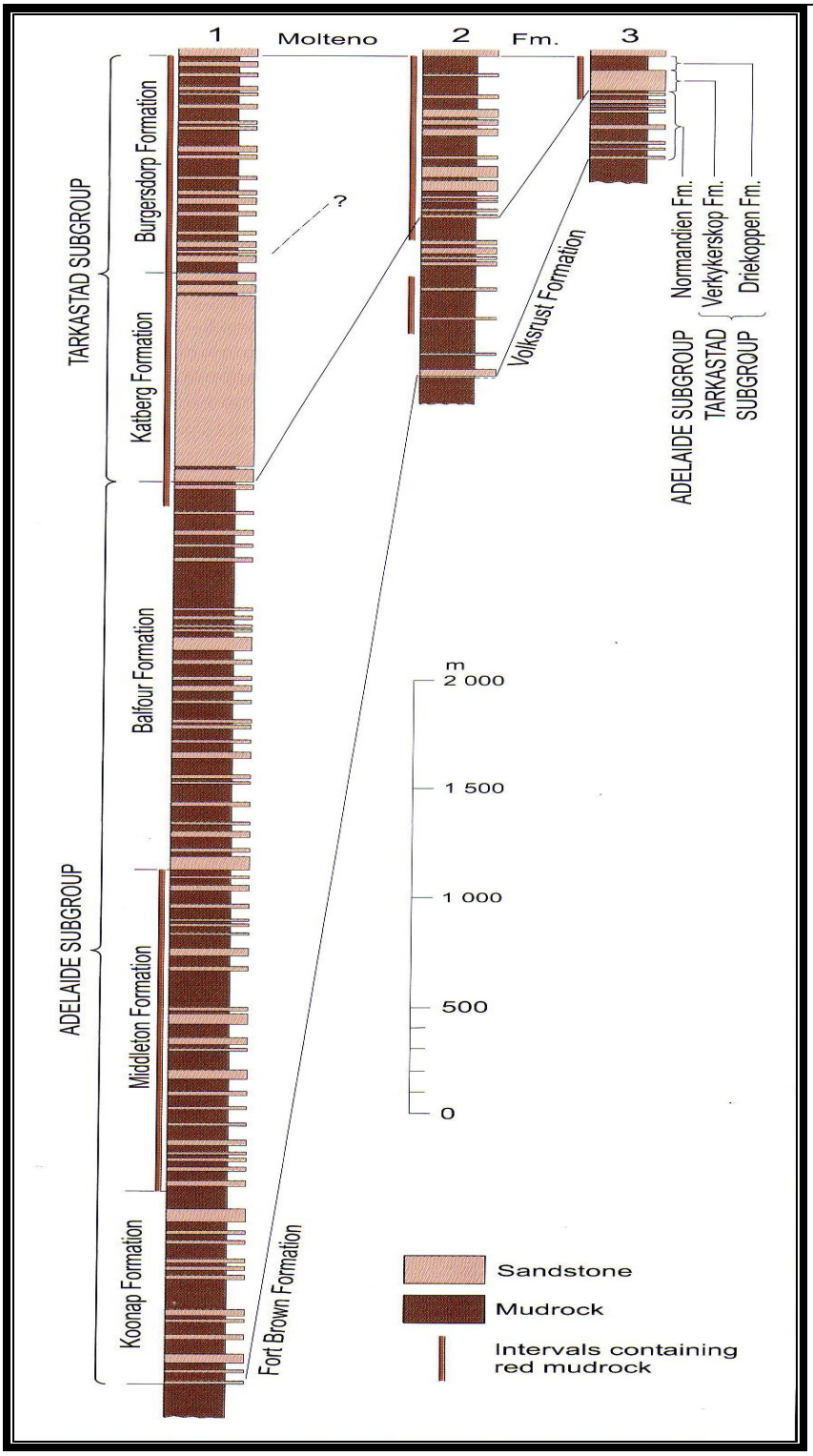

Figure 3.6 Lithostratigraphic units of the Beaufort Group which thickness decrease from south to north of the Main Karoo basin (after Johnson, 2006).

3.2.1 Lithostratigraphic units.

The geological sequence that is found in the East London area and particularly on the study site, is briefly discussed and presented in Table 3.1 below.

Table 3.1 Geological sequence of the fuel depot area

Super group	Group	Sub-group	Formation	Lithology
Karoo	Beaufort	Adelaide	Balfour	Mudstone, Sandstone
			Middleton	Red mudstone, sandstone
			Koonap	Mudstone, Sandstone

The Adelaide sub-group thickness decreases from 5000 m in the south-eastern Karoo to about 800 m in the centre of the Karoo basin. In that same area, the Koonap Formation has a maximum thickness of about 1300 m while the Middleton Formation has about 1600 m and the Balfour Formation has about 2000 m. In the southern part of the Karoo basin the Adelaide Sub-group consists of alternating blueish-grey, greenish-grey or greyish-red mudstone and grey, very fine- to medium-grained lithofeldspathic sandstones (Johnson *et al.,* 2006). Sandstone and mudstone units normally form fining-upward cycles separated in many cases by a thin mud-pellet conglomerate (refer to Figure 3.7). Generally the sandstone constitutes only 20-30% of the total thickness, but it reaches 60% in certain areas. Individual sandstone units have thicknesses ranging from 6 to 60m (Johnson *et al.,* 2006).

Figure 3.7 Contact between mudstone and sandstone in the Adelaide Subgroup in the Study area. (Photograph from SRK).

3.2.2 East London Karoo formations

The Karoo Formations which underly East London are characterized by fractured aquifers. The Karoo formations in that area are formed essentially by fractured sandstones and mudstones. The fracturing of these formations was caused by lava intrusions and the uplifting of the Karoo formations. Fractures in the Karoo formations are both horizontally and vertically orientated. The horizontal fractures, which are called bedding plain fractures, are found intersected by vertical fractures and could interconnect them (refer to Figure 3.8 for illustration). In most of these formations the occurrence, orientation and extent of the fractures will determine the groundwater and LNAPLs flow direction and rates, given that fractured media have a higher transmissivity and permeability than non-fractured media. (Botha *et al.,* 2001). Characterization of the East London Karoo formation will be a master key and first step in the studying and understanding of the fate and transport of LNAPLs, given that the fractured zones constitute preferential pathways for both groundwater and LNAPLs plumes.

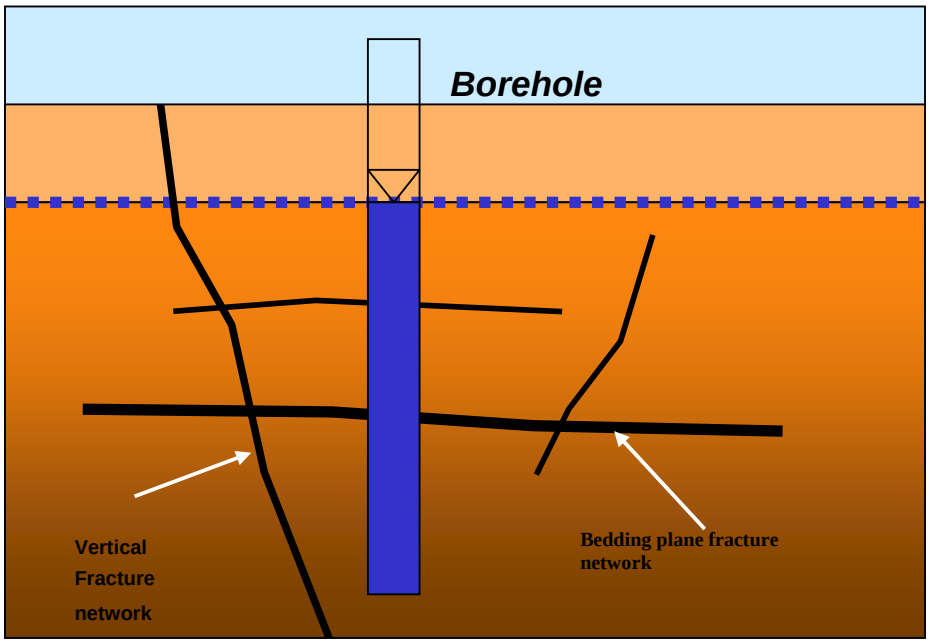

Figure 3.8 Illustration of Karoo fractured formations (adapted from Van der Voort 2001).

The East London area is part of the Karoo Igneous Province that contains extensive dolerite intrusions. Walker and Poldervaart (1949) studied the Karoo dolerite suite which is best developed in the Main Karoo Basin and is an interconnected network of dykes, sills and shaped sheets. The sills and inclined sheets range from a few meters to 200 m or more in thickness, forming the resistant caps of hills comprising softer sedimentary strata in the Karoo. The dykes are generally 2 to 10 m wide and 5 to 30 m long, although some can be followed for 80km (Johnson *et al.,* 2006).

It has been established that the Beaufort strata that underlies the joint fuel depot site is essentially intruded by doleritic sills of the Jurassic Age (Figures 3.9, 3.10 and 3.11). The dolerite sill is interpreted to have a thickness in excess of 200 m. Contact metamorphism is envisaged to have taken place between the mudstone/sandstone units of the Middleton Formation and the intrusive dolerite sill (Johnson *et al.,* 1994).

Figure 3.9 Site lithology (from SRK Consulting).

Figure 3.10 Contact of Mudstone and Dolerite sill at coastline (Modified after SRK consulting).

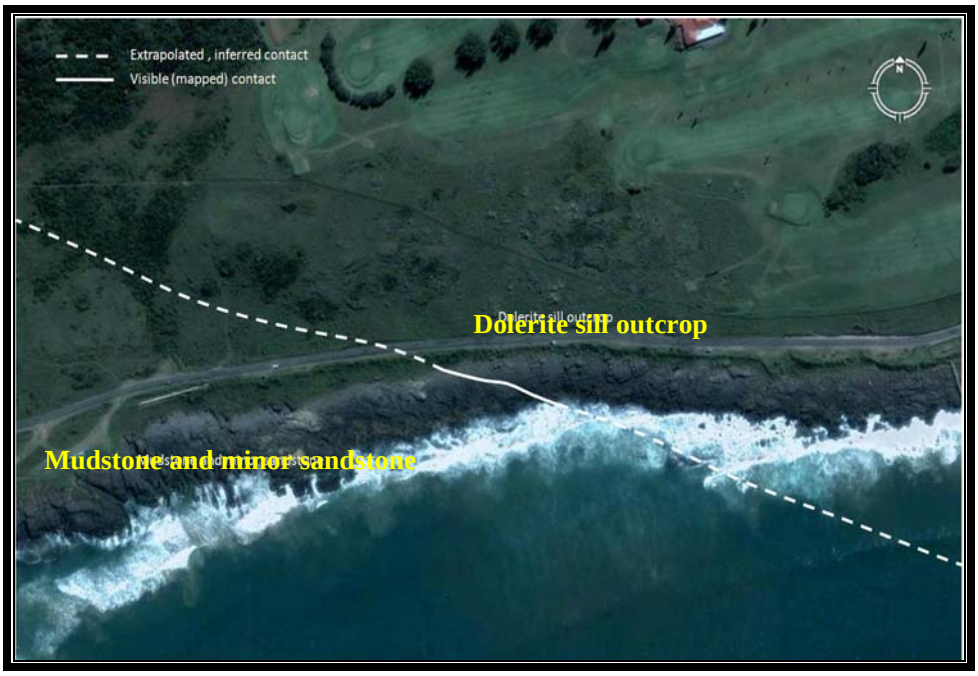

Figure 3.10 Location of coastline outcrop (Modified after SRK Consulting).

The drilling of the new borehole on site provided geological logs that generally revealed the presence of a sandy clayey layer on top, followed with various layers of clayey material before reaching the bedrock, which consisted of fresh dolerite.

3.3 Site Hydrogeology

3.3.1 Aquifers

In general, aquifers in the Adelaide subgroup are multi-layered and multi-porous with variable thickness (Botha *et al.*, 1998). As part of the Karoo bedding and parallel fractured formations, groundwater in the Beaufort formation occurs in joints and fractures of dolerite contact zones with country rock, in decomposed dolerites and in the semi-weathered zones between decomposed and solid dolerite (Meyer, 2003).

According to DWAF's National Groundwater Database (NGDB), the borehole productivity analysis using borehole information reveals that lithostratigraphy and the density of dolerite sills are the most important factors controlling

regional variations in the yield of boreholes (Chevallier et *al.*, 2005). Fracture zones, occurring at depths ranging from between 30m to 300m were identified at Qoqodala, in the Great Kei catchment where the dolerite ring complexes control, to a very large extent, the geomorphology, surface drainage patterns, aquifer recharge and location of many springs and seepages in such areas (Chevallier *et al.,* 2004). These fractured-rock aquifer systems appear to be relatively extensive (Figures 3.12 and 3.13).

Figure 3.11 A thin dolerite dyke intruding Karoo mudstones and sandstones (Photo by R Murray).

Figure 3.12 Fractured and baked sandstones overlying a dolerite sill (Photo by R Murray).

Investigations undertaken by SRK Consulting established that the groundwater flow is driven by the dominant joint sets striking toward the southeast and southwest of the site and directed toward the Ocean. The mudstone and sandstone of the Middleton formation are highly fractured compared to the dolerite sill, therefore the groundwater movement is likely to be higher in fractured mudstone and sandstone sequences then in the dolerite sill (Du Plooy, 2008).

3.3.2 Historical groundwater data

- Water Level Measurements and groundwater flow

According to SRK Consulting, the monthly water levels were recorded using a Solinst Model 122 Interface meter from May to July 2007. The records indicated the normal seasonal change in water levels for the current boreholes monitored. Figure 3.14 displays the water level contour map according to SRK records.

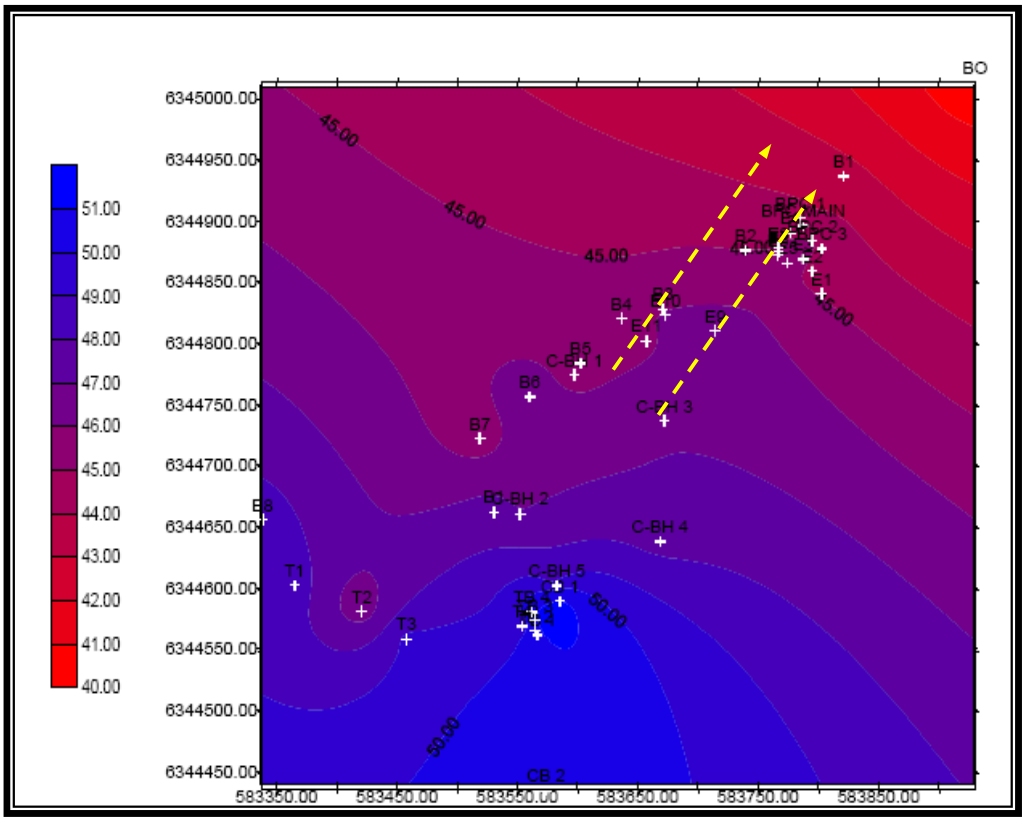

Figure 3.13 Water level contour map (Modified from SRK consulting).

From the water level data, it was possible to derive a general preferred groundwater flow direction which is in a north-easterly direction.

- **LNAPLs contaminant plume**

From the SRK investigation, free product was found in well 3 on Engen site, in borehole 5 on Chevron site and in The cut-off trench on BP site, probably originated from the spill that occurred at the BP site during 2003 (refer to Figure 2.2). The free product was analysed to estimate the degree of degradation. The result indicated that the free product found in the wells presented no chemical variation compared to the commercial diesel. It has been concluded that the free product discovered at the BP originated from a recent contamination event.

4. METHODOLOGY

The methodology used to characterize the geology and hydrogeology of the East London Fuel Depot site and the LNAPLs groundwater contamination, included the following steps:

- desk study;
- pedestrian surveys;
- geophysics methodology; and
- soil characterization methodology

4.1 Desk Study

The desk study consisted of a collection and a detailed review of all the relevant available information, including:

- a literature review of previous reports, aerial and geological maps and previous hydrogeological findings;
- a literature review on the use of geophysics to characterize LNAPLs sites;
- a literature review of Karoo formations and LNAPLs transport mechanisms; and
- a collection of borehole geological logs and water chemical data for the study area.

4.2 Pedestrian Surveys

A site visit in the East London Joint-Fuel Depot facility was initiated for two major reasons, including the location of surface spills around the tanks, the

piping and in the existing wells, as well as the identification of appropriate transects for geophysics surveys and appropriate electrode array.

No fuel spill was found around the piping (refer to Figure 4.1), therefore they were excluded from being sources of contamination. But free phase products were clearly found in the BP cut-off trench, the Chevron borehole 5 (Figure 4.2) and the Engen Well 3.

Figure 4.1 No products found around exposed fuel piping (Du Plooy 2007).

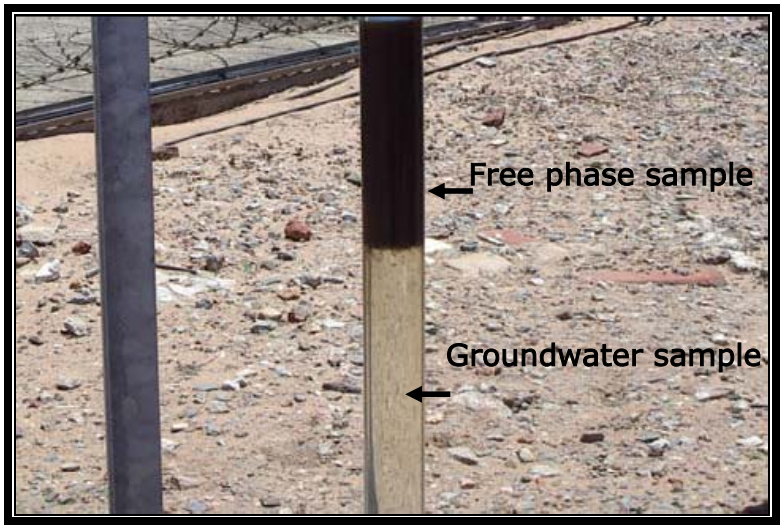

Figure 4.2 Free phase product sample Collected from Chevron borehole BH 5 (adapted from Du Plooy 2006).

Concerning the choice of appropriate transects for geophysics surveys, four transects were chosen outside the joint fuel Depot enclosure and five transects inside, based on the availability of uncovered spaces without major noisy sources.

4.3 Geophysics Methodology

4.3.1 Electrical resistivity tomography

The resistivity method is based on injecting a DC current (I) through two electrodes (C1, C2) and measuring the potential differences (V) through two other electrodes (P1, P2) (Figure 4.3). Data from the resistivity survey are presented and interpreted in the form of values of apparent resistivity (ρ_a) in a cross-section of the subsurface.

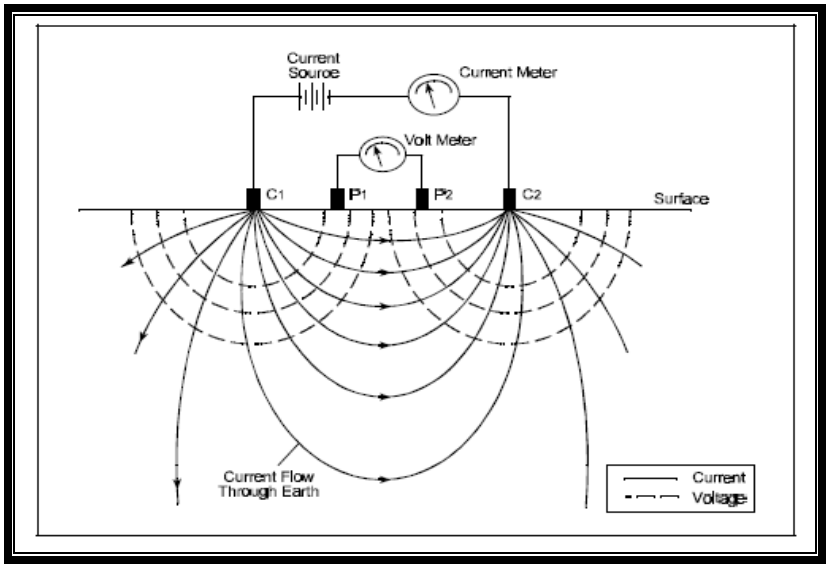

Figure 4.3 Schematic of operating principles of electrical resistivity (after Hitzig, 1997).

Apparent resistivity is defined as the resistivity of an electrically homogeneous and isotropic half-space that would yield the measured relationship between the applied current and the potential difference for a particular arrangement

(array) and the spacing of electrodes. The apparent resistivity of a medium is calculated by the following equation:

$$\rho_a = k\frac{V}{I} \qquad (8)$$

The resistivity of the medium is thus estimated from measured V, I and k, the geometric factor being dependent on the geometry of the electrode arrangement (array). In practice, the type of arrays that are most commonly used for 2-D imaging surveys include the Wenner, dipole-dipole, Schlumberger, pole-pole, pole-dipole. Among the characteristics of an array that should be considered are (Loke, 1999):

- the sensitivity of the array to vertical and horizontal changes in the sub-surface resistivity;
- the depth of the investigation;
- the horizontal data coverage; and
- the signal strength.

The depth of investigation is proportional to the separation between the electrodes in homogeneous material, and varying the electrode separation provides information about the stratification of the ground (Dahlin, 2001).

The ERT technique is a 2-D electrical imaging survey which is carried out using a large number of electrodes connected to a multi-core cable (Griffiths and Barker, 1993) (refer to Figure 4.4). In order to obtain a 2-D electrical image, horizontal and vertical data coverage is achieved by automatic sequential measurements of current and potential locations, as is demonstrated by 1, 2a, 3a in Figure 31. In order to extend the survey transect laterally, a roll-along technique is used, which consists of shifting a quarter of the layout length for a new measurement set.

The ERT technique can be used to locate fracture zones, faults, karsts, groundwater/contaminant pathways, perched water zones, depth to groundwater and occasionally a large quantity of residual and floating product (Hitzig, 1997).

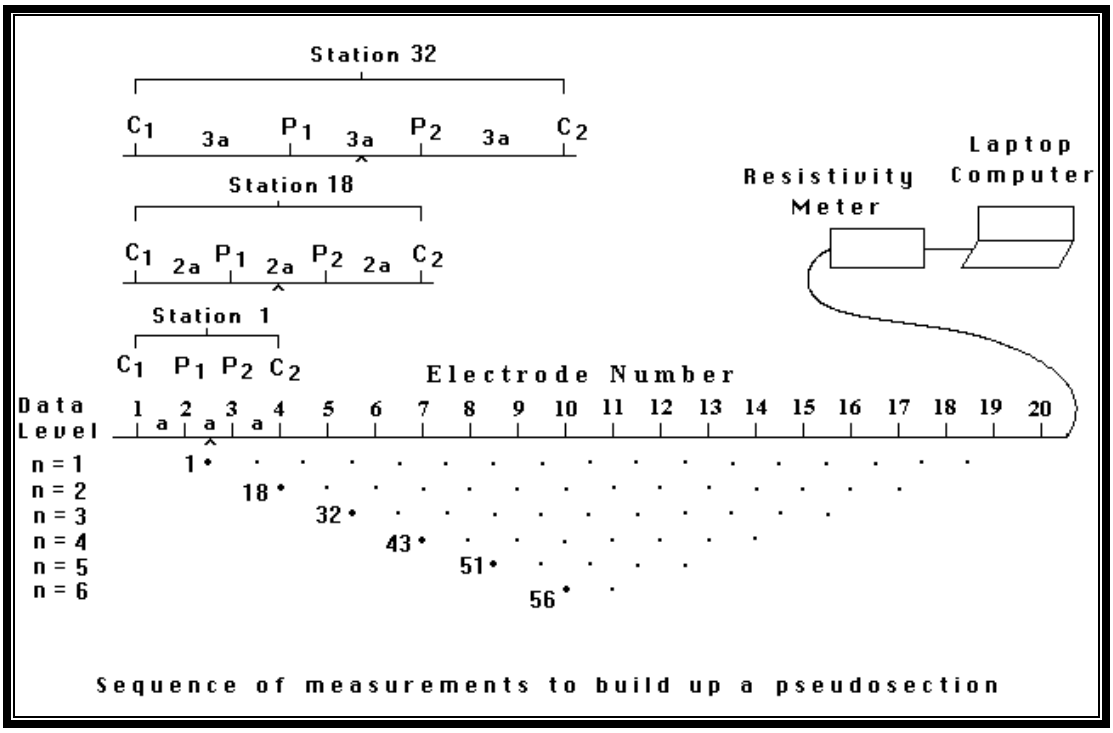

Figure 4.4 The arrangement of electrodes for a 2-D electrical survey and the sequence of measurements used to build up a pseudo-section (Loke 1999).

4.3.2 Induced polarization technique

Induced polarization (IP) method is based on measuring the transient decay of the voltage over a number of time intervals when the injected current is turned off. In passing an electrical current through the ground, certain subsurface units may become electrically polarized, essentially forming a battery. Once the source current is removed, the material gradually discharges, returning to equilibrium. The study of the decaying potential difference as a function of time is known as time-domain IP. In time-domain

IP, the studied parameter is the chargeability of the ground, expressed in milliseconds or in millivolt per volt (mV/V) and is calculated by the following equation:

$$M_{t_i t_{i+1}} = \frac{1}{V_0}\int_i^{i+1} V(t)dt \qquad (9)$$

Where:

$V(t)$ = decaying voltage,

t_i and t_{i+1} = start and stop times of the interval

V_0 = voltage measured before the current is turned off.

Polarization phenomena occur mainly at locations where the ground contains disseminated metallic (e.g. pyrite, magnetite), clay or graphite particles (Telford et al., 1990). The IP method is typically used for groundwater/clay distinction, salt-water invasion, waste mapping/characterization and ores in hard rock areas.

4.3.3 Data acquisition

The ABEM Lund Imaging System together with a Terrameter SAS 1000 was used on site for data acquisition. The Lund system consists of a basic charging unit, an Electrode Selector ES10-64, four Lund spread cables, a suitable quantity of cable joints and cable jumpers, a supply of electrodes, tools and spare kit (Figure 4.5).

Figure 4.5 ABEM LUND Imaging System with Terrameter SAS 1000.

The instrument has been designed to operate in three modes, the resistivity surveying mode, the induced polarization mode and the self-potential measuring mode. In the resistivity mode the instrument measures a range from 0.05 Milliohms up to 1999 Kiloohms. When the IP mode is run, the instrument measures both the chargeability and the apparent resistivity.

4.3.4 Electromagnetic method

An Electromagnetic method was also tested on site using an EM 38 instrument to assess anomalies due to pipes or shallow soil conductivity. The EM 38 measures the apparent electrical conductivity of the soil resulting from the induction of time-varying magnetic fields into the sub- surface. The EM 38 was used on the ground (0m): Vertical Dipole (VD) and Horizontal Dipole (HD).

The EM 38 has an intercoil spacing of 1m and measures up to 1.5 m depth in vertical dipole mode and up to 0.75 m depth in horizontal dipole mode.

4.4 Soil Characterisation Methodology

4.4.1 Sampling method

Both the core and auger methods were used to collect soil samples at different depths on site. The core method involves pressing a thin walled cylinder into the soil and withdrawing it with a relatively undisturbed sample. Some core samples were extracted from excavated trench sites. The augered samples were bagged and sealed to serve as samples for describing the profile and for conducting textural analyses.

4.4.2 Soil testing method

In order to characterise the unconsolidated units of the site, soil testing was performed in situ as well as in the laboratories. Soil tests carried out on soil samples and the methods used are described below.

- Initial gravimetric water content

Water in the soil is a vital link in hydrological cycle that controls the exchange with the atmosphere above and with the groundwater below. It exerts a controlling influence on most of the physical, chemical and biological processes that occur in soils (Dane *et al*., 2002).

Because electrical resistivity is influenced by soil water content, it appears important to evaluate the degree of saturation of the soil using gravimetric method. In this gravimetric method, water content is estimated by weighing it, oven-drying it at 105^{o}C for 24 hours and weighing it again. The difference of the two weights divided by the dry weight gives the initial gravimetric water content.

- **Soil profile description**

Soil profile description aims to identify and describe the texture, structure and color of soil samples using the feel method and it indicates their probable location in a soil profile. Soil texture is defined as the relative percentage of sand, silt and clay in a soil sample while structure refers to the arrangement of sand, silt, clay and organic matter into larger units called aggregates.

- **Particle size analysis**

The particle size analysis is a measurement of the size distribution of individual particles in a soil sample (Dane *et al.,* 2002). Particle size analysis was applied on soil samples to evaluate the soil texture. Soil texture is based on the distribution of sand, silt and clay in the soil sample. Table 4.2 below gives a particle size limit classification according to US department of Agriculture.

Table 4.1 Three main size classes, according to the U.S Department of Agriculture.

<table>
<tr><td colspan="8">Classification of Soil Particles by Maximum Diameter

US Department of Agriculture</td></tr>
<tr><td>0.002mm</td><td>0.05mm</td><td>0.10mm</td><td>0.25mm</td><td>0.50mm</td><td>1.0mm</td><td>2.0mm</td><td>>2.0mm</td></tr>
<tr><td rowspan="2">Clay</td><td rowspan="2">Silt</td><td>Very Fine</td><td>Fine</td><td>Medium</td><td>Coarse</td><td>Very Coarse</td><td rowspan="2">Gravel</td></tr>
<tr><td colspan="5">Sand</td></tr>
</table>

The method used for particle size analysis combines sieving and hydrometer methods:

- The sieving method uses a suitable sieve size, placed in order of decreasing size from top to bottom, in a mechanical sieve shaker. A pan is placed underneath the nest of sieves to collect the aggregate that passes through the smallest. The entire nest is then agitated, and material which is smaller than the mesh opening, passes through the sieves. After the aggregate reaches the pan, the amount of material retained in each sieve is then weighed.

- The hydrometer method involves dispersing a soil sample in water and determining the sedimentation rate of the sand, silt and clay particles (Dane *et al.,* 2002).

5. ERT SURVEY FOR SITE CHARACTERIZATION

5.1 Background on ERT Method

The DC resistivity survey is a non-intrusive and intensively used geophysical technique for subsurface resistivity structure investigations which represent geologic structure.

Electrical resistivity measurements are made by inserting four electrodes in the soil or rock. A current is caused to flow in the earth between one pair of electrodes while the voltage across the other pair of electrodes is measured. The measured voltage is being considered as a weighted mean value of the conductivity of all the current paths between the potential electrodes. This measurement allows for receiving information about the average electrical resistivity of certain subsurface volume determined by soil, rock and pore fluid resistivity. By changing the distance between the electrodes, different volumes of the subsurface are sensed and additional information about resistivities on different depths is obtained.

Normally, apparent or bulk (effective) resistivity values are calculated and used to create pseudo-sections and these are then interpreted and inverted to determine subsurface resistivity anomalies.

In general, resistivity measurements can be performed in three ways including profiling, which is carried out by moving a fixed electrode spacing laterally, sounding (1-D) which is carried out by increasing electrode spacing at a fixed location, as well as 2-D and 3-D imaging or tomography, which is carried out by using multi-electrode arrays.

Soil and rocks have intrinsic resistivity which governs the relation between the current density and the gradient of the electrical potential. The electrical resistivity of a geological unit or target is measured in ohmmeters and is dependant on water saturation and the concentration of dissolved solids

present in pore fluids. The resistivity measured is therefore a function of the porosity and permeability of the subsurface.

5.1.1 Basic resistivity theory

The purpose of electrical resistivity survey is to determine the subsurface resistivity distribution by taking measurements on the ground surface. From these measurements the true resistivity of the subsurface can be estimated (Loke, 2004). Data from a resistivity survey is customarily presented in the form of values of apparent resistivity ρ_a, which is defined as the resistivity of an electrically homogeneous and isotopic half-space that would yield the measured relationship between the applied current and potential difference for a particular arrangement and spacing of electrodes.

Considering a single point electrode located on an electrically homogeneous medium, carrying a current (I) measured in amperes, the potential at any point in the medium is given by:

$$\phi = \rho_a \frac{I}{2\pi r} \qquad (10)$$

Where:

ϕ = potential in volt

ρ_a = apparent resistivity

r = difference from the electrode.

Considering an electrode pair with current (I) at electrode C_1 and (–I) at electrode C_2, the potential at a point is given by the algebraic sum of the individual contributions:

$$\phi = \rho_a \frac{I}{2\pi r_{C_1}} - \rho_a \frac{I}{2\pi r_{C_2}} = \rho_a \frac{I}{2\pi}\left[\frac{1}{r_{C_1}} - \frac{1}{r_{C_2}}\right] \quad (11)$$

Where r_{C_1} and r_{C_2} are distances from the point to electrodes C_1 and C_2.

In addition to current electrodes C_1 and C_2, Figure 5.1 shows a pair potential electrode P_1 and P_2 measuring the potential difference V between current electrodes. From the previous equation, the potential difference V may be written as follows:

$$V = \phi_{P_1} - \phi_{P_2} = \rho_a \frac{I}{2\pi}\left[\frac{1}{r_{C_1P_1}} - \frac{1}{r_{C_2P_1}} - \frac{1}{r_{C_1P_2}} + \frac{1}{r_{C_2P_2}}\right] \quad (12)$$

Where ϕ_{P_1} and ϕ_{P_2} are potential at P_1 and P_2.

The above equation (12) gives the potential that would be measured over a homogeneous half space with a 4 electrode array (Figure 5.1).

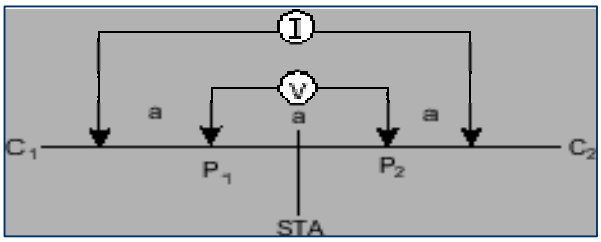

Figure 5.1 Wenner electrode array.

In the field, a resistivity survey is conducted over an inhomogeneous medium where the subsurface resistivity has a 3-D distribution. The resistivity measurements are still made by injecting a current into the ground through the two current electrodes C_1 and C_2 and measuring the voltage difference at

two electrodes P_1 and P_2. From the current (I) and potential (V) value, an apparent resistivity ρ_a value is calculated by the equation (8):

$$\rho_a = k\frac{V}{I}$$

Where $k = \dfrac{2\pi}{\left[\dfrac{1}{r_{C_1P_1}} - \dfrac{1}{r_{C_2P_1}} - \dfrac{1}{r_{C_1P_2}} + \dfrac{1}{r_{C_2P_2}}\right]}$ (13)

k = geometric factor

The types of electrode arrays that are most used are Wenner, Schlumberger, dipole-dipole, pole-dipole and pole-pole (Figure 5.2). In any case, the geometric factor k for any four electrode system can be found from the Equation (13) and can develop a far more complicated system.

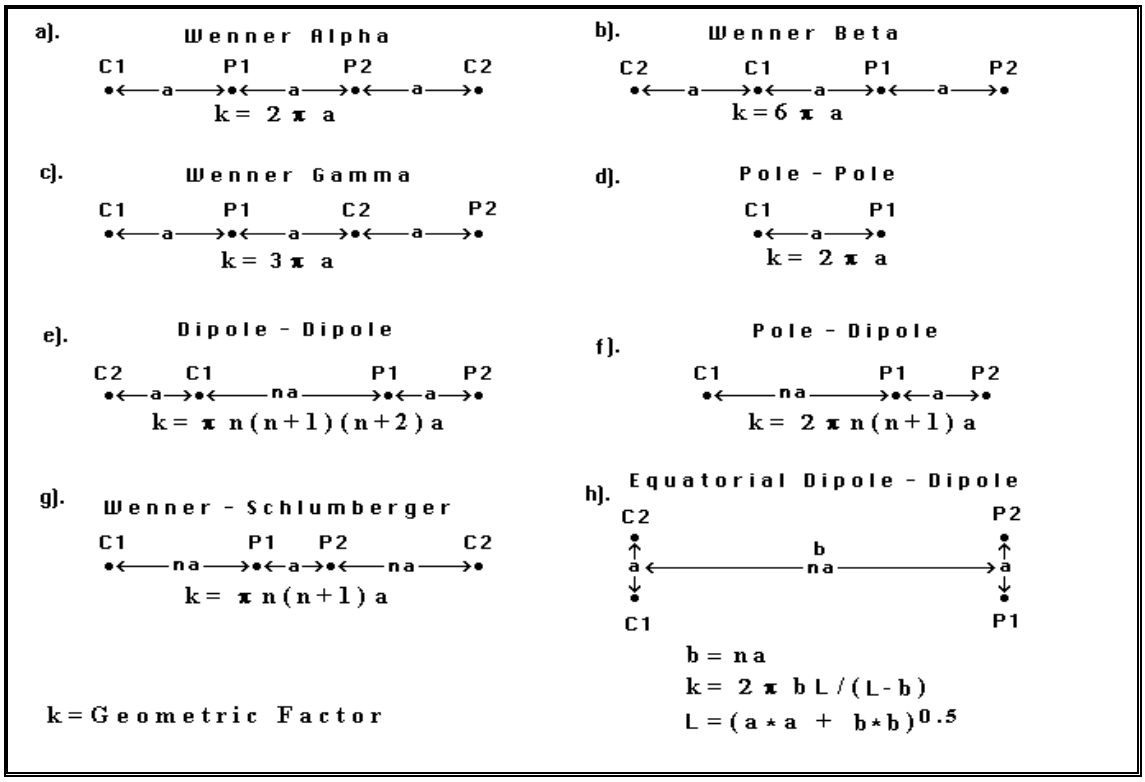

Figure 5.2 Common arrays used in resistivity surveys and their geometric factors (Loke, 1999).

- Comparison of the different arrays

It is critically important to understand that these common arrays shown by Figure 34 produce different shapes of the resistivity pseudo-section for the same structure. This is because each array has its own characteristics which must lead the choice of the "best" array for a field survey. Among the characteristics of arrays that need to be considered are:

  - The depth of the investigation;
  - The sensitivity of the array to vertical and horizontal changes in the subsurface resistivity;
  - The horizontal data coverage; and
  - The signal strength.

The depth of investigation and the sensitivity of the array to vertical and horizontal changes are two characteristics that can be determined from the sensitivity function of the array for a homogeneous earth model (Loke, 1999). In Figure 5.3, Loke (1999) shows a plot of the sensitivity function for the Wenner, Dipole-dipole and Schlumberger arrays applied for a homogeneous earth model. Loke (1999) defined the sensitivity function as the degree to which the change in the resistivity of a section of the subsurface will influence the potential measured by the array. The higher the value of the sensitivity function, the greater is the influence of the section on the measurement. It can be noticed on Figure 5.3 that the highest sensitivity values are near the electrodes for all three arrays. At larger distances from the electrodes, the shape of the contours differs for the three arrays.

The difference in the contour shape of the sensitivity function plot explains the different responses of the arrays to different types of structures in terms of resolution of vertical and horizontal changes and depth of investigation.

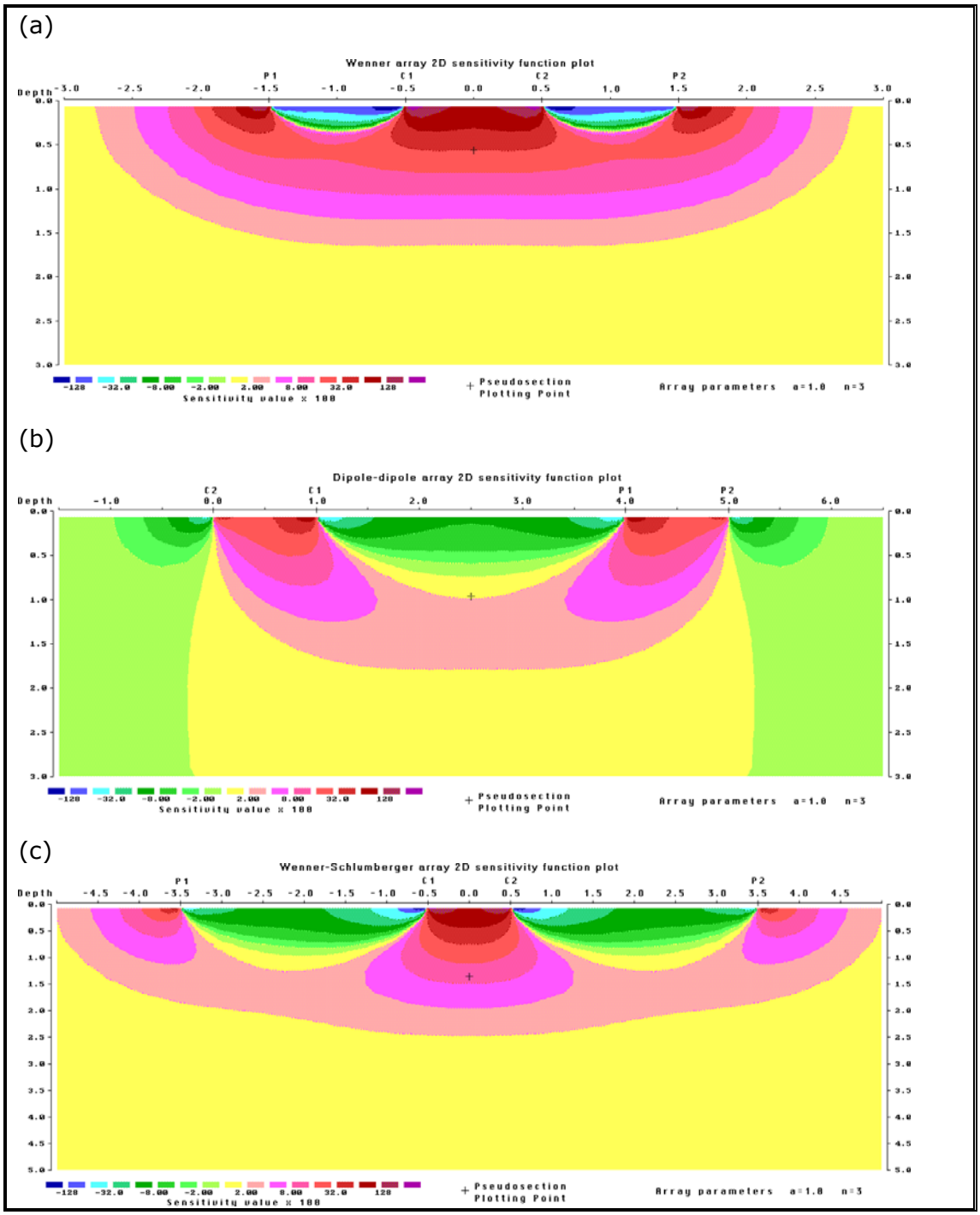

Figure 5.3 The sensitivity patterns for the (a) Wenner (b) dipole-dipole and (c) Wenner-Schlumberger arrays (After Loke, 1999).

Table 5.1 The median depth of investigation (Ze) for the different arrays, with "a" the smallest electrode spacing. "L" is the total length of the array. Please refer to Figure 5 for the arrangement of the electrodes for the different arrays.

Array type	z_e / a	z_e / L
Wenner alpha	0.519	0.173
Dipole-dipole n = 1	0.416	0.139
n = 2	0.697	0.174
n = 3	0.962	0.192
n = 4	1.220	0.203
n = 5	1.476	0.211
n = 6	1.730	0.216
n = 7	1.983	0.220
n = 8	2.236	0.224
Wenner-Schlumberger n = 1	0.520	0.173
n = 2	0.930	0.186
n = 3	1.320	0.189
n = 4	1.710	0.190
n = 5	2.090	0.190
n = 6	2.740	0.190
Pole-pole	0.867	

- Wenner array

In Figure 5.3(a), it has been noticed that the sensitivity plot for the Wenner array has almost horizontal contours beneath the centre of the array. The Wenner array is therefore relatively sensitive to vertical changes in the subsurface resistivity below the centre of the array. However, it is less sensitive to horizontal changes in the subsurface resistivity. In general, the Wenner array is good in resolving vertical changes (i.e. horizontal structures), but relatively poor in detecting horizontal changes (i.e. narrow vertical structures) (Loke, 1999).

Concerning the depth of investigation, the Wenner array has a moderate depth of investigation compared to other arrays, with an effective depth of

investigation approximately 0.5 times the "a" electrode spacing used. For example, using an "a" electrode spacing of 10 meters, the subsurface will be reliably mapped to a depth of approximately 5 meters.

The signal strength being inversely proportional to the geometric factor, the Wenner array has the strongest signal strength with a geometric factor of 2πa, which is smaller than that for other arrays. This factor makes the Wenner array a first choice when the survey has to be carried out in areas with high background noise.

One disadvantage of this array for 2-D surveys is the relatively poor horizontal coverage as the electrode spacing is increased. This could be a problem if we use a system with a relatively small number of electrodes (Loke 1999).

- Dipole-Dipole array

Referring to Figure 5.3(b), the sensitivity function plot for the Dipole-Dipole array has vertical contours between the C1 and C2 pair, as well as between the P1 and P2 pair. Therefore the Dipole-Dipole array is very sensitive to horizontal changes in resistivity, but relatively insensitive to vertical changes in the resistivity (Loke, 1999). Dipole-Dipole is then the most appropriate in mapping vertical structures, such as dykes and cavities, but relatively poor in mapping horizontal structures such as sills or sedimentary layers.

Concerning the depth of investigation, the Dipole-Dipole array (Figure 5.2) has the same spacing "a" between the current electrode pair C1 -C2, and between the potential electrode pair P1 -P2. This array has another factor marked as "n", which is the ratio between the distance between C1-C2 and P1-P2 pairs. For surveys with this array, the "a" spacing is kept totally fixed and the "n" factor is increased from 1 to 2 to 3, up to about 6, in order to increase the depth of investigation. The effective depth of the investigation is dependant on the "n" factor, as well as the "a" factor (Table 5.1).

Its signal strength being inversely proportional to the geometric factor, the Dipole-Dipole array has the very small signal strength when the "n" factor is increased. To use this array, the resistivity meter must have a comparatively high sensitivity and a very good noise rejection circuitry. However, for 2-D surveys this array has better horizontal data coverage than the Wenner array.

- Schlumberger array

The sensitivity pattern for the Schlumberger array, as shown in Figure 5.3(c) is slightly different from the Wenner array, with a slight vertical curvature below the centre of the array. This means that this array is moderately sensitive to both horizontal and vertical structures. In areas where both types of geological structures are expected, this array might be a good compromise between the Wenner and the Dipole-Dipole array (Loke, 1999).

The effective depth of investigation for this array is about 10% larger than the Wenner array, for the same distance between the outer (C1 and C2) electrodes. Note that the "n" for this array is the ratio between the C1-P1 (or P2-C2) electrodes to the spacing between the P1-P2 potential pair. The signal strength for this array is smaller than that of the Wenner array, but is higher than the Dipole-Dipole array. The horizontal data coverage is slightly better than the Wenner array, but smaller than obtained with the Dipole-Dipole array.

- Summary

  - The Wenner array is the best choice to be used if the survey is to be carried in a noisy area and/or if a good vertical resolution is needed;
  - The Dipole-Dipole array is the best option if good horizontal resolution and coverage are needed using a sufficiently sensitive resistivity meter; and
  - The Schlumberger array can be considered if none of the above is required.

5.1.2 Electrical properties of earth materials

Electrical currents flow in the earth's materials either through electronic conduction or electrolytic conduction. In electronic conduction, the current flow is via electrons such as in metals. In electrolytic conduction, the current flow is via the movement of ions in groundwater.

Igneous and metamorphic rocks: they typically have higher resistivity values. The resistivity of these rocks is greatly dependent on the degree of fracturing and the percentage of the fractures filled with groundwater. A given rock type can have a large range of resistivity, from 1000 to 10 million $\Omega.m$, depending on whether it is wet or dry. This characteristic is useful in the detection of fracture zones and other weathering features.

Sedimentary rocks: they are more porous and have a higher water content. They normally have lower resistivity values compared to igneous and metamorphic rocks. The resistivity values range from 10 to about 1000 $\Omega.m$, with most values below 1000 $\Omega.m$. The resistivity values are largely dependent on the porosity of the rocks, and the salinity of the contained water.

Unconsolidated sediments: they generally have even lower resistivity values than sedimentary rocks, with values ranging from about 10 to less than 1000 $\Omega.m$. The resistivity value is dependent on the porosity (assuming all the pores are saturated) as well as the clay content. Clayey soil normally has a lower resistivity value than sandy soil.

Groundwater has a resistivity values ranging from 10 to 100 $\Omega.m$, depending on the concentration of dissolved salts.
Sea water has a very low resistivity of about 0.2 $\Omega.m$ due to the relatively high salt content.

Metallic sulphides such as pyrrhotite, galena and pyrite have typically low resistivity values of less than $1\Omega.m$.

Industrial contaminants such as hydrocarbons (LNAPLs) typically have very high resistivity values of about $10^6\ \Omega.m$. However, in practice, the percentage of hydrocarbons in a rock or soil is usually quite small, and might not have a significant effect on the bulk resistivity. According to ASTM D3114-72 (1982), electrical conductivity of hydrocarbon oils is exceedingly small, of the order of 10^{-19} to$10^{-12}\Omega/cm$. Table 5.2 and 5.3 below give some resistivity and conductivity values for some common rocks, minerals, chemicals and metals.

Table 5.2 Resistivities of Some hydrocarbons compounds

Hydrocarbons	Resistivity (Ω.m)	Conductivity (S/m)
Benzene	2.27 10^{14}	4.4 10^{-15}
Kerosene	2 -22 10^{10}	50 – 450 10^{-12}
Xylene	6.998x10^{16}	1.429x10^{-17}

Table 5.3 Resistivities of Some Common Rocks, Minerals, Chemicals and Metals (after Loke, 1997).

Material	Resistivity (Ω.m)	Conductivity $(\Omega.m)^{-1}$
Igneous & metamorphic rocks	$5x10^{3}$ - 10^{6}	10^{-6} – $2x10^{-4}$
Granite	10^{3} - 10^{6}	10^{-6} - 10^{-3}
Basalt	$6x10^{2}$ – $4x10^{7}$	$2.5x10^{-8}$ - $1.7x10^{-3}$
Slate	10^{2} -$2.5x10^{8}$	$4x10^{-9}$ - 10^{-2}
Marble	10^{2} – $2x10^{8}$	$5x10^{-9}$ - 10^{-2}
Quartzite	$8 – 4x10^{3}$	$2.5x10^{-4}$ - 0.125
Sedimentary Rocks	$20 – 2x10^{3}$	$5x10^{-4}$ - 0.05
Sandstone	$50 – 4x10^{2}$	$2.5x10^{-3}$ - 0.02
Shale	1 - 100	0.01 - 1
Limestone	10 - 800	$1.25x10^{-3}$ - 0.1
Soils and Waters	10 - 100	0.01 - 0.1
Clay	0 - 15	6.7
Alluvium	$9.074x10^{-8}$	$1.102x10^{7}$
Groundwater (fresh)	0.708	1.413
Sea water	0.843	1.185
Chemicals and Metals	6.130	0.163
Iron		
0.01 M Potassium chloride		
0.01 M Sodium chloride		
0.01 M acetic acid		

5.1.3 Traditional resistivity surveys

- Data acquisition

The resistivity method has been used since the 1920's due to the work of the Schlumberger brothers. For the next 60 years, the conventional sounding survey was normally used for quantitative interpretation (Koefoed, 1979).

One dimensional (1-D) surveying is carried out with either profiling or vertical electrical sounding (VES). Profiling implies moving a constant spacing electrode array along a line and plotting the variations against profiled distances. Vertical electrical sounding involves the increase of the electrode separations around a mid-point, usually with a logarithmic electrode separation distribution, in order to find the layering of strata.

- **Data interpretation**

The interpretation of data acquired from the 1-D resistivity survey is conducted with the assumption that the subsurface consists of horizontal layers. The apparent resistivity data are normally plotted against the electrode separation and interpreted qualitatively through visual inspection and rule of thumb. Previously quantitative interpretation was conducted using a method of curve matching where data is plotted on double logarithmic diagrams and matched against a 2 or 3 layer master curve. Then a trial and error method was used, where the interpreter tried to find the best fit between the measured data and the model's response by adjusting layer thicknesses and resistivities. The actual method is an automatic inversion using RES1D.EXE software, which is a simple inversion and a forward modelling program for 1-D model interpretation (Figure 5.4). This method has given useful results for geological situations (such us water-table) where the one-dimensional model is approximately true (Loke, 2004).

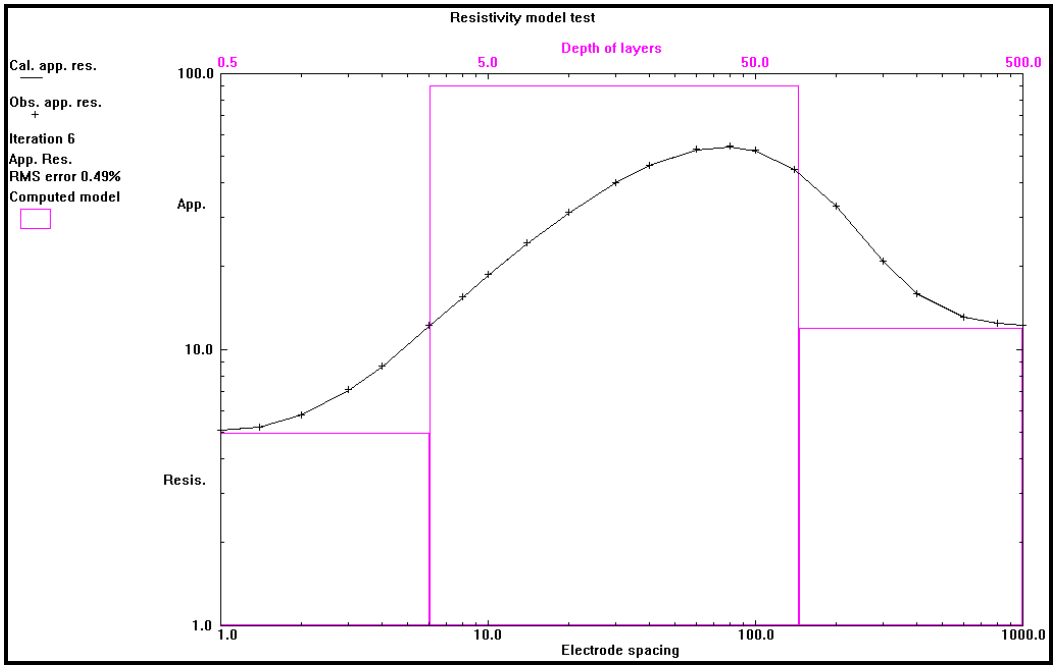

Figure 5.4 A typical 1-D model used in the interpretation of resistivity sounding data for the Wenner array.

- **Limitation of 1-D resistivity method**

The greatest limitation of the resistivity sounding method is that lateral changes in layer resistivity are not taken into account. Errors in interpreted layer resistivity and thickness are therefore possible. The profiling method is also limited, as it cannot detect vertical changes in resistivity and it is used mainly for qualitative interpretation.

5.1.4 Electrical resistivity tomography surveys

Because of the limitations of 1-D resistivity surveys, a two-dimensional (2-D) survey was introduced which is a more accurate model of the sub-surface, where the resistivity changes in both vertical and horizontal direction are estimated along the survey line. The 3-D survey should be even more accurate, as it covers the resistivity changes in a direction perpendicular to the survey line. Electrical resistivity tomography (ERT) or imaging is a technique in which many individual resistivities measured are combined to produce a 2-D resistivity cross-section or 3-D resistivity of the sub-surface.

- **Data acquisition for 2-D resistivity survey**

A linear array of electrodes is set into the ground and a computer system controls which two electrodes act as the potential electrodes and which two electrodes act as the current electrodes. Measurements are acquired at various electrode separations and positions along the line to provide information at various lateral and vertical locations beneath the array.

Figure 4.4 shows the typical set up for a 2-D survey with a number of electrodes along a straight line attached to a multi-core cable. Normally a constant spacing between the adjacent electrodes is used. The sequence of measurements to take, which type of array to use and other survey parameters, such as which current to use, are normally entered into a text file which can be read by a computer program on a laptop computer. After reading the control file, the computer program automatically selects the appropriate electrodes for each measurement. The ABEM Lund Imaging system used in

this study and described below has an in-built microprocessor system, so that a laptop is not directly connected.

In a typical survey, most of the field work involves laying out the cables and electrodes. After that the measurements are taken automatically and stored in the computer. The measurements are taken in certain sequences related to the protocol file chosen by the user. As shown in Figure 4.4, the first sequence of measurements with the Wenner array, for example, is made using electrode spacing of "1a". For the first measurement, electrodes number 1, 2, 3 and 4 are taken as C1, P1, P2 and C2 respectively. For the second measurement, electrodes number 2, 3, 4 and 5 are taken as C1, P1, P2 and C2 respectively. This selection of electrodes for measurements is repeated down the line until the last four electrodes are used for the last measurement with "1a" spacing. The same process is repeated for measurement with "2a", "3a", "4a", "5a" and "6a". As the electrode spacing is increased, measurements are made for deep layers.

The roll-along method is used when there is a need for horizontally extending the area covered by the survey. It consists of moving the first cable to the end of the last cable and adding new data points to the previous one.

- Abem Lund Imaging System

The Abem Lund Imaging System is an automatic electric imaging system, suited for automatic resistivity, induced polarization and self-potential surveys. It is a multi-electrode system for cost-effective and high-resolution 2-D and 3-D resistivity surveys. For data acquisition, the following equipment is used:

Abem terrameter SAS 1000: This is a one channel signal averaging system operating with SAS 1000 data acquisition software. The terrameter SAS 1000 allows:

- automatic measurement processes;
- in-field quality control of measurement with electrode tests and statistical measurement control;
- automatic roll-along with coordinates in x direction or y direction;
- to define survey strategies and arrays because of electrode cables geometry and switching sequence defined in address and protocol files; and
- on-screen echo of measurement progress.

Abem electrode selector ES10-64: This is a switching unit used to select electrodes in sequence of measurement defined by address and protocol files.

Lund spread cables and suitable cable joints and cable jumpers.

Suitable quantity of electrodes.

PC-software for downloading and converting data to several data formats:

- Utility software is used to download data and to convert it in other formats as well as to create protocols and visualize their pseudosection in colour or greyscale; and
- 2-D inversion software for model section plotting of inverted section in colour or greyscale as well as for graphical output with topography in bitmap format.

It is important to notice that the terrameter SAS 1000 can operate in both resistivity surveying mode and Induced polarization mode.

In resistivity mode, the terrameter calculates the apparent resistivity automatically and displays the values from 0.05 milliohms to 1999 kilo ohms. Figure 37 shows an example of measurement intervals for a resistivity measurement. The measurement for one data point takes place with different intensities where the voltage is measured at the same time as the current is

sent into the ground. On default, the intensity will be chosen by the Terrameter automatically, choosing different intensities according to the n- and a-factors and the reading depth respectively within a user defined range. The minimum and maximum intensity ranges from 1 mA to 1 A, with a maximum voltage of 400 V.

Alternatively, the intensity can also be controlled manually. The measurement for one data point takes place in several measurement cycles that are called stacks, whereas there are a maximum of four stacks for one data point. The resistivity value will be calculated using the median and mean of the results of the stacks, which are the receiving intervals as shown in Figure 5.5.

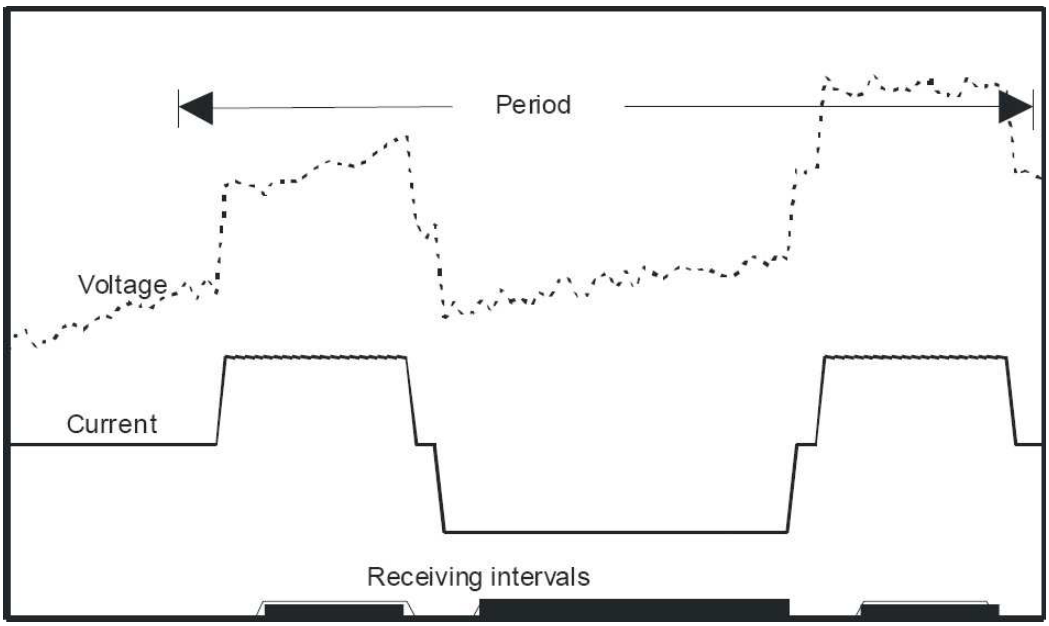

Figure 5.5 Timing diagram in resistivity mode (Abem, 2005).

In Induced polarization mode, the terrameter measures the transient decay of the voltage when the transmitted current is turned off. The time domain IP methods measure the voltage decay over a specified time interval after the induced voltage is removed. The terrameter can measure up to ten such time intervals. The total integration time is limited to 8 seconds (ABEM 2005)

The IP surveys are very useful to pick up the difference between soils with high water contents and clays that usually have a very similar resistivity spectrum. Water does not have any chargeable properties, but clays usually show very large values of voltage decay.

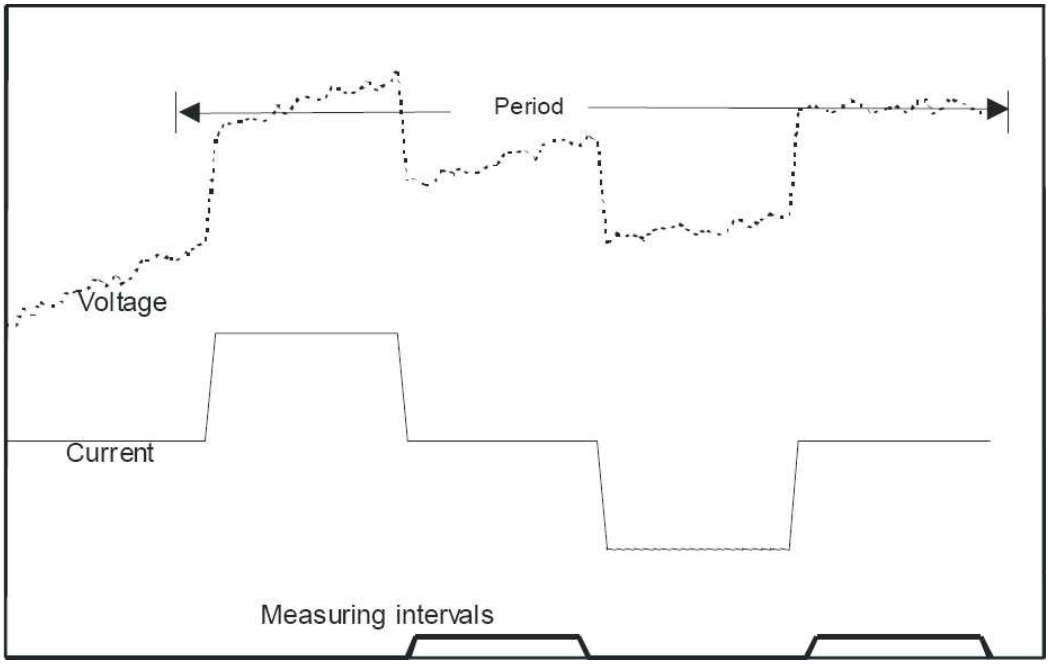

Figure 5.6 Timing diagram for a measurement sequence in IP-mode. (Abem 2005)

- Data interpretation

    - 2-D forward modelling

In the forwards modelling problem, the sub-surface resistivity distribution is specified and the purpose is to calculate the apparent resistivity that would be measured by a survey over such a structure.

A forward modelling sub-routine is in fact also an integral part of any inversion program since it is necessary to calculate the theorical apparent resistivity values for the model produced by the inversion routine. There are three main methods to calculate the apparent resistivity values for a specific model (Loke, 2004). These are: (i) the analytical method; (ii) the boundary element

method; and (iii) the finite-difference and finite element method. The finite-difference and finite element methods are usually the only viable choice. These methods can subdivide the subsurface into thousands of cells with different resistivity values.

In the RES2DMOD software, the user can use the finite-different or finite element method. The subsurface is subdivided into a large number of rectangular cells and the user can specify the resistivity values of each cell.

While our main interest is in the inversion of field data, the forward modelling program is also useful, particularly in the planning stage of the survey. Before carrying out a field survey, some information about the shape and size of expected targets is frequently known. By digitally trying different array types which have different sensitivity functions, it is possible to come up with the correct choice of the array type that will give a reasonably good response over a particular class of structures, and to avoid using an unsuitable array. It is also possible to get an idea of the suitable spacing between adjacent electrodes and the maximum electrode separation needed. This program helps in choosing the "best" array for a particular survey area after carefully balancing factors such as cost, depth of investigation and resolution.

- 2-D inversion modelling

The inversion modelling consists of converting apparent resistivity values into a resistivity model section that can be used for geological interpretation. The data needs to be converted in the RES2DINV format.

To get a good model, the data must be of equally good quality. Bad data points fall into two broad categories i.e. "systematic" and "random" noise. Systematic noise is usually caused by failure during the survey, such as breaks of cables, very poor ground contact at an electrode so that sufficient current cannot be injected into the ground, forgetting to attach the clip to the electrode and connecting the cable in the wrong direction. Random noise, at the other hand, includes effects such as telluric currents that affect all the

readings. The noise can cause the readings to be lower or higher than the equivalent noise-free readings.

As a general rule, before carrying out the inversion of data set, all bad data points from systematic noise are manually removed from a profile plot using "edit data" in RES2DINV program (Figure 5.7).

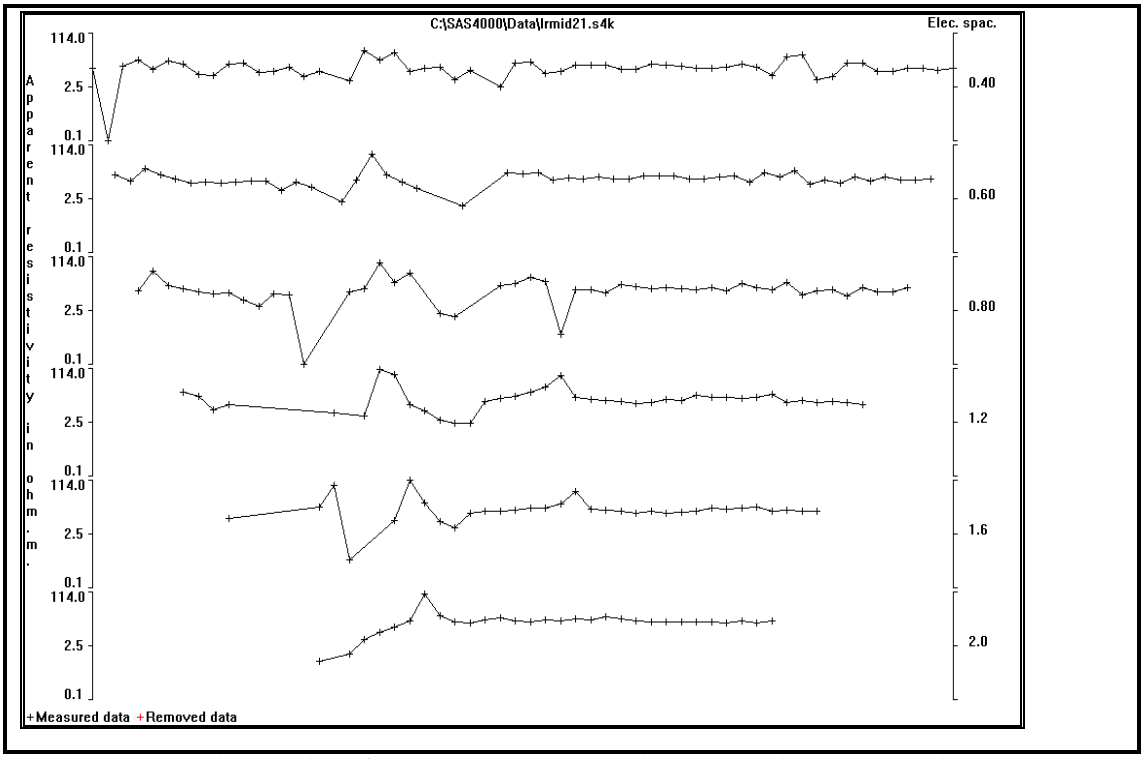

Figure 5.7 Plot to identify bad data points in the survey (Abem, 2005).

For random noise, RES2DINV has a general technique to remove the bad data points with minimal input by the user and it is practical for any array and any distribution of data points. In this method, trial inversion is carried out first, then a "display" window in RES2DINV is selected to read the INV file containing the inversion results. After that, the "RMS error statistics" option is selected displaying the distribution of percentage difference between the logarithm of measured and calculated apparent resistivity values. The error distribution is shown in the form of a bar chart. Normally the higher bar is the one with the smallest error, and the height of the bars should decease

gradually with increasing error values. Data points with high error values are removed by moving the green cursor line to the left of the 60% error bar.

The RES2DINV program is designed to operate, as far as possible, in an automatic and robust manner, with minimal input from the user. It has a set of default parameters that guide the inversion process. In most cases the default parameters give reasonable results. The program has some parameters that the user can modify to fine-tune the inversion, including options such as inversion methods, model discretization, model sensitivity, which are located under "Inversion" menu, as well as options such as inversion dumping parameters and inversion progress, located under the "Change Settings" menu. More detail on the change of these parameters can be found in the RES2DINV User Manual.

Apparent resistivity data measured during the field survey is recorded by the terrameter in ".S4k" format files. Using S4kWin 3.21 software, these data files are converted into ".Dat" format files in order to be read by Res2Dinv program for the inversion process.
The inversion routine starts by selecting the conventional least-squares smoothness-constrained inversion method which is considered applicable to all cases with good results. If the user is not satisfied with the results obtained, the Res2dinv program provides other options which are used to improve the results.

The result obtained from the inversion process is an inverse model section which is used for geological interpretation. For ground surfaces with a significant change in elevation, the Res2Dinv provides an option to include topography data in the inverse model section.

5.2 ERT Survey on East London Fuel Depot Site

5.2.1 Method of Resistivity and IP data acquisition on site

The geophysical survey lines are classified into two groups. The first includes five transects chosen outside the fuel depot, which aim to characterize the geology and hydrogeology of the site. This group is denoted as the pink lines 1, 2, 3 and 5 in Figure 5.8. The second group includes five transects selected inside the fuel depot to locate or to detect the LNAPLs contaminant plume and to characterize shallow soils. These are shown as the blue lines 6, 8, 10, 9 and 12 (Figure 5.8). Data has been acquired on site as follows:

- The Wenner protocol of measurement was chosen because of its ability to discriminate noise.
- The electrode spacing was chosen as 2 m for the external transects and 0.5m for transects inside the site.
- Four cables were laid out from the start of the traverse, denoted as the first measurement station. The first and the last cables had only odd-numbered take-outs connected to eleven electrodes and the two middle cable take-outs were connected to all 21 electrodes.
- A roll-along technique was used for lateral data coverage by repeatedly moving the first cable to the fourth one.
- A GPS reading was taken using a differential GPS with 2 cm precision.

All data detected in the terrameter is saved in .S4K format and is converted to .DAT format for the inversion process.

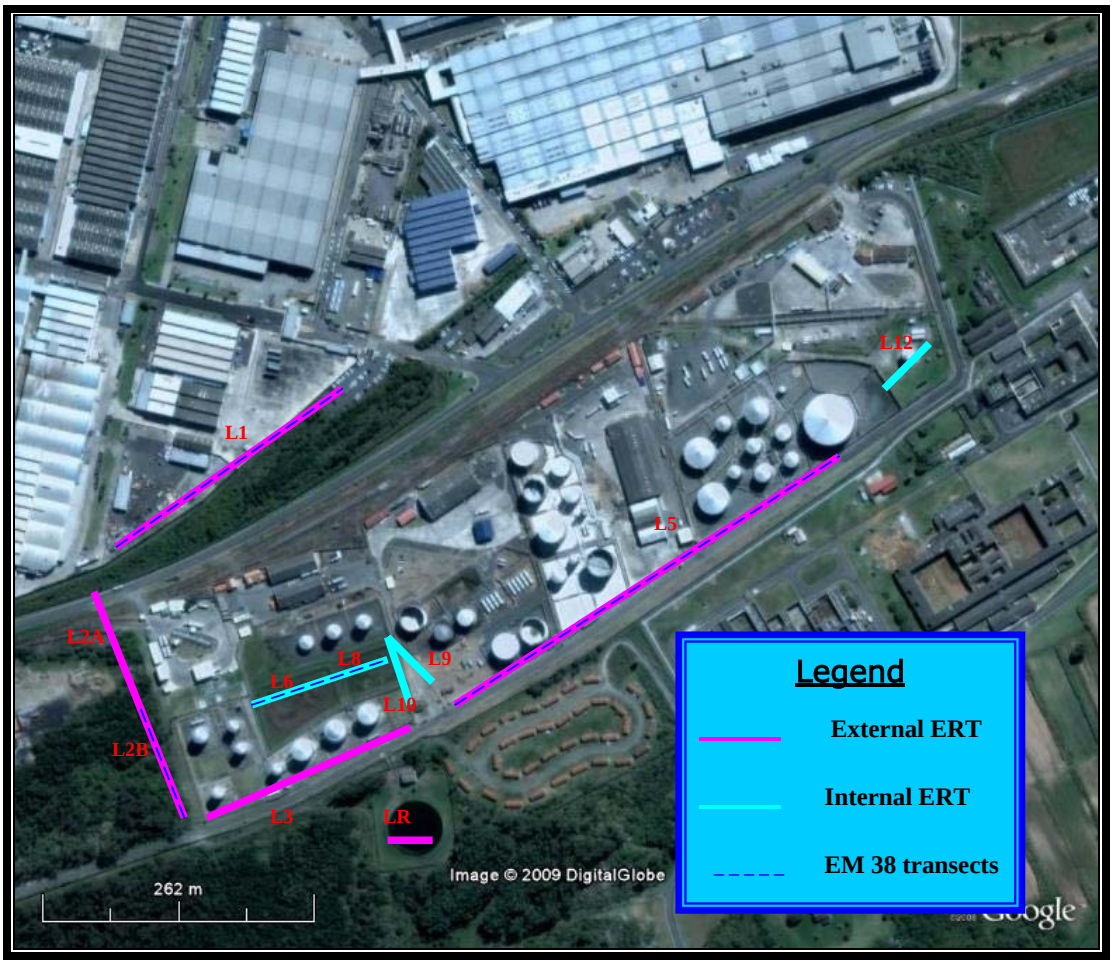

Figure 5.8 ERT survey transects at the East London site.

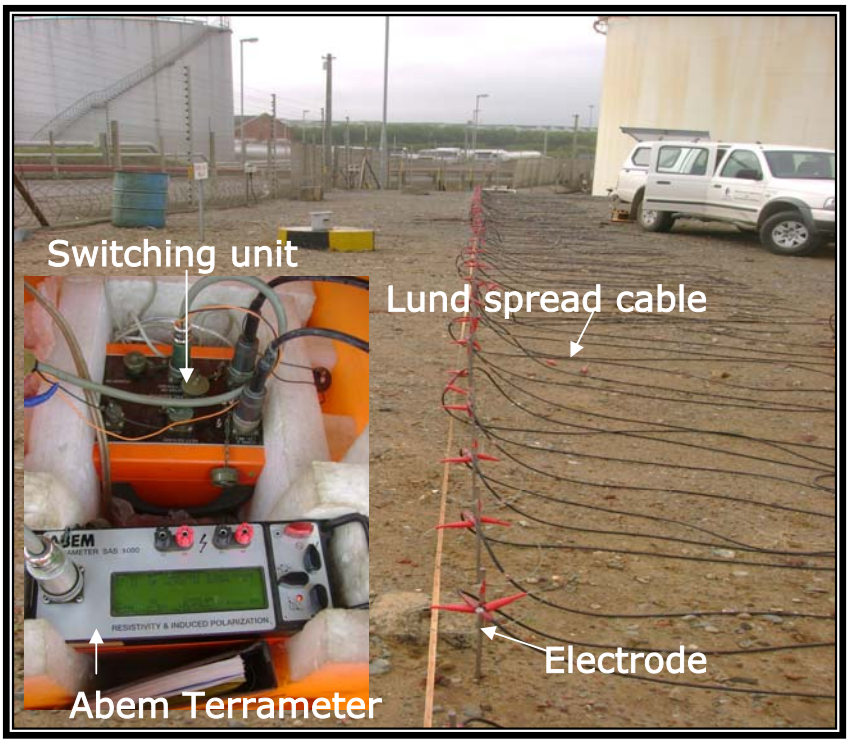

Figure 5.9 **Layout of ABEM LUND Imaging System with Terrameter SAS 1000 at Chevron Site during data acquisition.**

5.2.2 ERT and IP data inversion

The data obtained from all survey transects were analyzed using the RES2DINV program which makes use of the smoothness-constrained least-squares method and automatically determines a 2-D resistivity/chargeability model of the subsurface.

5.2.3 Analysis of results

In order to characterize the geological and hydrogeological conditions of the Joint Fuel Depot site, four transects have been found to be practical for ERT surveys. The ERT results are compared with borehole geological logs and geochemistry data in chapter 7 for an integrated interpretation.

For each transect, two or three 2-D resistivity sections are presented. The first section, without topography data, gives the true depth of the different layers. The second section, with topography data, gives the true lateral lengths of the

geological features. The third section shows the chargeability distribution for Transect 1 and 5 where the IP was applied.

- **Geology and hydrogeology characterization**

Transect 1

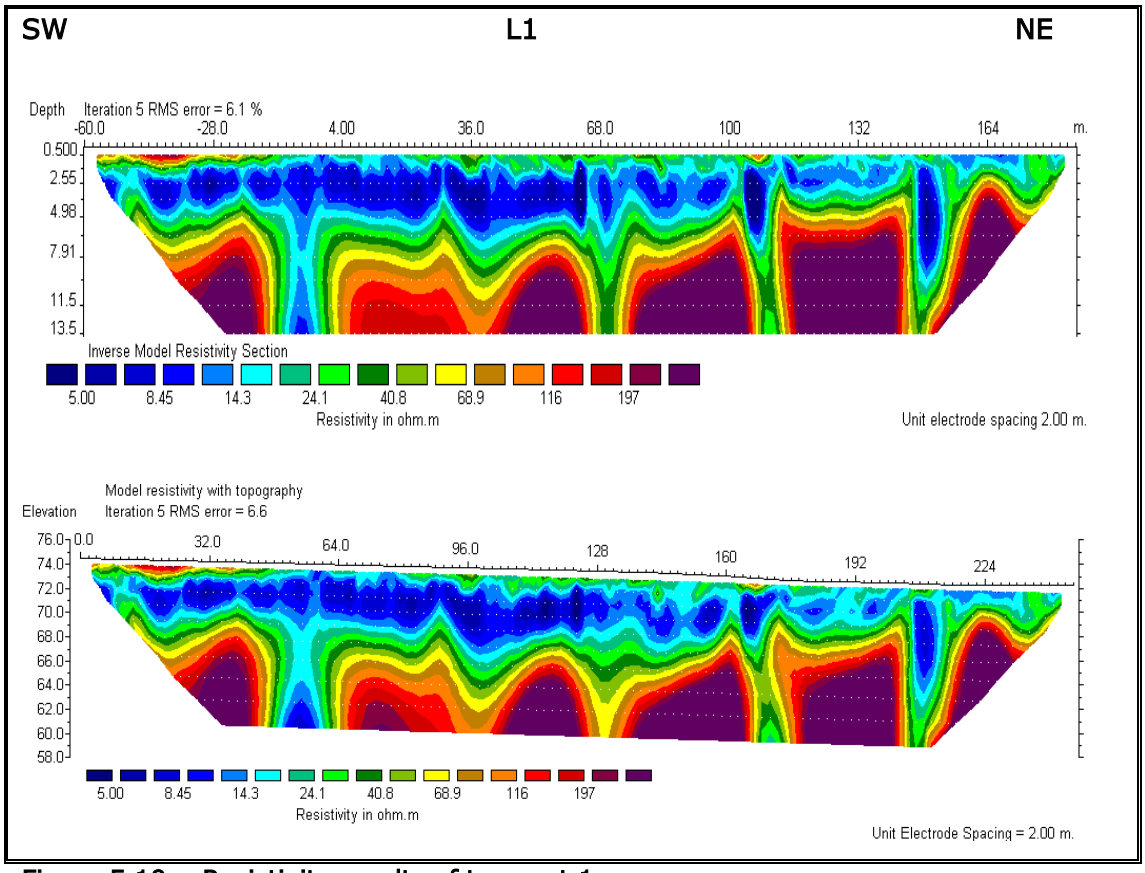

Figure 5.10 Resistivity results of transect 1.

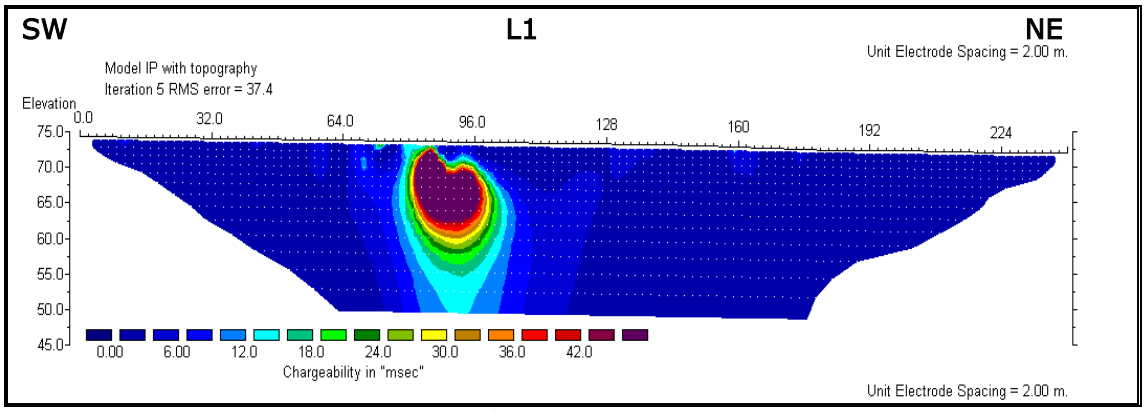

Figure 5.11 Chargeability results of transect 1.

The inverse Model Resistivity section is obtained from accurate data with an RMS error of 6.1%. Three zones of resistivity contrasts can be distinguished on the model (Figure 5.10):

- A resistive layer covering about 32 m distance and about 1m depth (resistivity of about >100 Ω.m);
- A middle conductive layer from 50cm to ± 5m (resistivity of 5-15 Ω.m); and
- A resistive layer goes from ± 8 m to the bottom of the section which could be a fractured bedrock (resistivity of >110 Ω.m).

The chargeability model (Figure 5.11) is not reliable because of the higher inversion error of 37.4%.

Transect 2

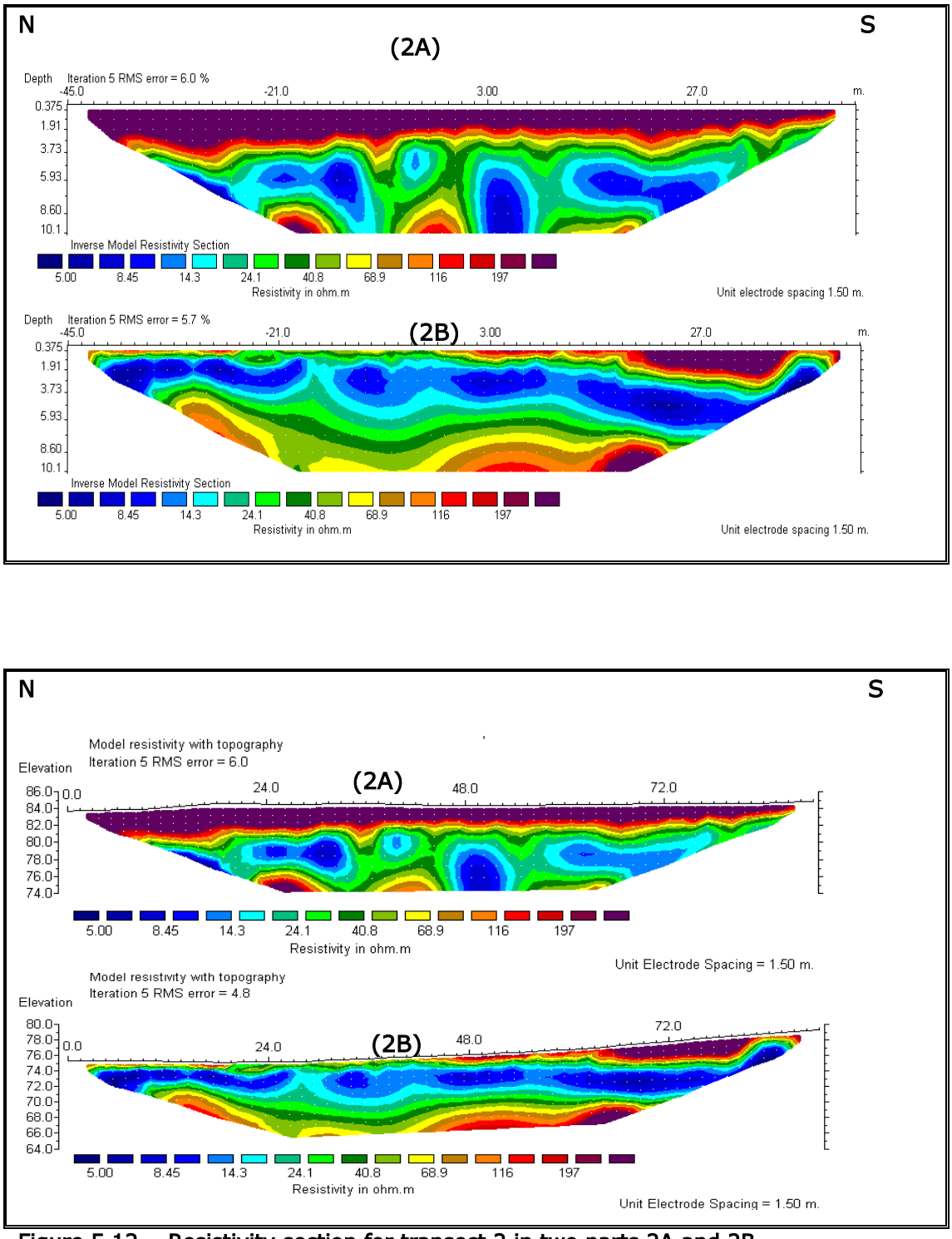

Figure 5.12 Resistivity section for transect 2 in two parts 2A and 2B.

This Transect 2 includes two parts (2A) and (2B) on a line divided by a fence. The survey was carried out separately on each section. A space of about 20 m separated them. The section 2A presents three contrasted zones (Figure 5.12):

- A shallow and resistive layer completely covering the section from 0 to 3.5 m (resistivity of > 200 Ω.m);
- A conductive zone which indicates a higher water content between 4 m and 7 m (resistivity of 5-15 Ω.m); and
- The bottom layer is more resistive, which represents the fractured bedrock (resistivity of > 200 Ω.m).

The section 2B presents two similarly bottom zones above, with a resistive cover partially present.

Transect 3

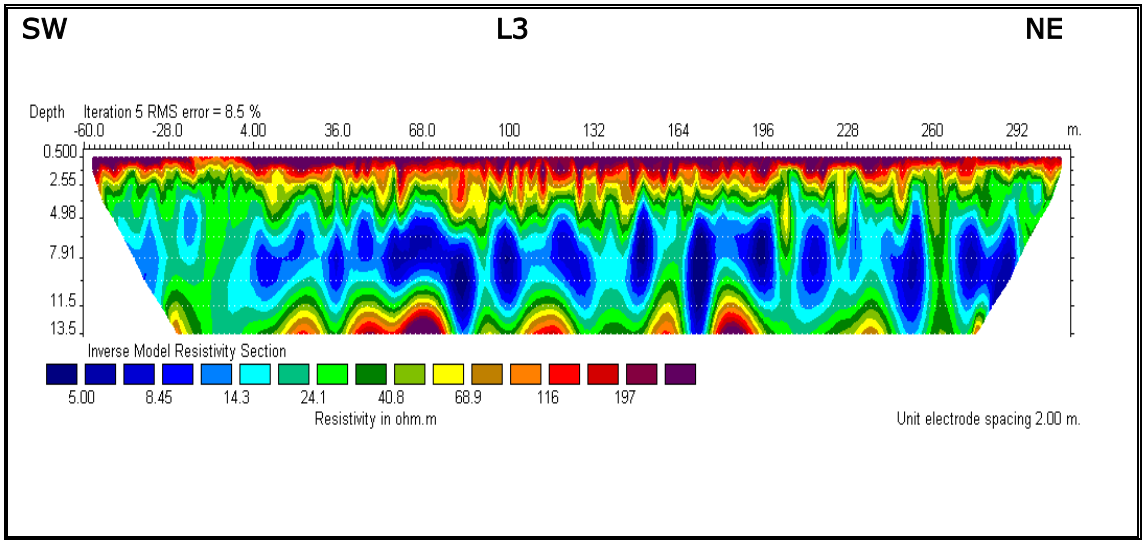

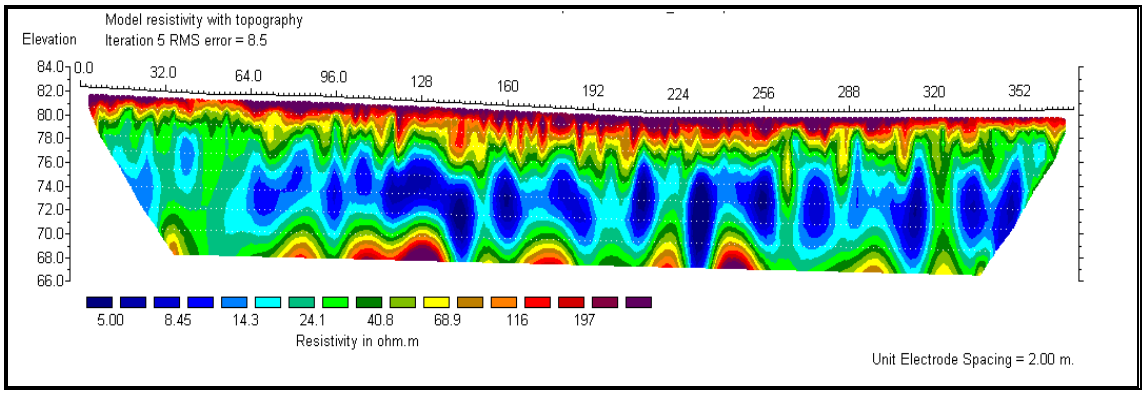

Figure 5.13 Resistivity section for transect 3.

The section presents three contrasted zones in Figure 5.13:

- a shallow resistive layer of about 2 m (resistivity of > 150 Ω.m);
- a conductive layer of about 9 m (resistivity of 5-15 Ω.m); and
- the bottom resistive bedrock separated from the conductive layer above (resisitvity of >200 Ω.m)

Transect 5

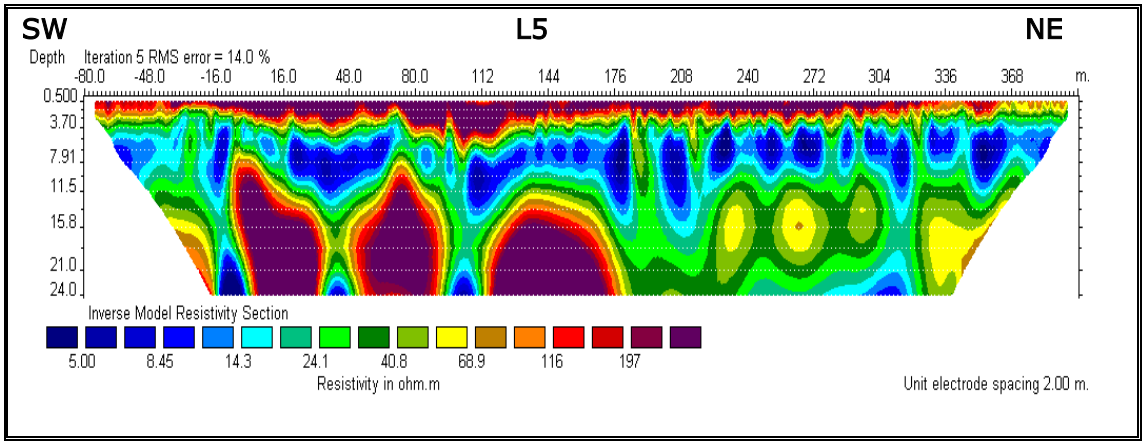

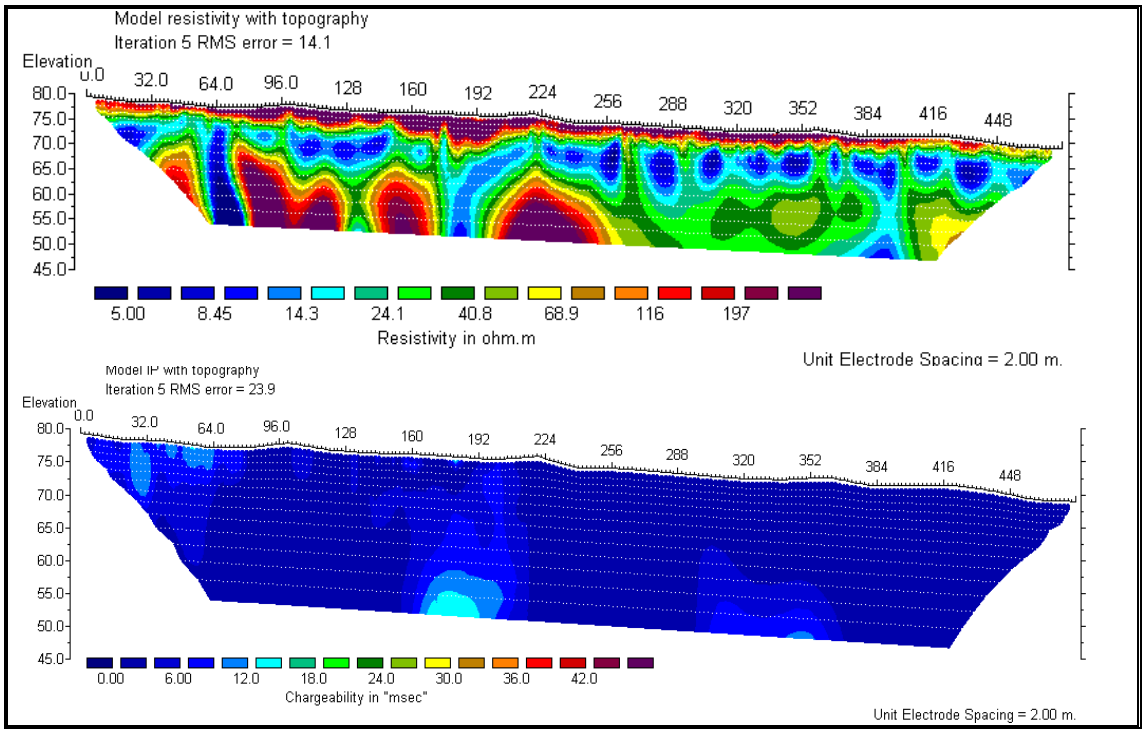

Figure 5.14 Resistivity and chargeability results of transect 5.

The data recorded on this transect was influenced by noise originating from the fence enclosing the prison site. Therefore some bad data points were found and were eliminated from the data set before the inversion process. The inversion RMS error is consequently higher than 16.4 % for the resistivity model and 23.9% for the chargeability model (figure 5.14). The Resistivity section present three contrasting zones:

- 3 m of resistive layer on top of the section (>200 Ω.m);
- a conductive layer follows up to 12 m (5 to 15 Ω.m); and
- resistive fractured bedrock at the bottom (>200 Ω.m)

The chargeability section is not reliable because of the high inversion error of 23.9%.

Transect R (Reservoir).

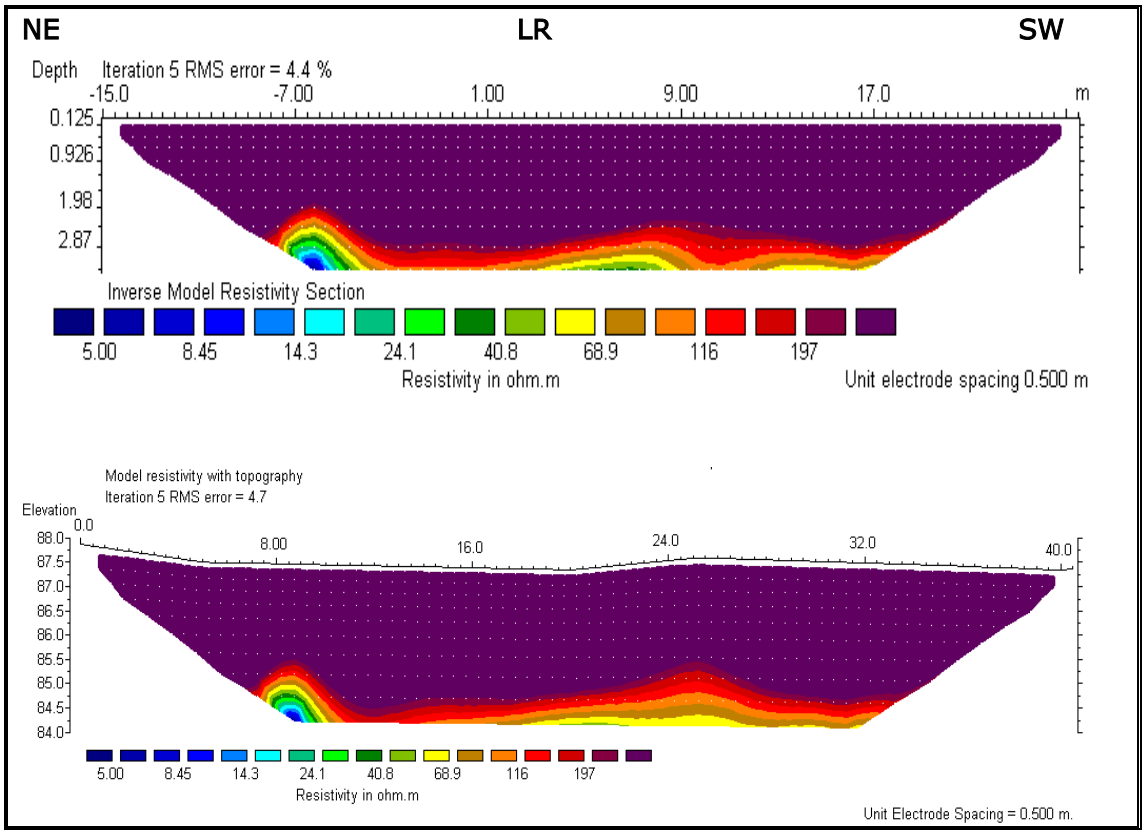

Figure 5.15 Resistivity section of transect R.

The transect R is located outside the Joint Fuel Depot facility and next to an underground water storage reservoir. The ERT section in Figure 5.15 reveals a resistive layer of about 2.5 m overlaying a conductive formation. This profile is the shortest with only 40 m long and could sample up to 3 m depth. It only reveals the first resistive layer (>200 Ω.m) which is similar to the first layer of profiles L2A, L3 and L5.

- **Hydrogeological and LNPAL Plume characterization**

Transect 6

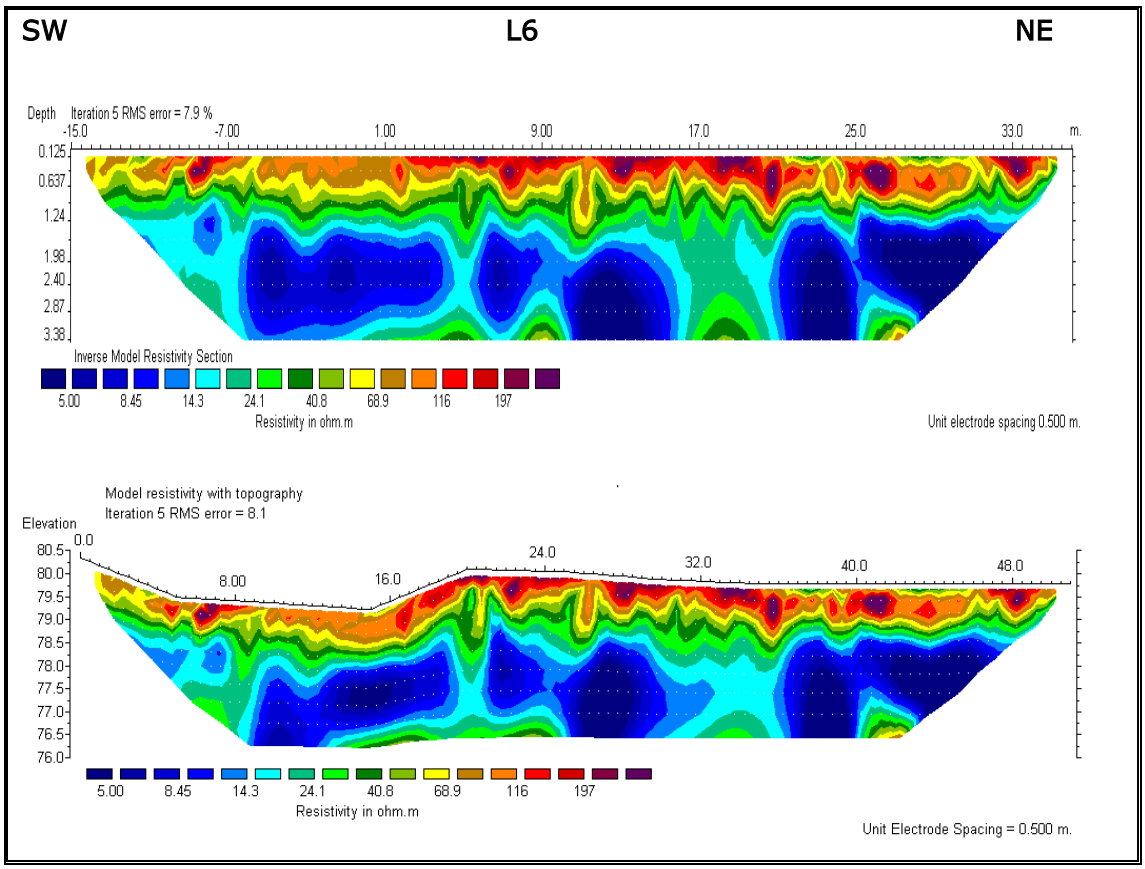

Figure 5.16 Resistivity section of transect 6.

Data acquired on Transect 6 is accurate with an inversion error of 7.9%. Three contrasting zones are identified (Figure 5.16):

- a resistant layer of about 1 m thickness is found near the surface (> 60 Ω.m);
- the following layer is 2 m thick and conductive (5-15 Ω.m); and
- Followed by the top of a resistive layer (20-100. Ω.m)

Transect 8

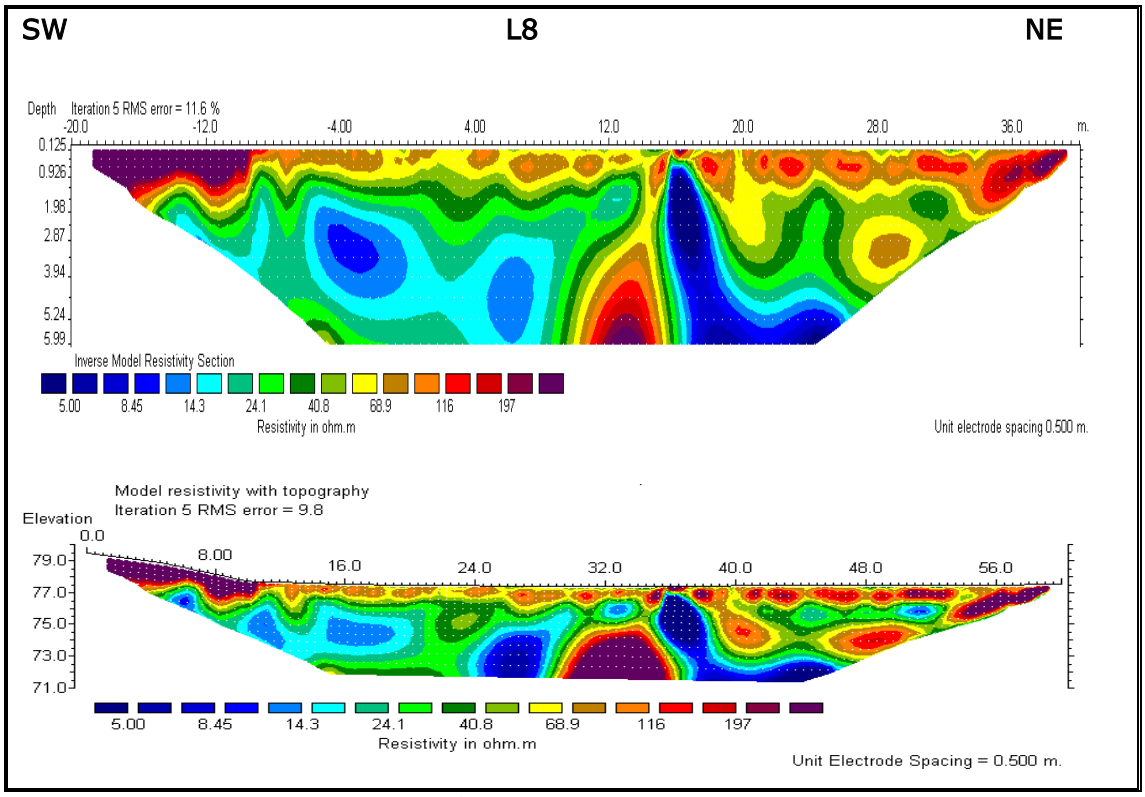

Figure 5.17 Resistivity section of transect 8.

The inversion of this ERT section reveals the presence of bad data which was eliminated (RMS error 11.6%). Because of bad data elimination, the model section is not accurate and layers are consequently distorted (Figure 5.17). In general there is:

- shallow resistive and heterogeneous layer on top (>70 Ω.m);
- a 2 m conductive and heterogeneous layer follows (5-15 Ω.m); and
- the resistive bedrock in the middle of the section (>200 Ω.m).

Transect 9

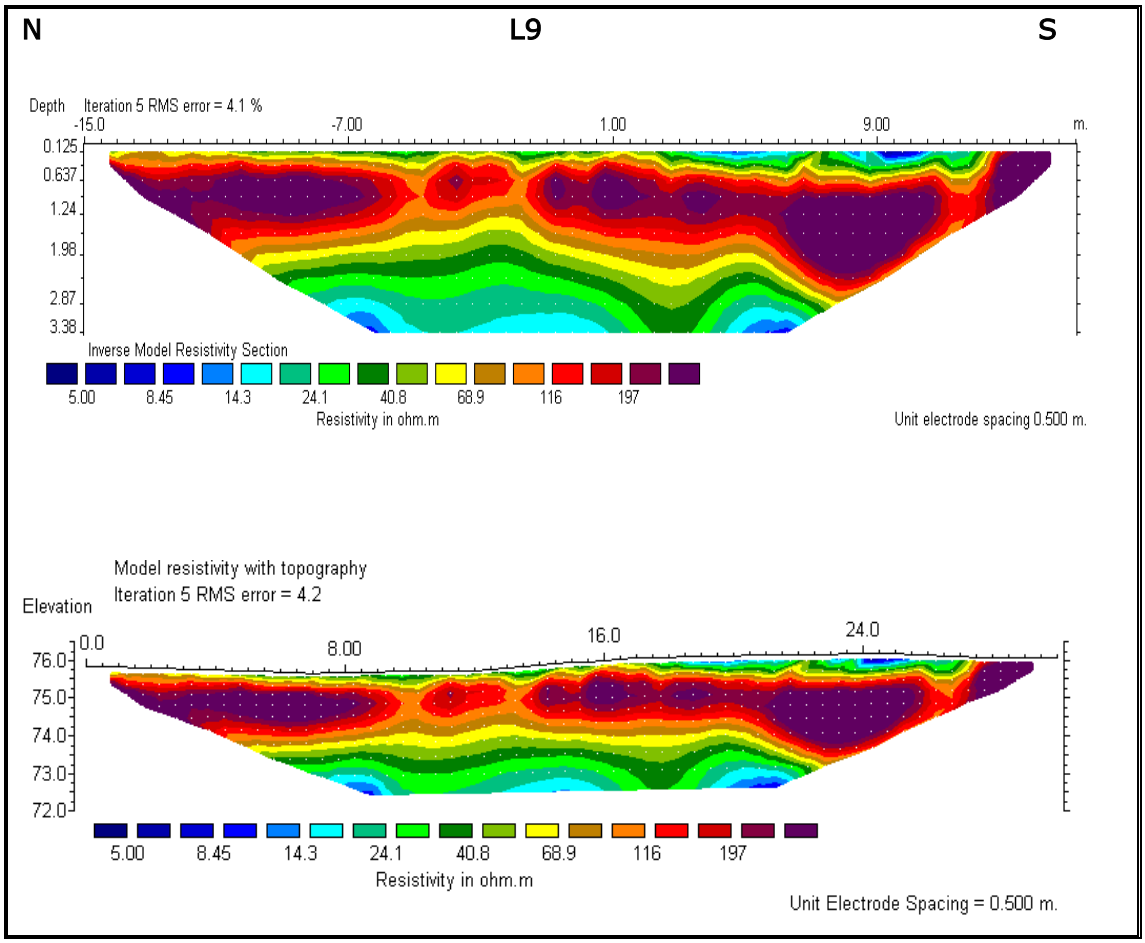

Figure 5.18 Resistivity section of transect 9.

The inversion of this data set indicates that data acquisition was very accurate (RMS error 4.1 Ω.m). The model therefore gives an accurate true resistivity distribution under Transect 9. Three contrasted zones are identified (Figure 5.18):

- a thin shallow and conductive layer of about 0.2 m (0-15 Ω.m);
- the second layer of about 2 m thickness is very resistive (>100 Ω.m) and quite heterogeneous; and
- the third conductive layer is at the bottom of the section with resistivity values ranging from 5 to 15 Ω.m.

Transect 9, in which 2.9 cm of free phase product was found during the pedestrian visit, is located next to borehole BH5 in the Chevron site (Figure 2.2).

Transect 10

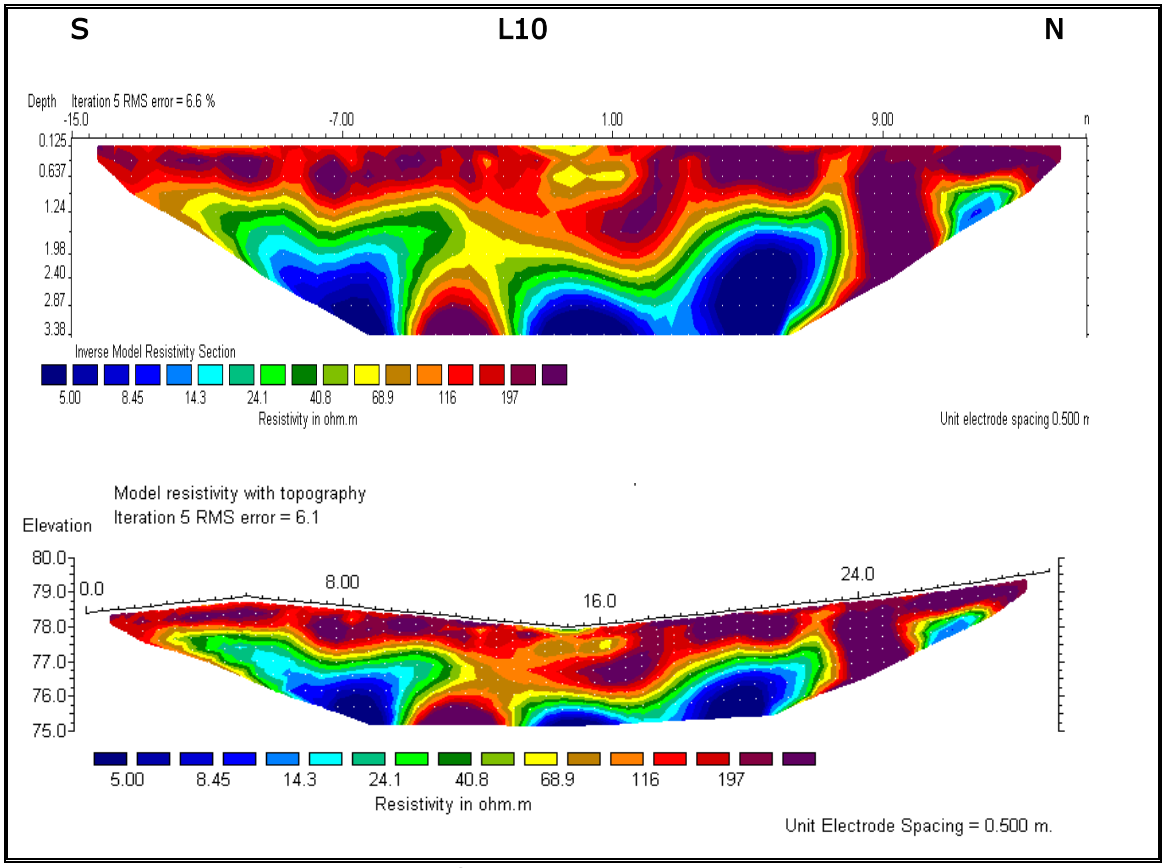

Figure 5.19 Resistivity section of Transect 10.

From this resistivity model, two contrasted zones are identified (Figure 5.19):

- The top layer of about 1.5 m is resistive with a resistivity value greater then 100 Ω.m; and
- The bottom layer is conductive and is intercepted by resistive zones which are part of the top formation.

Transect 12

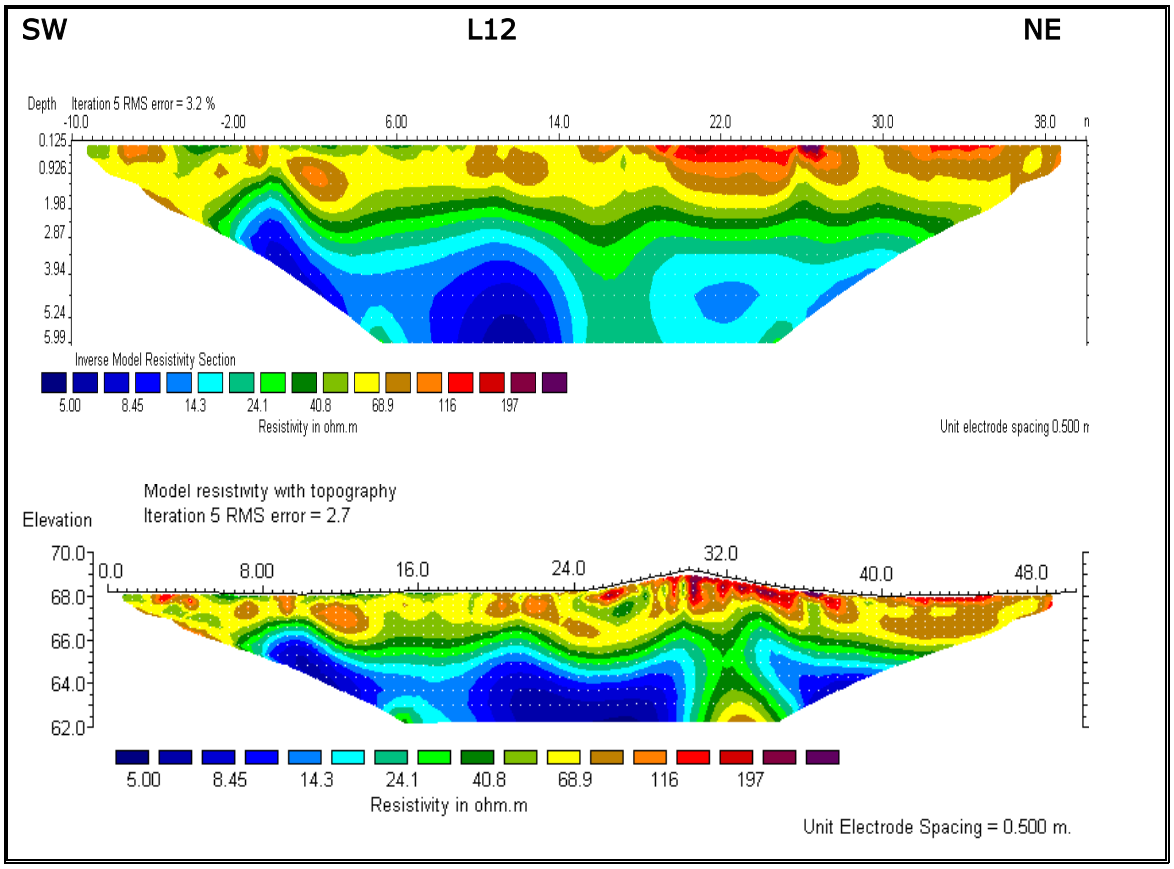

Figure 5.20 Resistivity section of transect 12.

The ERT results obtained for Transect 12 depicted two layers (Figure 5.20):

- the top layer of about 1 m thick and heterogeneous is less resistive (50 to 60 Ω.m); and
- the bottom layer is conductive and heterogeneous.

5.3 Electromagnetic (EM) Survey Results

The EM 38 measures the apparent electrical conductivity of the soil resulting from the induction of time-varying magnetic fields into the sub-surface. The electromagnetic method was also tested on site using an EM 38 instrument to assess anomalies caused by pipes or shallow soil conductivity.

The EM 38 has an intercoil spacing of 1m and measures up to a depth of 1.5 m in vertical dipole mode and up to 0.75 m depth in horizontal dipole mode. The EM 38 instrument shown in Figure 5.21 was used on site at Transect 1 and 5, the southern part of Transect 2 and Transect 6 and 8 combined.

Figure 5.21 EM 38 instrument.

Transect 1

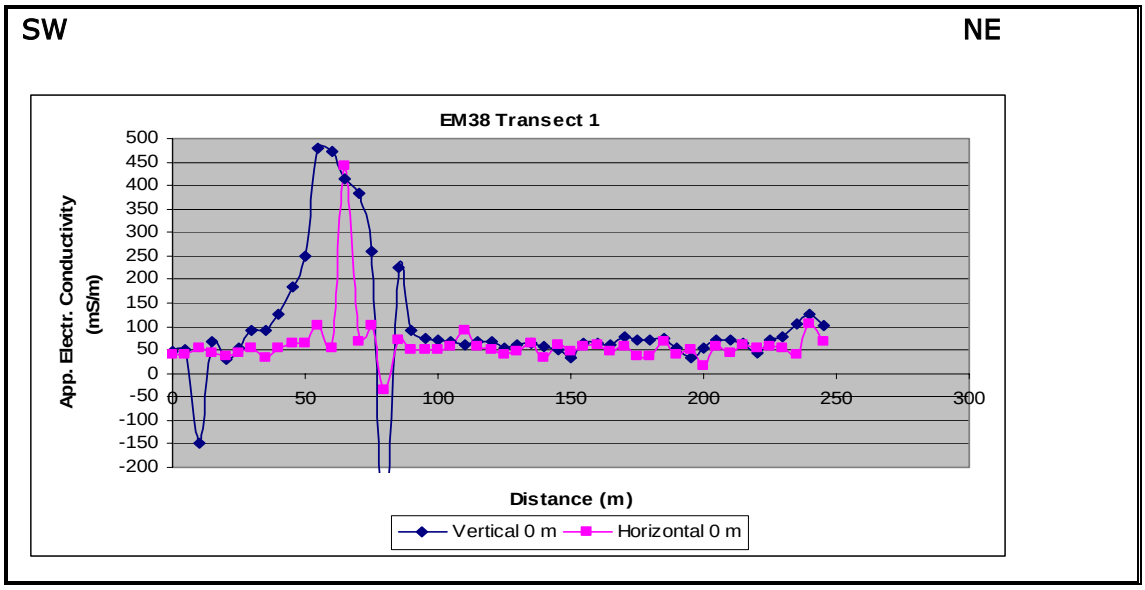

Figure 5.22 EM 38 result on Transect 1.

The EM 38 result on Transect 1 presents an anomalous conductive zone between 50 m and 100 m distance from the start of the transect (Figure 5.22).

Transect 5

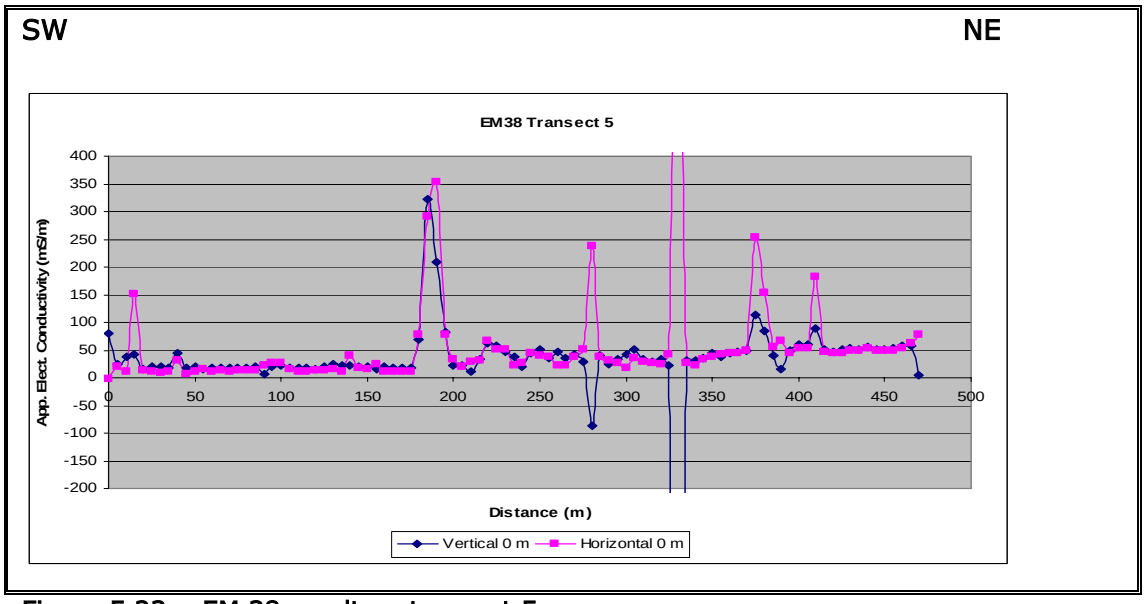

Figure 5.23 EM 38 result on transect 5.

Anomalies are detected on Transect 5 (Figure 5.23) probably due to the presence of underground pipes.

Transect 6 & 8

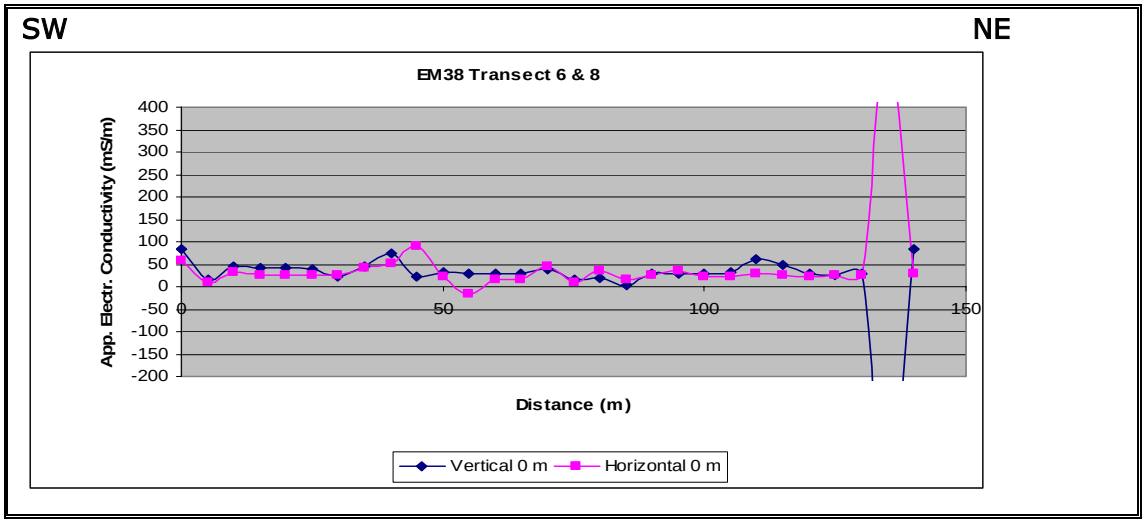

Figure 5.24 EM 38 result on transect 6&8.

On Transect 6 and 8, EM measurements are combined and pick up an anomaly at the north-eastern extremity which could be an underground pipe (Figure 5.24).

Transect 2B

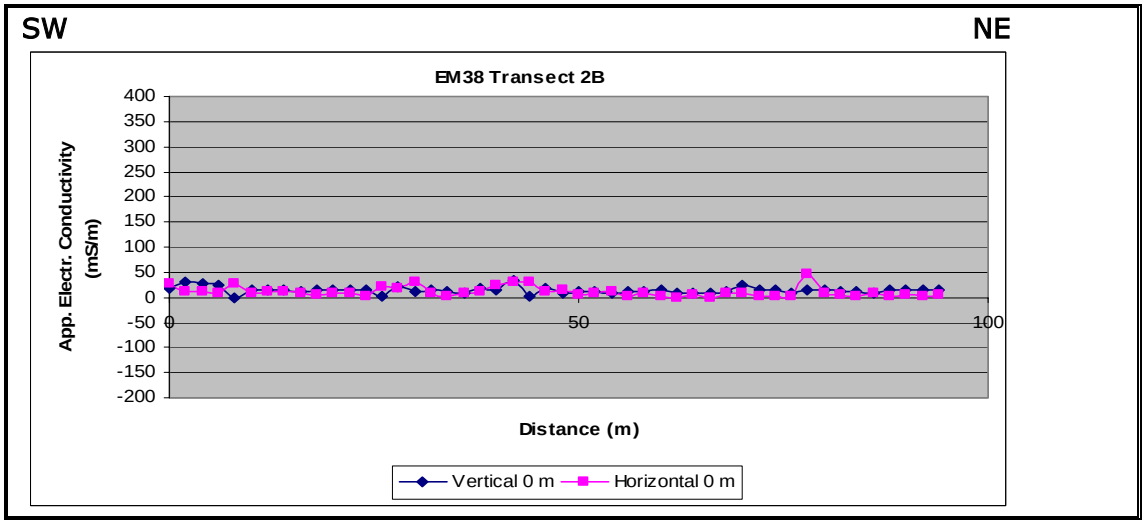

Figure 5.25 EM 38 results on Transect 2B.

The EM result obtained on Transect 2B above does not present the same level of noise as compared to the results on Transects 5, 6 and 8 (Figure 5.25).

The interpretation of the EM results shown above is to be done by comparing them with the ERT results, in order to confirm the source of the observed anomalies. The conductivity anomaly observed in Figure 5.22, compared to the chargeability anomaly observed in Figure 5.11, reveals the presence of either an underground pipe or a pocket of clayey soil. The EM result on Transect 5 (Figure 5.23) compared to ERT result, reveals the presence of sources of noise such as surface pipes as well as nearby electrical fences. The EM results on Transect 2B and Transect 6 and 8 present a steady soil conductivity, besides a conductivity anomaly appearing at the extremity of Transect 8 which was certainly caused by noise from the fences. It should be noticed that no dolerite was depicted by the EM survey.

6. FIELD TESTING

6.1 Initial Site Conceptual Model

Based on the previous investigation undertaken on the Joint Fuel Depot site, the Middleton Formation mudstones and sandstones setting are characterised by higher fracturing especially as fault planes. The intrusive rocks observed on site are dolerite sills which appear to be less fractured.

Joints observed on site are part of the geological structure which plays a major role in groundwater and contaminant movement. The dominant joint sets which dip sub-vertically toward the south-east and south-west, constitute the major pathway for groundwater flow in the direction of the Indian Ocean.

6.2 Soil Testing Results

6.2.1 Soil profiling and initial water content

The feel method was applied to describe the soil profile on site. The result indicates a general soil profile of sand, clayey sand and clay, composed from top to bottom.

The initial water content in the soil sample taken at different depths in the vadose zone was estimated using the gravimetric method. It appears, in general, that the soil water content throughout the site increases with depth.
Table 6.1 presents the results of one soil profile description and gravimetric water content distribution over the same soil profile for illustration. The results of the other sampling points can be found in Appendix A.

Table 6.1 Profile texture and description at BP1.

Depth (mm)	mass wet (g)	mass dry (g)	water content(g/g)	Soil Profile Description
0	28.26	27.87	0.014	
300	22.96	22.71	0.011	
600	23.79	23.41	0.016	
900	33.17	32.25	0.029	fine sands throughout the profile
1200	33.11	31.83	0.040	
1500	54.63	48.77	0.120	
1800	36.07	33.43	0.079	
2100	39.11	35.28	0.109	
2400	28.26	25.02	0.129	orange colour coming up
2700	20.17	16.71	0.207	
3000	34.11	29.21	0.168	
3300	36.07	31.78	0.135	from this point clayey prevail till depth
3600	27.15	23.04	0.178	orange clays

The initial soil water content for the profile J1 was plotted against depth to analyze its distribution in the vadoze zone (Figure 58). It appeared that the water content increased with depth.

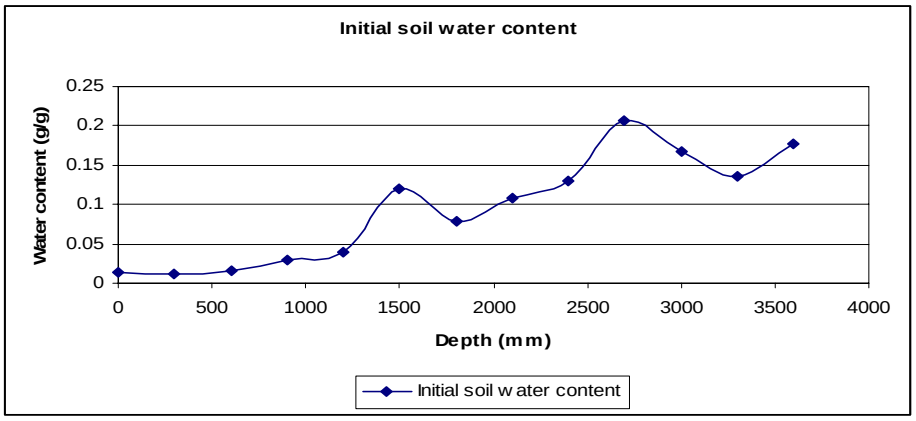

Figure 6.1 Gravimetric water content distribution curve for the profile J1 (28 October 2008).

6.2.2 Particle size analysis results

In general the particle size analysis results revealed that the unconsolidated sediments were composed of well-graded sand near the surface, becoming clayey with depth. To illustrate this, by an example of the soil sample BPT4 taken in BP site at 0.6 m and at 1.7 m depth, the soil was classified as a sand at 0.6m and as a clayey sand at 1.7 m depth (Figure 6.2 and 6.3). A full set of textural data is presented in Appendix A.

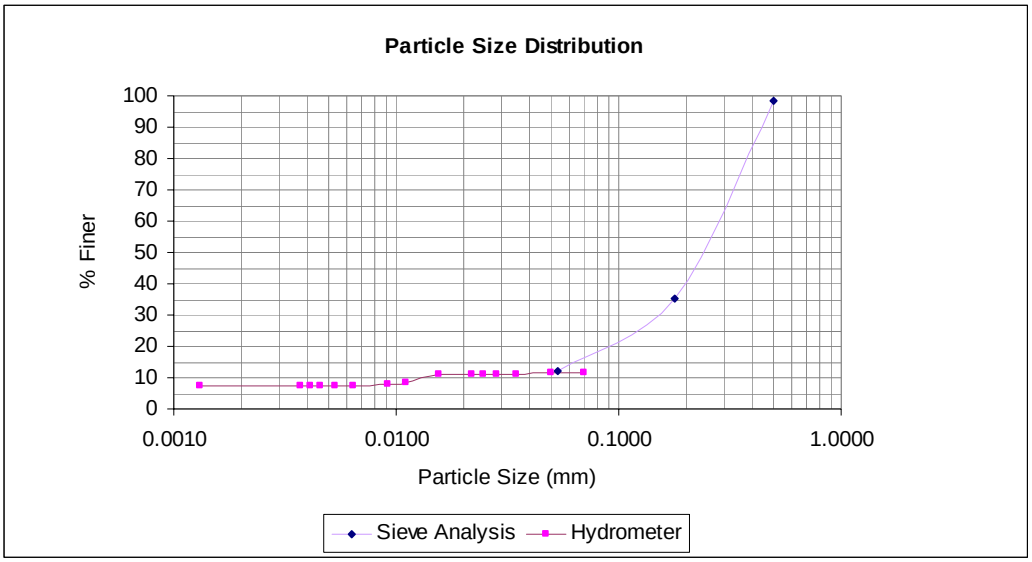

Figure 6.2 Particle size distribution curve for the sample BPT4 600.

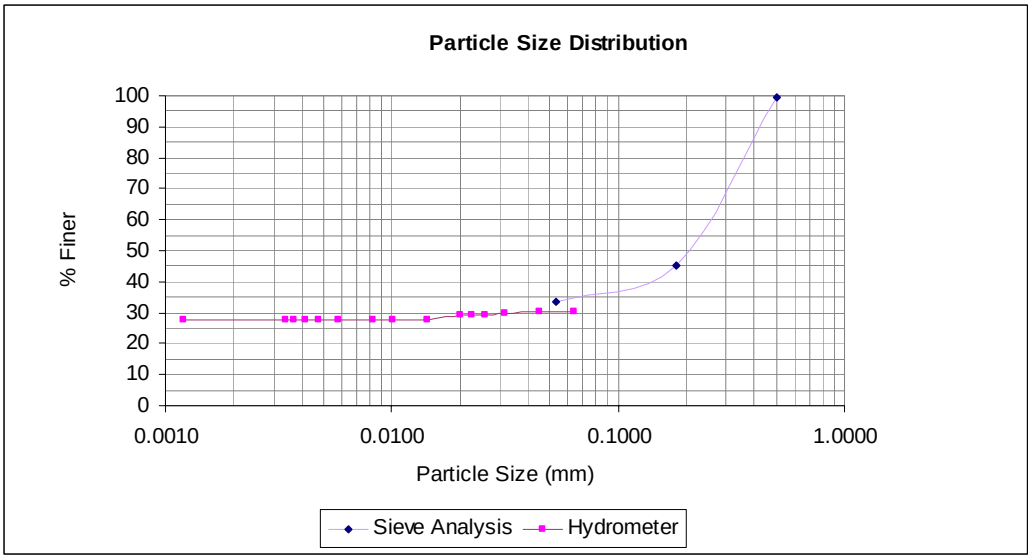

Figure 6.3 Particle size distribution curve for the sample BPT4 1700.

6.2.3 Soil vapour survey

A soil vapour survey was aimed to map the extent of the LNAPLs plume on site by detecting Volatile Organic Carbons (VOCs) contaminants in the vadose zone. Elevated VOC concentrations were an indication of LNAPLs in the vadose zone near the sample location. In the vadose zone equilibrium was established between the volatile fraction of the LNAPLs and other soil gases (?).

In the Joint Fuel Depot site, a soil vapour survey was undertaken using a Photo Ionisation Detector. This instrument measures the VOCs at various points on a grid spacing of between 5 and 20 m in the near-surface soils. Figure 6.4 represents the results in ppm of the survey.

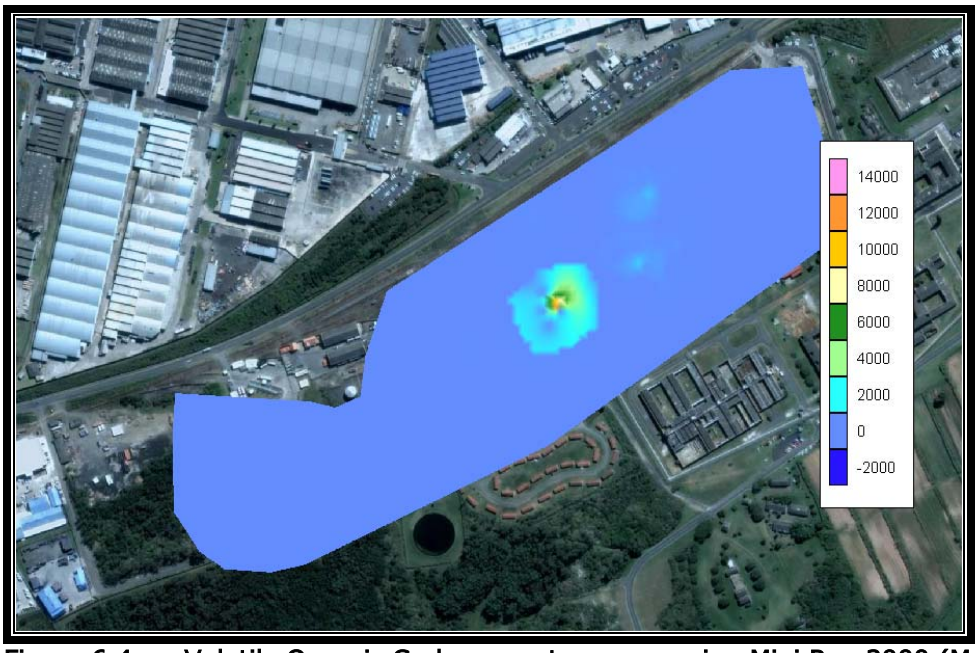

Figure 6.4 **Volatile Organic Carbons contour map using Mini Rae 3000 (Modified after Usher *et al.*, 2009).**

From the results presented in Figure 6.4, the volatile organic carbons were detected more toward the middle and the north of the site.

6.2.4 Contaminant analyses of soils

An organic chemical analysis was performed on soil samples collected across the site on twenty locations, as shown in Figure 6.5.

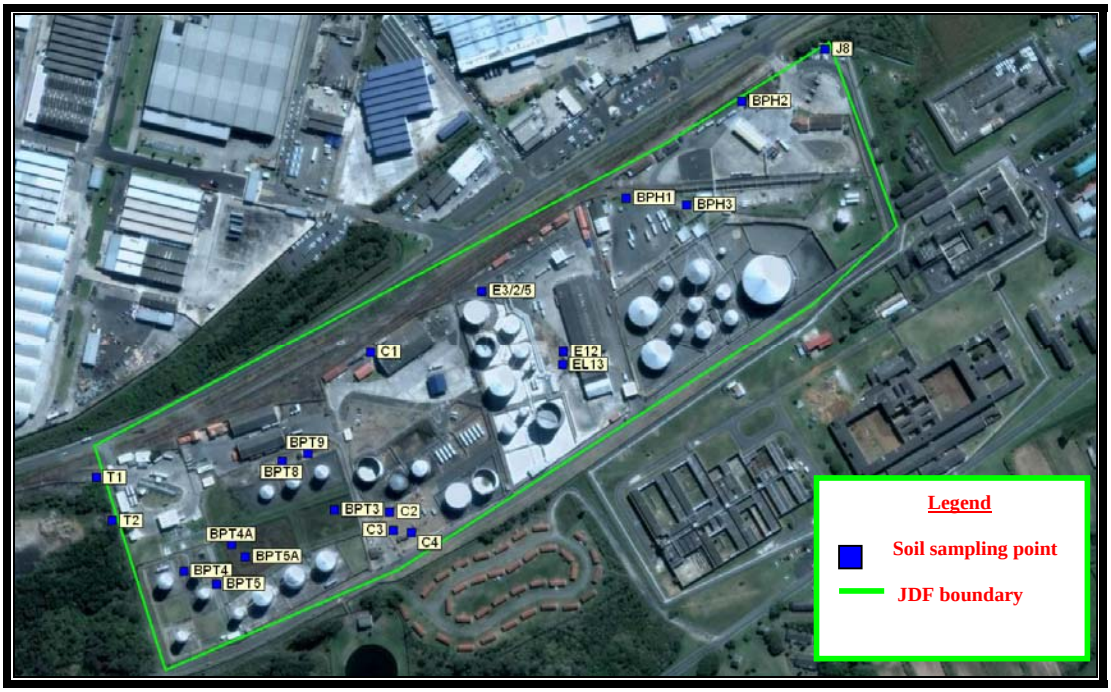

Figure 6.5 **Positions of soil samples submitted for organic analysis (Modified after Usher *et al.*, 2009).**

The results given in Figure 6.6 and 6.7 reveal the contamination of the soil with the heavier fraction of petroleum hydrocarbons toward south-west of the site and with the lighter or more volatile fraction (BTEX and TPH (C5 to C12)) toward the middle of the site. This corresponds well with results from the SVS, where high VOCs were measured in the shallow soil profile.

Figure 6.6 Partial distribution of BTEX (Sum) mg/kg (Modified after Usher *et al.,* 2009).

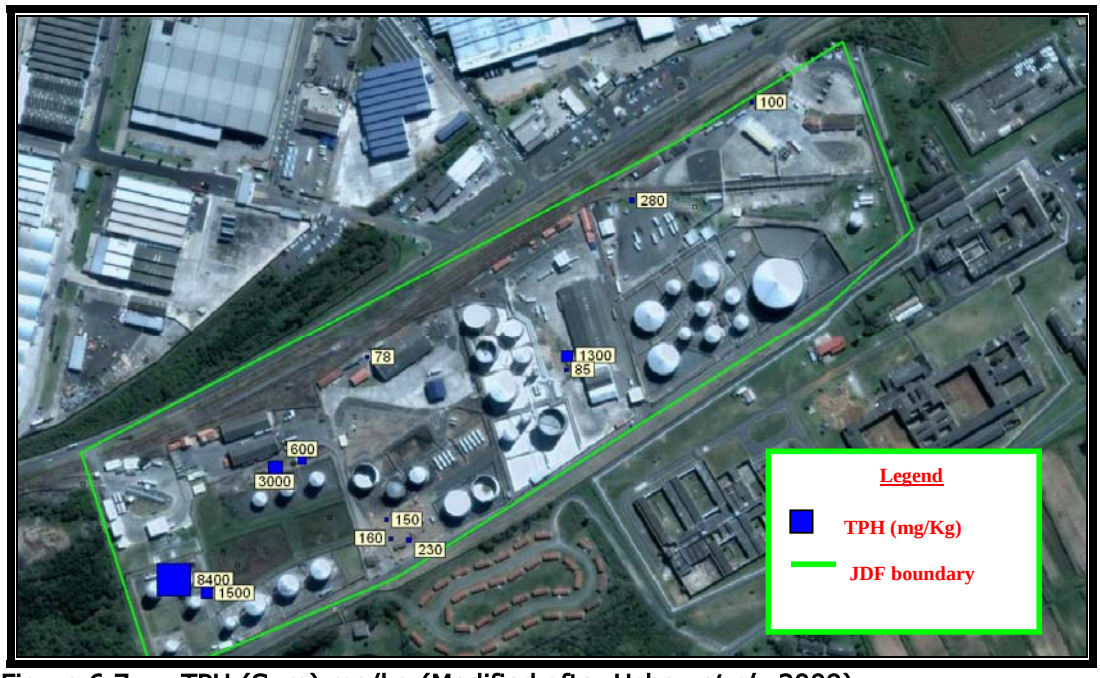

Figure 6.7 TPH (Sum) mg/kg (Modified after Usher *et al.,* 2009).

6.3 Groundwater Testing Results

6.3.1 Analysis of organic parameters

Groundwater samples collected from boreholes across the site were analysed in order to evaluate the presence of petroleum hydrocarbons in the saturated zones. The following figures give the spatial distribution of selected organic parameters measured.

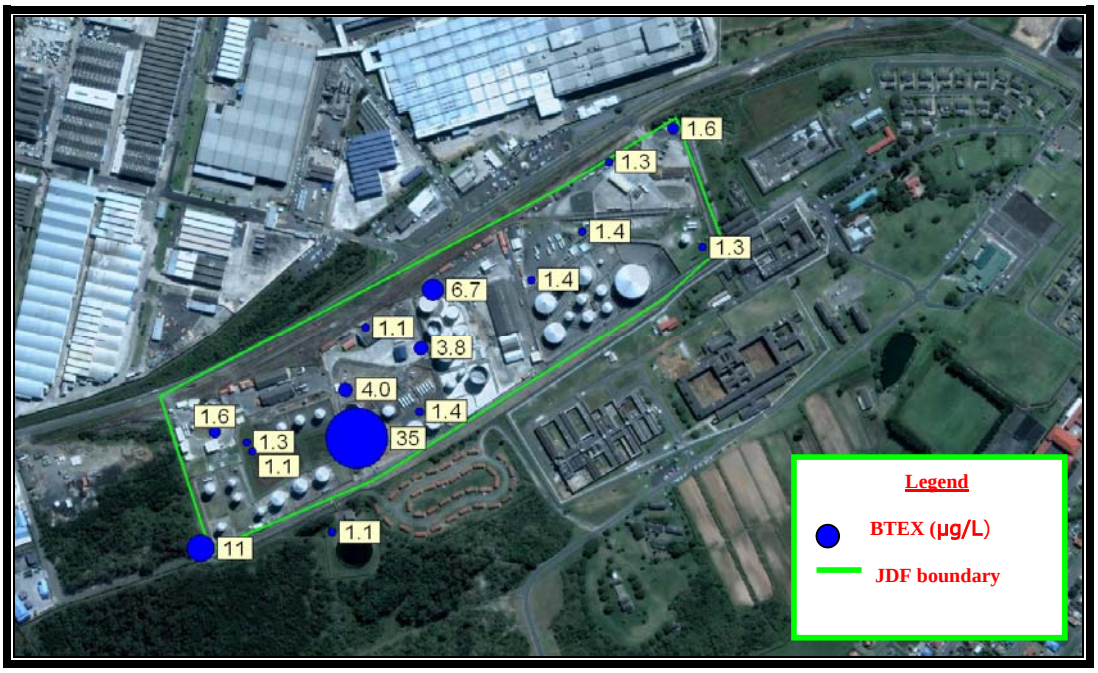

Figure 6.8 Partial distribution of BTEX (Sum) µg/L in boreholes (Modified after Usher *et al.,* 2009).

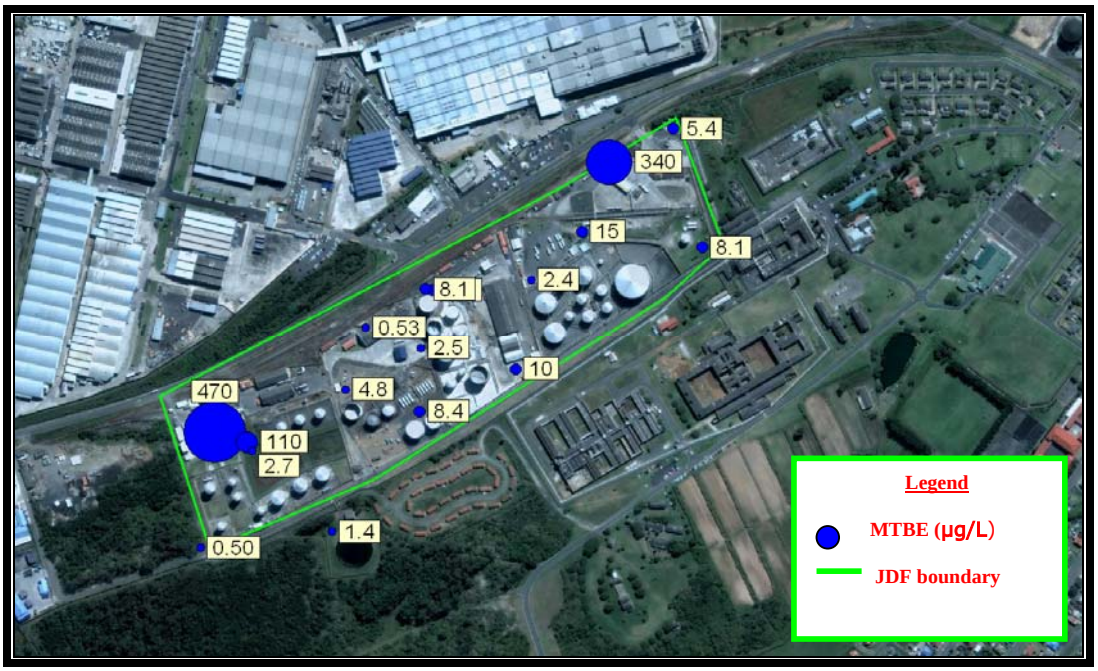

Figure 6.9 Partial distribution of MTBE µg/L in boreholes (Modified after Usher *et al.,* 2009).

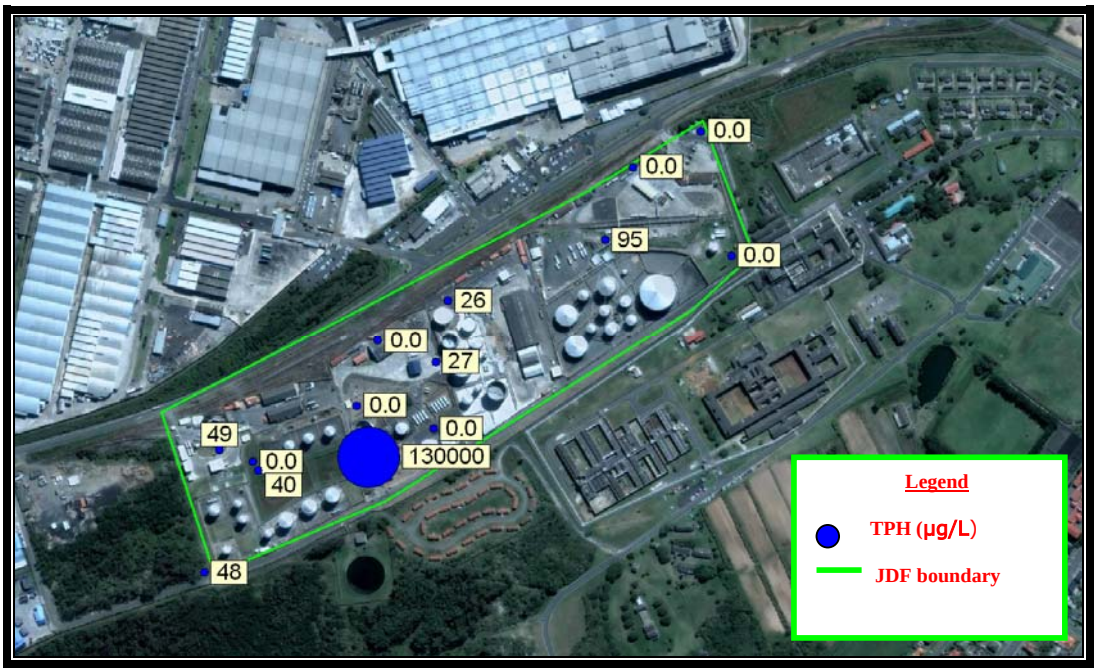

Figure 6.10 Partial distribution of TPH (C10 – C16) µg/L in boreholes (Modified after Usher *et al.,* 2009).

The results above reveal the presence of mobile fractions of the contaminants BTEX and MTBE throughout the site as well as TPH with the highest concentration found in borehole ELD 18, which is located next to CHEV1 and BH5 (refer to Figure 6.14). It is important to notice that high concentration of organic contaminant contributes to deteriorate the quality of the groundwater.

6.3.2 Analysis of inorganic parameters

It is important to verify the evidence of LNAPLs biodegradation on site as this process influences the response of LNAPLs-contaminated soil to the electrical resistivity measurements. The occurrence of biodegradation of the LNAPLs plume in the saturated zones is reflected in spatial changes in concentrations of dissolved electron acceptors (oxygen, nitrate and sulphate) and dissolved biodegradation products (reduced manganese, ferrous iron, hydrogen, organic acids and methane)

Microbial activities in the saturated zone contributed naturally to degrade LNAPLs constituents to organic acid intermediates and finally to carbon dioxide and water. The microbes preferentially use oxygen as an electron acceptor. As oxygen is depleted, other electron acceptors are used, such as nitrate, sulphate, ferric iron and manganese (Cozzarelli and Baedecker 1992, Salanitro *et al.*, 1993). This process results in the depletion of oxygen, nitrate, sulphate, ferric iron, pH, and oxidation-reduction potential measurements and enrichment of ferrous (reduced) iron in the saturated zones (Cozzarelli and Baedecker, 1992, Salanitro *et al*. 1993).

The biodegradation analysis can be done in this study according to data available by verifying whether there are decreases in dissolved NO_3^- and SO_4^{-2} and increases in Mn^{2+} between up-gradient and down-gradient boreholes, as shown in Table 6.2.

Table 6.2 Dissolved groundwater concentration.

Position	BH	Electron Acceptors		Biodegradation transformation products
		Nitrate (NO_3^- mg/l)	Sulphate (SO_4^{-2} mg/l)	Manganese (Mn^{2+} mg/l)
Downgradient Borehole	ENG1	0.81	129	0.755
	ENG2			
Up-gradient Borehole	BPD2	1.07	125	0.626
	RES1			

From the results presented by the table 6.2 above, it appears that the concentrations of acceptors and biodegradation transformation products remain constant in both upstream and downstream boreholes. Therefore, because there is no decrease in the dissolved nitrate and sulphate down-gradient and there is no increase in manganese downgradient, there is no evidence of biodegradation occurring. Consequently, the LNAPLs plume respond to electrical resistivity, as a resistive plume is likely to be evident.

It is important to notice that, in general, the inorganic groundwater quality is good at the site by considering only its salinity. The salinity was firstly observed by using the Durov diagram (Figure 6.11), and secondary, by using Electrical Conductivity (EC) and pH plots (Figure 6.12).

The Durov diagram reveals a high salinity and high chlorite content in the groundwater quality. This is a generally-expected situation in coastal regions. The Electrical Conductivity and pH measurements indicate that, in general, the values are within the ranges of drinking water requirements.

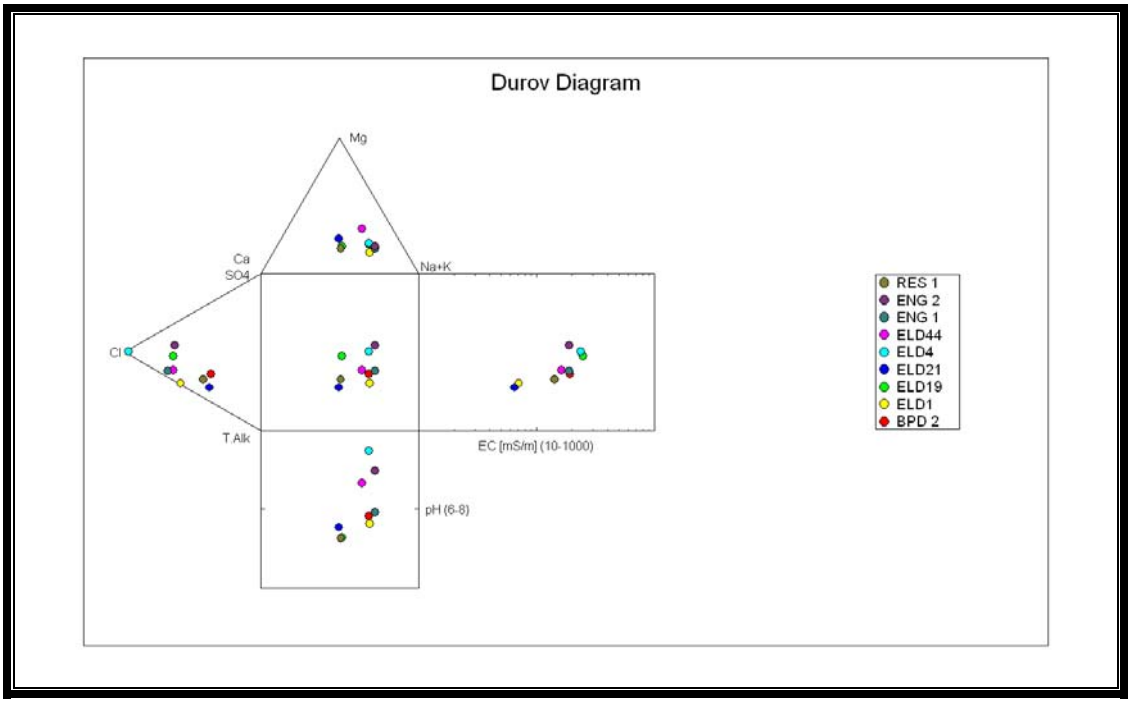

Figure 6.11 Durov diagram for borehole sampled (Modified after Usher *et al.*, 2009).

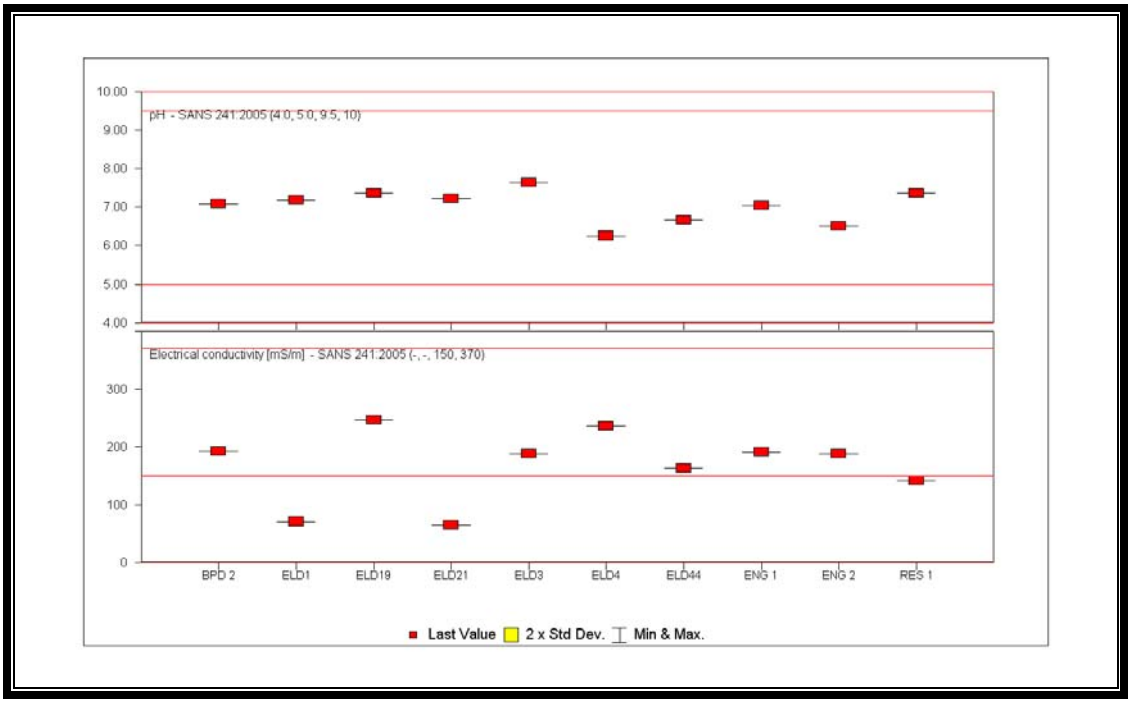

Figure 6.12 EC (mS/m) and pH of sampled boreholes (Modified after Usher *et al.*, 2009).

6.4 Drilling

Six new boreholes were drilled on the Joint Fuel Depot site using the air percussion drilling method (Figure 6.13). The location of the new drilled boreholes on site is shown in the Figure 69 below. These boreholes allowed for characterising the site in terms of its subsurface lithostratigraphy, hydrogeology and LNAPLs contaminant condition.

Figure 6.13 Drilling of borehole BPD1 (Usher *et al.*, 2009).

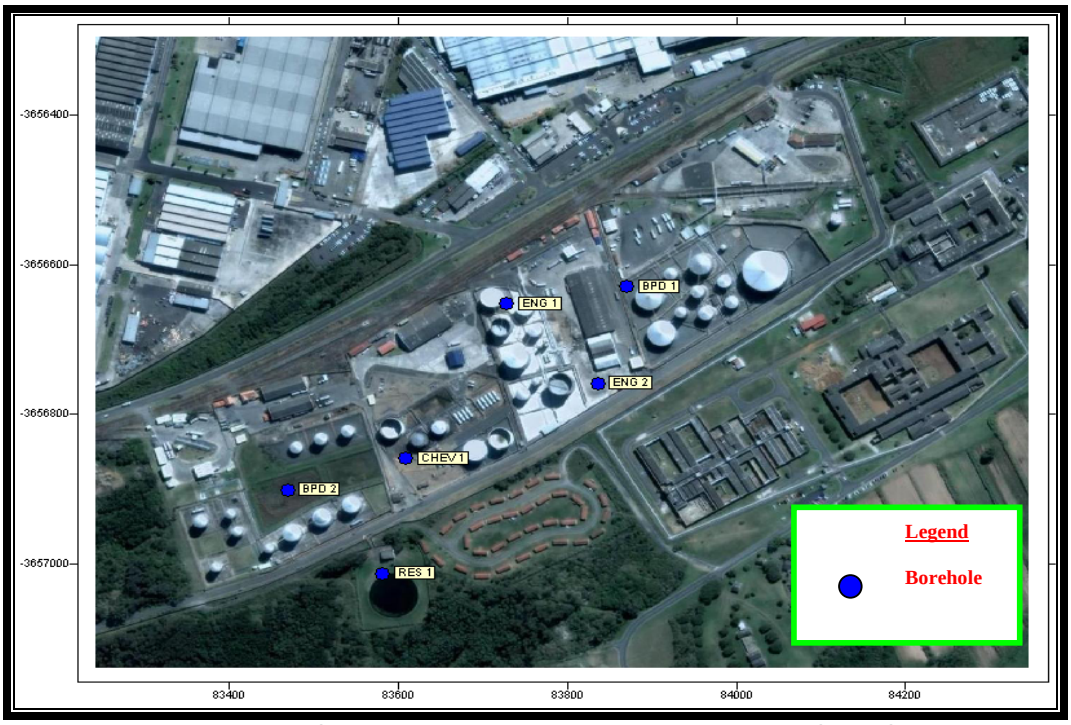

Figure 6.14 Location of the 6 new monitoring boreholes (Modified after Usher *et al.*, 2009).

6.4.1 Geological logs

The geological logs below present the lithology of the site subsurface, together with the position of the water strikes, fractures, weathered zone, water level (WL) below the ground level taken on the 27th of October 2008 and the Volatile Organic Carbons (VOCs) measured in the new boreholes.

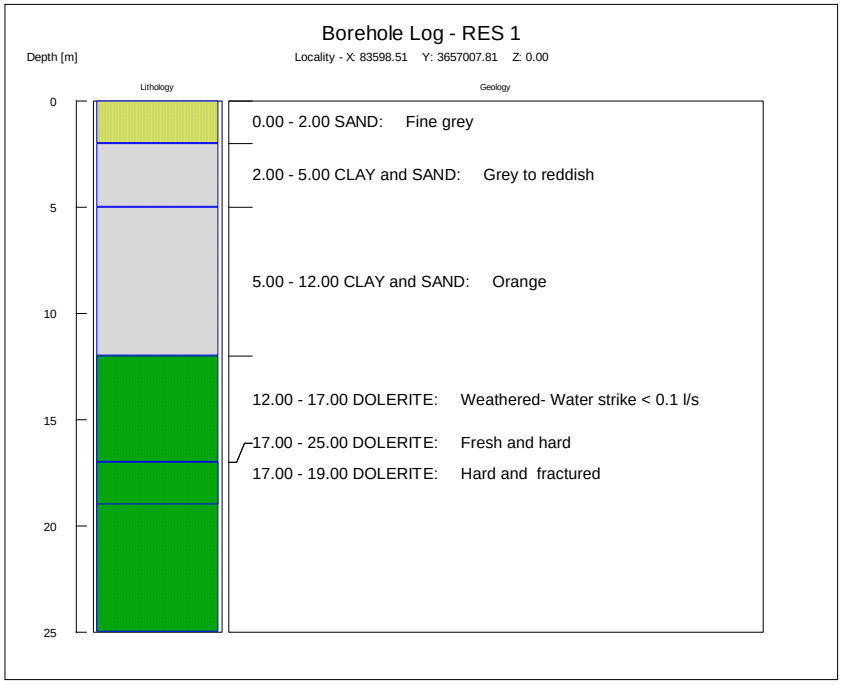

Figure 6.15 Borehole log for RES1 (WL: 10.55m).

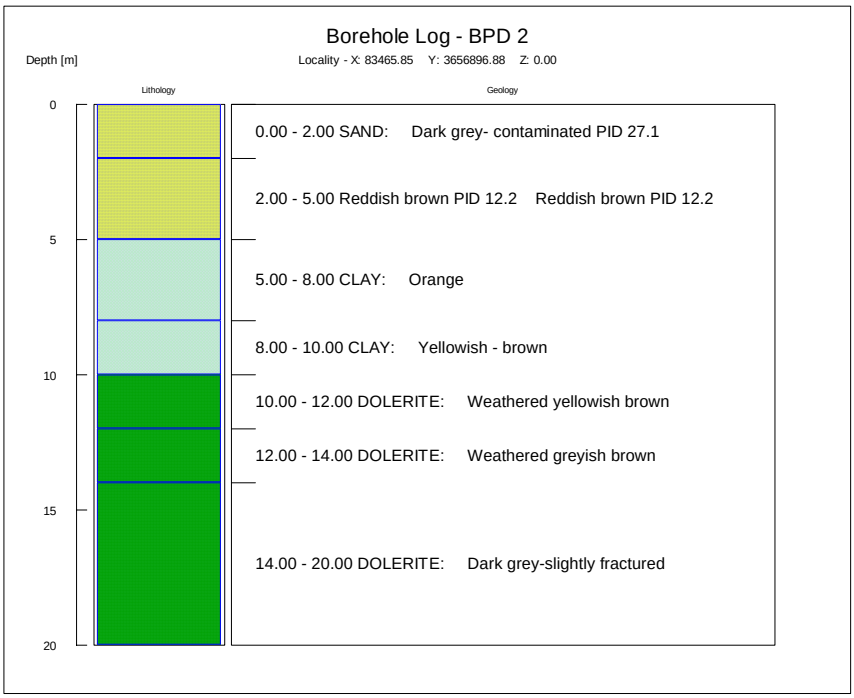

Figure 6.16 Borehole log for BPD2 (WL: 2.62m).

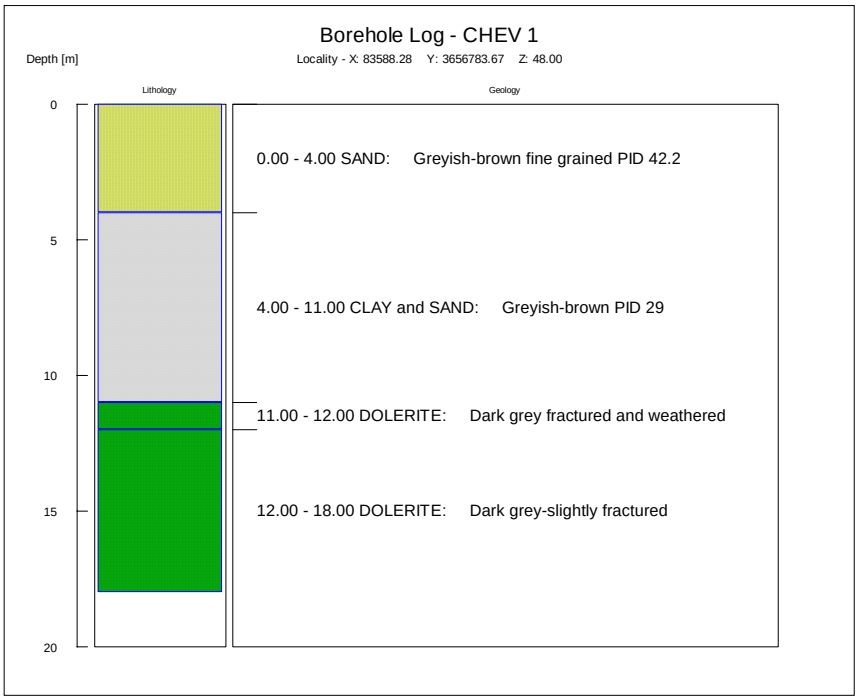

Figure 6.17 Borehole log for CHEV1 located close to ELD18 where free phase was observed (WL: not taken).

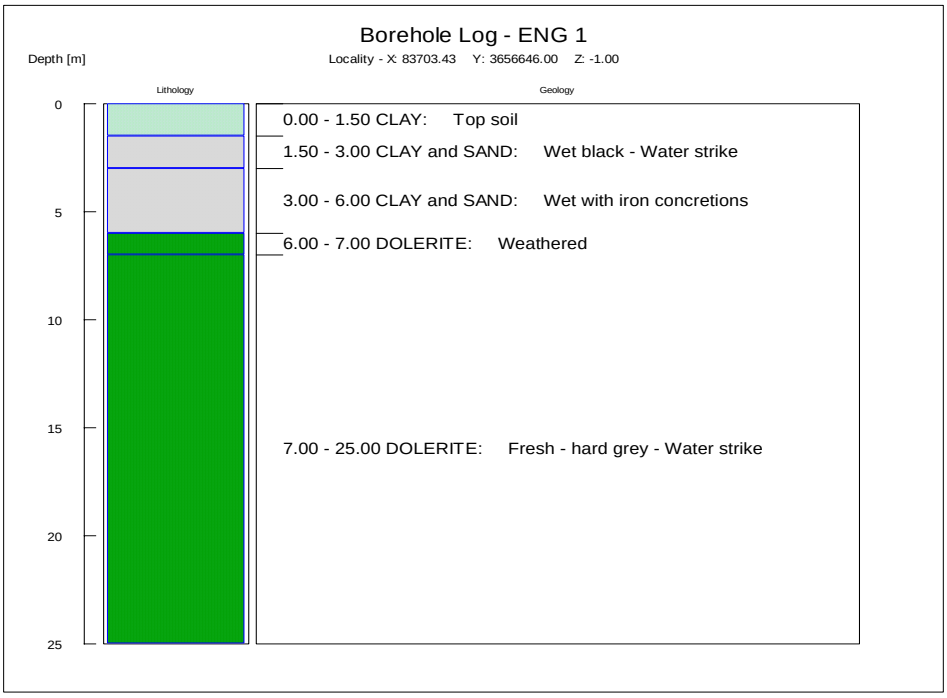

Figure 6.18 Borehole log for ENG1 (WL: 2.68m).

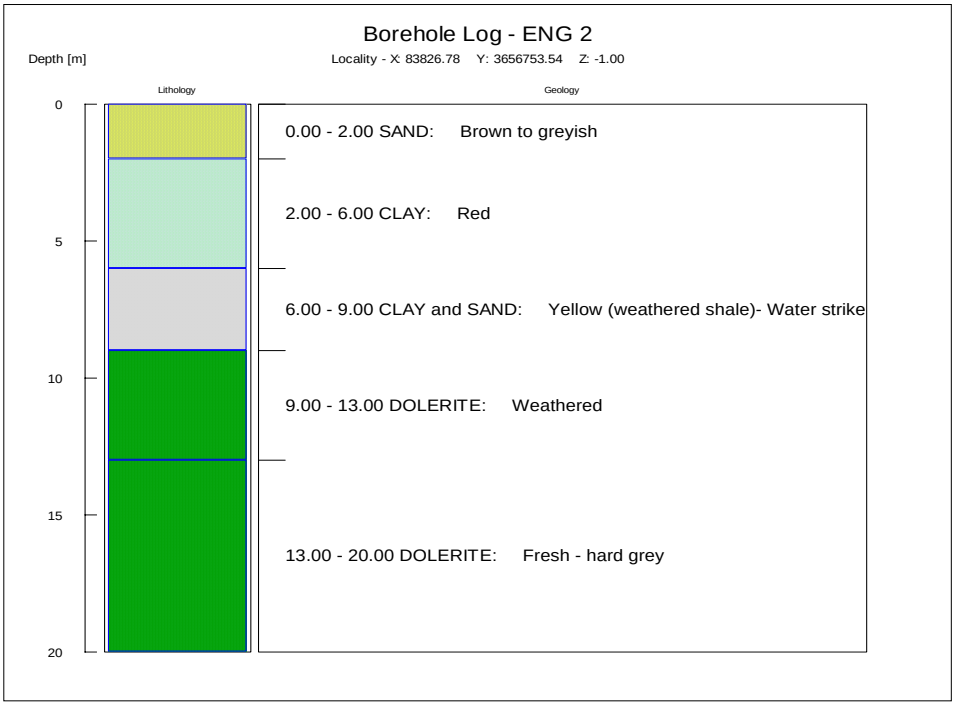

Figure 6.19 Borehole log for ENG2 (WL: 1.47m).

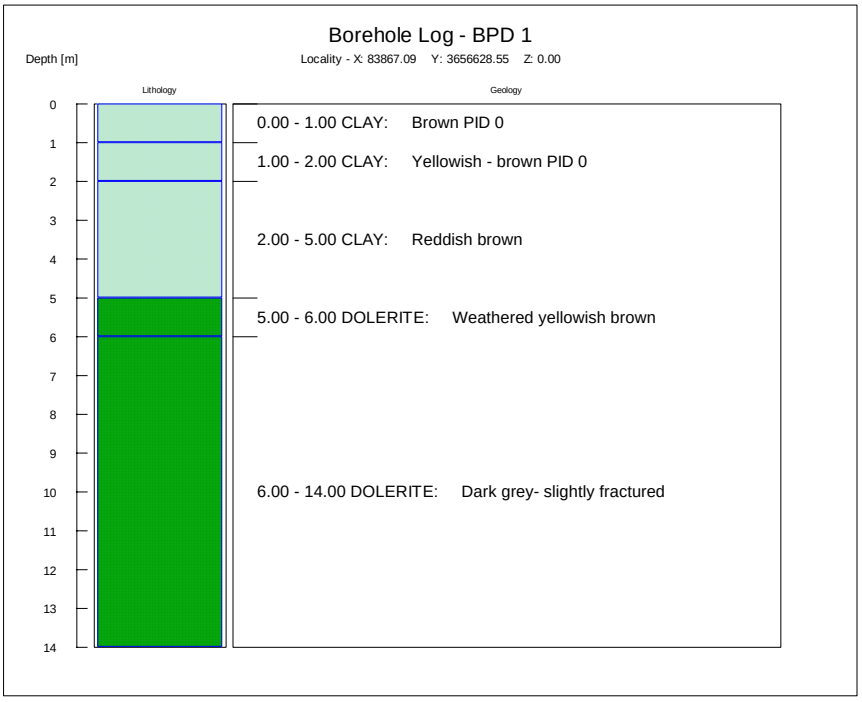

Figure 6.20 Borehole log for BPD1 (WL: 0.2m).

6.4.2 Groundwater level

On the site, the groundwater elevation was found to follow the topography. It decreases with the distance away from the Total site to the BP site toward the north-east. The water table is in the range of 0.6 to 3 m below the ground surface.

Topography versus water level elevations were plotted to determine the correlation between the two. There was a linear relationship with R^2 value of 0.98, as shown in Figure 6.21. For this reason the Bayesian method of interpolation was used to construct a water level contour map of the Joint Fuel Depot site and its surroundings (Figure 6.22). The appendix C gives a table of water level elevation and topography data.

The water level contour map indicates the north-eastern and south-eastern groundwater flow directions (Figure 6.22).

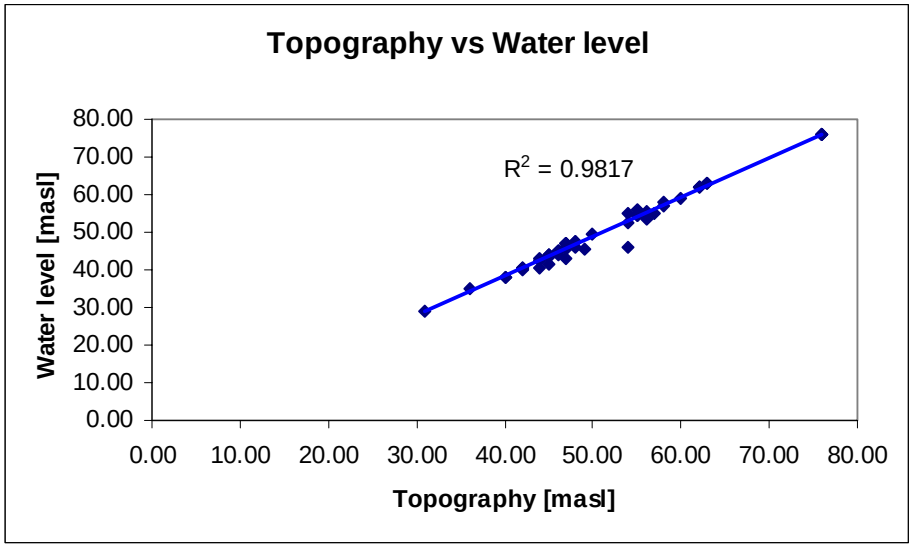

Figure 6.21 Topography versus water level elevations (Usher *et al.,* 2009).

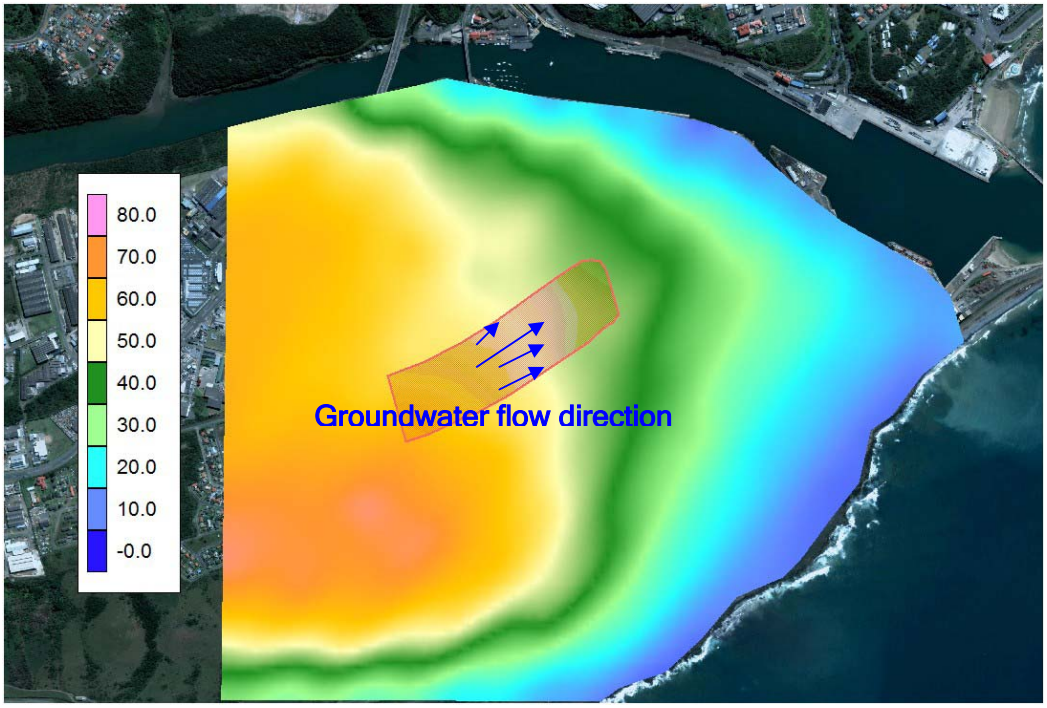

Figure 6.22 Water level contour map of the Joint fuel depot site and surroundings with groundwater flow direction (Modified after Usher *et al.,* 2009).

7. INTEGRATED INTERPRETATION

An integrated interpretation of ERT surveys results and field testing results were aimed to characterise the geological and hydrogeological condition. It aimed to also locate weathered and fractured zones which were considered as preferential flow paths and to detect the presence of hydrocarbon plumes.

The 2-D resistivity survey results obtained on external transects (refer to Figure 5.8) will be compared with field testing results including water levels, boreholes positions and geological logs which describes the geological setting of the site. They are also compared each other in order to identify a general extend of vadose zone, aquifers and bed rock throughout the Joint Fuel Depot.

ERT profiles obtained on internal transects are compared with the results of contaminant analysis of soils and groundwater. An indication of the presence of LNAPLs can be identified by noting anomalously high or low resistivity values. There were high anomalous resistivity values for fresh LNAPLs spills and low anomalous resistivity values for old LNAPLs spills that have been biodegraded over time. These results are also compared with hydrocarbon analyses from soil and water samples in the next section.

7.1 ERT Results for Hydrogeological Characterization

The ERT results have distinguished three major resistivity contrasts related to three geological layers in the following sequence from top to bottom, as shown by ERT results in Figures 7.1, 7.2, 7.3 and 7.4:

- sand : resistive layer > 200 Ωm;
- sand-clay or clay: conductive layer 5-15 Ωm; and
- dolerite sill (resistive layer > 200 Ωm)

The middle layer could be clayey sand or clay, or both a clayey sand layer and a clay layer. Resistivity measurements do not distinguish between groundwater and the clay layer because they fall in the same range of low resistivity values.

From a careful comparison between ERT results on Transects L3, L2 and L5 and the groundwater level measurements, the water table which is located at about 0.6 to 3 m below ground level is consistently coincident with the top of the conductive layer (sand-clay). The water table dips in a southwesterly to northeasterly direction, following the topography of the site. The groundwater therefore flows in the same direction.

Fracture zones and weathered zones can be observed at the top of the third resistive layer which is the dolerite sill. These observations are confirmed by the positions of the fractured and weathered zones on the geological logs.

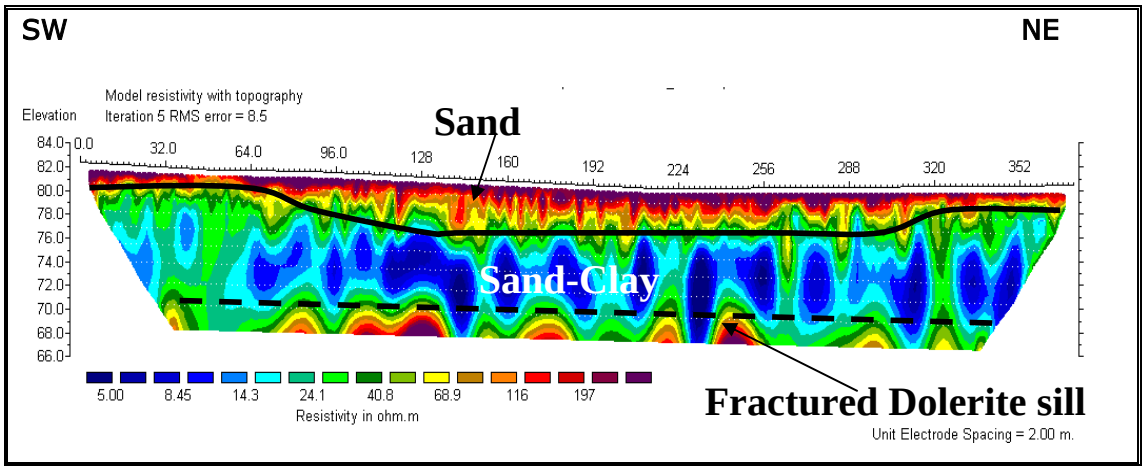

Figure 7.1 ERT results on Transect L3.

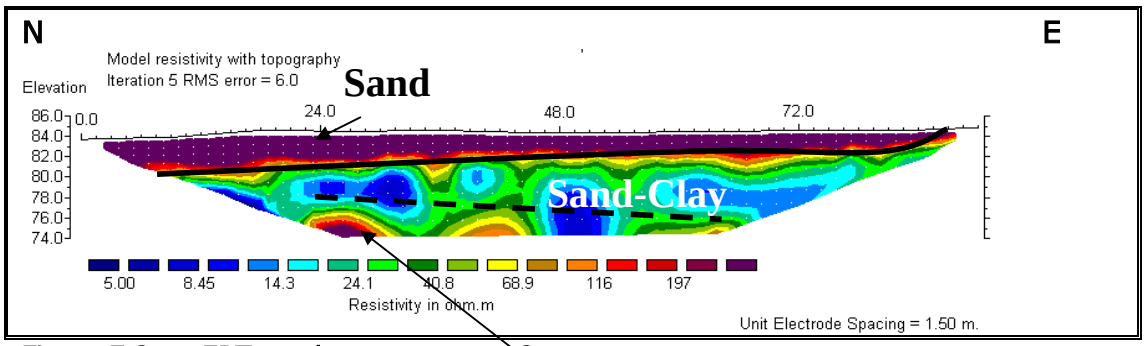

Figure 7.2 ERT results on transect L2a.

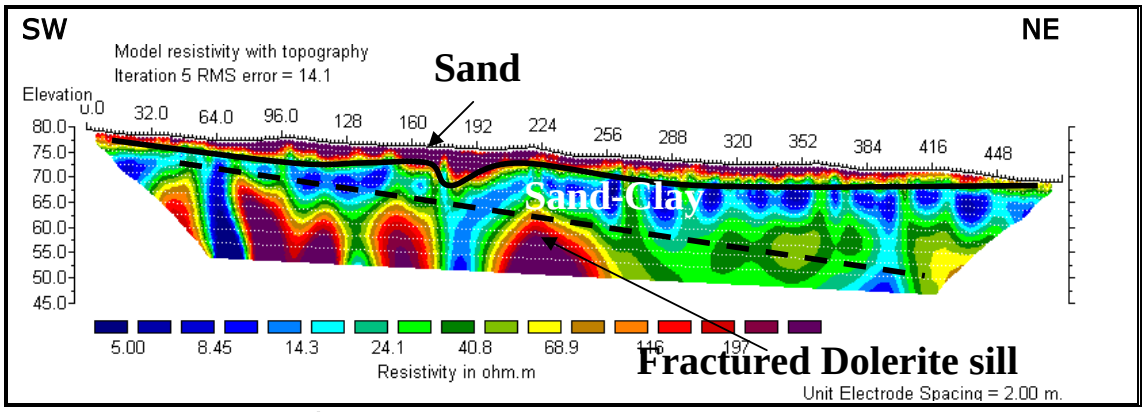

Figure 7.3 ERT results on transect L5.

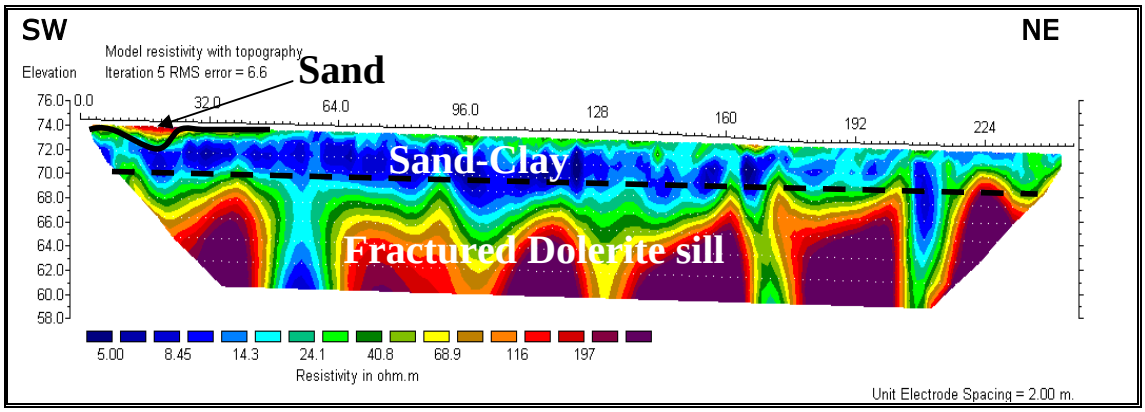

Figure 7.4 ERT result on transect L1.

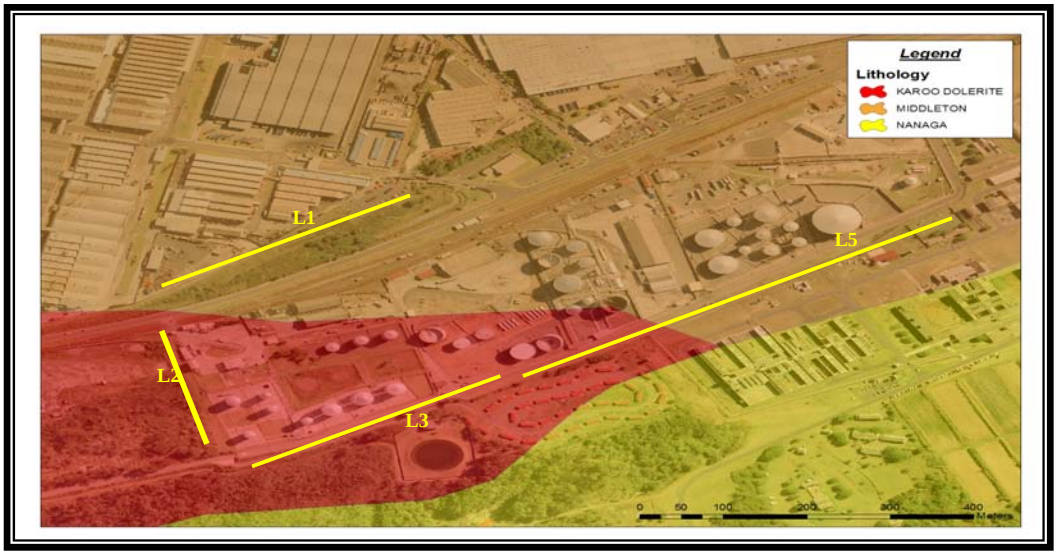

Figure 7.5 Geology with external ERT transects. (Modified form SRK, 2006).

The following are the observations made on the ERT results:

- The overburden dolerite sill interface is dipping SW-NE of the site and located at about 10 m below ground level;
- The inverse model error is very high at 16.4% for line 5 compared to other lines. That means that the measured data was affected by the high level of noise caused by the prison electrical fences located in the proximity of Line 5. The removal of bad data points due to random noise, as required by the inversion process, has cut off a portion of the dolerite sill.
- Because the Wenner array was used, it would be expected to reveal an exaggeration of vertical features. The Wenner array can only resolve horizontal changes accurately, therefore the thickness of fractures and light depressions on the dolerite sill surface were exaggerated by the modelling process (refer to L1 and L5).

7.2 ERT Results for LNAPLs Plume Delineation

The ERT results obtained on Transect 9 present a resistivity anomaly of about 1.5 to 2 m thickness with high resistivity values of more then 200 Ωm. Transect 9 was chosen purposely to be next to borehole CHEV1 where the following higher concentration of petroleum hydrocarbons was measured:

- BTEX : 35µg/L (highest value);
- TPH (C10 – C16) 130000µg/L (highest value);
- PID 42.2 p/pp (highest value); and
- During the site visit, free product was found floating on the groundwater surface in borehole BH5, also located next to the Transect 9.

Referring to Figure 6.7, a total petroleum hydrocarbon of 150 to 350 µg/kg was analysed in soil samples taken around Transect 9. This confirms that the soil is contaminated. Referring to soil vapour survey results in Figure 6.4, 2000 to 10000 p/pp of volatile organic carbon was depicted in the area of Transect 9, as shown on the volatile organic carbon contour map.

According to Du Plooy (2007), the free product found in the wells was analysed for the degree of degradation. It has been concluded that the free product discovered at the lower site originates from a recent spill/contamination event (Du Plooy J., 2007). As discussed in Section 6.3.2 above, the biodegradation transformation of the LNAPLs plume is not evident on site as well as around Transect L9. The ERT results on transect L9 were compared to the results obtained on Transect L12 (Figure 7.7) and Transect L1 (Figure 7.8). It appears that the resistivity anomaly is not present in Transect 12 and Transect L1.

Based on the above observations, the resistivity anomaly under Transect 9 is likely be a no degraded LNAPLs contaminant plume in the sand layer which has probably reached the water table.

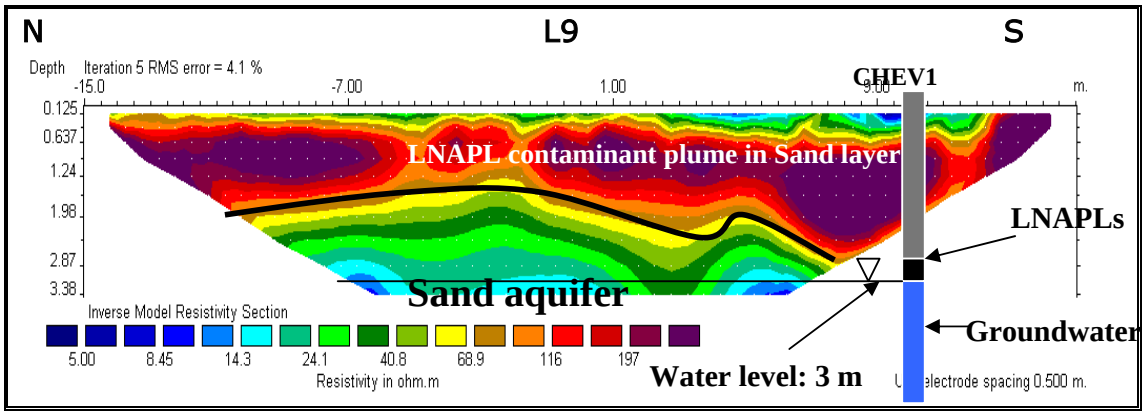

Figure 7.6 ERT result on transect L9.

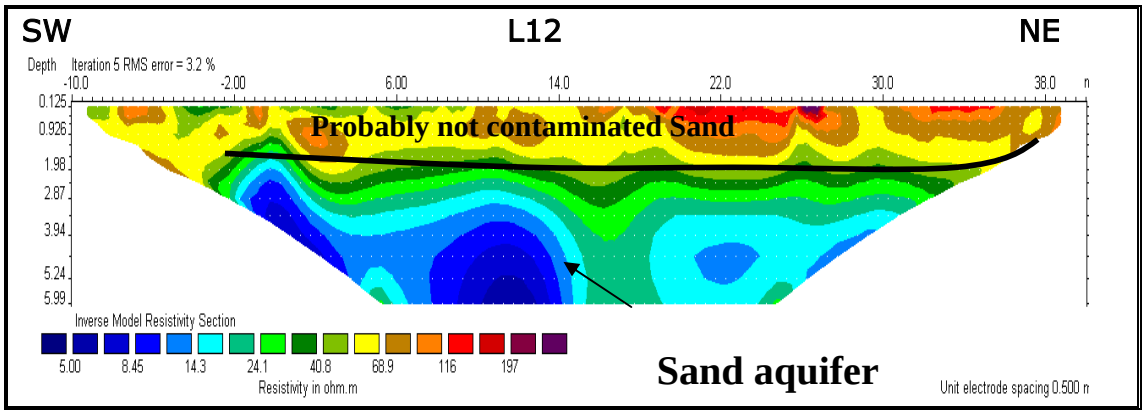

Figure 7.7 ERT result on transect L12.

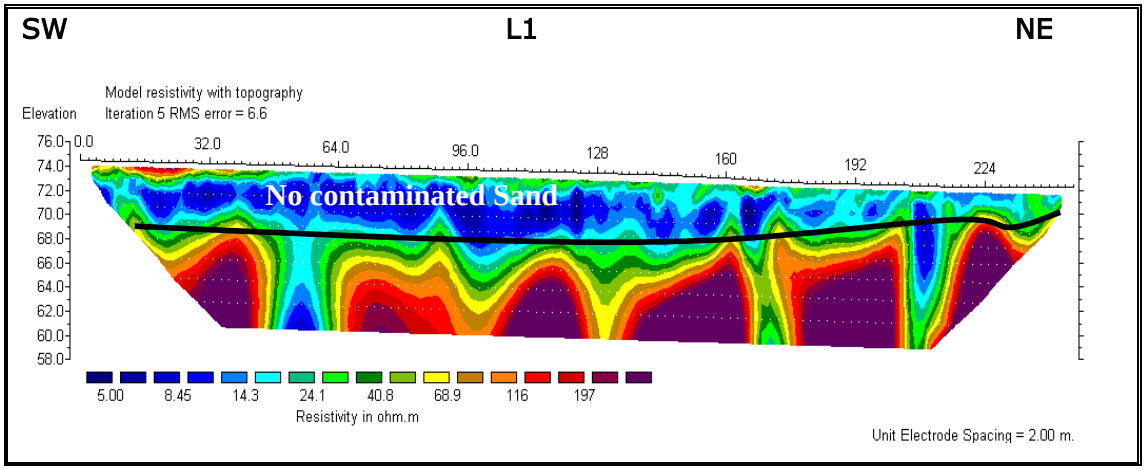

Figure 7.8 ERT result on transect L1.

The Transect 10 which is the closer to L9 than other internal transects, presents the first resistive layer (>200 Ωm). This layer is likely to be the sand layer hosting the LNAPLs contaminant plume.

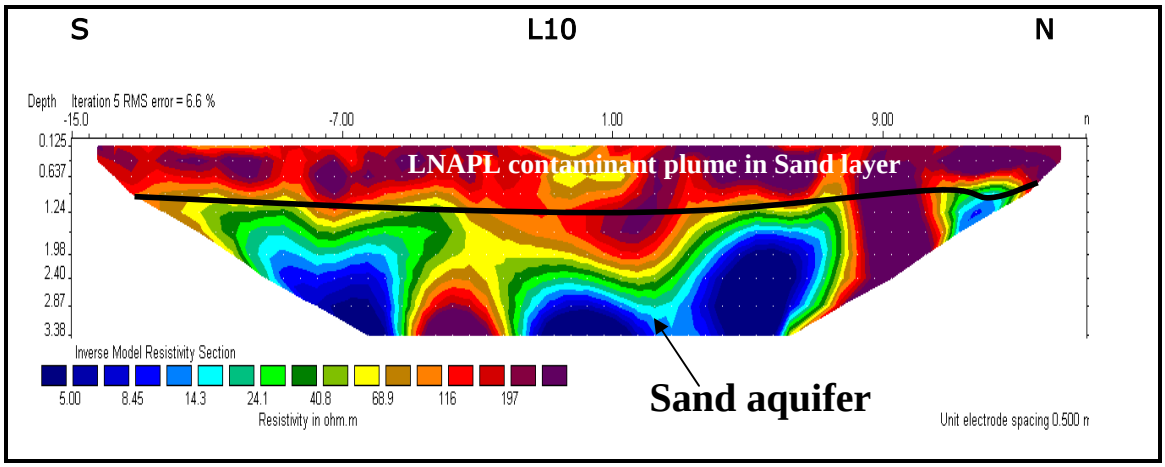

Figure 7.9 ERT result on transect L10.

It was noticed that the more apart an internal transect is from Transect 9, the less resistive their first layers become. Thus Transects L8 and L6 (refer to Figures 7.10 and 7.11) present less resistive (100–200 Ωm) indicating the spatial disappearance of the LNAPLs plume. This is confirmed by the partial distribution of the volatile organic carbons as shown in Figure 61.

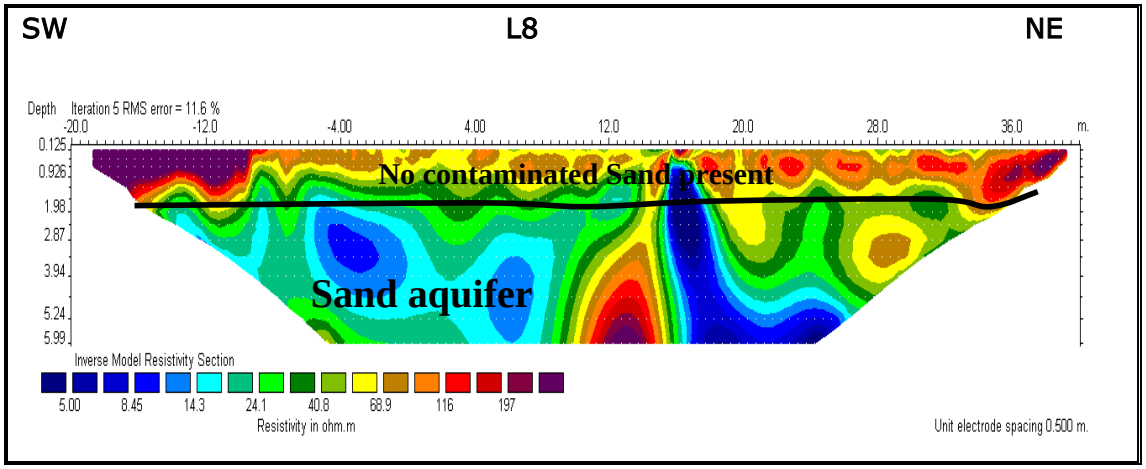

Figure 7.10 ERT result on transect L6.

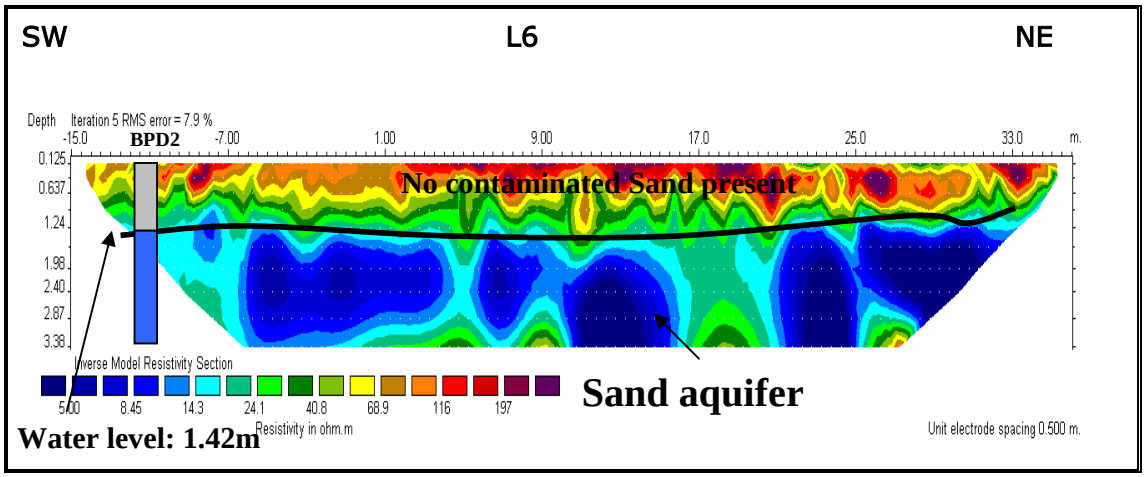

Figure 7.10 ERT result on transect L8.

In conclusion, the ERT results have revealed the presence of the LNAPLs plume by revealing a higher resistivity value (>200 Ωm) around Transect L9, which decreases with the distance away from it. This was confirmed by the partial distribution of volatile organic carbons (Figure 6.4) which coincides with the partial distribution of the LNAPLs contaminant plume on site and the PID measurements in borehole CHEV1 (42.2 p/pp).

8. UPDATED CONCEPTUAL MODEL

The initial conceptual model is updated in this section with information gained from the ERT results and from field testing results in terms of the geology and hydrogeology and in terms of LNAPLs plume delineation.

8.1 Geology and Hydrogeology

8.1.1 Geology of the site

The lithology of the site can be divided into two parts including the upper unconsolidated units or overburden and the lower consolidated unit or bedrock.

- The overburden is the Middleton Formation composed generally from top to bottom of sand, sand-clay and clay. The overburden is about 10 m thick. From the ERT results and borehole geological logs, it appears that the overburden thickness and extent varies;
- The bedrock top surface is located at about 10 m depth. The bedrock is a dolerite sill which is fractured as is revealed in the borehole logs and resistivity section models. The interface between the dolerite sill and the overburden is not a smooth surface, but accidental; and
- The clayey layer in depth which overlay the dolerite sill is likely to be a weathered dolerite.

8.1.2 Hydrogeology of the site

The sub-surface can be divided in two major parts, the unsaturated or vadose zone and the saturated zones or aquifers.

- Vadose zone

The vadose zone is the unsaturated zone composed essentially of fine-grained sand. Because of its higher drainage rate, the sand plays a significant role in the groundwater and LNAPLs movement of the area. The water table in this aquifer which separates the vadose zone from the saturated zone, is located at a depth of about 0.6 to 3 m. A shallow water table aquifer is located in the unconsolidated units which is in sand and clayey sand.

- Aquifers

A fractured aquifer is located in the fractured dolerite sill forming a confined aquifer. A clay layer acting as aquitard separates these two aquifer types. Groundwater will flow in the direction following the topography of the site surface. In this case, the flow direction is therefore in a north-easterly direction toward the Buffalo River and in a south-easterly direction toward the Indian Ocean.

8.1.3 LNPLs delineation

The migration of LNAPLs in the vadose zone toward the groundwater surface is facilitated by the first layer of sand because of its higher drainage rate. Therefore LNAPLs spills that could have happened on site were easily percolated through the vadose zone and eventually reached the water table of the unconfined aquifer.

The lateral migration of LNAPLs is driven by the lateral flow of groundwater in the north-easterly and south-easterly direction of the site. The Buffalo River and Indian Ocean can be considered as eventual receptor zones of LNAPLs contaminants.

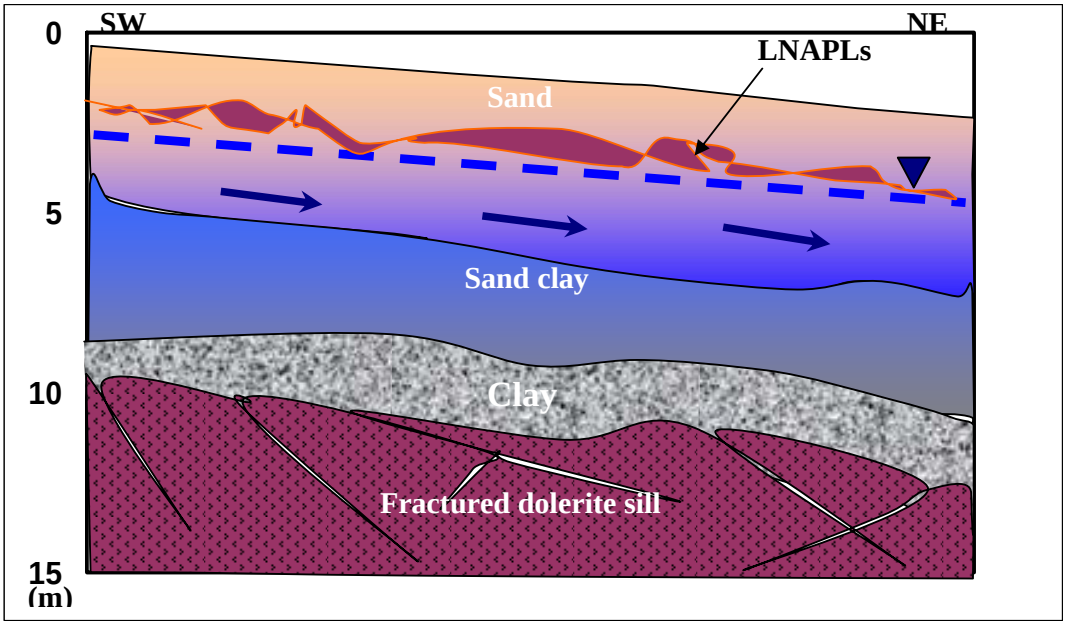

Figure 8.1 Geological and hydrogeological Conceptual representation of the East-London test site. Groundwater and LNAPLs flow North-easterly following the topography.

9. DISCUSSION

9.1 Limitation

The use of the ERT technique to characterise a site contaminated by (LNAPLs) is subject to certain limitations in terms of data acquisition requirements, subsurface conditions of the site, data processing and modelling and varying response of LNAPLs to resistivity measurements.

9.1.1 Data acquisitions requirements

The quality of resistivity data will always influence the quality of the model resistivity image expected. The following factors are considered to be the cause of poor quality data acquisition:

- The setting of 2-D resistivity transect parallel to an elongated good conductor can cause distortion data. Elongated good conductors such as a metallic fence in galvanic contact with the ground, buried metallic pipes or cables with metallic casing, dykes, ditches and streams can divert the electrical current injected during data acquisition and can alter the quality of the data. Therefore data quality can be ensured if the distance between the 2-D resistivity profile and these sources of noise should be set at no less than 1.5 to 2 times the expected penetration depth (www.burval.org); And

- At the Joint Fuel Depot site, typical noisy situation was encountered. Alteration of data quality should be expected as electrical fences, buried metallic pipes and tanks could not be avoided because of confined spaces between them. They were definitely closer to the ERT transect than required. In these conditions more interesting electrode arrays such Dipole-Dipole and Schlumberger were excluded because their ability to discriminate noise is very limited

compared to the Wenner array. The Wenner array used on site is also limited in terms of lower data density.

In order to achieve a good resolution of resistivity images, higher data density is required. Sparse data can cause important features to be overlooked or create false sub-surface images. In the case of the Joint Fuel Depot site, the Wenner array used was a good compromise between noise discrimination and data density. The noisy condition of the site has restricted the ability of the induced polarization methods to distinguish the clay layer from the aquifer. Therefore the clay layer found certain geological logs and could not be resolved by resistivity measurements.

Another limitation related to the surface resistivity investigation is that the resolution decreases as an exponential function of depth (Barker, 1989; Loke and Dalhin, 2002). As the data density decreases with depth, the constraint on the model is greatly reduced in this zone, therefore allowing more alternate solutions. This direct consequence from the basic laws of physics cannot be improved unless borehole measurements are available (Nguyen *et al.,* 2005).

9.1.2 Sub-surface condition of the site

It has been established that the delineation of LNAPLs contaminant or pollution is greatly dependant on the resistivity contrast between the host geological formation and plume. For instance, a fresh LNAPLs spill floating above the water table exhibits a much higher resistivity value in contrast with the conductivity of the aquifer such as a sandy formation (Adepelumi *et al.,* 2006). But once the biodegradation, which contributes to enhancing the conductivity of the LNAPLs plume, has taken place over time, the detection of the LNAPLs contaminant is made difficult (Atekwana *et al.,* 1998).

9.1.3 Data processing

The 2-D electrical resistivity data processing is related to the use of inversion modelling. It consists of converting apparent resistivity values into a resistivity model section that can be used for geological interpretation. The use of the

RES2DINV program, which is numerical model, is limited in covering the true structure of the target. Many factors are responsible for this limitation including the quality and density of the data available for modeling and the smoothing of the model inversion process (Binley *et al.,* 2005).

The removal of bad data points caused by systematic noise before inversion can make the model not reflect the natural system. Using the Wenner array on site, the removal of bad data contributed to create scattered data set which, after modeling, yielded poor resolution. In addition, the Wenner array tends to exaggerate vertical features such as vertical fractures and joints (Binley *et al.,* 2005).

Finally, Olayinka and Yaramanci (2000) suggested that the inversion procedure cannot be very precise because: (i) the solution from the inverse problem is often not unique; (ii) the models determine a continuous function of the space variables, whereas the amount of data is usually finite in real experiments; (iii) when the solution is unique, exact inversion techniques are often unstable; and (iv) real data is often contaminated by noise. Inversion can only provide an approximate guide to the true geometry of the subsurface heterogeneities.

9.2 Applicability

Despite limitations associated with the use of a 2-D electrical resistivity technique to characterize sites contaminated by LNAPLs, several authors have demonstrated the applicability of the technique successfully.

The ERT technique has the ability to detect an area impacted by LNAPLs by imaging anomalies of both low and high resistivity which are confirmed by chemical analysis. Higher resistivity is evident for fresh hydrocarbon spills and low resistivity for degraded hydrocarbons plumes, depending on its residence time in the subsurface (Moreira, 2009). Results obtained at various spill sites around the world are varied and appear to be site- dependent.

Schneider and Greenhouse (1992), affirmed that electrical methods are very useful geophysical techniques in the detection and monitoring of immiscible contaminants in porous soils and rocks due to the large difference in electrical properties between the groundwater and contaminants.

Godio and Naldi (2003) showed the reliability of using the Wenner array of electrical resistivity method in monitoring the effects of induced biodegradation at a contamination site.
In the literature review (refer to Section 2), a number of previous studies on the detection and delineation of subsurface LNAPLs using electrical geophysical methods have been described, indicating the possible effectiveness of these methods.

In the case of the Joint Fuel Depot site, the electrical resistivity tomography has successfully contributed to locate the overburden bedrock interface and the depth of groundwater level. Resistivity contrasts compared to geological logs provided consistency in terms of the lithostratigraphy of the area which includes sand, sand-clay, clay and dolerite sill. Fractured zones and weathered zone are depicted in the dolerite sill as confirmed by the geological logs.

The delineation of the LNAPLs plume in the Joint Fuel Depot site was extremely difficult because of very limited space to undertake proper geophysical surveys and because of the inevitable noisy environment. Nevertheless the ERT result obtained on Transect 9 has contributed by confirming the presence of LNAPLs above the water table, as found in the borehole located nearby and as revealed in the organic and chemical testing.

10. CONCLUSION AND RECOMMENDATIONS

10.1 Conclusion

This study has shown the usefulness and the limitations of using electrical resistivity tomography to characterize the geology, the aquifer condition and the LNAPLs contaminant state of the Joint Fuel Depot site in East London.

In terms of the geology and aquifer conditions, the following findings can be highlighted:

- The resistivity contrasts have contributed to identify the vertical limits and lateral extents of three geological layers interpreted as sand, sand-clay and dolerite sill;
- The identification of fractured zones and weathered zones related to zones of low resistivity zones on the dolerite sill;
- The identification of overburden bedrock interface depth and its dipping direction;
- The identification of water table depth and groundwater direction; and
- The sandy clay and clay interface found in geological logs could not be resolved by resistivity measurements.

In terms of LNAPLs delineation on site, a higher resistivity anomaly was observed under Transect 9, which could be interpreted as being caused by the presence of LNAPLs in the first sandy layer. Factors such as higher concentration of petroleum hydrocarbons and free phase found in the boreholes next to Transect 9 support the interpretation. Therefore the LNAPLs

which infiltrated easily through the sandy layer, migrated in the direction of groundwater flow.

From all these finding a conceptual model of the site is drawn which present the lithostratigraphy of the site, LNAPLs and groundwater flow direction as well as the presence of weathered and fractured zones.

10.2 Recommendations

The following recommendations remain pertinent when electrical resistivity tomography needs to be used for LNAPLs site characterization:

- Boreholes should be drilled on the ERT transects to allow a good correlation between hydrogeological features and resistivity responses.

- Surface electrical resistivity tomography measurements should be combined with downhole resistivity probes to refine characterization of conductive zones associated with the biodegradation of LNAPLs in the subsurface, or resistive zones associated with recent LNAPLs contamination;

- it is recommended that to reduce the inversion ambiguity and so improve the quality of the interpretation, data from several different prospecting methods should be integrated;

- A three-dimensional ERT survey around Transect L9 could be a recommended option to delineate the extent of the LNAPLs contaminant plume; And

- A time-lapse survey is another recommended option that allows for monitoring the changes in resistivity distribution over time.

11. REFERENCES

Aaltonen, J. 2001. Seasonal resistivity variations in some different swedisch soils. Cited in: Samoueliana A., Cousina I., Tabbaghc A., Bruandd A., Richarde G., 2005. Electrical resistivity survey in soil science: a review. *Soil & Tillage Research* 83:173–193.

ABEM. 2005. Instruction Manual, ABEM Instrument AB. ABEM printed Matter 93105. Hamngatan 27, S-17266 Sandbyberg, Sweden.

Acworth, R.I. 1999. Investigation of dryland salinity using the electrical image method. In: Samoueliana, A., Cousina, I., Tabbaghc, A., Bruandd, A. and Richarde G. 2005. Electrical resistivity survey in soil science: a review. *Soil & Tillage Research* 83:173–193.

Adepelumi, A.A., Solanke, A.A., Sanusi, O.B. and Shallangwa, A.M. 2006. Model tank electrical resistivity characterization of LNAPL migration in a clayey-sand formation. *Journal of Environmental Geology*: vol. 50: 1221-1233.

Archie, G.E., 1942. The electrical resistivity log as an aid in determining some reservoir characteristics. Trans. AM. *Inst. Min. Metall. Pet. Eng*. 146:54–62.

Aristodermou, E. and Thomas-Betts, A. 2000. DC Resistivity and Induced polarization investigation at a waste disposal site and its environments. *Journal of Applied geophysics*.

Atekwana, E.A., Sauck, W.A. and Werkema, D.D. Jr. 1998. Characterization of a complex refinery groundwater contamination plume using multiple geoelectrical methods. In: Proceedings the symposium on the application of geophysics to engineering and environmental problems, EEGS, Chicago, 427–436.

ASTM D3114-72. 1982. Method of Test for D-C Electrical Conductivity of Hydrocarbon Fuels. ASTM International, 100 Barr Harbor Drive, PO Box C700, West Conshohocken, PA, 19428-2959 USA.

Baedecker, M.J., Cozzarelli, I.M., Eganhouse, R.P., Siegel, D.I. and Bennett, P.C. 1993. "Crude Oil in a Shallow Sand And Gravel Aquifer: III. Biogeochemical Reactions and Mass Balance Modeling in Anoxic Groundwater". In: ITRC, 2009. Evaluating Natural Source Zone Depletion at Sites with LNAPL. *The Interstate Technology & Regulatory Council LNAPLs Team.*

Barker, R.D. 1989. Depth of investigation of collinear symmetrical four-electrode arrays. *Geophysics*, 54:1031– 1037.

Bernstone, C., Dahlin, T., Ohlsson, T. and Hogland, W. 1998. DC resistivity mapping of internal landfill structures: two pre-excavation surveys. In: Samoueliana, A., Cousina, I., Tabbaghc, A., Bruandd, A. and Richarde, G. 2005. Electrical resistivity survey in soil science: a review. *Soil & Tillage Research* 83:173–193.

Binley, A. and Kemna, A. 2005. DC resistivity and induced polarization methods. *Water science and technology library*, volume 50:129-156.

Binley, A., Cassiani, G., Middelton, R. and Winship, P. 2002. Vadose zone flow model parameterisation using cross-borehole radar and resistivity imaging. In: Samoueliana, A., Cousina, I., Tabbaghc, A., Bruandd, A. and Richarde, G. 2005. Electrical resistivity survey in soil science: a review. *Soil & Tillage Research* 83:173–193.

Botha, J. F., Verwey, J. P., Van der Voort, I., Vivier, J. J. P., Colliston, W. P. and Loock, J. C. 1998. Karoo Aquifers. Their Geology, Geometry and Physical Behaviour. Water Research Commission. South Africa.

Bottraud, J.C., Bornand, M. and Servat, E. 1984b. Mesures de résistivité et étude du comportement agronomique d'un sol. In: Samoueliana, A.,

Cousina, I., Tabbaghc, A., Bruandd, A. and Richarde, G. 2005. Electrical resistivity survey in soil science: a review. *Soil & Tillage Research* 83: 173–193.

Campbell, R.B., Bower, C.A. and Richards, L.A. 1948. Change of electrical conductivity with temperature and the relation of osmotic pressure to electrical conductivity and ion concentration for soil extracts. In: Samoueliana, A., Cousina, I., Tabbaghc, A., Bruandd, A. and Richarde, G. (2005). Electrical resistivity survey in soil science: a review. *Soil & Tillage Research* 83:173–193.

Chevalier, L., Gibson, L.A., Nhleko, L.O., Woodford, A.C., Nomquphu, W. and Kippie, I. 2004. Hydrogeology of fracturedrock aquifers and related ecosystems within the Qoqodala dolerite ring and sill complex, Great Kei catchment, Eastern Cape. WRC Report No. 1238/1/04. Water Research Commission, Pretoria, South Africa.

Christensen, B.N. and Sorensen, K. 1998. Surface and borehole electric and electomagnetic methods for hydrological investigation. *Eur. J. Environ. Eng. Geophys*. 3:75–90.

Cozzarelli, I.M., and Baedecker, M.J. 1992. "Oxidation of Hydrocarbons Coupled to Reduction of Inorganic Species in Groundwater. In: ITRC. 2009. Evaluating Natural Source Zone Depletion at Sites with LNAPL. *The Interstate Technology & Regulatory Council LNAPLs Team*.

Dahlin, T. 2001. The development of DC resistivity imaging techniques. *Computers & Geosciences*, Volume 27:1019-1029.

Dane, J.H. and Topp, G.C. 2002. Methods of Soil Analysis, Part 4, Physical methods. *Soil Science Society of America*, Inc. Madison, Wisconsin, USA.

Dannowski, G. and Yaramanci, U. 1999. Estimation of water content and porosity using radar and geoelectrical measurements. *Eur. J. Environ. Eng. Geophys*. 4:71–85.

Du Plooy, J. 2007. East London Joint Fuel Depot Facility Environmental Contamination Investigation. SRK Project Number 369204. SRK Consulting. Suite 3, Sherwood House, Batting Road, Beacon Bay, East London. 5241, South Africa.

Du Plooy, J. 2006. East London Joint Fuel Depot Facility Contamination Assessment – Desk Study. SRK Project Number 369204. SRK Consulting. Suite 3, Sherwood House, Batting Road, Beacon Bay, East London. 5241, South Africa.

Du Plooy, J. 2008. Geological Mapping Investigation letter report. SRK Project Number 396691. SRK Consulting.Port Elizabeth 6000.

Fukue, M., Minatoa, T., Horibe, H. and Taya, N., 1999. The microstructure of clay given by resistivity measurements. In: Samoueliana, A., Cousina, I., Tabbaghc, A., Bruandd, A. and Richarde G. 2005. Electrical resistivity survey in soil science: a review. *Soil & Tillage Research* 83:173–193.

Garambois, S., Senechal, P. and Perroud, H. 2002. On the use of combined geophysical methods to assess water content and water conductivity of near-surface formations. *J. Hydrol*. 259: 32–48.

Godio, A. and Naldi, M. 2003. Two-dimensional electrical imaging for detection of hydrocarbon contaminants. *Near surface geophysics*, 131-137.

Goyal, V.C., Gupta, P.K., Seth, P.K. and Singh, V.N. 1996. Estimation of temporal changes in soil moisture using resistivity method. In: Samoueliana, A., Cousina, I., Tabbaghc, A., Bruandd, A. and Richarde G. 2005. Electrical resistivity survey in soil science: a review. *Soil & Tillage Research* 83:173–193.

Griffiths, D.H. and Barker, R.D. 1993. Two-dimensional resistivity imaging and modelling in areas of complex geology. *Journal of Applied Geophysics*, 29:211-226.

Gupta, S.C. and Hanks, R.J. 1972. Influence of water content on electrical conductivity of the soil. In: Samoueliana, A., Cousina, I., Tabbaghc, A., Bruandd, A. and Richarde G. 2005. Electrical resistivity survey in soil science: a review. *Soil & Tillage Research* 83:173–193.

Hamzah, U., Ismail, M.A. and Samsudin, A.R. 2009. Geoelectrical Resistivity and Ground Penetrating Radar Techniques in the Study of Hydrocarbon-Contaminated Soil. Sains Malaysiana Vol38(3):305-311.

Hardisty, P.E., Roher, J. and Dottridge, J. 2004. LNAPL Behavior in Fractured Rock:Implications for Characterization and Remediation. In: *2004 U.S. EPA/NGWA Fractured rock conference*: State of the science and Measuring success in Remediation. Maine, Portland, September 13-15 2004:129-134. Holiday Inn by Bay.

Hitzig, R. 1997. Expedited Site Assessment Tools For Underground Storage Tank Sites. A Guide for Regulations. [Internet], *Environmental Protection Agency*, Washington DC, USA. Available from: [http://www.epa.gov/OUST/pubs/esa-ch3.pdf]. [Accessed 12 June 2008].

Johnson, M.R., Anhaeusser, C.R. and Thomas, R.J. 2006. The Geology of South Africa. *Geological Society of South Africa*, Johannesburg, and Council for Geoscience, Pretoria.

Johnson, M.R. and Le roux, F.G. 1994. The Geology of the Grahamstown area Geological Survey of South Africa. In: Du Plooy, J. 2008. 396691/2008 Geological Mapping Investigation letter report. SRK consulting. Port Elizabeth 6000.

Koefoed, O. 1979. Geosounding Principles 1: Resistivity sounding measurements. *Elsevier Science Publishing Company*, Amsterdam.

Lago, A.L., Elis, V.R., Borges, W.R. and Penner, G.C. 2008. Geophysical investigation using resistivity and GPR methods: a case study of a lubricant oil waste disposal area in the city of Ribeira˜o Preto, Sa˜o Paulo, Brazil. *Environ Geol* (2009) 58:407–417.

Loke, M.H. 1999. Electrical imaging surveys for environmental and engineering studies. A practical guide to 2-D and 3-D surveys**.** 5, Cangkat Minden Lorong 6, 11700 Penang, Malaysia.

Loke, M.H. 2004. *Tutorial: 2-D and 3-D electrical imaging surveys*.

Loke, M.H., and Barker, R.D. 1995. Least-square deconvolution of apparent resistivity pseudo-sections. *Geophysics* 60(6):499–523.

Loke, M.H. and Barker, R.D. 1996. Rapid least-squares inversion of apparent resistivity pseudosection by a quasi –Newton method. *Geophysical prospecting* 44: 131-152.

Loke, M.H. and Dalhin, T. 2002. A comparison of the Gauss–Newton and quasi-Newton methods in resistivity imaging inversion. *Journal of Applied Geophysics*, 49:149–462.

McCarter, W.J. 1984. The electrical resistivity characteristics of compacted clays. In: Samoueliana, A., Cousina, I., Tabbaghc, A., Bruandd, A. and Richarde G. 2005. Electrical resistivity survey in soil science: a review. *Soil & Tillage Research* 83:173–193.

Michot, D., Benderitter, Y., Dorigny, A., Nicoullaud, B., King, D. and Tabbagh, A. 2003. Spatial and temporal monitoring of soil water content with an irrigated corn crop cover using electrical resistivity tomography. In: Samoueliana, A., Cousina, I., Tabbaghc, A., Bruandd, A. and Richarde

G. 2005. Electrical resistivity survey in soil science: a review. *Soil & Tillage Research* 83:173–193.

Michot, D., Dorigny, A. and Benderitter, Y., 2000. Mise en évidence par résistivité électrique des écoulements préférentiels et de l'assèchement par le maıs d'un calcisol de Beauce irrigué. In: Samoueliana, A., Cousina, I., Tabbaghc, A., Bruandd, A. and Richarde G. 2005. Electrical resistivity survey in soil science: a review. *Soil & Tillage Research* 83:173–193.

Moreira, C.A. and Braga, A.C.D. 2009. Applications of geophysical methods in monitoring contaminated area under natural attenuation. UNESP, IGCE, Dept Geol Aplicada, BR-13506900 Rio Claro, SP Brazil.

Newell, C.J., Acree, S.D., Ross, R.R. and Huling, S.G. 1995. Light Nonaqueous Phase Liquids, Ground Water Issue. *Environmental Protection Agency*, United States, Washington DC.

Nguyena, F.T., Garambois, S., Jongmans, D., Pirarda, E. and Loke, M.H. 2005. Image processing of 2D resistivity data for imaging faults. *Journal of Applied Geophysics* 57:260–277.

Nowroozi, A.A., Horrocks, S.B. and Henderson, P. 1999. Saltwater intrusion into the freshwater aquifer in the eastern shore of Virginia: a reconnaissance electrical resistivity survey. In: Samoueliana, A., Cousina, I., Tabbaghc, A., Bruandd, A. and Richarde G. 2005. Electrical resistivity survey in soil science: a review. *Soil & Tillage Research* 83:173–193.

Olayinka, A.I. and Yaramanci, U. 2000. Assessment of the reliability of 2D inversion of apparent resistivity data. *Geophys. Prospec*. 48:293–316.

Pretorius, J.A., Usher, B.H., Gomo, M., Reyneke, R., Linde, G., Surridge, K., Lorentz, S., Gemel, A. and Ngeleka, J. (2008). Field investigations to study the fate and transport of light non-aqueous phase liquids (LNAPLs) in groundwater: Deliverable 2: Literature Review. Published by the Water research Commission, Pretoria, South Africa.

Rhoades, J.D., Raats, P.A.C. and Prather, R.J. 1976b. Effect of liquid phase electrical conductivity, water content, and surface conductivity on bulk soil electrical conductivity. In: Samoueliana, A., Cousina, I., Tabbaghc, A., Bruandd, A. and Richarde G. 2005. Electrical resistivity survey in soil science: a review. *Soil & Tillage Research* 83:173–193.

Robain, H., Descloitres, M., Ritz, M. and Atangana, Q.Y. 1996. A multiscale electrical survey of a lateritic soil system in the rain forest of Cameroon. In: Samoueliana, A., Cousina, I., Tabbaghc, A., Bruandd, A. and Richarde G. 2005. Electrical resistivity survey in soil science: a review. *Soil & Tillage Research* 83:173–193.

Ruxton, B.P. and Berry, L. 1957. Weathering of granite and associated erosional features in Hong Kong, Bull. In: Gioa, P.H., Weller, A., Hien, D.H. and Adisornsupawat, K. (2008). An approach to construct the weathering profile In hilly granitic terrain based on electrical imaging. *Journal of Applied Geophysics*, volume 65:30-38.

Samoueliana, A., Cousina, I., Tabbaghc, A., Bruandd, A. and Richarde, G. 2005. Electrical resistivity survey in soil science: a review. *Soil & Tillage Research* 83:173–193.

Sauck, W.A. 2000. A model for the resistivity structure of LNAPL plumes and their environs in sandy sediments. *J. Appl. Geophys*. 44:151–165.

Schneider, G.W. and Greenhouse, J.P. 1992. Geophysical detection of perchloroethylene in a sandy aquifer using resistivity and nuclear logging technique. *Proceedings of the symposium on the application of geophysics to engineering and environmental problems*, EEGS,619–628.

Shea, P.F. and Luthin, J.N. 1961. An investigation of the use of the fourelectrode probe for measuring soil salinity in situ In: Samoueliana, A., Cousina, I., Tabbaghc, A., Bruandd, A. and Richarde G. 2005. Electrical resistivity survey in soil science: a review. *Soil & Tillage Research* 83:173–193.

Slater, L. and Reeve, A. 2002. Investigation peatland stratigraphy and hydrogeology using integrated electrical geophysics. *Geophysics* 67:365–378.

Technos, Inc. 2005. Characterizing Karst and Pseudokarst. Volume 4, Issue 2. Terrace Miami, Florida 33172.

Telford, W.M., Geldart, L.P. and Sheriff, R.E. 1990. *Applied Geophysics* (second edition). Cambridge University Press.

Usher, B.H., Van Tonder, G.J., Steyl, G., Gomo, M., Vermaak, K., Bothwell, J., Pretorius, J.A., Reyneke, R., Vd Linde, G., Surridge, K., Lorentz, S., Ngeleka, J., Sikosana, S., Dlamini. M., Zondi, N., Revil-Bourdard, S., Cock, B., Du Plooy, J., Nel, G., vBiljon, W. and Mohr, S. (2009). Field investigations to study the fate and transport of light non-aqueous phase liquids (LNAPLs) in groundwater: Deliverable 3: Initial Field Results. Published by the Water research Commission, Pretoria, South Africa.

Van der Voort, I and Van Tonder, G.J. 2001. Matrix diffusion: Is it important? In New Approaches characterizing groundwater flow (P. 667-672). Edited by Klaus-Peter Seiler and Stefan Wohnlich. *IAH Conference*, Munich, Sept. 2001.

Vegter, J.R. 2001. Groundwater development in South Africa and an introduction to the hydrogeology of groundwater regions. Water Research Commission. Report No TT134/00.

Walker, F. and Poldervaart, A. 1949. Karroo Dolerites of the Union of South Africa. In: Johnson, M.R., Anhaeusser, C.R. and Thomas, R.J. 2006. *The Geology of South Africa*. Geological Society of South Africa, Johannesburg, and Council for Geoscience, Pretoria.

Yaramanci, U. 2000. Geoelectric exploration and monitoring in rock salt for the safety assessment of underground waste disposal sites. In: Samoueliana, A., Cousina, I., Tabbaghc, A., Bruandd, A. and Richarde G. 2005. Electrical resistivity survey in soil science: a review. *Soil & Tillage Research* 83:173–193.

Zhou, Q.Y., Shimada, J. and Sato, A. 2001. Three-dimensional spatial and temporal monitoring of soil water content using electrical resistivity tomography. In: Samoueliana, A., Cousina, I., Tabbaghc, A., Bruandd, A. and Richarde G. 2005. Electrical resistivity survey in soil science: a review. *Soil & Tillage Research* 83:173–193.

Zhou, W., Beck, B.F. and Adams, A.L. 2002. Effective electrode array in mapping karst hazards in electrical resistivity tomography. *Environmental Geology* (2002) 42:922–928.

www.burval.org, 4.5 Geoelectrical methods (accessed 15th November 2009).

APPENDIX A

Profile Descriptions and Initial Water Content

BP1				
Depth	mass wet (g)	mass dry (g)	water content (g/g)	Profile Description
300	38.04	37.94	0.003	fine(roots) sand with fine black (organic) material
600	35.62	35.54	0.002	fine sand lighter in color
900	38.67	38.48	0.005	transition zone where below there is darker material with pegs forming
1200	51.34	42.85	0.198	darker and wetter fine sands with slight ped formation(consolidation)
1500	40.88	36.58	0.118	
1800	40.87	36.92	0.107	
2100	29.76	28.85	0.032	
BPT1				
Depth	mass wet (g)	mass dry (g)		Profile Description
300	30.78	29.48	0.044	fine sand with ped formation
700	43.1	37.99	0.135	fine sand to silty material
900	31.25	27.54	0.135	red mottling very sticky material
1200	48.73	41.63	0.171	colour changes to red with depth
1600	32.61	29.1	0.121	
2000	27.76	27.51	0.009	
2500	29.71	27.14	0.095	
2800				
BPT4				
Depth	mass wet (g)	mass dry (g)		Profile Description
600	40.87	34.99	0.168	fines with a black taint possible organics
1300	50.94	42.93	0.187	increasing clay content; signs of greying (mottles) (G)
1700	83.66	45.81	0.826	
BPT6				
Depth	mass wet (g)	mass dry (g)		Profile Description
300	34.88	33.87	0.030	Concrete pebble size materials in fine sands. Dense reddish brown mass
600	42.73	40.48	0.056	
2100	94.28	85.09	0.108	
Be 2 (BACK ROAD)				
Depth	mass wet (g)	mass dry (g)		Profile Description
500	38.22	31.98	0.195	grey soil displaying signs of alluviation

D1				
Depth	Mass wet (g)	mass dry (g)		Profile Description
300	28.62	28	0.022	fine loose silty material greyish black in colour
1500	48.7	43.27	0.125	consolidated silty material with orange mottling
E1				
Depth	mass wet (g)	mass dry (g)		Profile Description
300	28.07	25.58	0.097	small consolidated pegs
700	36.86	33.29	0.107	fine wetter material possible an E-horizon
950	39.42	32.63	0.208	
1050	35.92	29.18	0.231	
1200	33.08	23.48	0.409	
1400	41.32	32.62	0.267	perceived higher clay, black color
1700	29.23	26.05	0.122	
1800	40.63	36.21	0.122	
1900	46.16	45.4	0.017	black consolidated material
E3				
Depth	mass wet (g)	mass dry (g)		Profile Description
300	43.33	38.04	0.139	Reddish yellow mottled fine material
600	17.18	14.46	0.188	
900	35.6	29.37	0.212	
1200	29.25	25.07	0.167	
1500	54.43	45.57	0.194	
1800	50.35	41.88	0.202	black/grey silty sandy material
2000	50.79	41.96	0.210	getting finer with depth
2100	39.56	28.65	0.381	black clayey material
2300	51.13	41.14	0.243	signs of eluviation material appears grey to white
2500	18.26	15.88	0.150	
2900	65.41	52.88	0.237	
E5				
Depth	mass wet (g)	mass dry (g)		Profile Description
300				
600				
900				
1200				
1500				
1800				
2100				

E7				
Depth	mass wet (g)	mass dry (g)		Profile Description
300	17.93	16.77	0.069	black material in fine matrix
400	15.61	14.93	0.046	becoming lighter/pale in colour with depth
600	23.78	21.88	0.087	
900	25.08	22.61	0.109	grey ped size material
1200	40.17	30.8	0.304	
1500	39.72	31.17	0.274	Black dense and consolidated
1900	26.42	23.84	0.108	hard black mass
2-3 ends	14.31	11.2	0.278	fine sands reddish yellow possible parent material
E9				
Depth	mass wet (g)	mass dry (g)		Profile Description
300	27.47	9.56	1.873	fine black soil
600	40.42	36.58	0.105	light coloured fine material could be through eluviations
1000	36.45	28.21	0.292	there is progressive darkening with depth
1200	48.45	41.18	0.177	
1400	58.55	50.28	0.164	the material feels denser
1700	37.03	32.09	0.154	possible a greyed horizon
E11				
Depth	mass wet (g)	mass dry (g)		Profile Description
300	35.16	33.59	0.047	
600	52.63	44.99	0.170	
900	25.77	22.3	0.156	small peds orange in colour
1000	33.61	28.6	0.175	orange coloured soil with signs of greying
1200	33.42	26.65	0.254	
1400	52.59	42.23	0.245	
1700	25.85	20.7	0.249	angulated peds orange in colour consistent with depth
2000	37.53	30.3	0.239	
J1				
Depth	mass wet (g)	mass dry (g)		Profile Description
0-300	28.26	27.87	0.014	
300-600	22.96	22.71	0.011	
600-900	23.79	23.41	0.016	
900-1200	33.17	32.25	0.029	
1200-1500	33.11	31.83	0.040	fine sands throughout the profile
1500-1800	54.63	48.77	0.120	
1800-2100	36.07	33.43	0.079	
2100-2400	39.11	35.28	0.109	
2400-2700	28.26	25.02	0.129	orange colour coming up
2700-3000	20.17	16.71	0.207	
3000-3300	34.11	29.21	0.168	from this point clayey prevail still with depth
3300-3600	36.07	31.78	0.135	
3600-3900	27.15	23.04	0.178	orange clays

J4				
0-300	28.03	25.8	0.086	fine sands
1000	30.56	27.46	0.113	dark material
2000	31.35	26.28	0.193	increased clay, black and red orange
2500	32.7	28.67	0.141	high clay content and black colour reduced
4000	26.54	22.02	0.205	no more orange colour black is reduced. Clay is high
TS1				
1000	33.01	31.17	0.059	material bright orange and consolidated
1500	39.82	36.39	0.094	
2000	43.83	37.43	0.171	orange in colour becoming angular peds

BP5				
Depth	mass wet (g)	mass dry (g)	water content (g/g)	Profile Description
300	34.18	33.85	0.010	fine sand dark in color with dense roots
600	28.52	28.42	0.004	light colored fine sand
900				dark and light material consolidated
1200	41.31	39.99	0.033	below this depth very dark material prevails
1500	43.34	42.3	0.025	with slight ped formation (consolidation)
1800				
BPT2				
Depth	mass wet (g)	mass dry (g)		Profile Description
300-500-700	39.37	36.07	0.091	fine material with signs of mottling
900	31.64	28.35	0.116	material gets more sticky with depth hence clay content increase
1800	37.98	35.8	0.061	
2100	21.62	19.25	0.123	
BPT5				
Depth	mass wet (g)	mass dry (g)		Profile Description
700	39.03	36.25	0.077	fines with a black taint
900				lighter colored material
1200	28.31	27.77	0.019	signs of red mottling
1900	30.21	29.49	0.024	
2100	61.9	52.09	0.188	Material very wet
BPT7				
Depth	mass wet (g)	mass dry (g)		Profile Description
0-500	40.02	37.44	0.069	shale fragments in clayey material
500-1000	46.99	46	0.022	black silt material with roots
1500-1700	85.25	78.66	0.084	black clayey
2000-2800	31.29	30.25	0.034	

E2				
Depth	mass wet (g)	mass dry (g)		Profile Description
1400				
1550	35.14	28.22	0.245	Black clayey material
1600	40.43	32.7	0.236	
1800				
	32.72	27.23	0.202	greyed soil: grey colour
E4				
Depth	mass wet (g)	mass dry (g)		Profile Description
400	33.09	30.64	0.080	reddish yellow mottled material concretes once dry
600	15.11	13.15	0.149	Concrete once dry
800	22.63	13.17	0.718	clayey black material
900	21.6	18.84	0.146	
1000	17.63	14.62	0.206	
1200	17.64	15.11	0.167	
1400	38.62	32.71	0.181	
1600	41.22	31.74	0.299	
1800	40.67	33.89	0.200	
2000	25.42	22.33	0.138	
2200	43.46	36.16	0.202	
2400	62.88	52.36	0.201	
3200	44.83	36.11	0.241	black material consistent with depth
4000	44.45	36.65	0.213	
E6				
Depth	mass wet (g)	mass dry (g)		Profile Description
700	23.13	20.2	0.145	light coloured fine(possible E)
1100	36.29	32.92	0.102	
1400	18.64	16.78	0.111	
1800	25.15	21.43	0.174	
2000	48.02	40.83	0.176	Progressive darkening and denser material with depth. At 2000mm the material is black
2100	34.66	30.09	0.152	
2500	41.48	34.64	0.197	
3000	48.02	40.83	0.176	clayey material coloured by black pigment
E8				
Depth	mass wet (g)	mass dry (g)		Profile Description
300	28.94	25.14	0.151	sandy coarse particles in fine matrix
600	42	35.77	0.174	reddish mottling yellow no coarse sands
700	41.52	37.22	0.116	
800	50.79	44.3	0.147	dark consolidated material
1000	49.83	41.45	0.202	lighter coloured fine soils with progressive darkening with depth
1200	37.39	27.5	0.360	
1400	45.99	38.7	0.188	dense black mass
1500	41.96	36.27	0.157	
1600	38.28	32.41	0.181	
2100	47.28	37.89	0.248	

E10				
Depth	mass wet (g)	mass dry (g)		Profile Description
400	37.98	33.2	0.144	gravel material in a fine sand matrix
600	25.35	23.16	0.095	
E12				
Depth	mass wet (g)	mass dry (g)		Profile Description
300	21.28	19.88	0.070	black silty material
600	43.97	38.21	0.151	black fine material due to organic matter
900	33.61	28.45	0.181	
1200	44.52	38.33	0.161	grey material with reddish mottling
J3				
Depth	mass wet (g)	mass dry (g)		Profile Description
300	23.37	23.11	0.011	silty sands (yellow)
1800	22.67	19.51	0.162	reddish brown soil with high clay
P1				
Depth	mass wet (g)	mass dry (g)		Profile Description
0-300	41.62	37	0.125	black structured soil with roots
300-600	41.15	35.76	0.151	black consolidated mass
1800	25.05	21.66	0.157	greyed with signs of mottling
2000	21.24	18.67	0.138	
3200	22.81	17.88	0.276	

APPENDIX B

Soil Particle Size Analysis

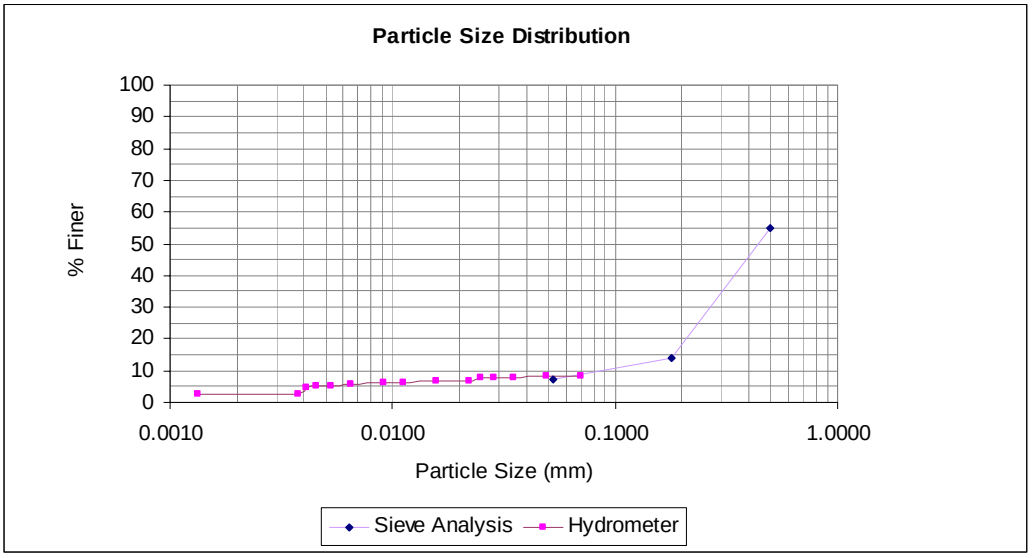

Figure B.1 Particle size distribution BP1 300

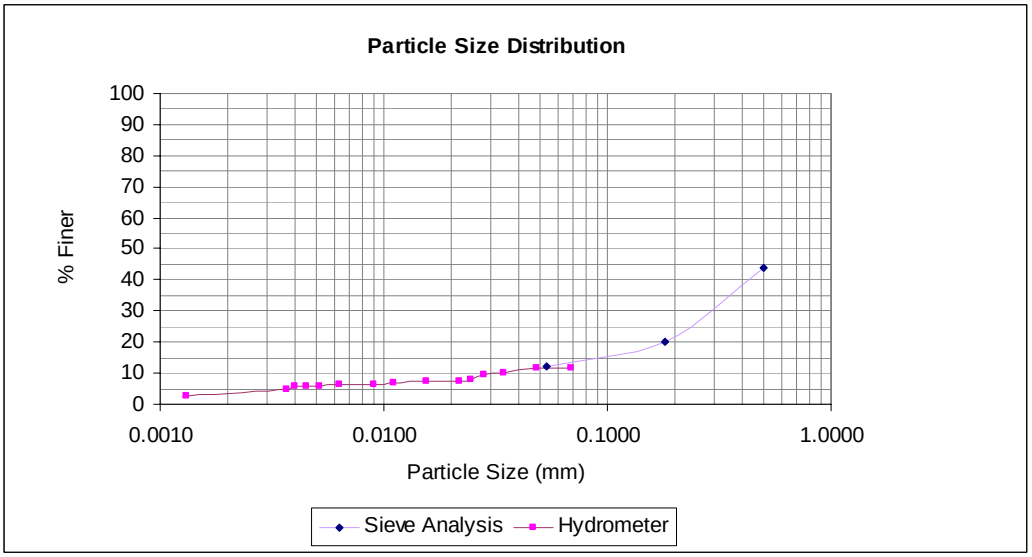

Figure B.2 Particle size distribution BP1 900

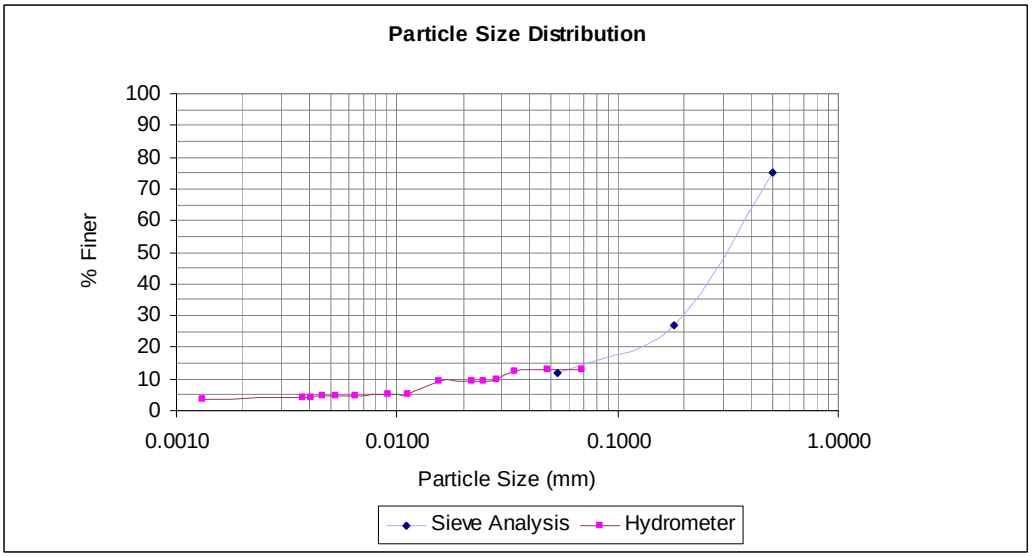

Figure B.3 Particle size distribution BP1 1500

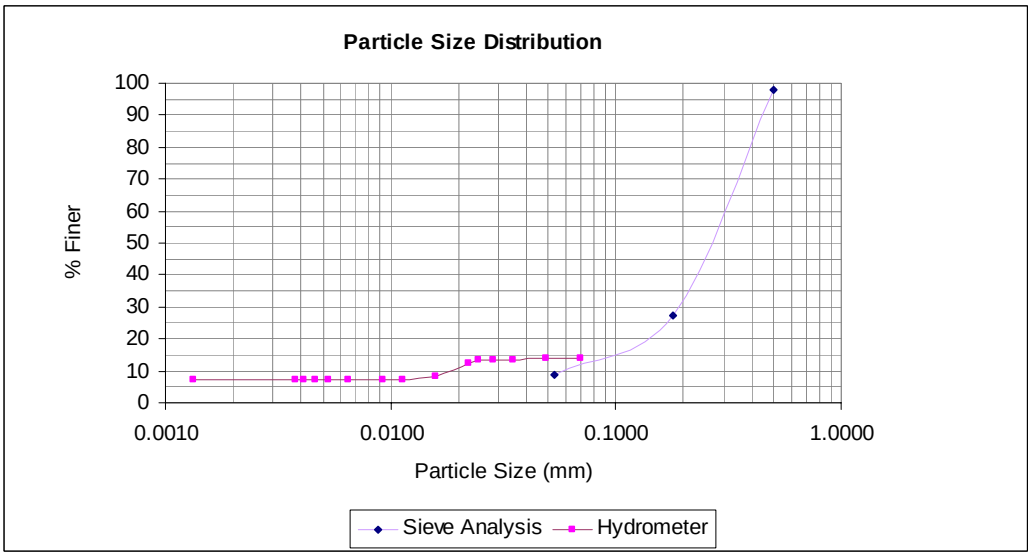

Figure B.4 Particle size distribution BP5 300

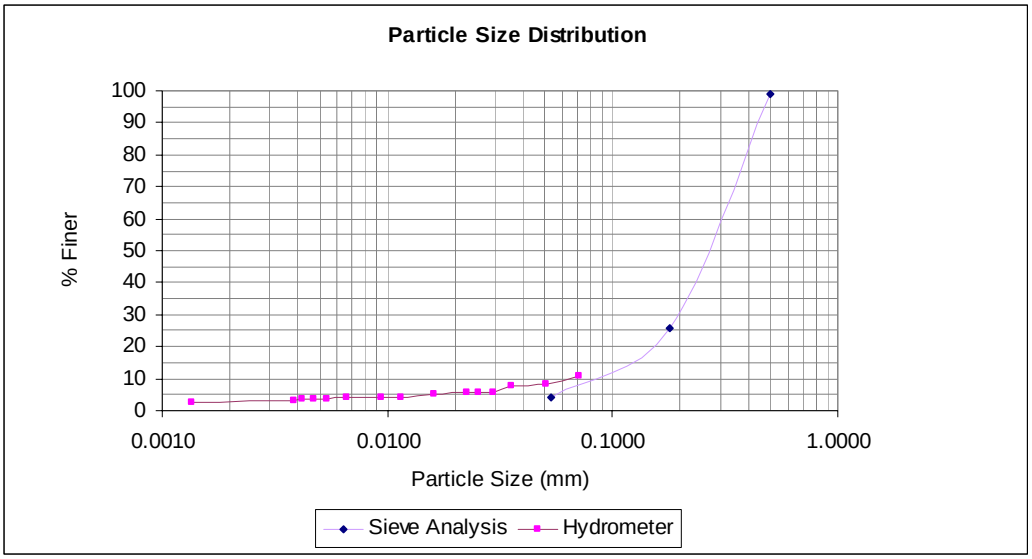

Figure B.5 Particle size distribution BP5 1200

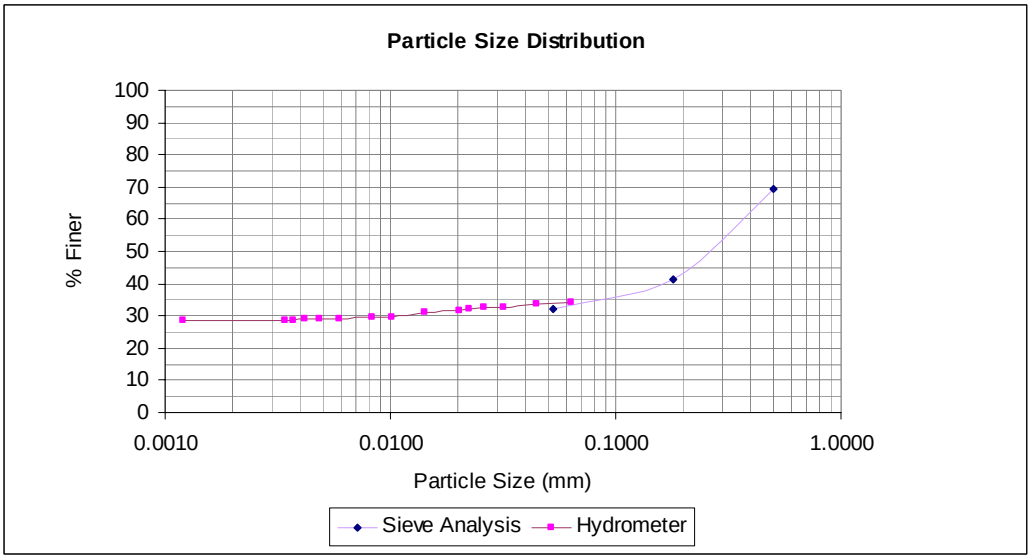

Figure B.6 Particle size distribution BPT1 900

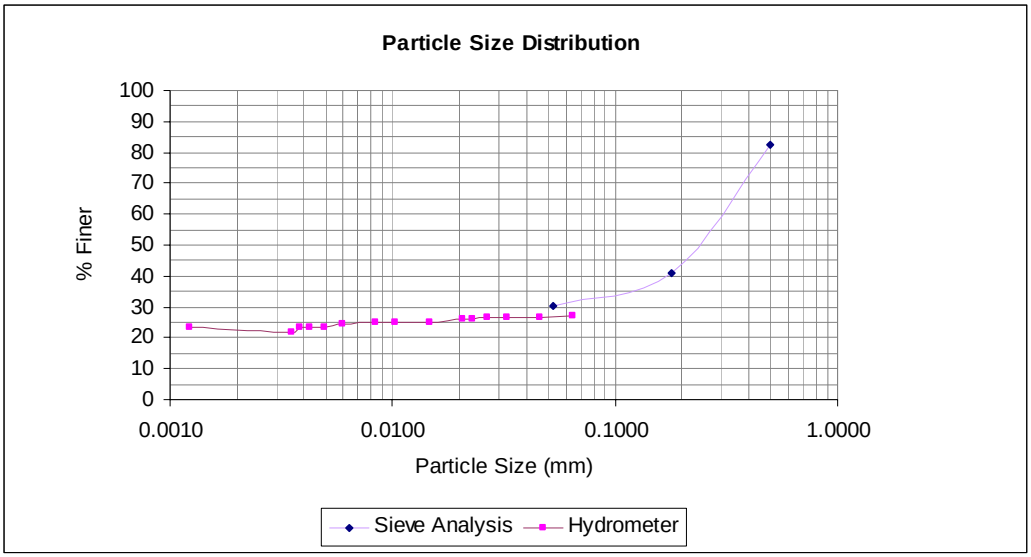

Figure B.7 Particle size distribution BPT1 2500

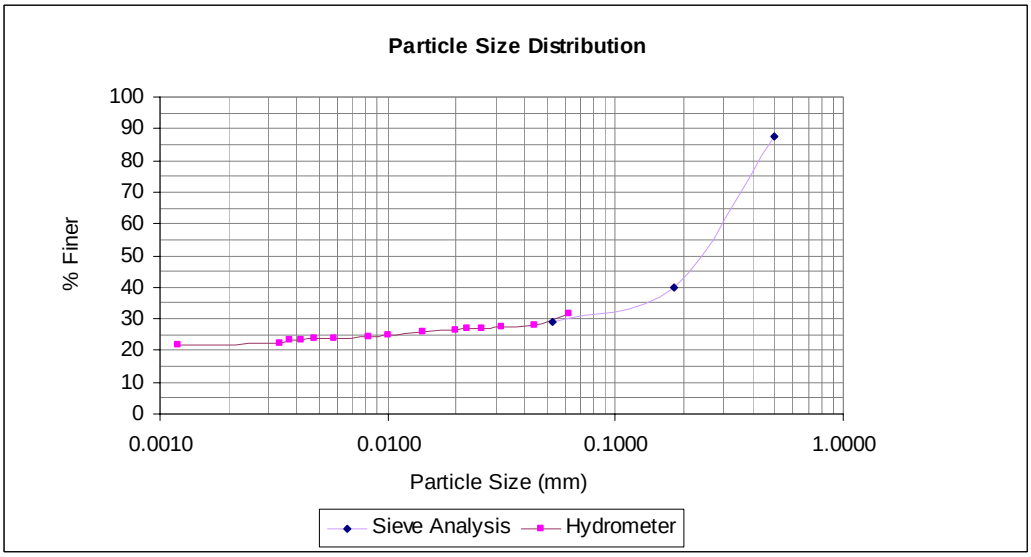

Figure B.8 Particle size distribution BPT2 900

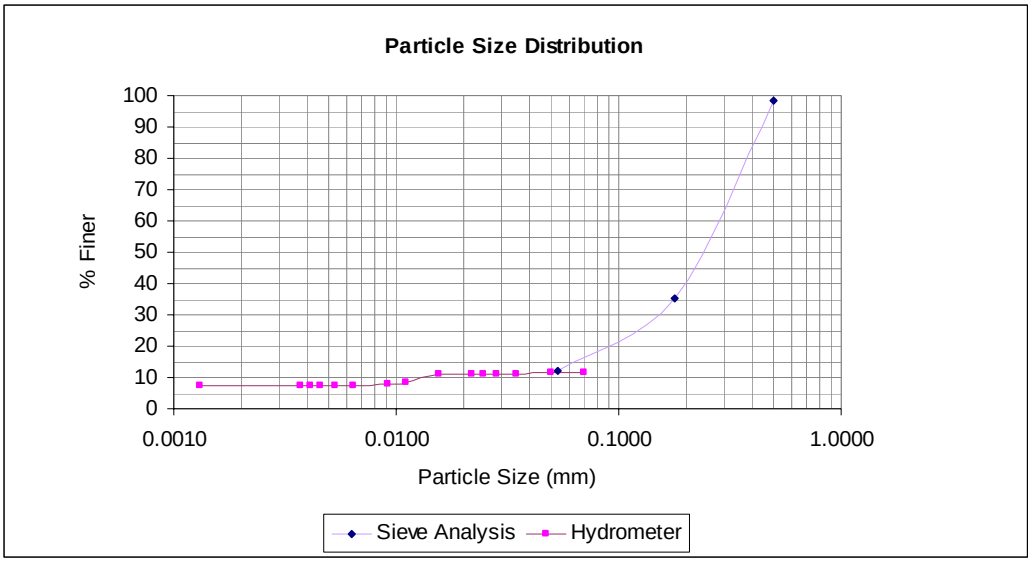

Figure B.9 Particle size distribution BPT4 600

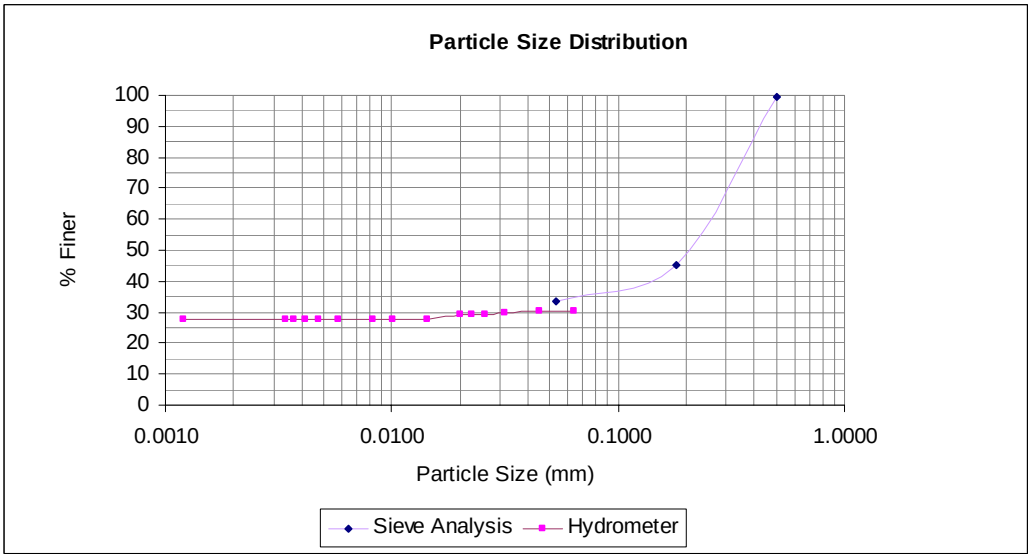

Figure B.20 Particle size distribution BPT4 1700

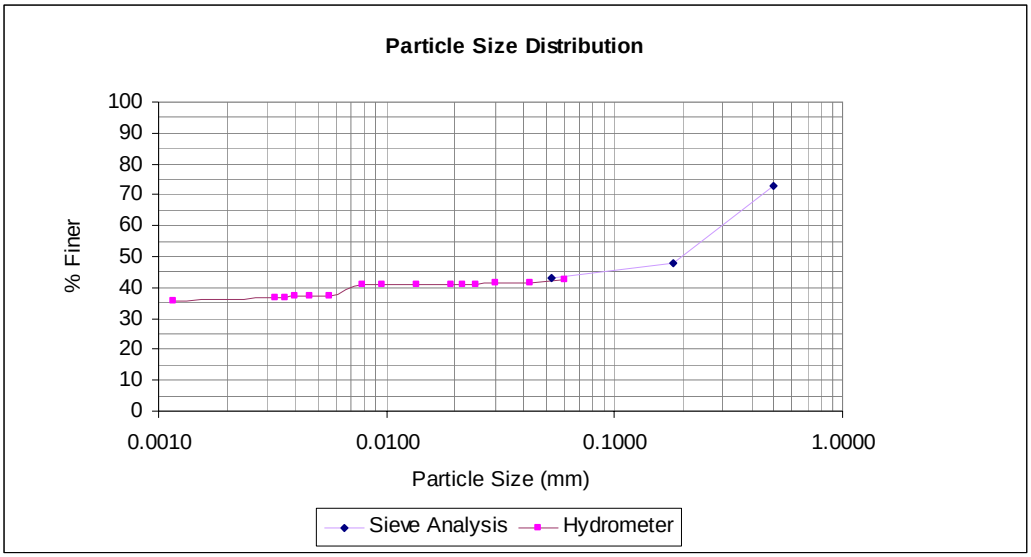

Figure B.11 Particle size distribution BPT5 1900

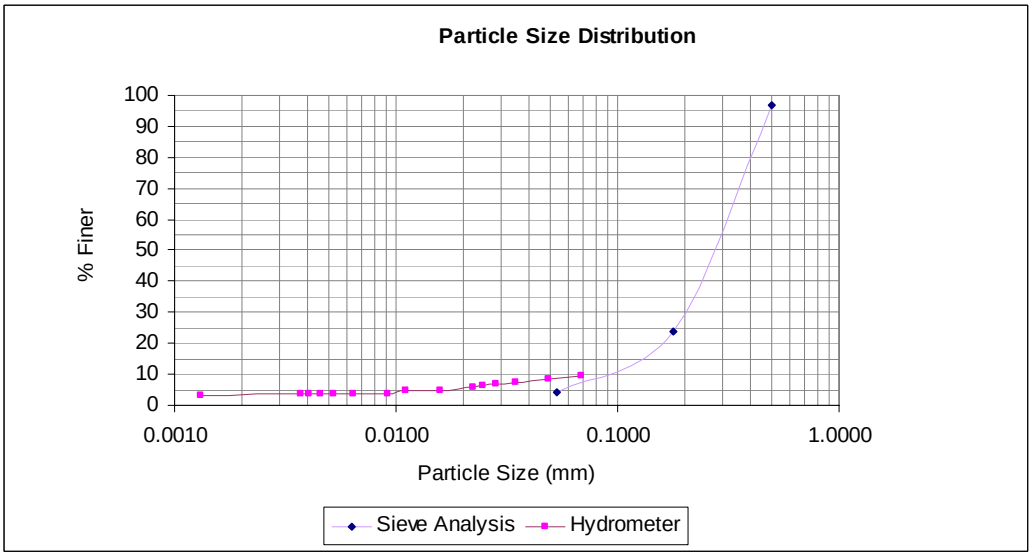

Figure B.12 Particle size distribution BPT6 1500

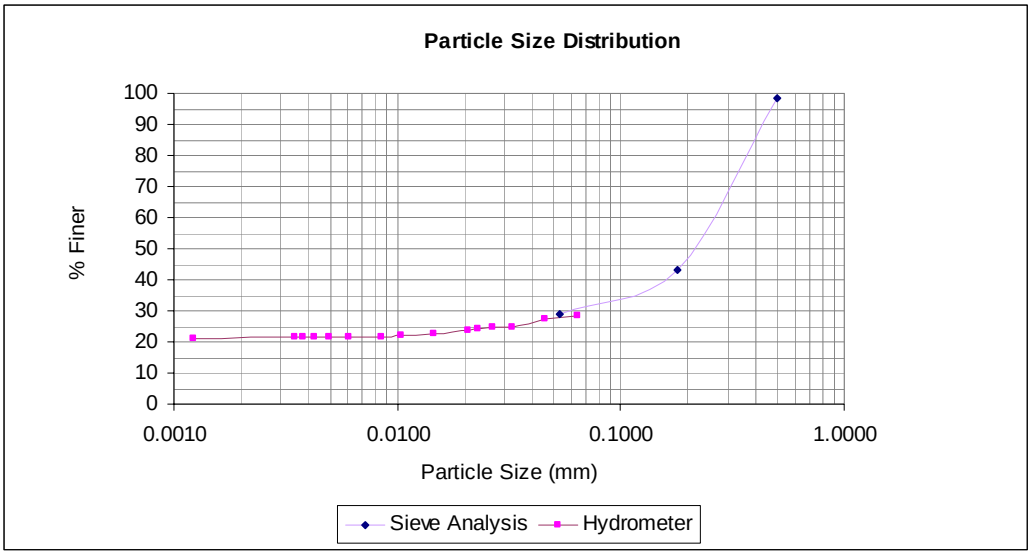

Figure B.13 Particle size distribution BPT7 0-500

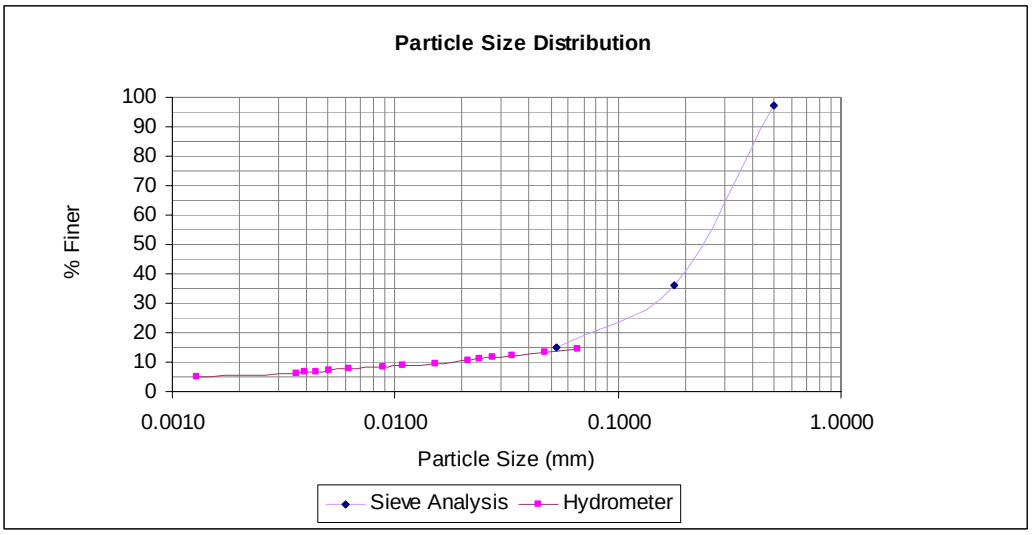

Figure B.14 Particle size distribution BPT7 500-1000

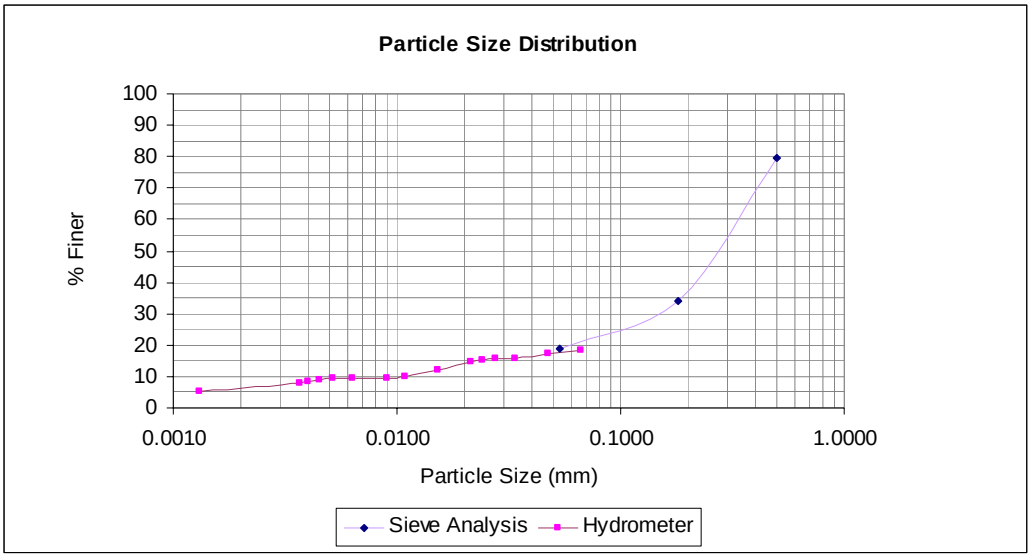

Figure B.15 Particle size distribution BLACK ROAD

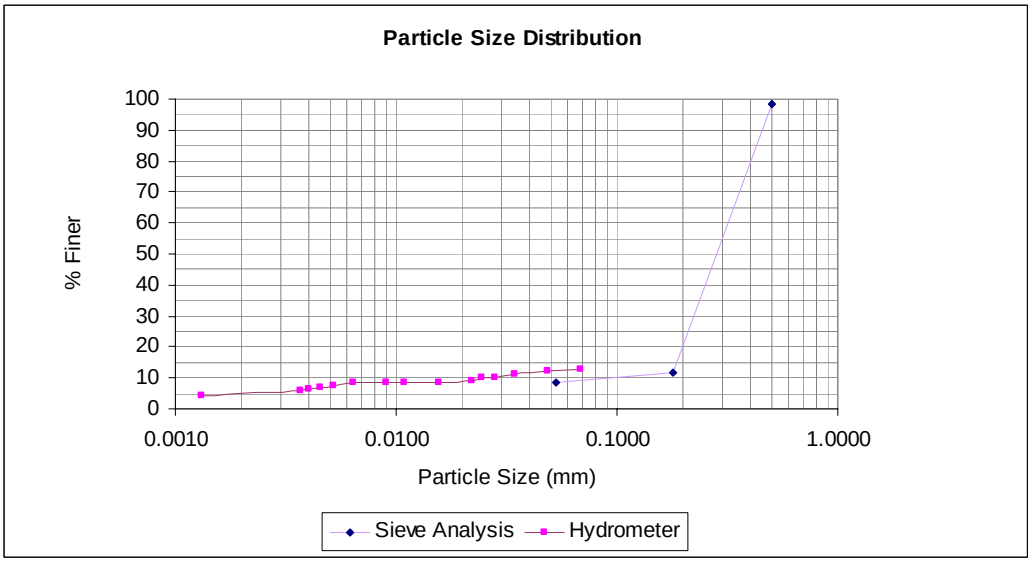

Figure B.16 Particle size distribution D1 300

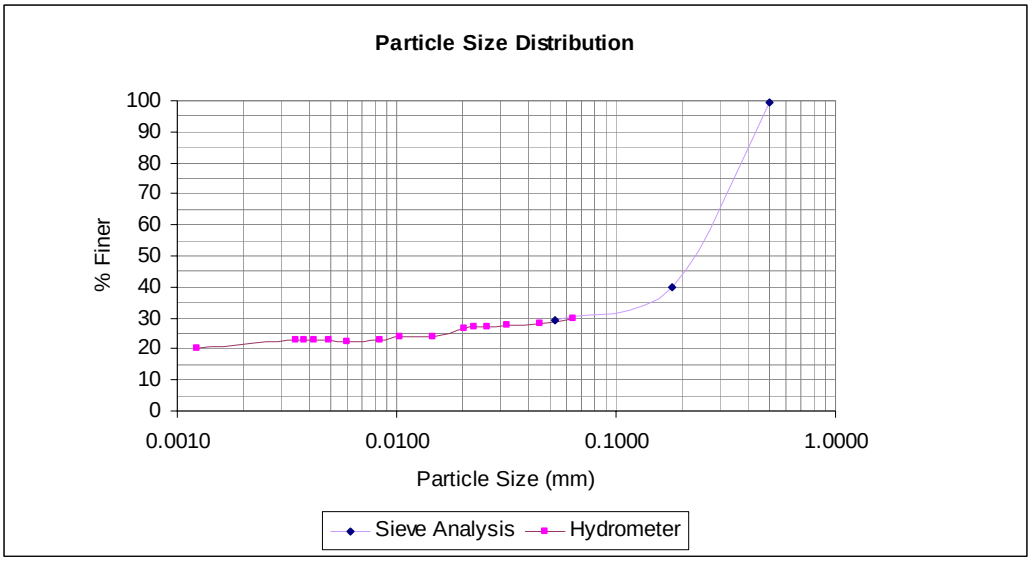

Figure B.17 Particle size distribution D1 1500

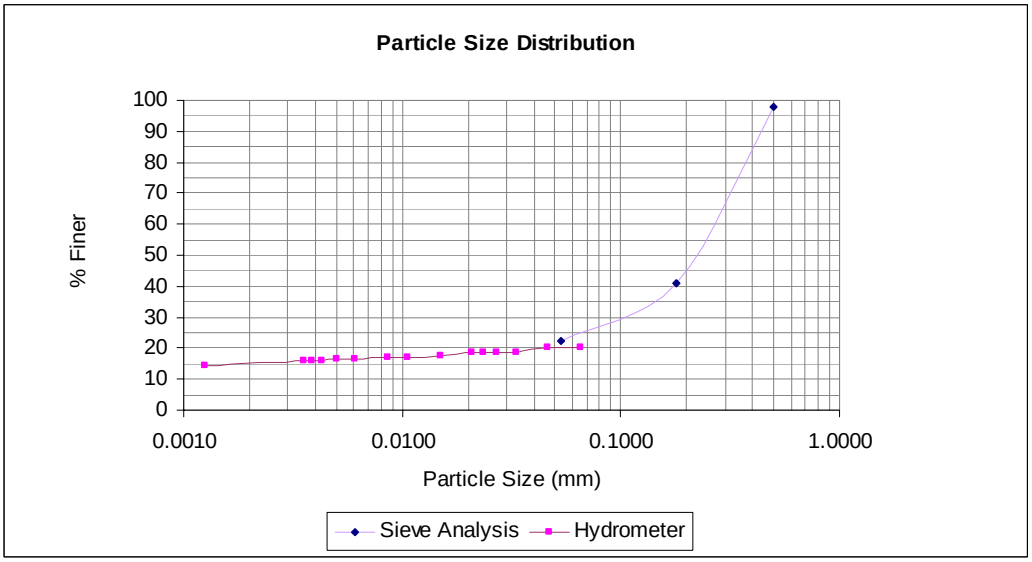

Figure B.18 Particle size distribution E1 300

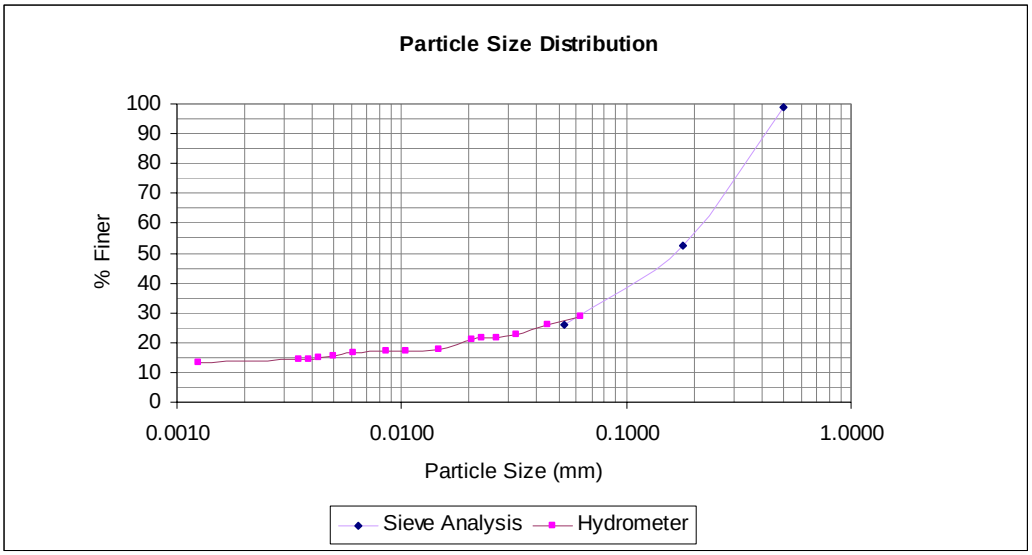

Figure B.19 Particle size distribution E1 950

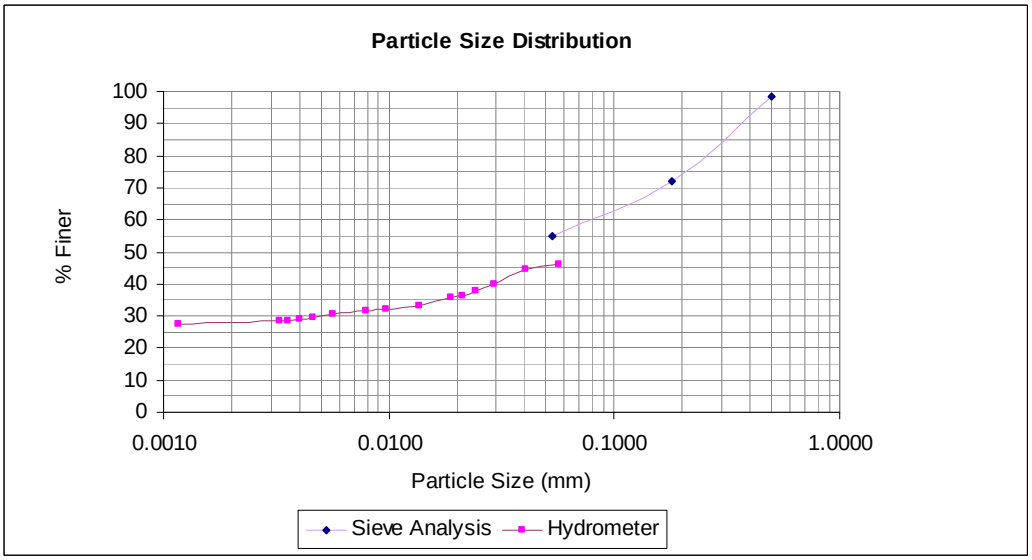

Figure B.30 Particle size distribution E1 1200

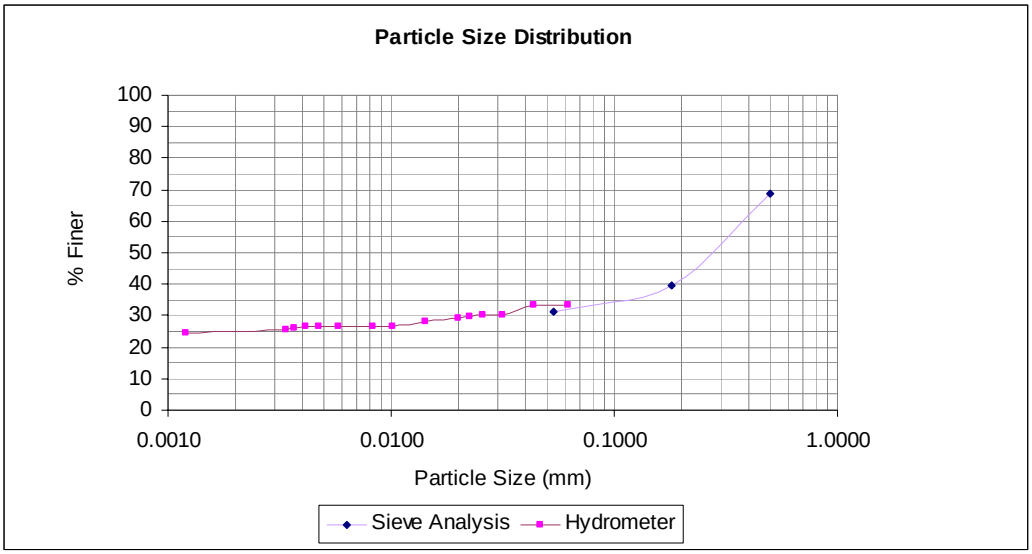

Figure B.21 Particle size distribution E1 1700

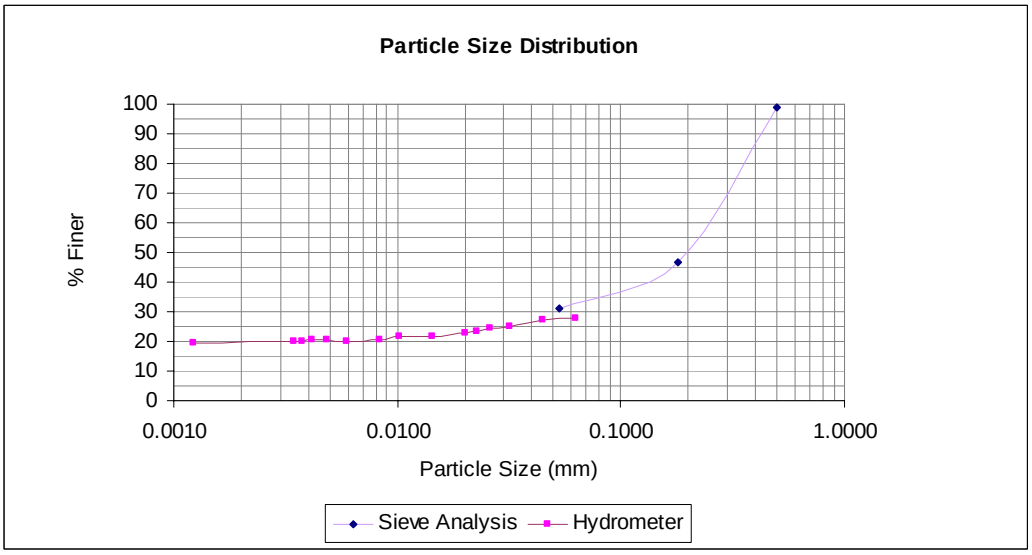

Figure B.22 Particle size distribution E2 1550

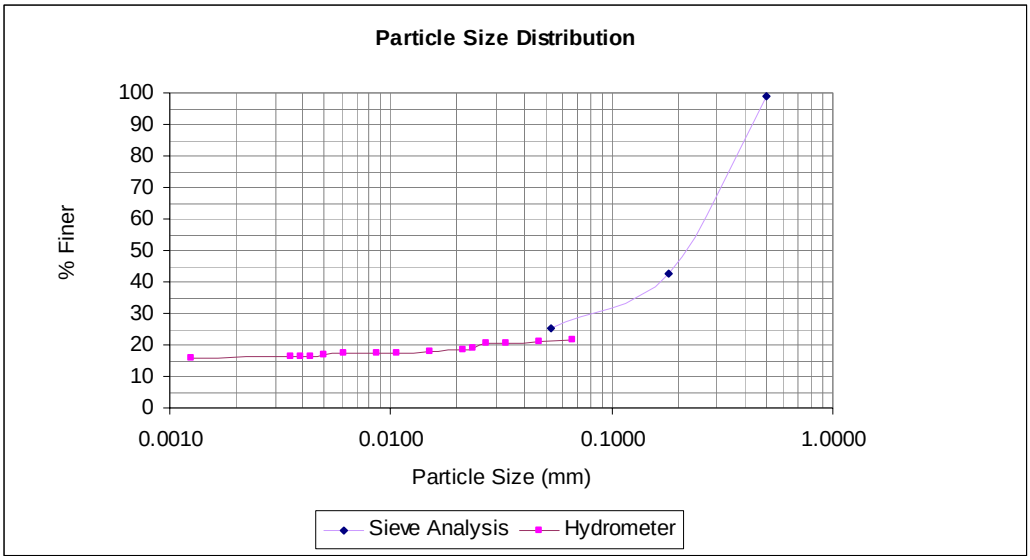

Figure B.24 Particle size distribution E2 2000

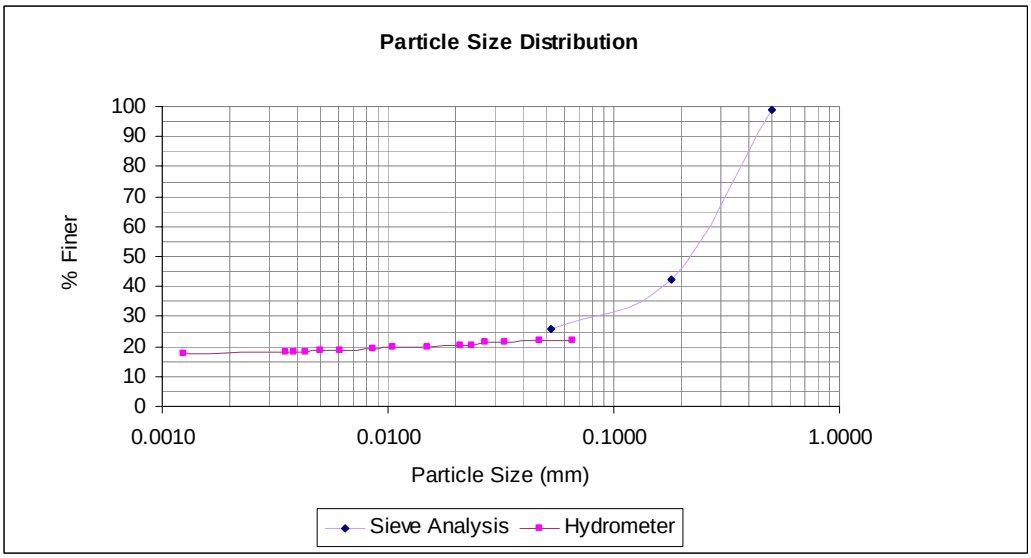

Figure B.24 Particle size distribution E3 300

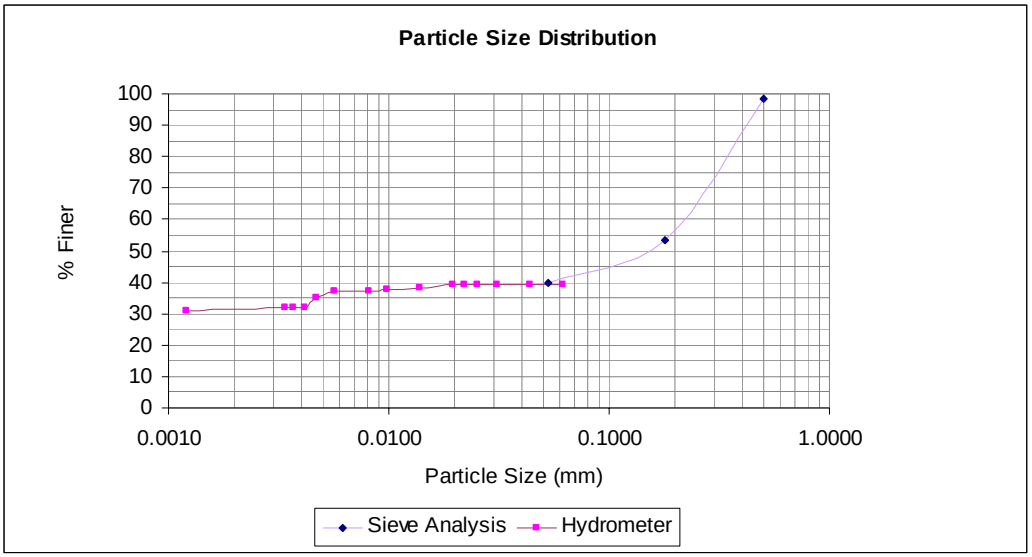

Figure B.25 Particle size distribution E3 600

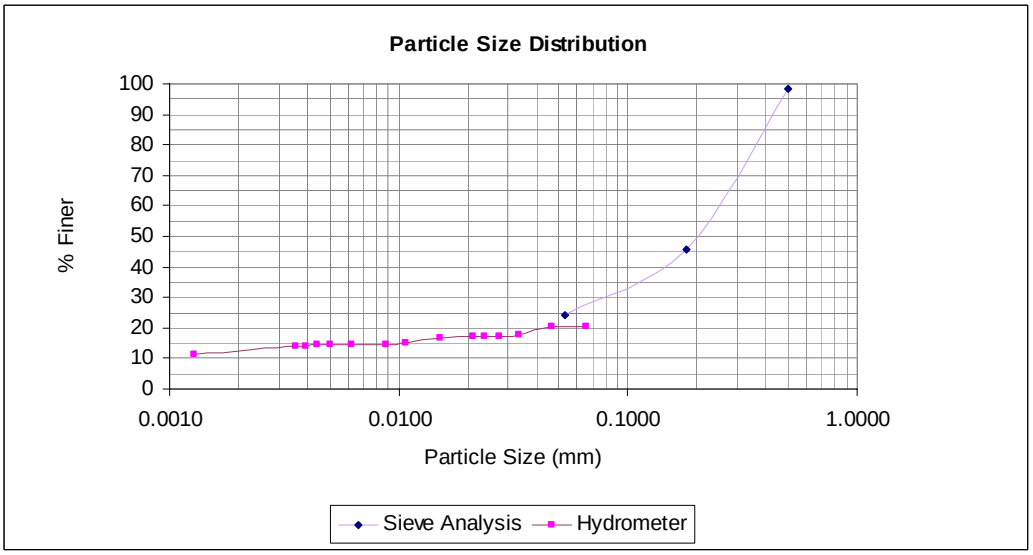

Figure B.26 Particle size distribution E3 1200

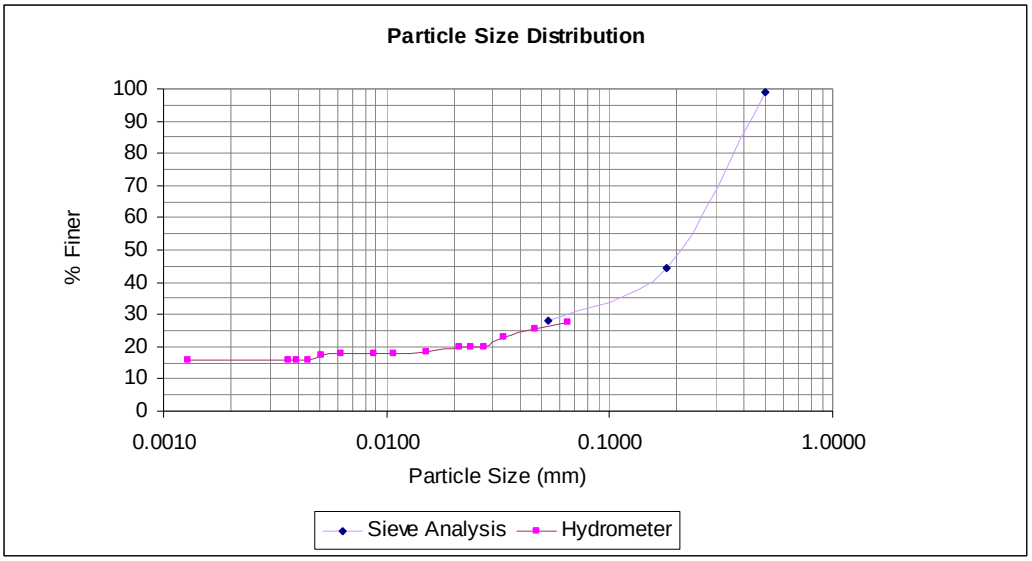

Figure B.27 Particle size distribution E3 1500

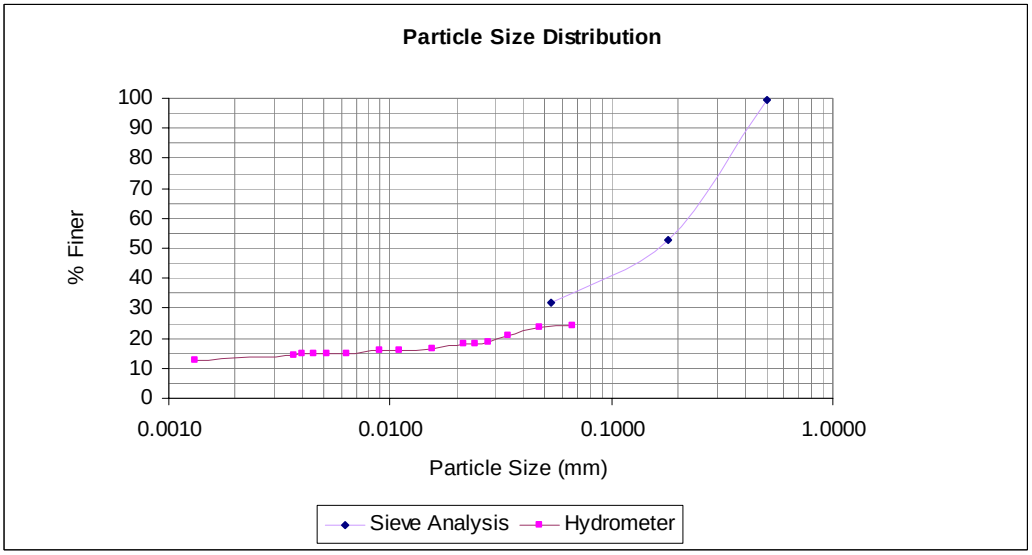

Figure B.28 Particle size distribution E3 2100

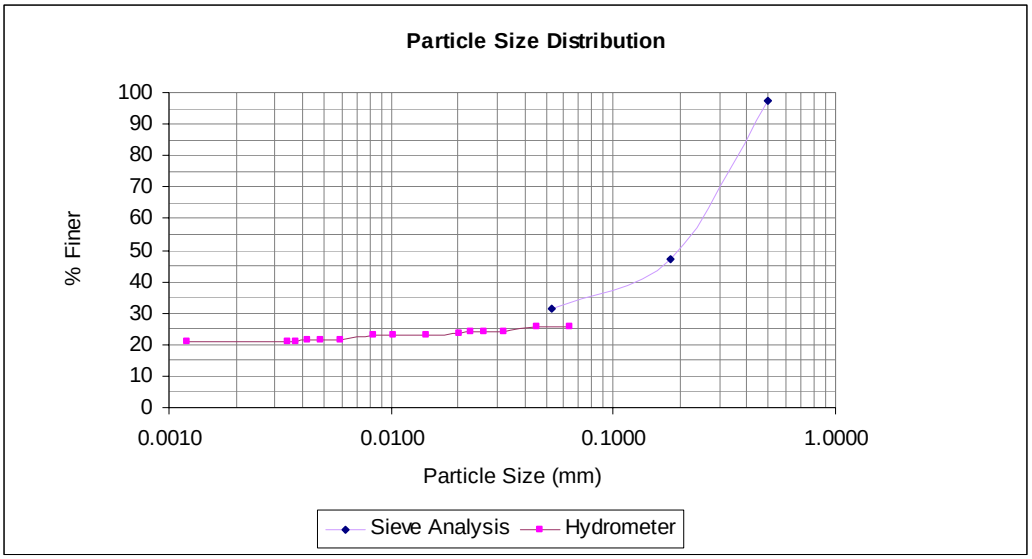

Figure B.29 Particle size distribution E3 2900

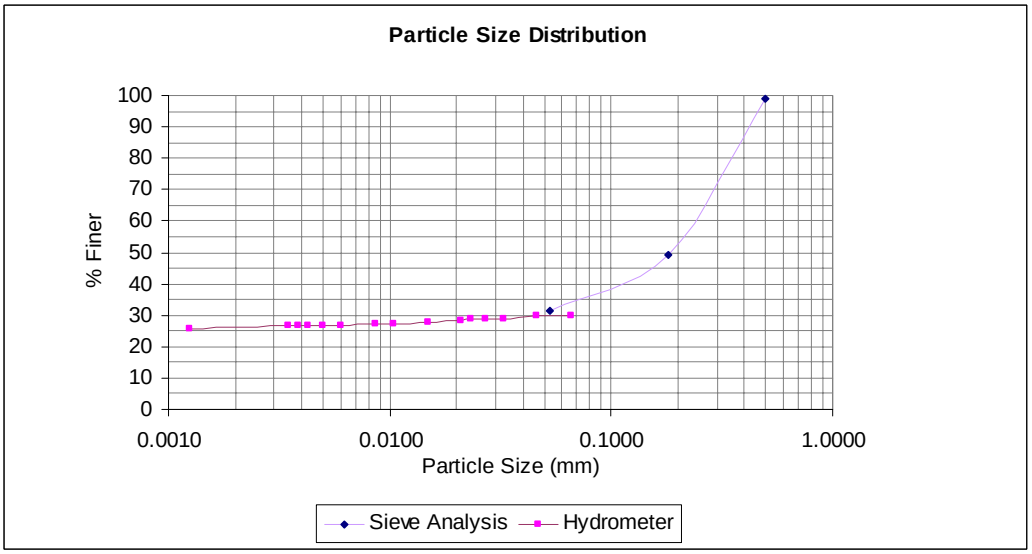

Figure B.31 Particle size distribution E4 400

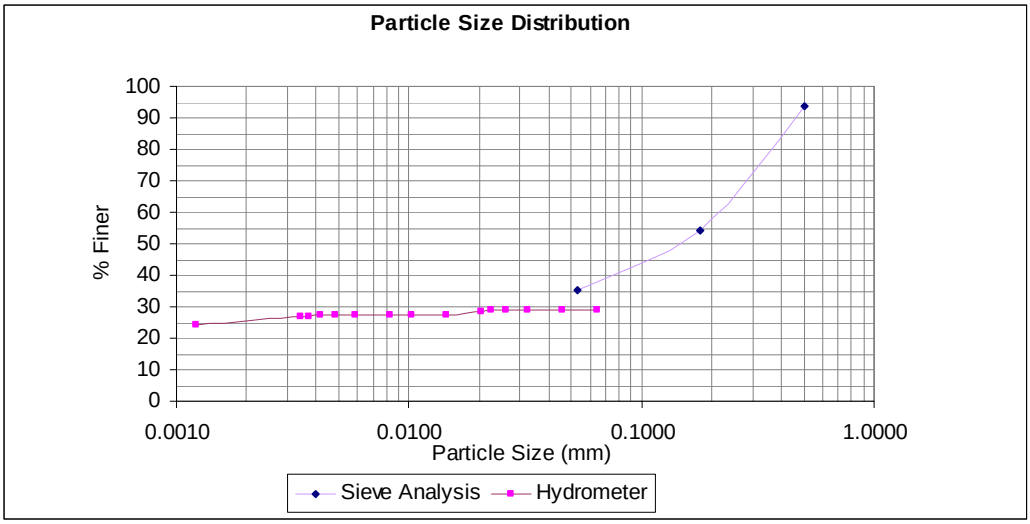

Figure B.32 Particle size distribution E4 900

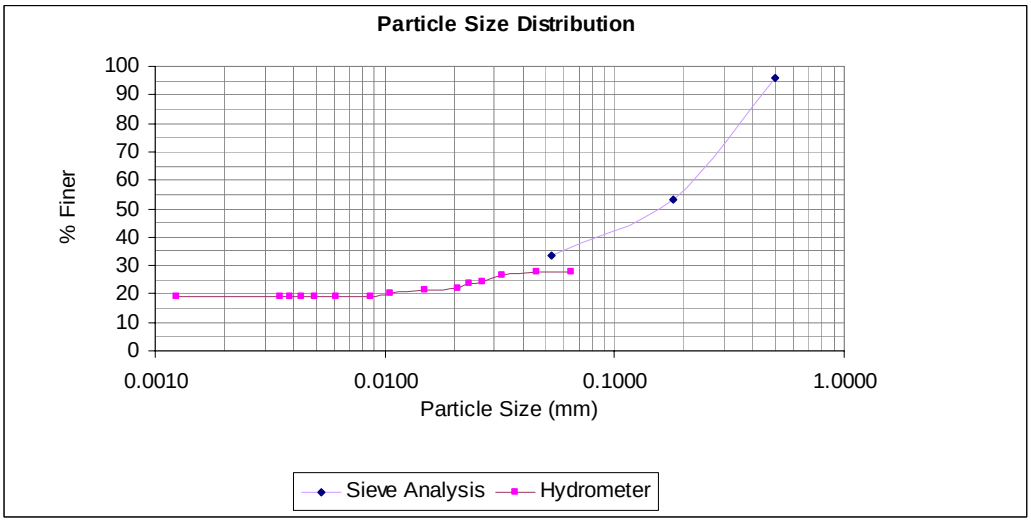

Figure B.33 Particle size distribution E4 1400

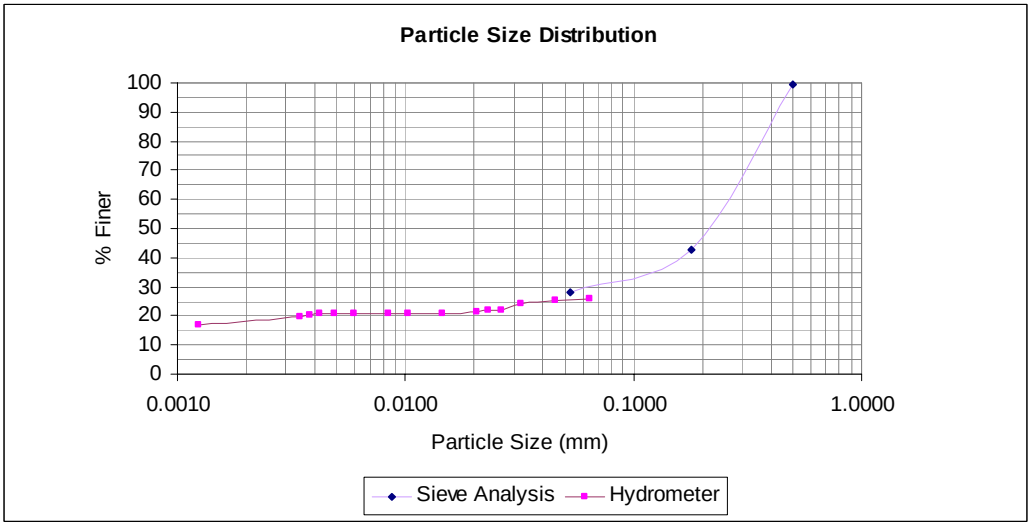

Figure B.34 Particle size distribution E4 2200

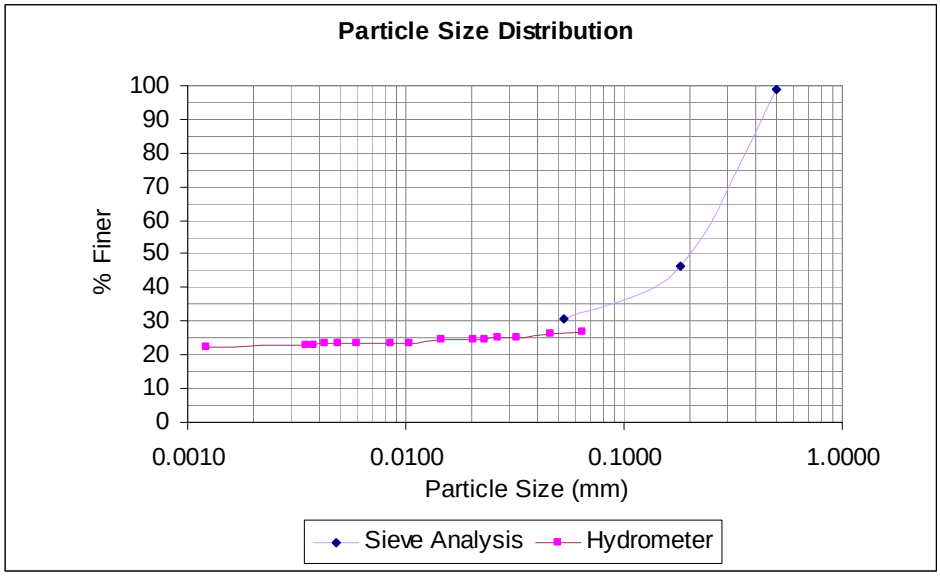

Figure B.35 Particle size distribution E4 4000.

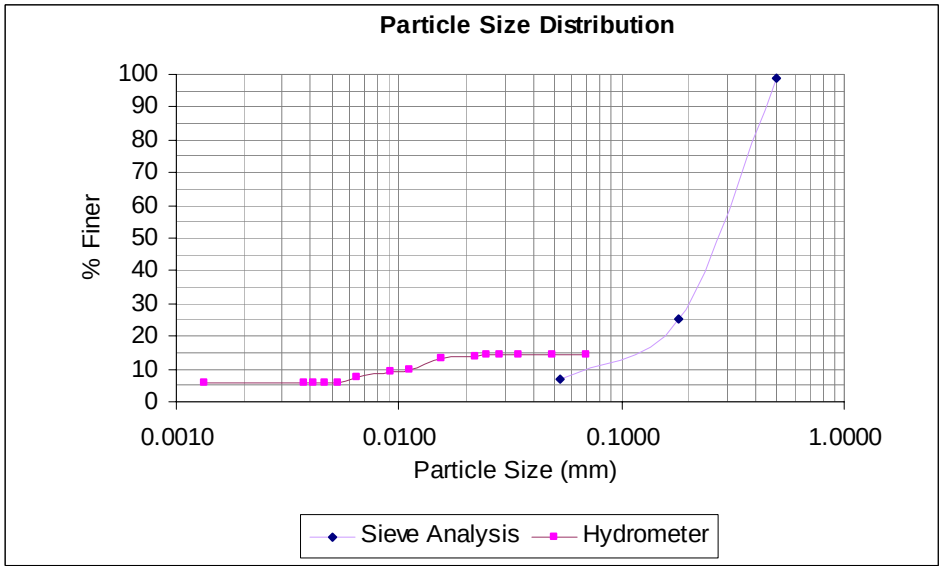

Figure B.36 Particle size distribution E6 700.

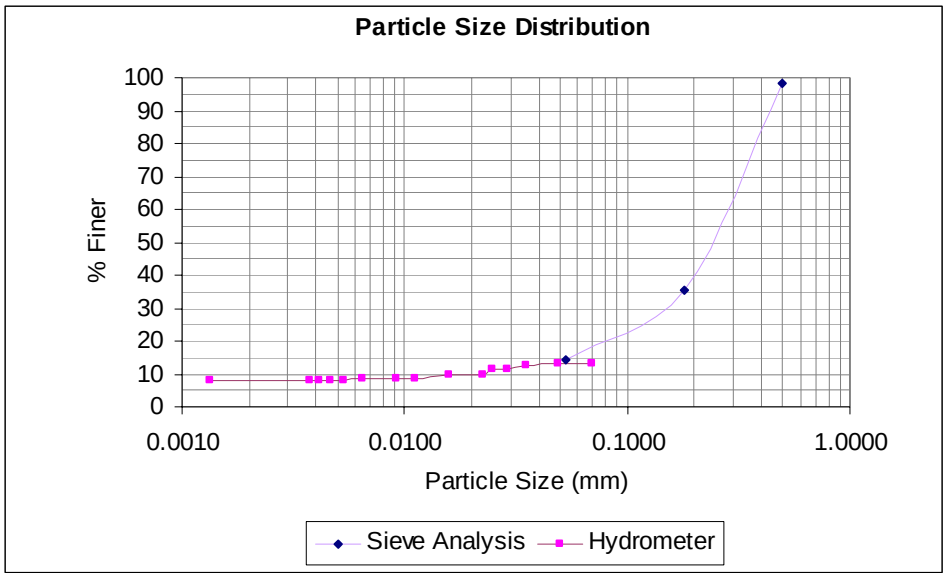

Figure B.37 Particle size distribution E6 1400.

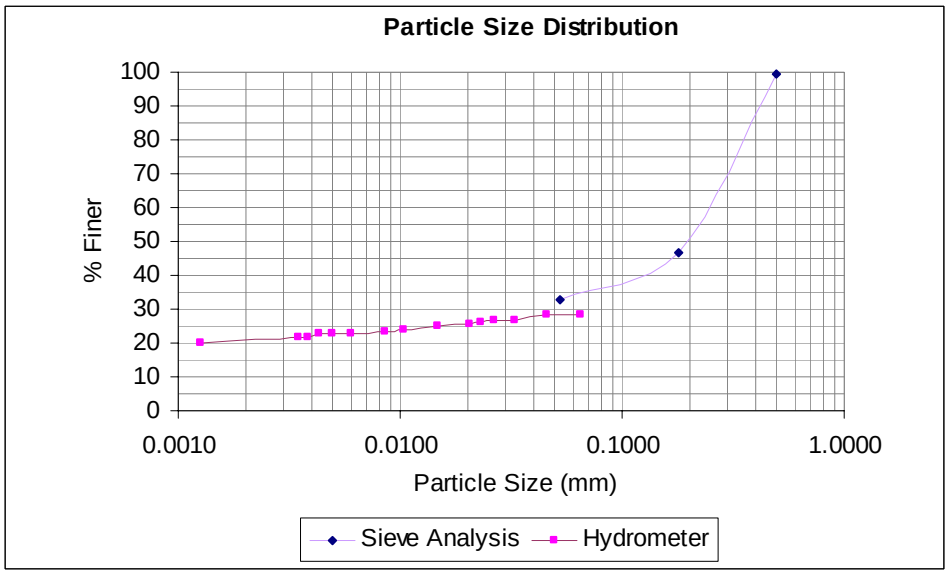

Figure B.38 Particle size distribution E6 2100.

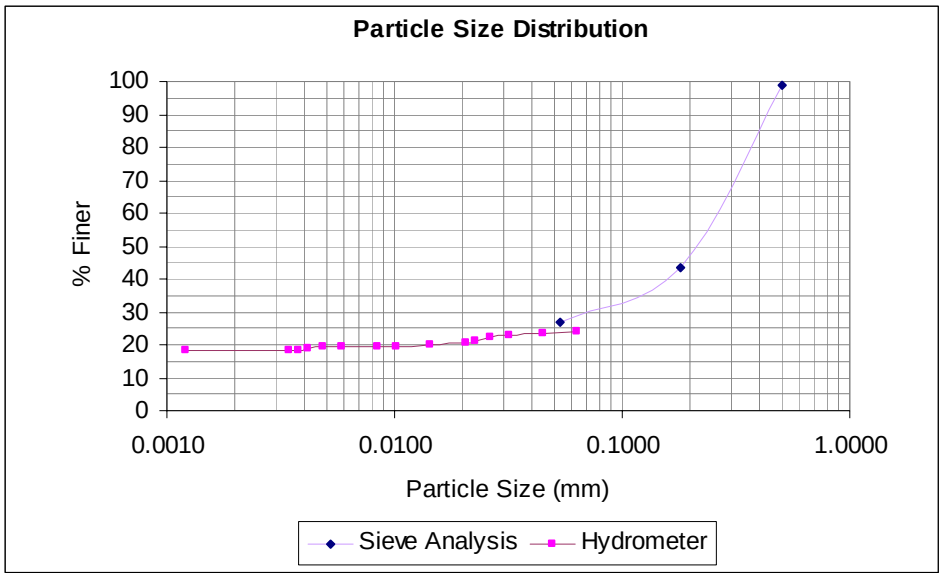

Figure B.39 Particle size distribution E6 3000

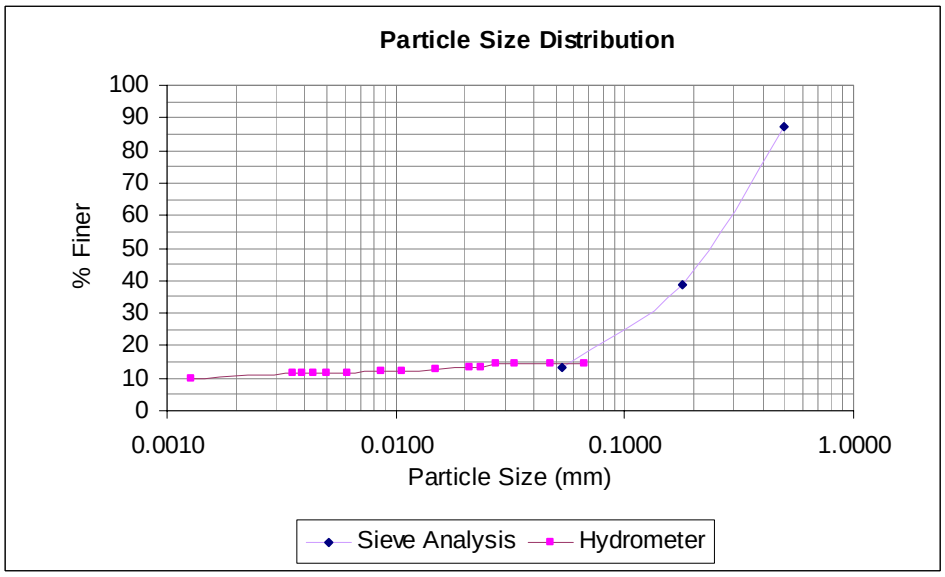

Figure B.40 Particle size distribution E7 300.

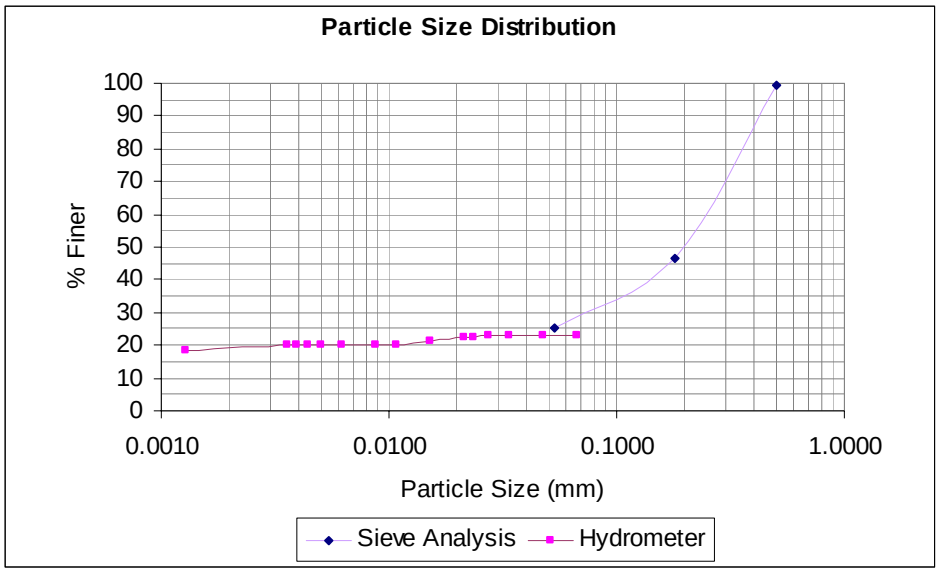

Figure B.41 Particle size distribution E7 600.

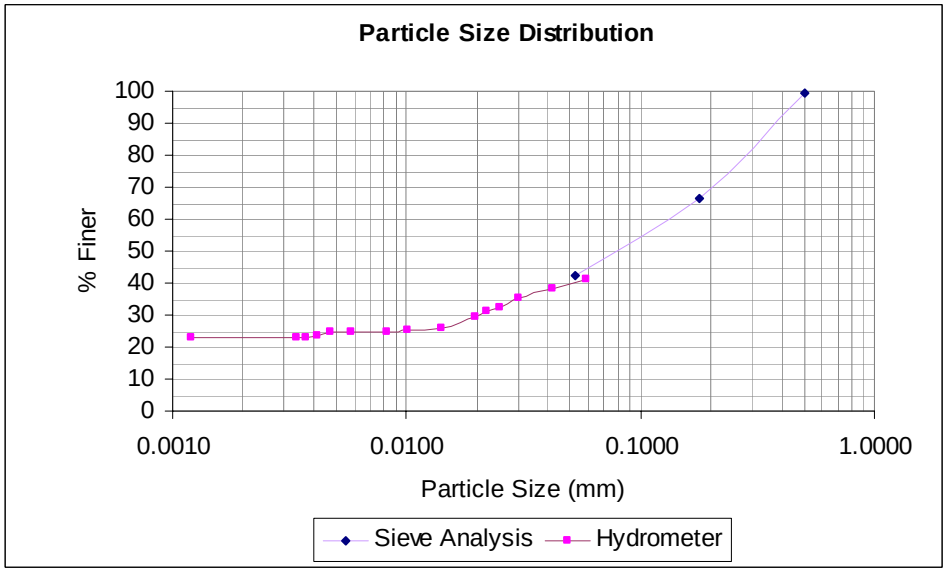

Figure B.42 Particle size distribution E7 1200

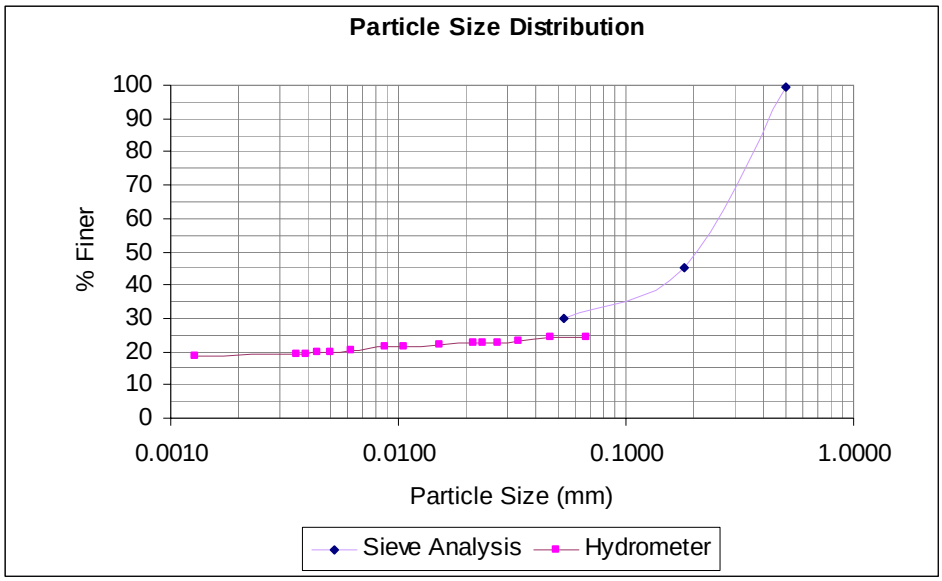

Figure B.43 Particle size distribution E7 1900.

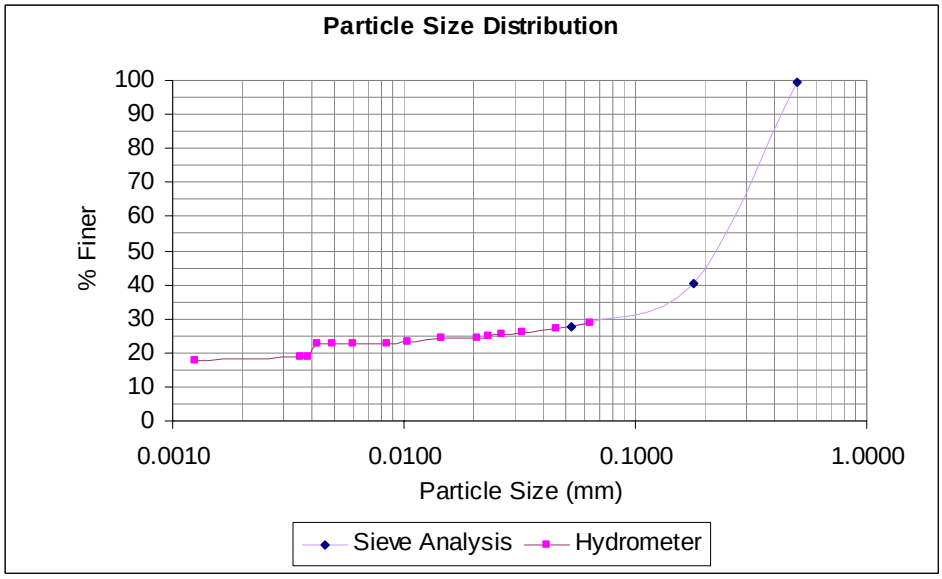

Figure B.44 Particle size distribution E7 2-3ends

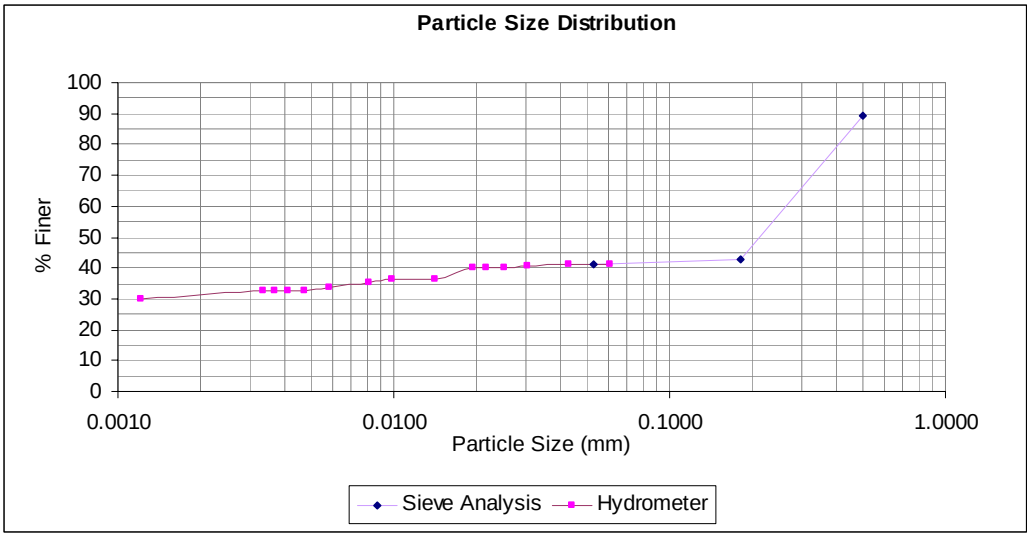

Figure B.45 Particle size distribution E8 300

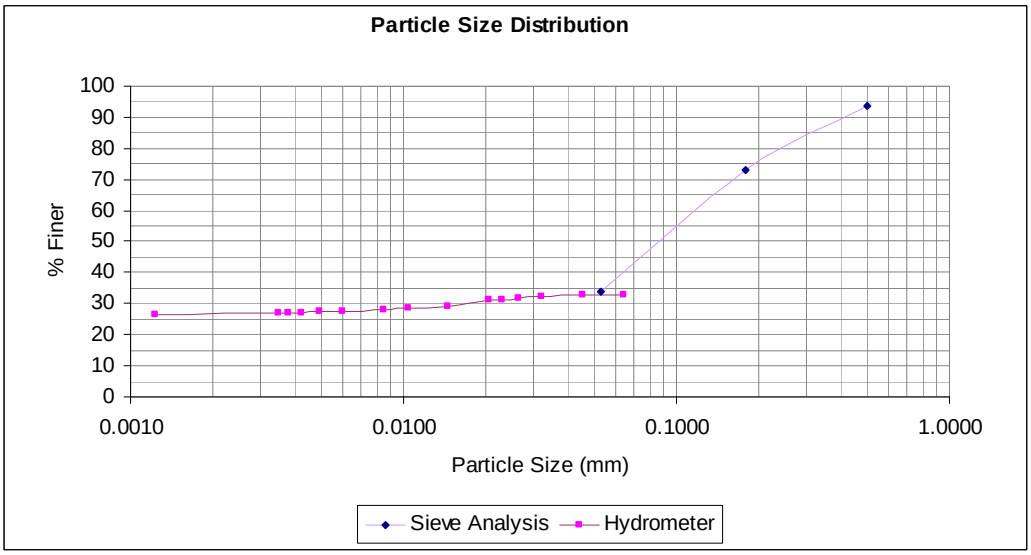

Figure B.46 Particle size distribution E8 600

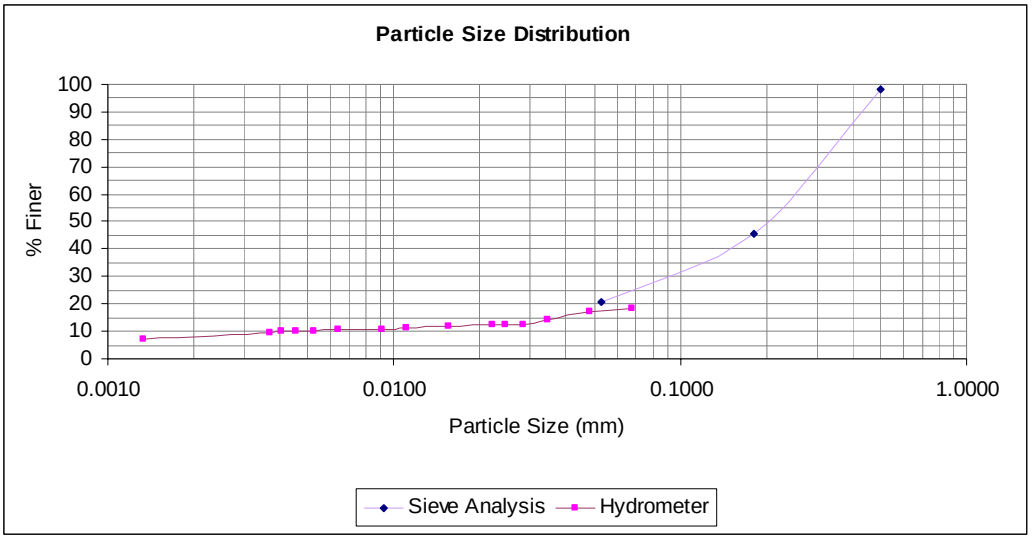

Figure B.47 Particle size distribution E8 1000

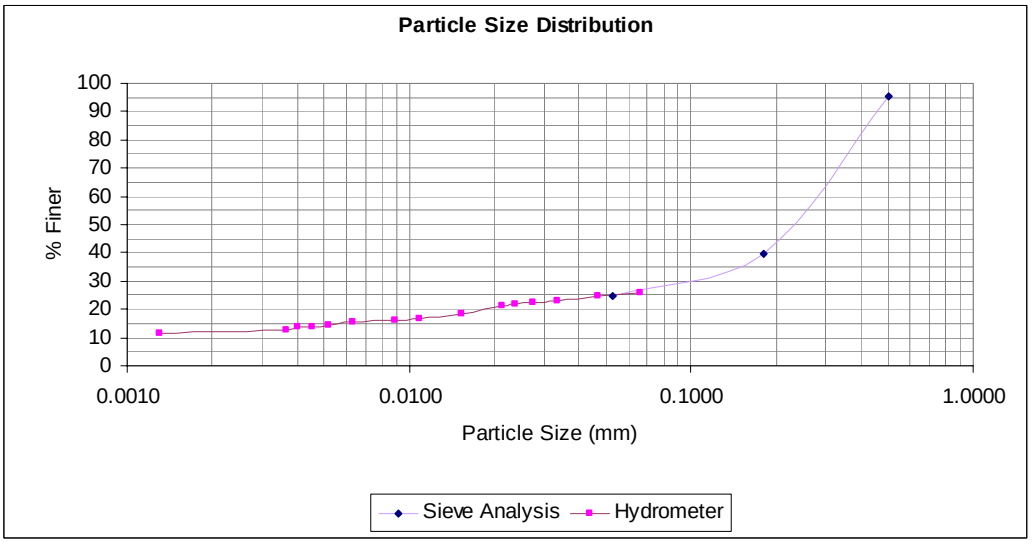

Figure B.48 Particle size distribution E8 1400

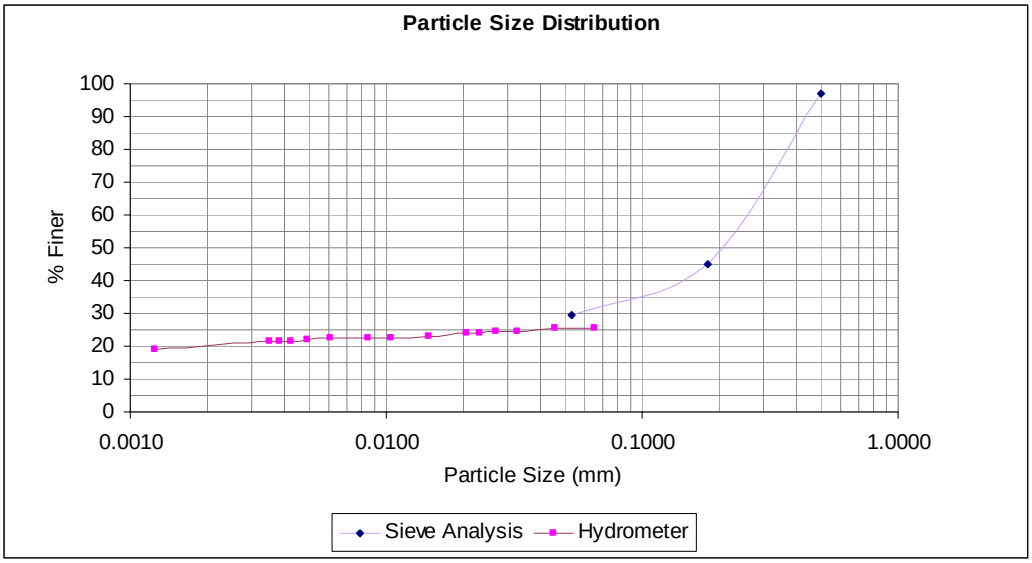

Figure B.49 Particle size distribution E8 2100.

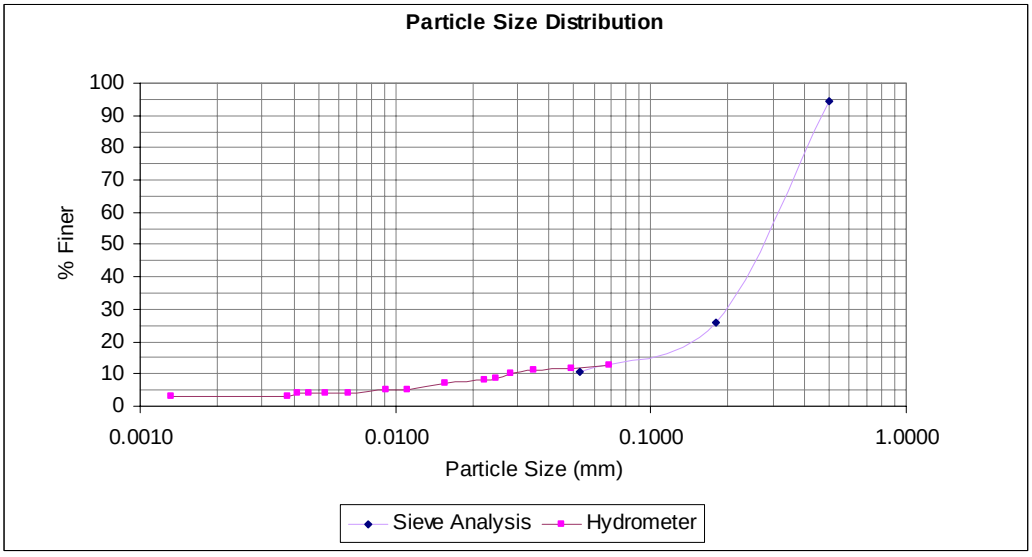

Figure B.50 Particle size distribution E9 300

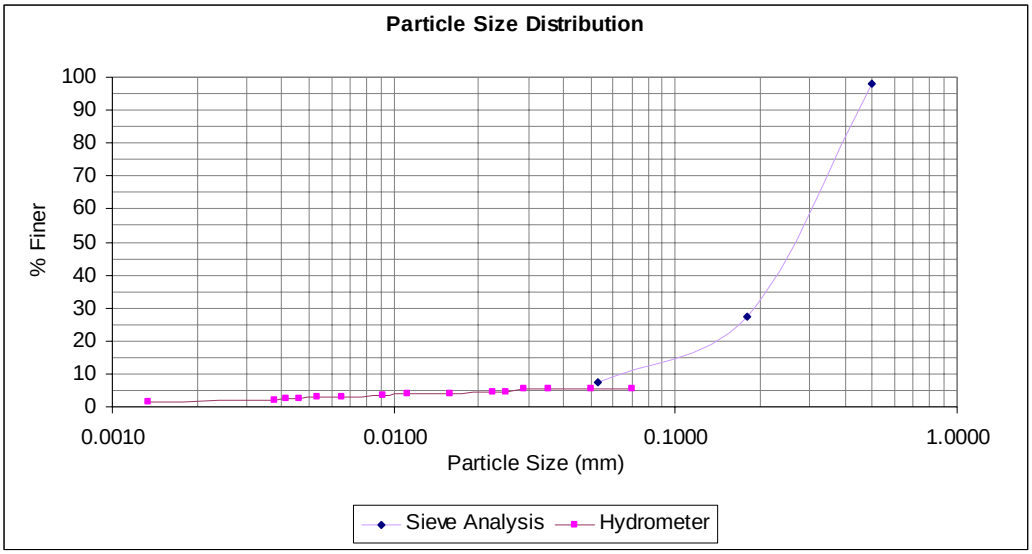

Figure B.51 Particle size distribution E9 600

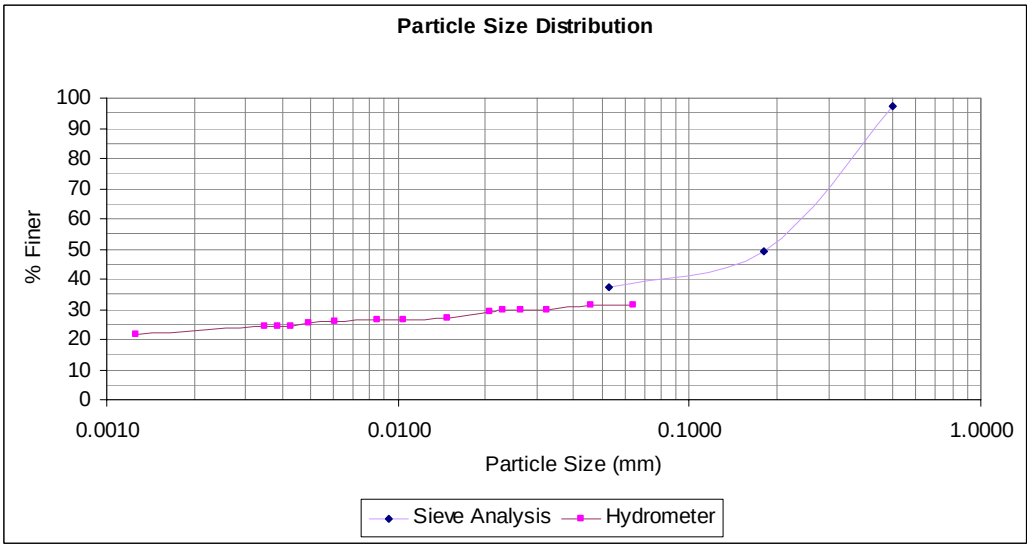

Figure B.52 Particle size distribution E9 1000

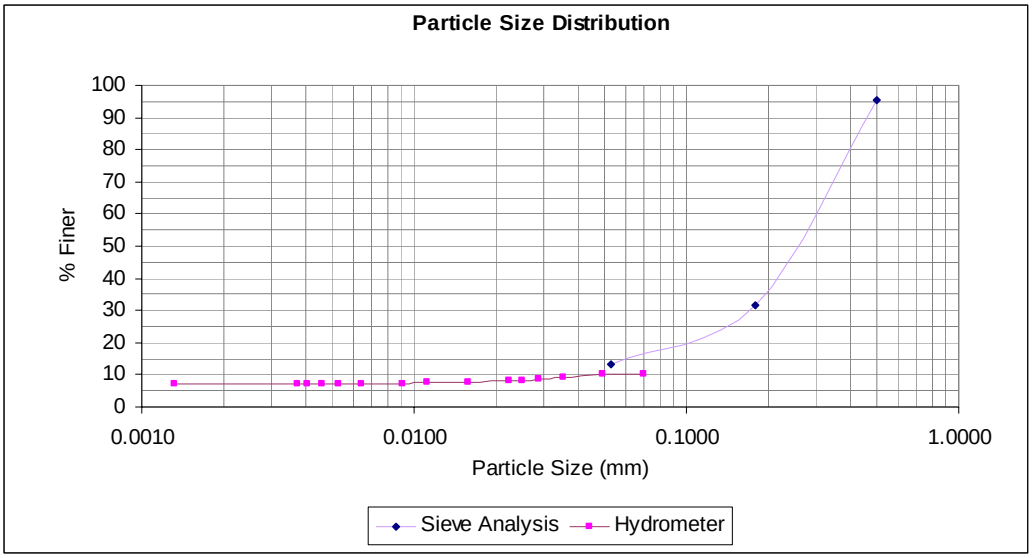

Figure B.53 Particle size distribution E9 1200

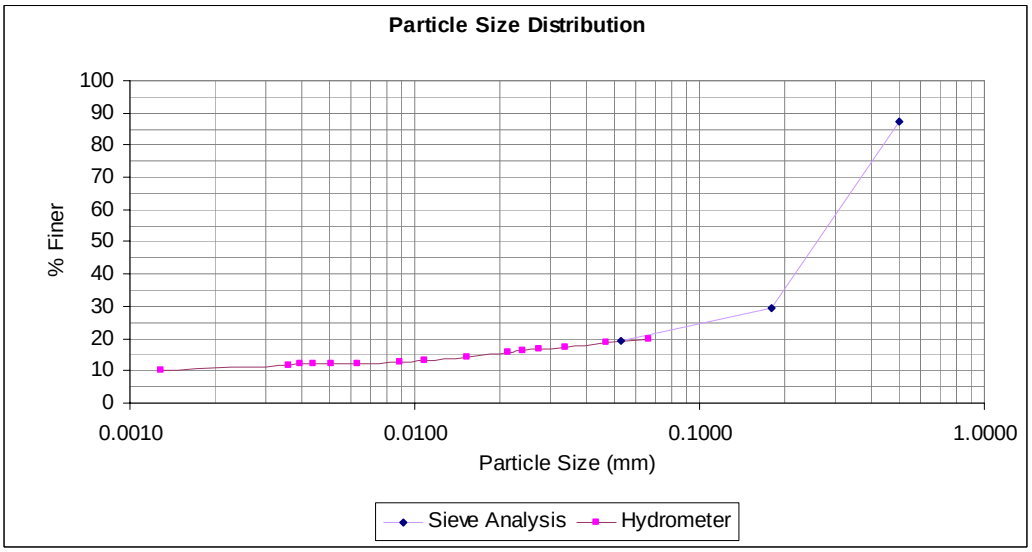

Figure B.54 Particle size distribution E9 1700.

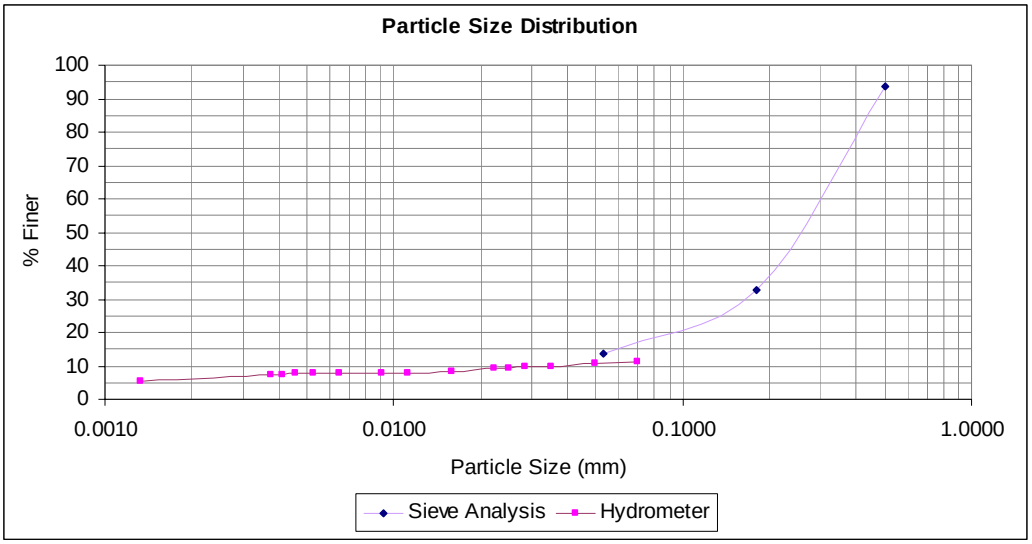

Figure B.55 Particle size distribution E10 600.

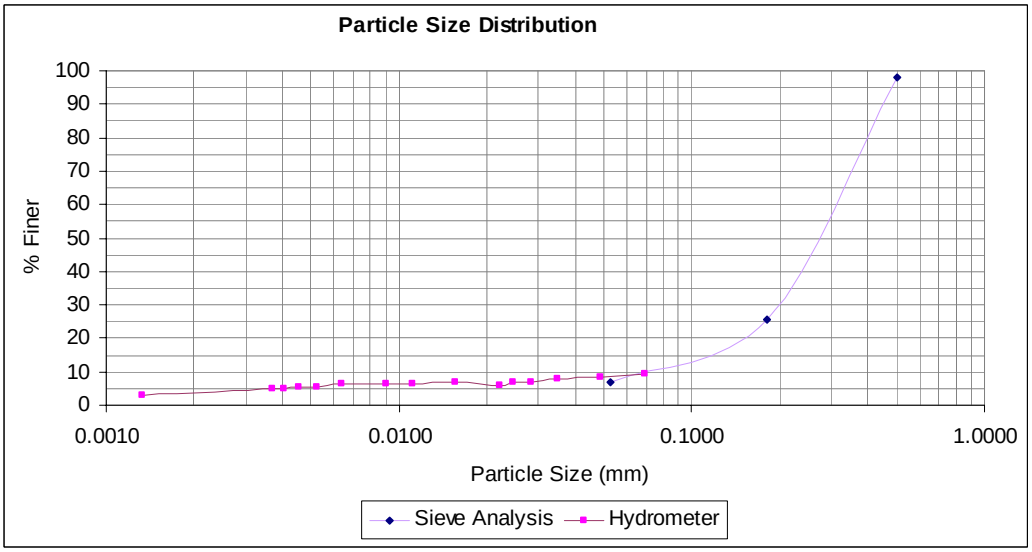

Figure B.56 Particle size distribution E11 300

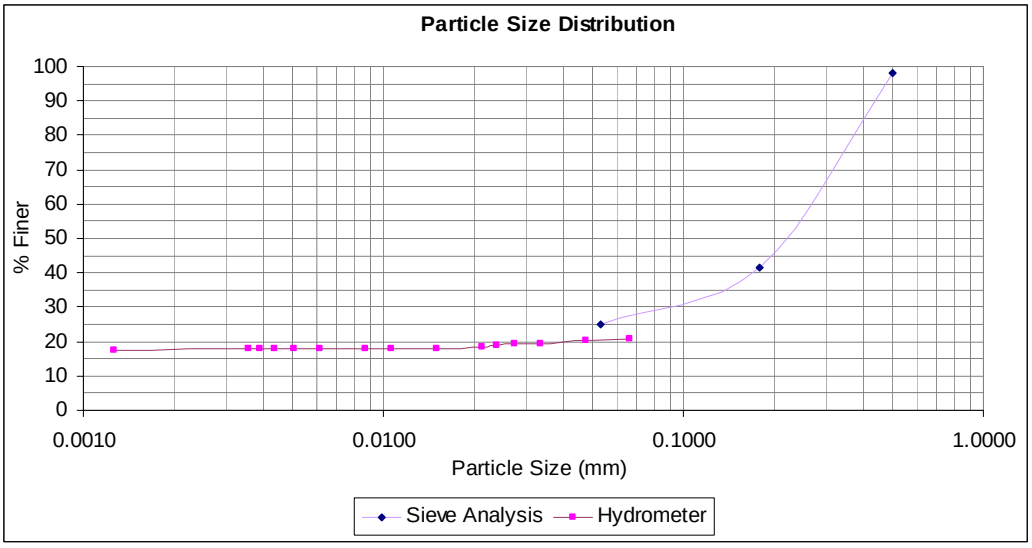

Figure B.57 Particle size distribution E11 900

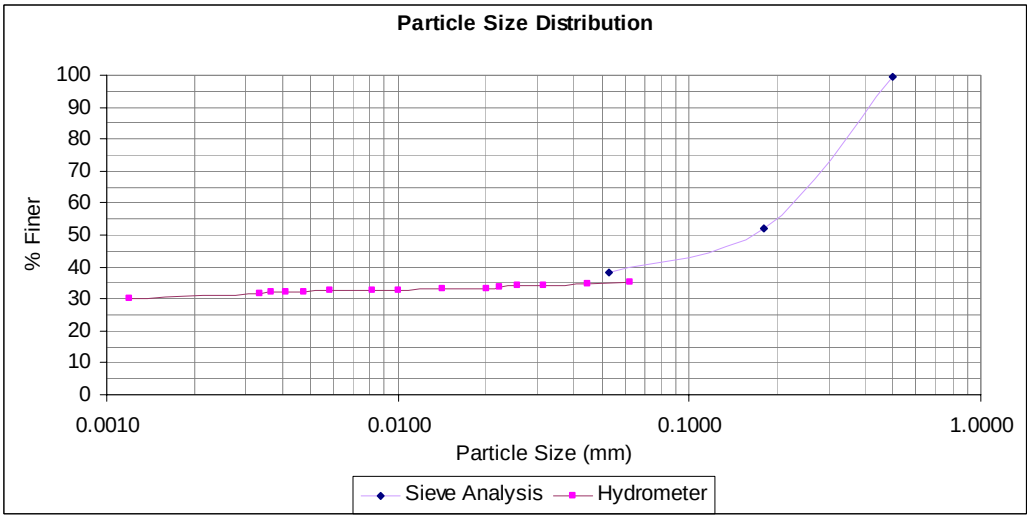

Figure B.58 Particle size distribution E11 1700

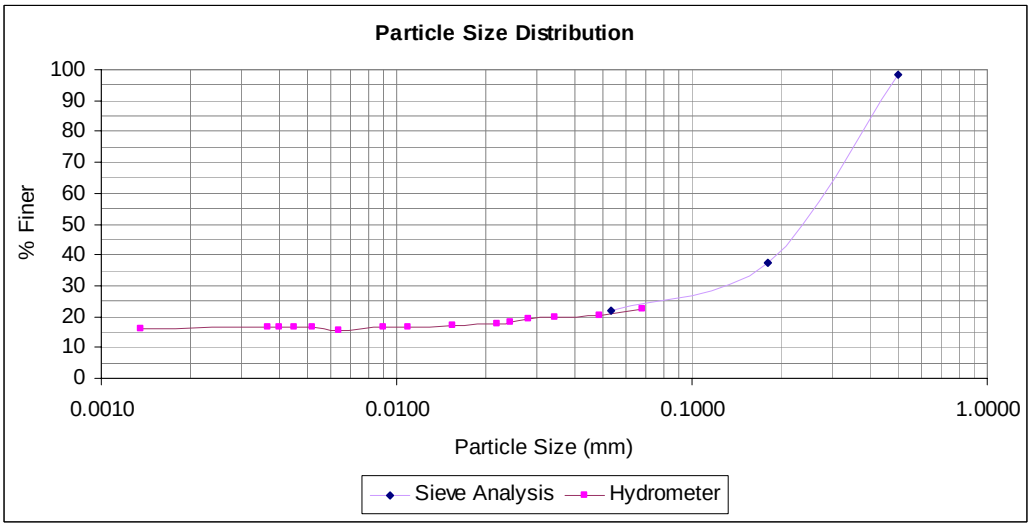

Figure B.59 Particle size distribution E12 600.

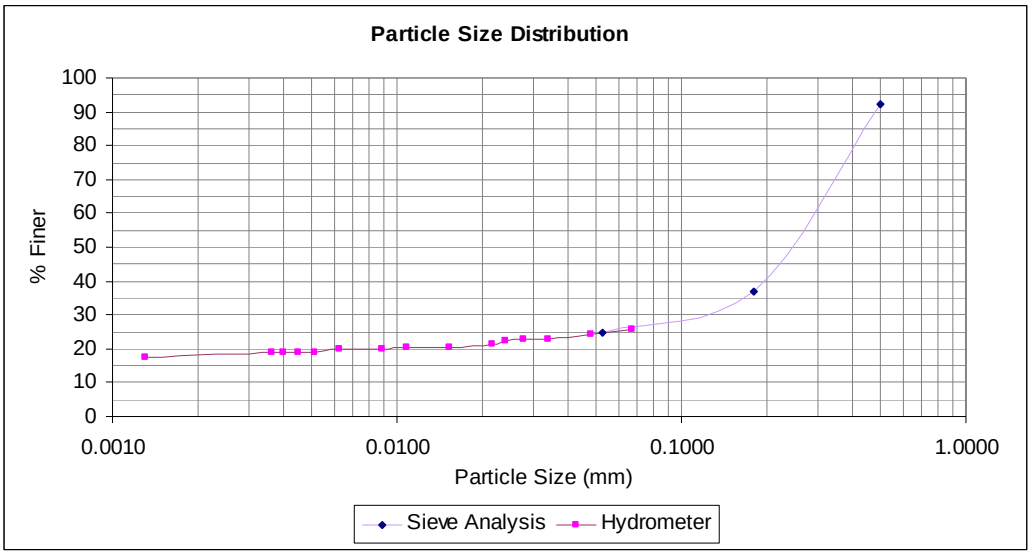

Figure B.60 Particle size distribution E12 1200

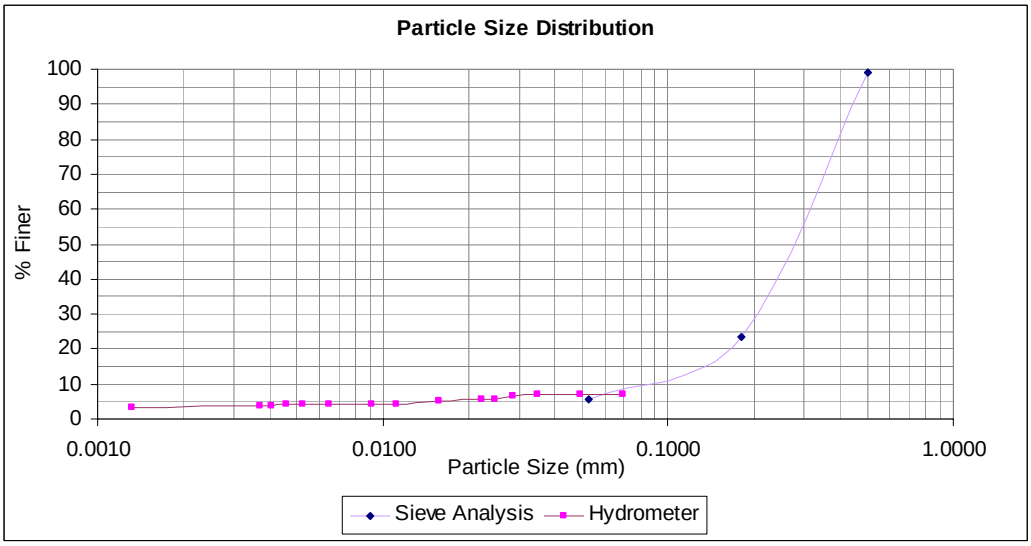

Figure B.61 Particle size distribution J1 0-300

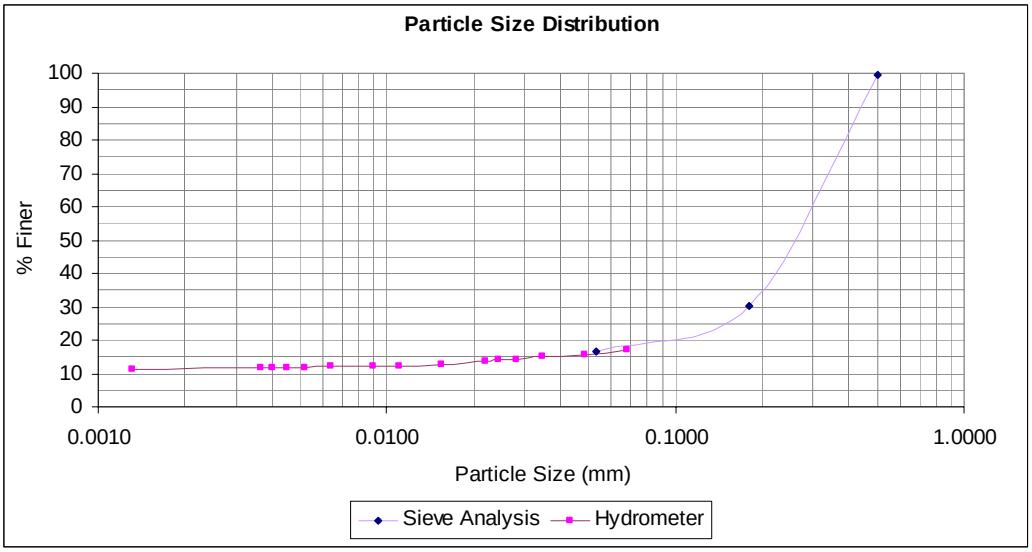

Figure B.62 Particle size distribution J1 1500-1800.

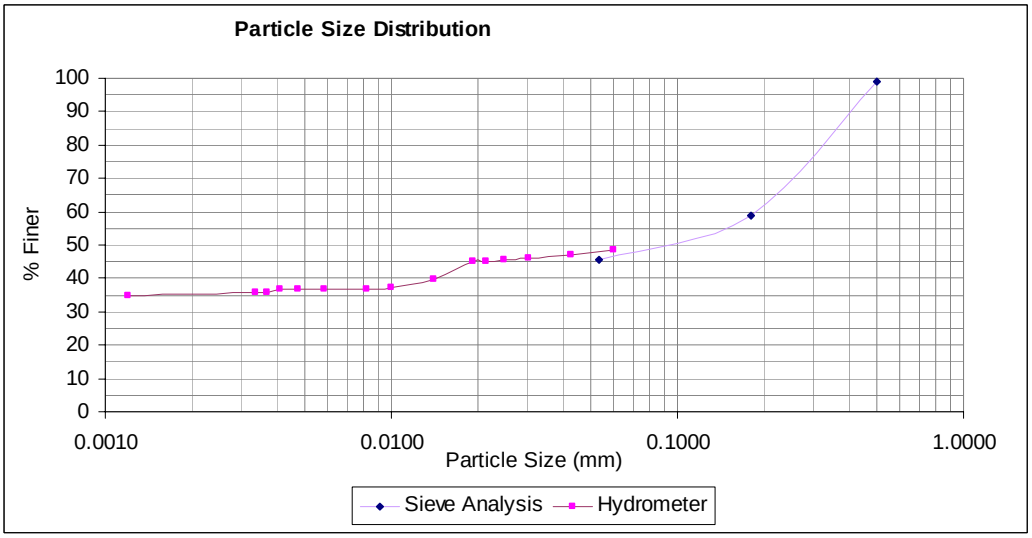

Figure B.63 Particle size distribution J1 3000-3300.

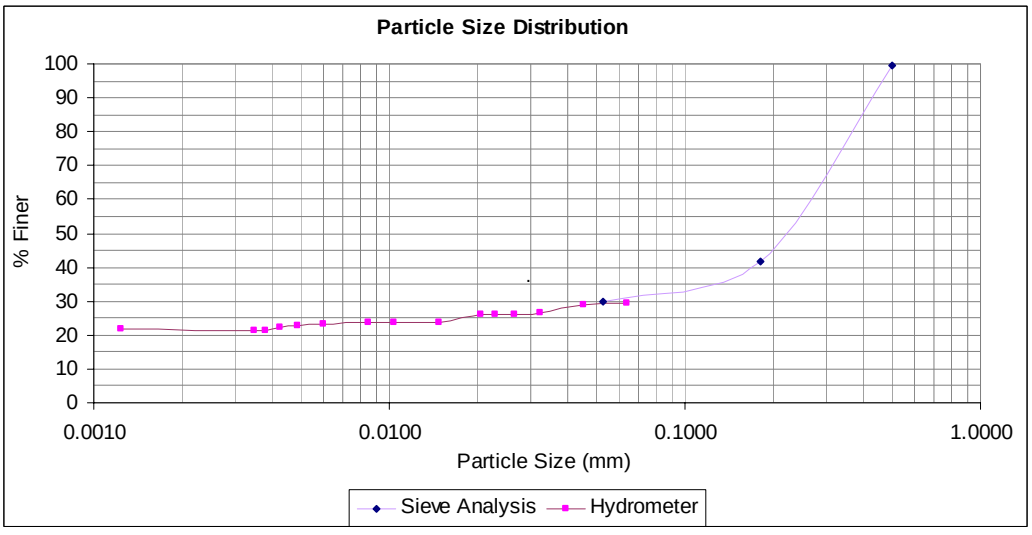

Figure B.64 Particle size distribution J1 3600-3900.

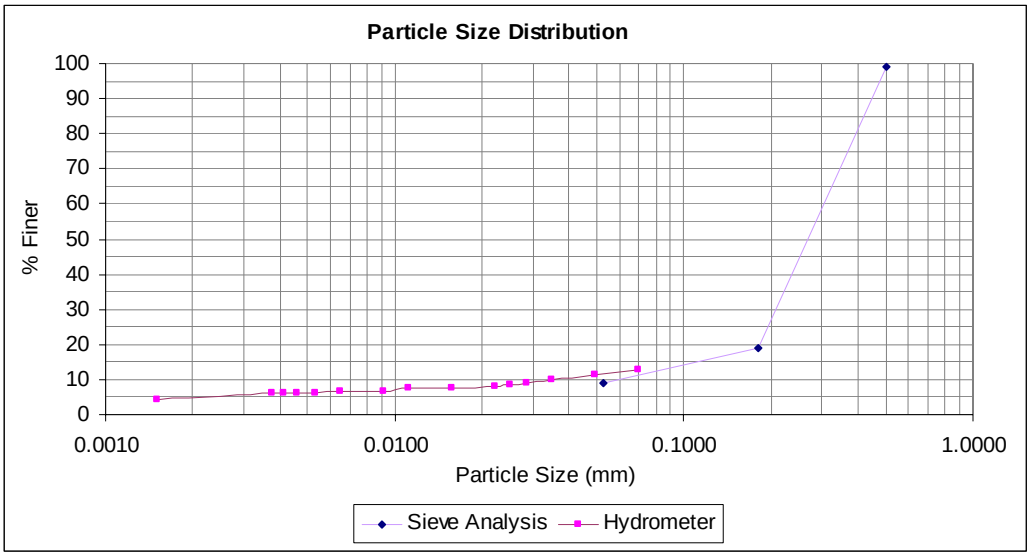

Figure B.65 Particle size distribution J3 300

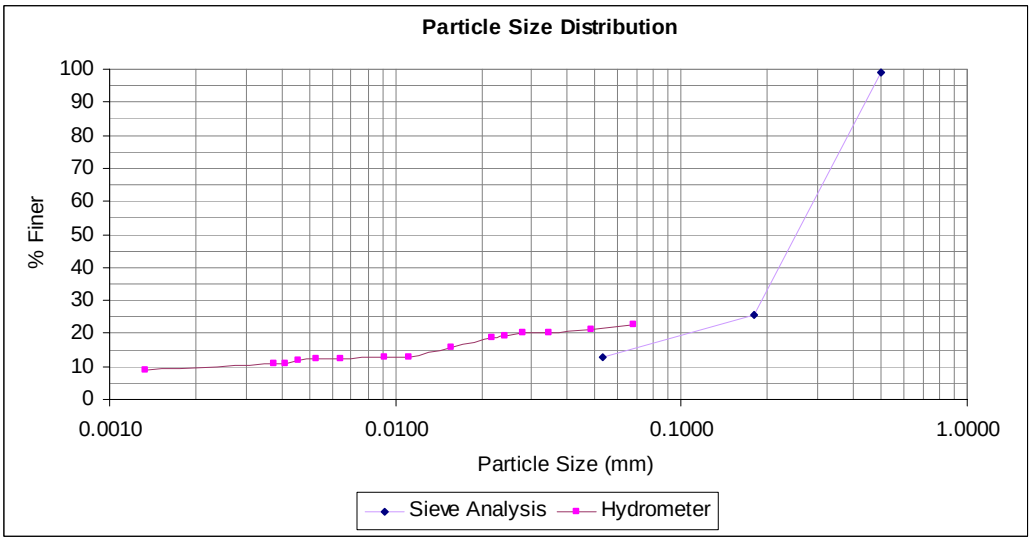

Figure B.66 Particle size distribution J4 1000.

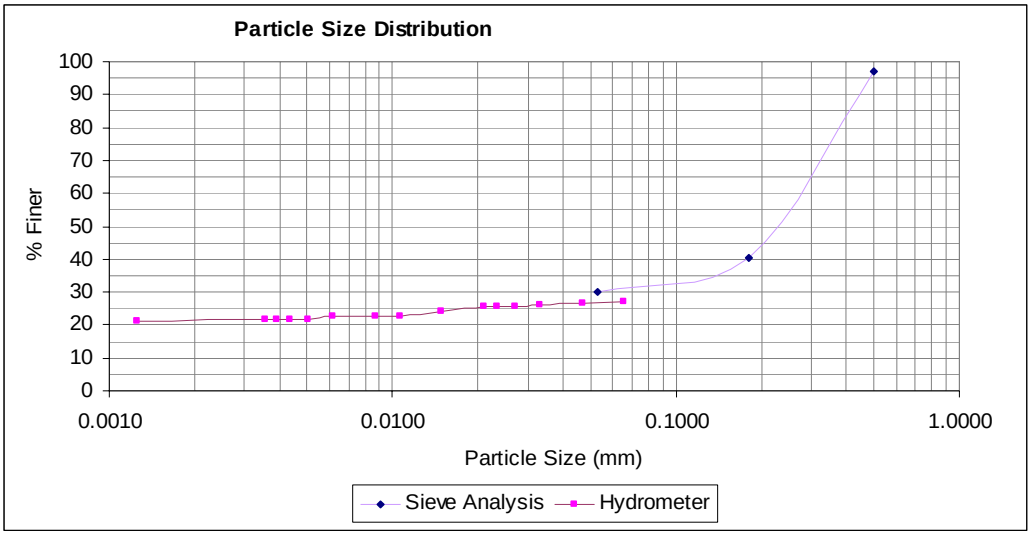

Figure B.67 Particle size distribution J4 4000.

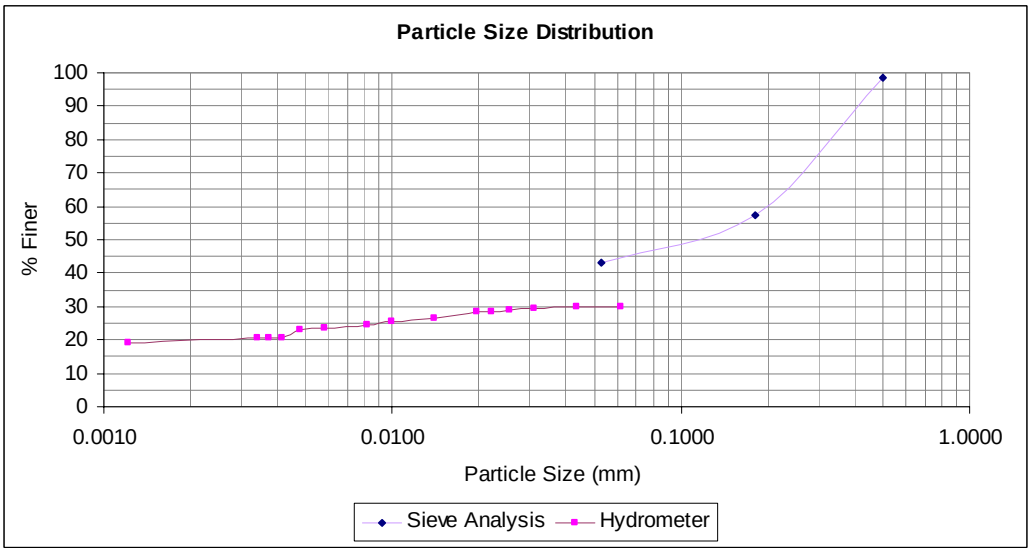

Figure B.68 Particle size distribution P1 0-300

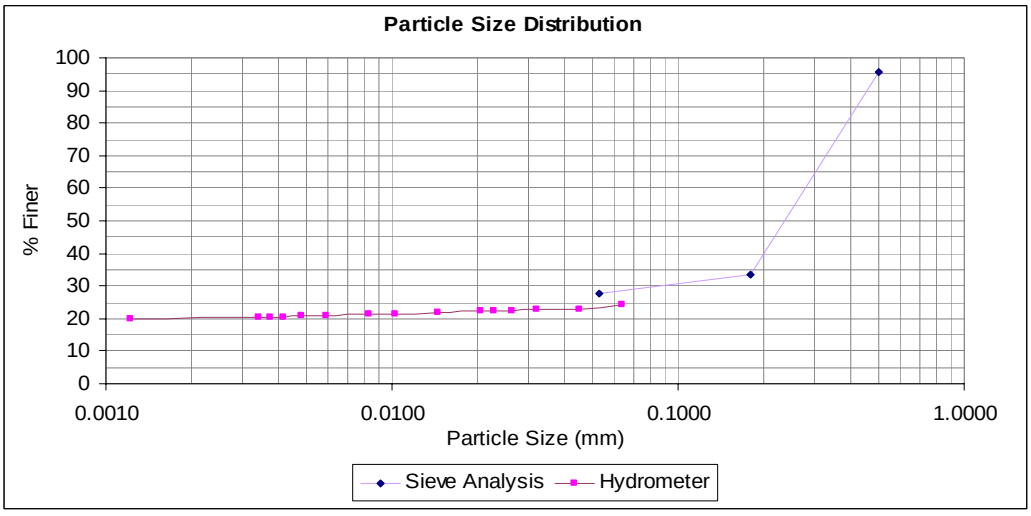

Figure B.69 Particle size distribution P1 1800.

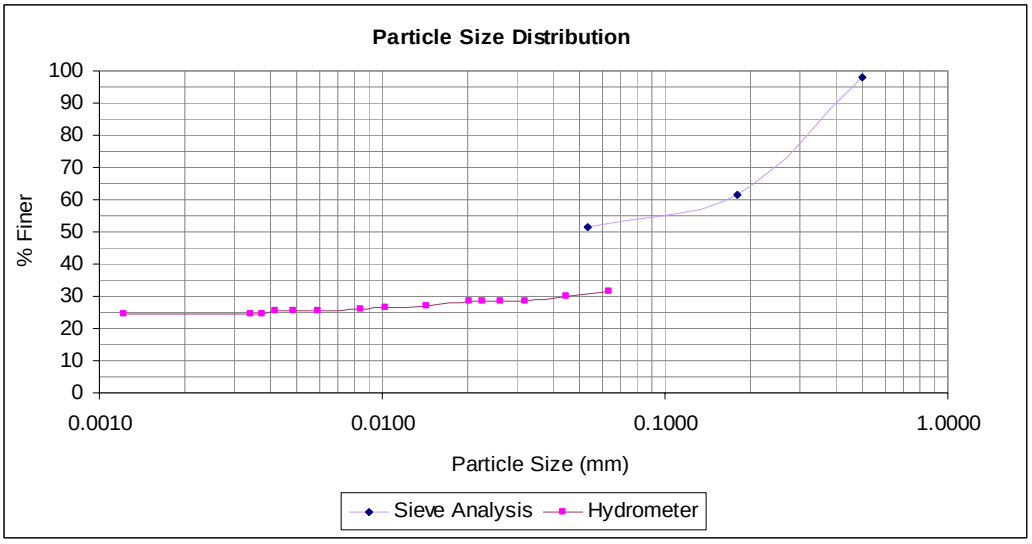

Figure B.70 Particle size distribution P1 3200.

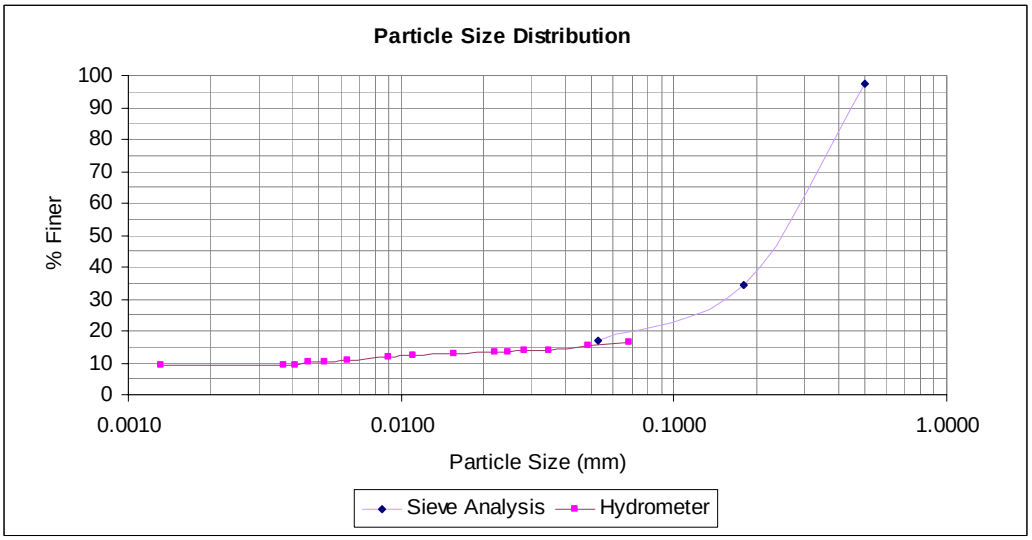

Figure B.71 Particle size distribution TS1 1000.

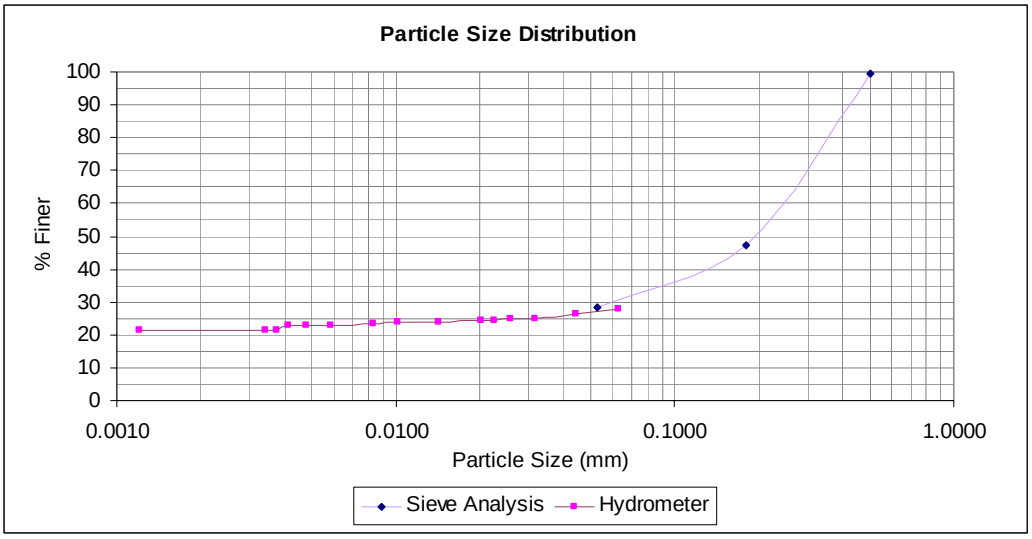

Figure B.72 Particle size distribution TS1 1500.

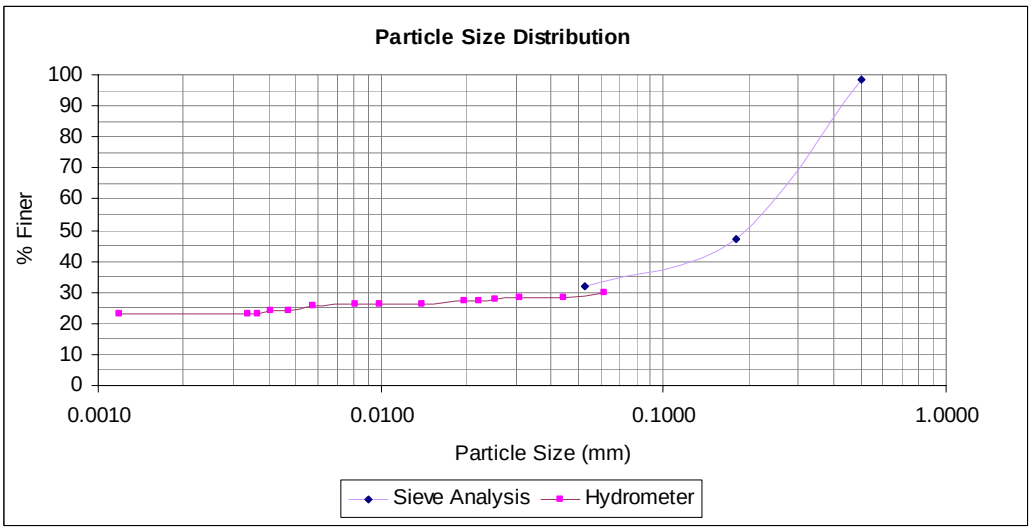

Figure B.73 Particle size distribution TS1 2000.

APPENDIX C

Groundwater Level and Topography Data

SiteName	WaterLevel (m)	Topography (m)
ELD43	40.6	42.00
ELD25	46.25	47.00
ELD44	28.94	31.00
ELD45	43.41	45.00
ELD46	40.06	42.00
ELD3	41.75	45.00
ELD18	45.7	49.00
ELD4	53.75	56.00
ELD1	45.86	54.00
ELD21	44.19	46.00
ELD22	43.55	45.00
ELD23	43.21	47.00
ELD19	45.93	48.00
ELD2	40.66	44.00
ELD27	49.35	50.00
B2	75.9	76.00
ELD50	34.76	36.00
ELD49	43.8	45.00
ELD48	38.2	40.00
ELD47	44.2	45.00
E1	42.3	44.00
E2	38.21	40.00
E3	40.64	42.00
E4	43.68	45.00
E5	45.13	46.00
ELD28	46.21	47.00
E9	52.52	54.00
E10	55.11	56.00
E12	54.65	55.00
E13	54.62	55.00
E15	55.63	56.00
E16	54.3	55.00
E17	57.24	58.00
E18	59.04	60.00
Wall1	43.17	44.00
ELD20	45.24	46.00
ELD8	44.87	46.00

ABSTRACT

This thesis is part of the project that the South African government and research institutions had initiated to study the fate and the transport of the LNAPLs contaminant in groundwater. The aim of the dissertation is to characterize the geology and hydrogeology of the Joint Fuel Depot site in East London, as well as to characterize the state of groundwater which is exposed to LNAPLs contamination from the tank's leakage. This characterization has lead to the drawing of a geological and hydrogeological conceptual model of the site.

Site characterization has been initiated as the first step of the investigation to provide detailed information on the geological and hydrogeological conditions of the site. Such information is important as it leads to a better understanding of the position and flow of LNAPLs in the sub-surface and how the groundwater is affected.

The electrical resistivity tomography (ERT) was selected as one of the techniques to delineate the geological units, to locate the aquifers as well as weathered and fractured zones which are considered as preferential pathways of groundwater and contaminants.

The literature review and site description had a permit to acquire relevant information on the previous use of the ERT techniques in LNAPLs site characterization and on the local geological and hydrogeological setting. ERT techniques have proved to be applicable and appropriate for this investigation. ERT is a 2-D electrical resistivity technique which uses an automatic multi-electrode instrument to inject a current into the ground through two electrodes, and which measures the voltage drop at two other electrodes. The injection of a current and the measurement of the voltage drop are sequentially repeated along a line of several electrodes to produce a 2-D resistivity distribution of the subsurface.

Like any other geophysical methods, the ERT results need to be complemented by other field testing results to permit an integrated interpretation which leads to the complete characterization of the LNAPLs site. The field testing includes soil testing, groundwater testing, borehole logs and groundwater levels. The soil testing provided the initial soil water content, soil particle distribution and the spatial distribution of volatile organic carbons on the site. Groundwater testing evaluates the presence of petroleum hydrocarbons in the saturated zones. Borehole logs gave the nature and thickness of geological units and water level data allowed to determine the direction of the groundwater on the site.

The field testing results were very useful in ERT interpretation. They have been used to compare to the contrasts revealed in the resistivity model sections provided by the ERT surveys. This integrated interpretation has lead to establish, firstly, that the Joint Fuel Depot site is underlain by four major geological units including the sand, clayey sand, clay and dolerite sill; and secondly, that there is evidence of LNPALs contaminant on the surface of the groundwater.

From the integrated interpretation of the results, it could be concluded that the ERT survey has proved to be applicable in the LNAPLs site characterization. It is recommended that the ERT survey be used for three-dimensional resistivity distributions for a more accurate delineation of LNAPLs plumes and that a time-lapse survey be considered to monitor the changes and progress of LNAPLs contaminant in the subsurface.